Faint Gamma-Ray Bursts and Other High-Energy Transients Detected with BATSE

by

Jefferson Michael Kommers

Submitted to the Department of Physics
in partial fulfillment of the requirements for the degree of

Doctor of Philosophy in Physics

at the

MASSACHUSETTS INSTITUTE OF TECHNOLOGY

February 1999

© Massachusetts Institute of Technology 1999. All rights reserved.

Author .....
Department of Physics
December 15, 1998

Certified by .....
Walter H. G. Lewin
Professor of Physics
Thesis Supervisor

Accepted by .....
Thomas J. Greytak
Professor of Physics
Associate Department Head for Education

Faint Gamma-Ray Bursts and Other High-Energy Transients Detected with BATSE

by

Jefferson Michael Kommers

Submitted to the Department of Physics
on December 15, 1998, in partial fulfillment of the
requirements for the degree of
Doctor of Philosophy in Physics

Abstract

The Burst and Transient Source Experiment (BATSE) onboard the *Compton Gamma Ray Observatory* detects gamma-ray bursts (GRBs) and other high-energy astronomical transients using a real-time burst detection system running onboard the spacecraft. This thesis describes a search of the archival BATSE data for GRBs, emission from soft gamma-ray repeaters (SGRs), bursts and flares from X-ray binaries, and other transients that were *not* detected by the onboard system. The search covers six years of the mission, from 1992 December 9.0 to 1997 December 17.0.

The search reveals 873 GRB candidates that did not activate the onboard burst detection because they were too faint, because they occurred while the onboard system was disabled for technical reasons, or because their time profile artificially raised the onboard detection threshold. The catalog of these bursts increases the number of GRBs detected with BATSE by 48% during the time period of the search.

The intensity distribution of the GRBs detected with the search reaches peak fluxes that are a factor of ~ 2 lower than could be studied previously. The value of the $\langle V/V_{\rm max}\rangle$ statistic (in Euclidean space) for these bursts, 0.177 ± 0.006, is the lowest so far obtained for a global sample of GRBs. The differential peak flux distribution is consistent with cosmological models in which the co-moving GRB rate approximately traces the star-formation history of the Universe. These results suggest that more sensitive detectors are likely to discover relatively few GRBs (of the kind currently known) that are fainter than the BATSE detection threshold.

Thesis Supervisor: Walter H. G. Lewin
Title: Professor of Physics

Acknowledgments

It has been a pleasure to spend the last 5.5 years working with the members of the MIT astrophysics community and the BATSE team at Marshall Space Flight Center. The time has come to acknowledge the extensive discussions and assistance that they have contributed to this thesis as well as to my other research projects.

I am grateful to my thesis advisor, Walter Lewin, for his support, encouragement, and dedication to my success as a scientist. His high standards in research and in pedagogy are a model for my own intellectual development. It has been a privilege and a pleasure to spend these years as a student, colleague, and friend.

I would like to thank the other readers on my thesis committee for their discussions at committee meetings and their valuable comments on the manuscript: Jackie Hewitt and Simon Mochrie of MIT and Jerry Fishman of the NASA Marshall Space Flight Center. I am grateful to Jerry, the Principal Investigator on the BATSE project, for acting as the agency sponsor on my NASA Graduate Student Researchers Program Fellowship, for serving as an official reader on this thesis, and for taking the time to travel to MIT for the defense.

The research I describe in this thesis was undertaken as part of a collaboration that includes myself, Walter, and Jerry as well as Jan van Paradijs, Chryssa Kouveliotou, Geoff Pendleton, and Chip Meegan. The idea to produce a catalog of nontriggered gamma-ray bursts and other transients from the BATSE archival data is due to Chryssa, who has served as my primary contact with the BATSE group at MSFC throughout this research. Indeed, the entire BATSE team has in one way or another helped make this thesis possible. I am grateful to all these collaborators for their guidance and assistance throughout this project. I would like to thank Jan and Chryssa in particular for their hospitality during my visits to Huntsville.

The wide-ranging interests of the MIT astrophysics community ensured that I did not spend all my time on topics directly related to my thesis. I am happy to acknowledge discussions on a variety of astrophysical subjects with Deepto Chakrabarty, Al

Levine, Ed Morgan, Vicky Kaspi, Ron Remillard, George Ricker, and Paul Schechter.

The graduate student community has been the source of countless hours of helpful discussions and lasting friendships. Bob Rutledge, Derek Fox, Patrick Wojdowski, and Bob Guerriero have been colleagues, running partners, and friends. There have been hours of serious and whimsical discussions with the other residents of our sixth-floor computer room—Dave Buote, Froney Crawford, Taotao Fang, Eric Gaidos, Jon Miller, Dave Pooley, and Julia Steinberger—as well as with those working downstairs with the CCD lab and the XTE group: Chris Becker, Glen Monnelly, Mike Pivovaroff, Bob Shirey, and Don Smith.

I am happy to acknowledge financial support from a National Science Foundation Graduate Fellowship during my first three years at MIT and from a NASA Graduate Student Researchers Program Fellowship under grant NGT 8-52816 for the remainder of my graduate studies.

My parents and grandparents, Jim, Nancy, Clarence, Vernetta, and Betty, deserve special thanks. Their support, encouragement, and strong family commitment to education motivated me to pursue the doctoral degree. Finally, I am personally indebted to Arthur Pugsley IV. His support, patience, and companionship over the last 3.5 years have been indispensable and deeply appreciated.

Contents

1 Introduction **17**

1.1 Organization 18

1.2 Terms, Naming Conventions, and Units 19

1.3 Publications 20

1.3.1 Refereed Journals 21

1.3.2 In Preparation 22

1.3.3 Conference Proceedings 22

1.3.4 IAU Circulars 23

2 Gamma-Ray Bursts and Other High-Energy Astronomical Transients **25**

2.1 Gamma-Ray Bursts 26

2.1.1 Historical Overview 26

2.1.2 Gamma-Ray Properties 29

2.2 Soft Gamma-Ray Repeaters 35

2.3 Bursts and Flares from X-ray Binaries 36

2.4 Solar and Terrestrial Phenomena 37

2.4.1 Solar Flares 38

2.4.2 Radiation Belts 38

2.4.3 Orbiting Nuclear Reactors 40

2.4.4 Terrestrial Gamma-Ray Flashes 41

2.5 Unknown Phenomena 42

2.6 Effects of High-Energy Transients on Earth 42

3 The Burst and Transient Source Experiment 45

3.1 The *Compton Gamma Ray Observatory* 45

3.2 BATSE Instrument Description 46

3.3 Onboard Data Processing and Burst Detection 49

3.4 Detector Characteristics 52

3.5 Detector Background 55

4 The Search for Nontriggered Events 61

4.1 Motivations for the Off-line Search 62

4.2 Data Selection and Scope 64

4.3 Off-line Search Algorithm 65

4.4 Detection Efficiency and Sky Exposure 72

4.5 Classification of Off-line Triggers 75

4.5.1 Occultation Steps and Aperiodic Variability 78

4.5.2 Phosphorescence Spikes 80

4.5.3 Magnetospheric Particle Precipitations 80

4.5.4 Solar Flares 81

4.5.5 Terrestrial Gamma-Ray Flashes 83

4.5.6 Gamma-Ray Bursts 83

4.5.7 Bursts and Flares Associated with Known Sources in Outburst 87

4.5.8 Soft Gamma-Ray Repeaters 87

4.5.9 "Unknown" Low-Energy Events 90

5 The Nontriggered Event Catalogs 93

5.1 Off-line Triggers 93

5.2 Nontriggered GRB Candidates 94

5.3 Estimation of Physical Parameters 96

5.3.1 Source Directions 97

5.3.2 Durations 98
5.3.3 Peak Photon Fluxes 99
5.3.4 Fluences 100
5.3.5 $C_{\max}/C_{\min}$ 100
5.3.6 Accuracy of Off-line Burst Parameters 100
5.4 Classification Accuracy 104
5.4.1 Contamination by Non-GRB Events 104
5.4.2 Incompleteness by Misclassification of GRBs 109
5.5 GRB Direction Distribution 111
5.6 GRB Duration Distribution 114
5.7 GRB Rate 114
5.8 SGR Events 116
5.9 "Unknown" Low-Energy Events 118
5.9.1 Direction Distribution 118
5.9.2 Spectral Hardness 119
5.9.3 Event Rate 123

6 Gamma-Ray Burst Intensity Distribution 127
6.1 Abstract 127
6.2 Introduction 128
6.3 The Search for Nontriggered GRBs 131
6.3.1 Trigger Efficiency 133
6.3.2 $(C_{min}/C_{max})^{3/2}$ Distribution 137
6.3.3 Peak Fluxes 140
6.4 Cosmological Model Comparison 141
6.4.1 Purely Cosmological Models 141
6.4.2 Limits on a Possible Homogeneous Sub-population 152
6.5 Discussion 154

7 Conclusions 165

A Catalog of Nontriggered Gamma Ray Bursts **169**

B Catalog of Unknown 25–50 keV Transients **217**

C "A Search for Nontriggered Gamma-ray Bursts in the BATSE Data Base" **223**

C.1 Abstract 223

C.2 Introduction 224

C.3 Search Algorithm 226

C.4 Sensitivity 231

C.4.1 Trigger Efficiency 231

C.4.2 Sensitivity to "Slow-risers" 237

C.5 Classification and Analysis of Events 238

C.6 Results 247

C.6.1 Gamma-ray Burst Candidates 247

C.6.2 Unknown Events 262

C.7 Conclusions 263

C.8 Acknowledgments 264

List of Figures

2-1 Examples of GRB time profiles 31

2-2 GRB duration histogram 32

2-3 Examples of GRB energy spectra 34

3-1 *Compton Gamma Ray Observatory* 47

3-2 BATSE detector module 48

3-3 Discriminator channel response 54

3-4 Angular response of LADs 56

3-5 BATSE detector count rates over one day 57

4-1 Off-line trigger criteria 68

4-2 Off-line sky exposure 76

4-3 Off-line sky exposure as a function of declination 77

4-4 Occultations of bright X-ray sources 79

4-5 Magnetospheric particle precipitation 82

4-6 Solar flares and GRB plotted in 8 detectors 84

4-7 Solar flare plotted in 4 discriminator channels 85

4-8 GRB plotted in 4 discriminator channels 86

4-9 X-ray burst from GRO J1744−28 88

4-10 Burst from SGR 1806−20 89

5-1 Rate of off-line triggers 95

5-2 Comparison of off-line measurements with those of BATSE team . . . 102

5-3 Histogram of angles between nontriggered GRB sources and the Sun . 106
5-4 Histogram of angles between nontriggered GRB sources and the Earth's center 107
5-5 *CGRO* geographic locations at time of nontriggered GRBs 108
5-6 *CGRO* geographic latitudes at times of nontriggered GRBs 110
5-7 Direction distribution of nontriggered GRBs 113
5-8 Duration distribution of nontriggered GRBs 115
5-9 Detection rate of GRBs 117
5-10 Sky map of nontriggered SGR events 120
5-11 Direction distribution of "unknown" low-energy bursts 121
5-12 Distribution of angles between "unknown" events and Earth's center . 122
5-13 Hardness ratios of "unknown" events and nontriggered GRBs 124
5-14 Rate of "unknown" events. 125

6-1 Trigger efficiency for off-line search 134
6-2 Histogram of peak duration 136
6-3 Cumulative distribution of $(C_{min}/C_{max})^{3/2}$ 138
6-4 Redshift distributions of the star-formation rate 147
6-5 Best-fit cosmological models with power-law luminosity distributions 149
6-6 Redshift distributions of observed bursts 151
6-7 Cumulative burst rate distributions 159

C-1 Off-line search detection criteria 230
C-2 Distribution of $S_d(k)$ 232
C-3 Off-line trigger efficiency 235
C-4 Off-line sky exposure. 236
C-5 Profile of a "slow riser." 239
C-6 Detection probability for "slow riser." 240
C-7 Sky map of all non-terrestrial nontriggered events. 250
C-8 Sky map of 91 nontriggered GRB candidates 255

C-9 Cumulative number vs. peak flux for nontriggered GRBs 257
C-10 Peak flux distributions for 83 nontriggered GRBs 258
C-11 Intensity profiles of nontriggered GRB candidates. 260
C-12 More light curves of nontriggered GRB candidates 261
C-13 Sky map of low-energy (25–50 keV) events. 265

List of Tables

3-1 Fast discriminator channel boundaries 59

4-1 Days for which no archival data were searched. 70

4-2 Parameters of off-line searches 70

4-3 Dipole and quadrupole moments of sky exposure 91

5-1 Some causes of off-line triggers 112

5-2 Dipole and quadrupole statistics for nontriggered GRBs 112

5-3 Dipole and quadrupole statistics for low-energy "unknown" events . 120

6-1 Values of $\langle (C_{min}/C_{max})^{3/2} \rangle$ obtained by various GRB detectors. . . . 161

6-2 Data for fitting differential peak flux distribution 162

6-3 Best fit parameters for monoluminous cosmological models 163

6-4 Best fit parameters for cosmological models with a power-law luminosity function 163

6-5 Co-moving $z = 0$ burst rate for monoluminous cosmological models . 163

6-6 Co-moving $z = 0$ burst rate for cosmological models with a power-law luminosity function 164

6-7 Upper limits on fractional GRB rate due to a possible homogeneous (in Euclidean space) sub-population of GRBs 164

A-1 Onboard triggers detected in off-line search 171

A-2 Nontriggered GRB catalog 173

B-1 Non-triggered SGR events 218
B-2 Non-triggered "unknown" events 220

C-1 Parameters of the time series formed from the DISCLA data. 236
C-2 Classification matrix of 317 onboard triggers 243
C-3 91 nontriggered GRB candidates. 249
C-4 Durations and intensities of nontriggered GRB candidates 253

Chapter 1

Introduction

Gamma-ray bursts (GRBs) are intense pulses of electromagnetic radiation that carry most of their energy above 100 keV. They arrive from random directions in space and are observed primarily with Earth-orbiting and interplanetary spacecraft. During their appearance, which may last from $\sim$ 10 ms to $\sim$ 1000 s, they are often brighter than all other gamma-ray sources in the sky combined.

The detection and study of GRBs are the primary objectives of the Burst and Transient Source Experiment (BATSE) onboard the *Compton Gamma Ray Observatory* (Fishman et al. 1989). BATSE is a set of eight gamma-ray detector modules facing outward from the corners of the spacecraft. Each detector module carries a Large Area Detector (LAD) and a smaller Spectroscopy Detector (SD). The onboard computer monitors the gamma-ray count rates in each of the detectors. A programmable burst detection algorithm identifies GRBs and other transients in real time. When the count rates in the LADs exceed a certain preset threshold, the computer signals a "burst trigger" and records data at higher temporal and spectral resolution for a limited time interval. The BATSE operations team scrutinizes and catalogs the transient events identified by the onboard computer. As of 1998 December 13, there are 2267 GRBs listed in the BATSE burst catalogs (Meegan et al. 1998a).

In certain cases a GRB or other astronomically interesting transient may *not* activate the onboard burst trigger. The event may be too faint to exceed the preset

threshold; it may occur while the onboard burst trigger is disabled for technical reasons; or it may artificially raise the onboard background estimate and be mistaken for a below-threshold event. The data on such "nontriggered" or "untriggered" events are recorded in the (nearly) continuous lower-resolution data streams from BATSE.

In this thesis I describe a search of the archival continuous data from BATSE for GRBs and other astronomically interesting transients that did *not* activate the onboard burst trigger. The goals of this investigation are to detect the faintest GRBs that have ever been observed and to search for a variety of other astrophysical transients.

The detection of the faint GRBs provides unique information on the intensity distribution of bursts below the BATSE onboard detection threshold. This information is useful for testing cosmological models of the burst sources and for planning the design and operation of future GRB detectors. GRBs are not the only transient phenomenon detected with BATSE, however. Because it is an all-sky monitor, BATSE also detects bursts and flares from soft gamma-ray repeaters (SGRs) and X-ray binaries. A systematic search for transients from these objects and others has the potential to identify new burst sources.

1.1 Organization

The main features of this thesis are the catalog of nontriggered GRBs in Appendix A and its application to cosmological models of the GRB intensity distribution in Chapter 6.

Chapter 2 provides background information on GRBs and other transients that can be studied in the energy range monitored with BATSE. Chapter 3 describes the BATSE instrument and its operation. Chapter 4 describes the search for nontriggered GRBs and other transients in the archival data. The search algorithm, its sensitivity to bursts with certain characteristics, and the procedures for separating the detected events into useful classes (GRBs, solar flares, terrestrial phenomena,

etc.) are described. Chapter 5 describes the catalogs of nontriggered events. It discusses the physical quantities that are tabulated for the GRBs, bursts from SGRs, and low-energy (25–50 keV) events of "unknown" origin.

Chapter 6 discusses the intensity distribution of the GRBs detected with the off-line search. This is the main scientific result of the search for nontriggered events. The burst rate as a function of peak photon flux contains information on the intrinsic peak luminosities and the spatial distribution of the burst sources. This chapter is a self-contained paper that has been submitted to *The Astrophysical Journal*.

Chapter 7 collects the main results and conclusions of the thesis.

Appendix A contains the catalog of GRBs that were detected by the off-line search. Appendix B contains the catalogs of bursts from SGRs and the bursts and flares of unknown origin. The catalogs in appendices A and B are also available in electronic form. A CD-ROM can be obtained from the author, and access is available via the World Wide Web at `http://space.mit.edu/BATSE`.

Appendix C contains the text of a paper describing preliminary results from the off-line search (Kommers et al. 1997).

1.2 Terms, Naming Conventions, and Units

The names of GRBs in the BATSE catalogs are generally given in the form "GRB YYMMDD," where YY specifies the year, MM the month, and DD the day that the burst was observed. When more than one burst is detected on a single day, an alphabetic letter starting with "b" is appended according to the approximate brightness of the burst. For example, GRB 930711 is the brightest burst observed on 1993 July 11 and GRB 930711c is the third-brightest (Meegan et al. 1996). In the catalog of nontriggered GRBs, this scheme can break down since the off-line search sometimes discovered bursts with brightness intermediate between two previously cataloged bursts with adjacent letters. Therefore, the nontriggered bursts are given names according to the time they occurred in the format "NTB YYMMDD.FF,"

where the suffix ".FF" specifies the first two digits of fractional part of the day. For example, NTB 961222.50 is a nontriggered burst observed on 1996 December 22 at 12:00:01.7 UT.

Physical quantities are quoted in units based on the Gaussian CGS system; however, standard high-energy astronomical usage and BATSE operations usage require that certain exceptions be made for ease of communication. Dates are given in terms of the Truncated Julian Day (TJD) number that is used in BATSE operations. The TJD is related to the standard astronomical Julian Day (JD) number by TJD = JD - 2,440,000.5. Note that dates in the TJD system begin at Greenwich mean midnight. The time of day is specified in terms of seconds (UT) on the given TJD. Distances on cosmological scales are quoted in mega-parsecs (Mpc) or giga-parsecs (Gpc) where 1 Mpc = 10^{-3} Gpc = 3×10^{24} cm. Where necessary, the Hubble constant is defined as $H_0 = 70\ h_{70}$ km s^{-1} Mpc^{-1}.

As is customary in gamma-ray astronomy, photon energies are quoted in kilo-electron volts (keV), where 1 keV = 1.6×10^{-9} erg. To conform with the BATSE catalogs, the peak fluxes of bursts are given in units of photons per square centimeter per second (ph cm^{-2} s^{-1}) in a given energy range. Similarly, burst fluences (total energy deposited in the detector by the event) are given in units of ergs per square centimeter (erg cm^{-2}) in a given energy range. Celestial coordinates of the burst source directions are quoted uniformly as equatorial right ascension (in decimal degrees) and declination (in decimal degrees) referred to epoch J2000.0.

1.3 Publications

Some of the work presented in this thesis has already appeared (or will appear) in refereed journals. This section is a complete list of the author's publications as of 1999 January 11. Some of the work reflected in these publications is separate from the research described in this thesis.

1.3.1 Refereed Journals

Kommers, J. M., Lewin. W. H. G., Kouveliotou, C., van Paradijs, J., Pendleton, G. N., Meegan, C. A., & Fishman, G. J. "The Intensity Distribution of Faint Gamma-ray Bursts Detected with BATSE," 1999, *Astrophysical Journal*, in press

Guerriero, R., Fox, D., Kommers, J., Lewin, W. H. G., Rutledge, R., Morgan, E., van Paradijs, J., van der Klis, M., Bildsten, L., & Dotani, T. "The Evolution of Rapid Burster Outbursts," 1999, *Monthly Notices of the Royal Astronomical Society*, in press

Kippen, R. M., Briggs, M. S., Kommers, J. M., Kouveliotou, C., Hurley, K., Robinson, C. R., van Paradijs, J., Hartmann, D. H., Galama, T. J., & Vreeswijk, P. M. "On the Association of Gamma-Ray Bursts with Supernovae," 1998, *Astrophysical Journal Letters*, **506**, 27

Kouveliotou, C., Dieters, S., Strohmayer, T., van Paradijs, J., Fishman, G. J., Meegan, C. A., Hurley, K., Kommers, J., Smith, I., Frail, D., & Murakami, T. "An X-ray Pulsar with a Superstrong Magnetic Field in the Soft Gamma-Ray Repeater SGR 1806−20," 1998, *Nature*, **393**, 235

Kommers, J. M., Chakrabarty, D., & Lewin, W. H. G. "Sidebands Due to Quasi-Periodic Oscillations in 4U 1626−67," 1998, *Astrophysical Journal Letters*, **497**, L33

Koshut, T. M., Kouveliotou, C., van Paradijs, J., Woods, P.M., Fishman, G. J., Briggs, M. S., Lewin, W. H. G., & Kommers, J. M. "Pulse Delay Observations of GRO J1744−28," 1998, *Astrophysical Journal Letters*, **496**, L101

Kommers, J. M., Lewin, W. H. G., Kouveliotou, C., van Paradijs, J., Pendleton, G. N., Meegan, C. A., & Fishman, G. J. "A Search for Nontriggered Gamma-Ray Bursts in the BATSE Data Base," 1997, *Astrophysical Journal*, **491**, 704

Augusteijn, T., Griener, J., Kouveliotou, C., van Paradijs, J., Lidman, C., Blanco, P., Fishman, G. J., Briggs, M. S., Kommers, J. M., Rutledge, R., Lewin, W. H. G., Henden, A. A., Luginbuhl, C. B., Vrba, F. J., & Hurley, K. "ROSAT Position of GRO J1744−28 and Search for Its Near-Infrared Counterpart," 1997, *Astrophysical Journal*, **486**, 1013

Kommers, J. M., Fox, D. W., Lewin, W. H. G., Rutledge, R. E., van Paradijs, J., & Kouveliotou, C. "Postburst Quasi-periodic Oscillations from GRO J1744−28 and from the Rapid Burster," 1997, *Astrophysical Journal Letters*, **482**, L53

Lewin, W. H. G., Rutledge, R. E., Kommers, J. M., van Paradijs, J., & Kouveliotou, C. "A Comparison Between the Rapid Burster and GRO J1744−28," 1996, *Astrophysical Journal Letters*, **462**, L39

Kouveliotou, C., van Paradijs, J., Fishman, G. J., Briggs, M. S., Kommers, J. M., Harmon, B. A., Meegan, C. A., & Lewin, W. H. G. "A New Type of Transient High-energy Source in the Direction of the Galactic Centre," 1996, *Nature*, **379**, 799

Wang, H.-H., Carlson, K. D., Geiser, U., Kini, A. M., Schultz, A. J., Williams, J. M., Montgomery, L. K., Kwok, W. K., Welp, U., Vanervoort, K. G., Boryschuk. S. J., Crouch, A. V. S., Kommers, J. M., Watkins, D. M., Schirber, J. E., Overmeyer, D. L., Jung, D., Novoa, J. J., & Whangbo, M. H. "New κ-phase Materials, κ-$(ET)_2Cu[N(CN)_2]X$, X = Cl, Br, and I—the Synthesis, Structure, and Superconductivity Above 11 K in the Cl (T_c = 12.8 K, 0.3 kbar) and Br (T_c = 11.6 K) Salts," 1991, *Synthetic Metals*, **42**, 1

Williams, J. M., Kini, A. M., Wang, H.-H., Carlson, K. D., Geiser, U., Montgomery, L. K., Pyrka, G. J., Watkins, D. M., Kommers, J. M., Boryschuk, S. J., Strieby-Crouch, A. V., Kwok, W. K., Schirber, J. E., Overmeyer, D. L., Jung, D., & Whangbo, M.-H. "From Semiconductor-Semiconductor Transition (42 K) to the Highest-T_c Organic Superconductor, κ-$(ET)_2Cu[N(CN)_2]Cl$ (T_c = 12.5 K)," 1990, *Inorganic Chemistry*, **29**, 3272

1.3.2 In Preparation

Kommers, J. M., Lewin, W. H. G., Kouveliotou, C., van Paradijs, J., Pendleton, G. N., Meegan, C. A., & Fishman, G. J. "The Nontriggered Supplement to the BATSE Gamma-Ray Burst Catalogs," 1999, in preparation

1.3.3 Conference Proceedings

Kommers, J. M., Lewin, W. H. G., Kouveliotou, C., van Paradijs, J., Pendleton, G. N., Fishman, G. J., & Meegan, C. A. "A Search for Non-triggered Events in the BATSE Data Base," 1998, in *Gamma Ray Bursts*, AIP Conference Proceedings, **428**, eds. C. A. Meegan, R. D. Preece, & T. M. Koshut (New York: AIP), 45

Hurley, K., Kouveliotou, C., Fishman, G. J., Meegan, C. A., Briggs, M., van Paradijs, J., Cline, T., Kommers, J., & Lewin, W. H. G. "Verifying the Accuracy of the 3rd Interplanetary Network with the Bursting Pulsar GRO J1744−28 and the Soft Gamma Repeater SGR 1806−20," 1998, 1998, in *Gamma Ray Bursts*, AIP Conference Proceedings, **428**, eds. C. A. Meegan, R. D. Preece, & T. M. Koshut (New York: AIP), 109

Hakkila, J., Meegan, C. A., Pendleton, G. N., Henze, W., McCollough, M., Kommers, J. M., & Briggs, M. 1998, in *Gamma Ray Bursts*, AIP Conference Proceedings, **428**, eds. C. A. Meegan, R. D. Preece, & T. M. Koshut (New York: AIP), 144

Kommers, J. M., Lewin, W. H. G., van Paradijs, J., Kouveliotou, C., Fishman G. J., & Briggs, M. S. "A Search for Untriggered Events in the BATSE Data Base," 1996, in *Gamma Ray Bursts*, AIP Conference Proceedings, **384**, eds C. Kouveliotou, M. S. Briggs, & G. J. Fishman (New York: AIP), 441

1.3.4 IAU Circulars

Guerriero, R., Lewin, W. H. G., & Kommers, J. M. "MXB 1730-335," 1997, IAU Circ. 6689

Fox, D. W., Kommers, J. M., Lewin, W. H. G., & Magnier, E. A. "GRB 970228," 1997, IAU Circ. 6643

Lewin, W. H. G., Fox, D. W., Kommers, J. M., Morgan, E. H., Rutledge, R. E., Bildsten, L., Dotani, T., Lubin, L., van der Klis, M., & van Paradijs, J. "MXB 1730-33," 1996, IAU Circ. 6506

Kommers, J. M., Rutledge, R. E., Fox, D. W., Lewin, W. H. G., Morgan, E. H., Kouveliotou, C., & van Paradijs, J. "GRO J1744−28," 1996, IAU Circ. 6415

Kouveliotou, C., Deal, K., Woods, P., Briggs, M. S., Harmon, B. A., Fishman, G. J., van Paradijs, J., Finger, M. H., Kommers, J. M., & Lewin, W. H. G. "GRO J1744−28," 1996, IAU Circ. 6395

Kommers, J. M., Lewin, W. H. G., Kouveliotou, C., Finger, M. H., Fishman, G. J., Meegan, C. A., Wilson, R., Briggs, M. S., van Paradijs, J., & Dotani, T. "GRO J1744−28," 1996, IAU Circ. 6371

Briggs, M. S., Harmon, B. A., van Paradijs, J., Kouveliotou, C., Fishman, G. J., Kommers, J. M., Lewin, W. H. G., Deal, K., & Woods, P. "GRO J1744−28," 1996, IAU Circ. 6290

Kouveliotou, C., Kommers, J. M., Lewin, W. H. G., van Paradijs, J. & Fishman, G. J. "Transient X-ray Burster GRO J1744−28," 1996, IAU Circ. 6286

Hurley, K., Kouveliotou, C., Harmon, B. A., Fishman, G. J., Briggs, M. S., van Paradijs, J., Kommers, J. M., & Lewin, W. H. G. "New X-ray Transient Repeater," 1995, IAU Circ. 6275

Fishman, G. J., Kouveliotou, C., van Paradijs, J., Harmon, B. A., Paciesas, W. S., Briggs, M. S., Kommers, J. M., & Lewin, W. H. G. "Galactic Center," 1995, IAU Circ. 6272

Chapter 2

Gamma-Ray Bursts and Other High-Energy Astronomical Transients

In this thesis, the term *transient* refers to pulses of radiation with durations ranging from less than 1 s to approximately 1000 s. This definition includes gamma-ray bursts (GRBs), bursts and flares from X-ray binaries, bursts from soft gamma-ray repeaters (SGRs), and other phenomena that appear to turn on and off on a time scale shorter than the duration of a single $\sim$ 90 minute spacecraft orbit. On the other hand, this definition intentionally excludes X-ray novae, which are sometimes called "X-ray transients." The X-ray novae are binary systems containing a neutron star or a black hole; they show outbursts lasting from weeks to months (Tanaka & Shibazaki 1996). In X-ray astronomy, the term *fast transient* is sometimes used to distinguish the short time-scale (milliseconds to hours) phenomena that are the subject of this thesis from the longer (weeks to months) outbursts of X-ray novae.

Lewin, Clark, & Smith (1968) made the first observation of an extra-solar fast X-ray transient during a balloon flight launched from Mildura, Australia. They observed the intensity of Sco X-1 to increase by a factor of 4 over the course of 10 minutes, followed by a decrease during the next 20 minutes. During the decade that followed, observations with high-altitude balloons and Earth-orbiting satellites revealed a variety of other transient phenomena in the X-ray and gamma-ray sky.

The sections that follow give brief introductions to the burst-like and flare-like transients that are detected with BATSE. GRBs, bursts from SGRs, and bursts and flares from X-ray binaries are the primary focus, but certain solar and terrestrial phenomena that are (or could have been) encountered in the BATSE data deserve mention as well.

2.1 Gamma-Ray Bursts

A comprehensive bibliography of papers about GRBs is maintained by Hurley (1998). As of mid-1998 the list contains over 3600 papers, a number comparable to the number of individual bursts that have been observed by all current and previous GRB detectors combined. It is therefore impractical to give a comprehensive survey of the GRB literature. The history of GRB observations through the mid-nineties is reviewed by Fishman & Meegan (1995) and by Hurley (1995); see also references therein. A more recent review by Piran (1998) summarizes observations of multi-wavelength afterglows of GRBs and discusses models of the burst and afterglow radiation processes. This section summarizes enough of what has been learned about GRBs to put the rest of the thesis in context.

2.1.1 Historical Overview

On 1967 July 2, two of the *Vela 4* satellites, separated by 240,000 km, recorded in near coincidence a pulse of gamma-rays lasting $\sim$ 8 s (Klebesadel 1988). The primary mission of these satellites was to detect gamma radiation from possible man-made nuclear explosions hidden behind a deployed (or natural) shield as fission debris expanded from behind that shield.[1] The temporal structure of the 1967 July 2 event was inconsistent with that expected from decaying debris from a nuclear detonation,

[1]The *Vela* missions themselves were not classified; but certain capabilities of their detectors were, and the data pertaining to their response (or lack thereof) to any nuclear weapons tests remain classified (Klebesadel 1997).

so there was little doubt that it represented a natural phenomenon rather than the testing of nuclear weapons in space (Klebesadel 1988). With data on at least 16 other such events from the improved instrumentation on the subsequent *Vela 5* and *Vela 6* spacecraft, Klebesadel, Strong, & Olson (1973) published the discovery of cosmic gamma-ray bursts (GRBs).

The discovery of GRBs led quickly to the development of models in which the sources were neutron stars in our own Galaxy. A review by Higdon & Lingenfelter (1990) summarized the arguments in favor of this interpretation. Rapid variations in the time profiles suggested a compact emitting region. Energy spectra from multiple instruments showed evidence of absorption lines between 20 keV and 70 keV, suggestive of cyclotron absorption in a neutron star magnetic field. Yet the source directions were isotropic, giving no indication of a Galactic origin. In 1990 it was expected that more sensitive GRB detectors would eventually reveal an excess of faint bursts in the Galactic plane, where most of the known neutron stars were found (Higdon & Lingenfelter 1990).

By 1992, results from the first year of observations with the Burst and Transient Source Experiment (BATSE) on the *Compton Gamma Ray Observatory* (*CGRO*) showed that the direction distribution of GRBs was isotropic for bursts of all observed intensities. Furthermore, the intensity distribution was unequivocally deficient in faint bursts, indicating spatial inhomogeneity (Meegan et al. 1992). Since the combination of directional isotropy and spatial inhomogeneity is unlike any known Galactic source population, but quite natural for sources at cosmological distances, the results from BATSE encouraged more vigorous examination of extragalactic models for GRB sources (Fishman & Meegan 1995).

Prior to 1997 a major impediment to understanding GRBs was the lack of a convincing counterpart at any other photon energy. Extensive searches for quiescent counterparts were carried out in the radio, infrared, optical, ultraviolet, X-rays, and gamma-rays, but none were definitively identified; see the review by Hurley (1995). Searches for emission simultaneous with (or shortly following) GRBs turned up sim-

ilarly disappointing results, with a few exceptions. Observations with the Energetic Gamma-Ray Experiment Telescope (EGRET) of a GRB on 1994 February 17 showed that the burst was followed by very high-energy gamma-rays (up to 18 GeV) for up to 5400 s following the main GRB emission (Hurley et al. 1994). Observations with *ROSAT* showed the first repeatedly detectable X-ray source coincident with a GRB error box (Hurley et al. 1996).

A breakthrough came in 1997 February, when GRB 970228 was detected with the *BeppoSAX* satellite. The Wide Field Cameras of *BeppoSAX* viewed the burst and provided the coordinates of the source to within a 3 arcmin uncertainty just a few hours after the burst (Costa et al. 1997). Rapid optical follow-up observations of the X-ray error box revealed a fading optical source apparently associated with an extended emission region, possibly a faint galaxy (van Paradijs et al. 1997). Subsequent observations with the *BeppoSAX* narrow-field X-ray instruments revealed an X-ray afterglow fading according to a $t^{-1.3}$ power-law (Costa et al. 1997). Observations with the *Hubble Space Telescope* confirmed the association of the optical transient with the extended emission, though the nature of the extended emission was not clear (Sahu et al. 1997). These developments attracted the attention of astronomers outside the GRB field, and the race was on to observe more GRB counterparts.

The next GRB to be associated with an optical transient was GRB 970508, again the result of a precise position furnished by *BeppoSAX* (Bond 1997). Metzger et al. (1997) obtained spectral constraints on the optical afterglow. They found that the presence of Mg II and Fe II absorption lines at $z = 0.835$ coupled with the absence of a Lyman-α forest constrained the redshift of the optical transient to $0.835 \leq z \leq 2.3$. This discovery confirmed that at least some GRBs come from cosmological distances, and that these events are the most powerful sources of electromagnetic radiation known. At a redshift of $z = 0.835$ the observed gamma-ray fluence of GRB 970508 yielded an equivalent isotropic energy release (in the 20–1000 keV band) of 7×10^{51} erg (Metzger et al. 1997).

A radio afterglow was observed from GRB 970508 by Frail et al. (1997). During

the first 30 days after the burst there were substantial variations in radio flux; the amplitude of the time variability subsided thereafter. This was interpreted as the signature of interstellar scattering as the angular size of the source region increased past the angular size of irregularities in the interstellar medium. With this interpretation, and the redshift $z = 0.835$, the size of the radio emitting region must have been smaller than $\sim 10^{17}$ cm (Frail et al. 1997).

As of 1998 August the *BeppoSAX* satellite has obtained positions for 15 GRBs, of which at least 11 showed fading X-ray afterglows, at least 8 showed fading optical afterglows, and at least 3 showed radio afterglows. Redshifts were obtained for 3 of the optical afterglows as well as for the unusual type Ib/c supernova SN 1998bw, which may be associated with GRB 980425. These totals were based on information available electronically from the GRB Coordinates Network (Barthelmy & Butterworth 1998).

The behavior of the X-ray and optical afterglows of GRB 970228 was quickly shown by Wijers, Rees, & Mészáros (1997) to be consistent with the predictions of the "fireball" model developed by Mészáros & Rees (1997). The fireball model did not describe the cause of the GRB; rather, it described the aftermath. The afterglow was the diminishing synchrotron emission from a relativistic blast wave. The model successfully predicted the shape of the light curves and relative intensities in the X-ray and optical bands for GRB 970228 (Wijers et al. 1997). For GRB 970508 the model successfully predicted the radiation spectrum of the afterglow over a factor of 10^9 in photon energy, from radio to X-rays, on a day 2 weeks after the burst (Galama et al. 1998).

2.1.2 Gamma-Ray Properties

The source directions of GRBs are isotropically distributed. This is expected if most or all of the sources lie at cosmological distances. A comprehensive study of the direction distribution of GRBs shows no evidence for anisotropy in a sample of 1005 GRBs observed with BATSE; nor is there any evidence for anisotropy in a variety

of subsets based on other burst properties such as intensity, spectral hardness, and duration (Briggs et al. 1996).

There is no evidence that GRBs represent a single physical phenomenon or source population, however. The isotropy of source directions can accommodate models in which as many as 20% of observed bursts originate from a source population within the Galaxy, while the remainder are cosmological (Loredo & Wasserman 1998a).

GRBs display a bewildering array of time profiles in the 50–300 keV energy band. Some bursts show single pulses with little or no additional structure; some show multiple pulses with well-defined peaks; some show distinct, well-separated episodes of emission; and some show a series of erratic, spiky pulses. Figure 2-1 shows some examples of time profiles observed with BATSE (Paciesas et al. 1999). The time scales are different in each panel. Despite the distinctive time structure of each burst, no other observational parameter (such as source direction, spectrum, or intensity) appears to correlate with temporal morphology (Fishman & Meegan 1995).

The durations of GRBs range from ~ 10 ms to over 1000 s. A precise measure of duration is difficult to obtain, because the time during which a GRB appears to be happening depends on the burst intensity relative to the background fluctuations and on the time resolution of the instrument. Two duration measures in common use with data from BATSE are the T_{50} and T_{90} measures. The value of T_{50} is the time during which the cumulative flux (i.e., fluence) from the burst increases from 25% of 75% of its total value. Similarly, the value of T_{90} is the time during which the cumulative flux increases from 5% to 95% of the total burst fluence (Koshut et al. 1996). Kouveliotou et al. (1993) showed that the duration distribution of 222 bursts from early in the BATSE mission was clearly bimodal. This separated GRBs into 2 classes: short ($T_{90} < 2$ s) and long ($T_{90} > 2$ s) bursts. To illustrate, Figure 2-2 shows a histogram of T_{90} durations for 1233 bursts from the BATSE 4B catalog (Paciesas et al. 1999). The bimodality is clearly evident.

The short ($T_{90} < 2$ s) bursts show slightly different spectral properties than the longer bursts (Kouveliotou et al. 1993). A crude measure of spectral characteristics is

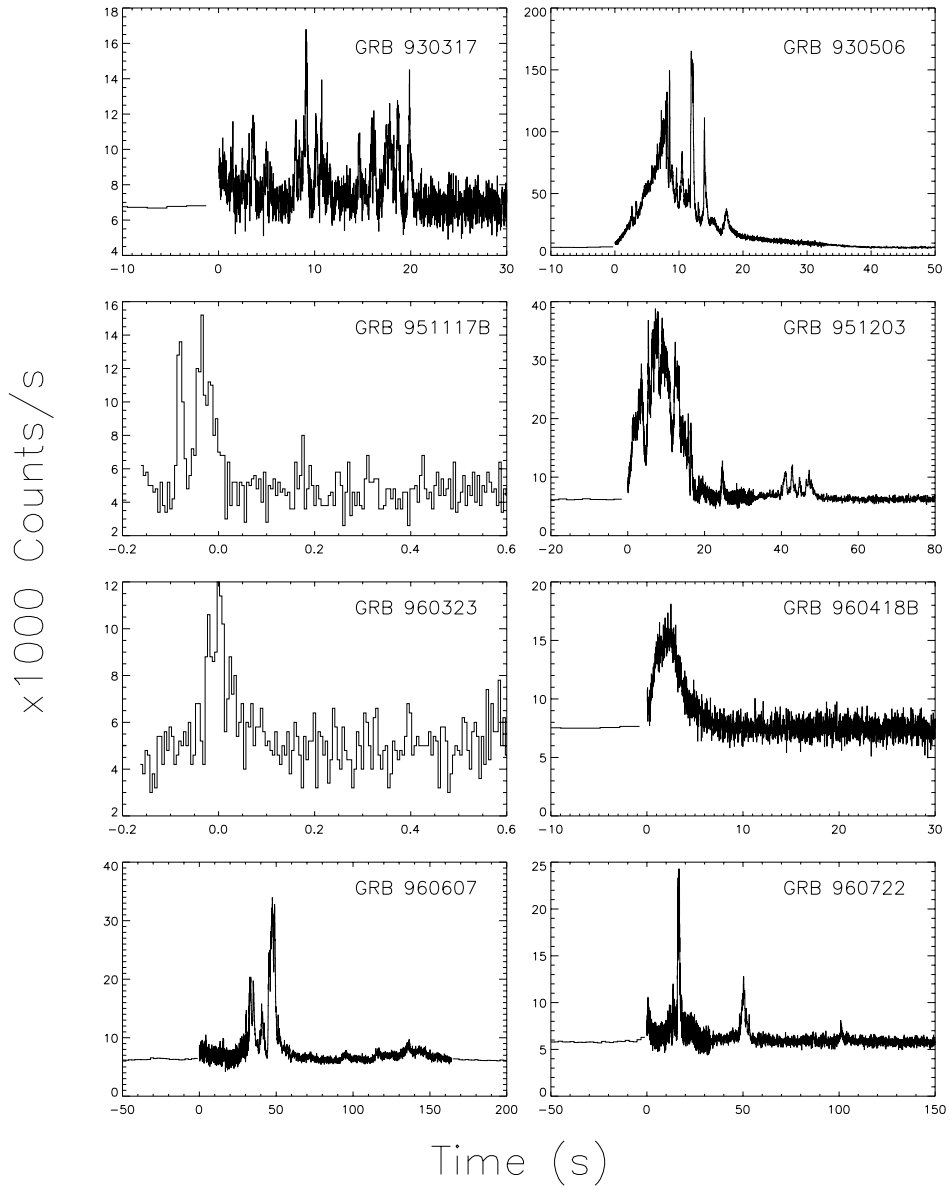

Figure 2-1 Examples of GRB time profiles, to illustrate the many different kinds of temporal variability. Note the different vertical (count rate) and horizontal (time) scales. In each panel, time is measured relative to the BATSE onboard burst trigger time. Lower time resolution prior to the trigger time is a result of the onboard data processing (see Chapter 3).

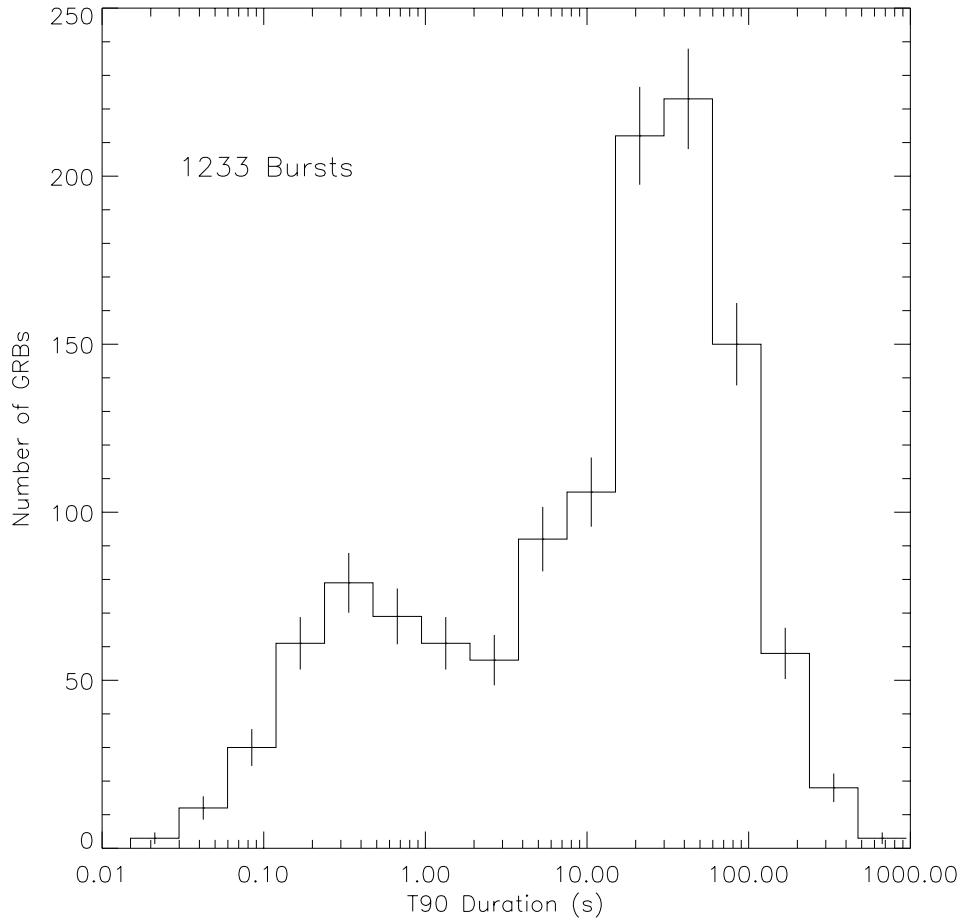

Figure 2-2 Histogram of GRB durations. The cutoff for very short bursts (< 60 ms) is partly instrumental, because the shortest time scale on which BATSE detects bursts is 64 ms.

an instrumental hardness ratio: the ratio of gamma-ray counts in one energy band to counts in another (usually lower) energy band. (This measure is similar to the notion of source "color" in optical astronomy, which is the logarithm of a ratio of source fluxes in different photon energy bands.) As a population, the short ($T_{90} < 2$ s) bursts have higher hardness ratios than long bursts. Thus the short bursts show systematically harder spectra, that is, relatively more high-energy photons. Since both the long and short classes of bursts show isotropic source distributions and inhomogeneous intensity distributions, the differences in their spectral characteristics probably do not indicate separate source populations. Rather, they may be due to different geometries (relative to the observer) of the burst emission regions (Kouveliotou et al. 1993).

The relatively short duration of GRBs coupled with the origin of most (possibly all) of them at cosmological distances suggests that their durations should show the signature of cosmological time dilation. This signature should manifest itself as an anti-correlation between intensity and duration: assuming the more intense bursts are predominantly nearby, they should be shorter on average than the faint bursts, which presumably arise from more distant sources and so experience larger cosmological time dilation. Whether this effect exists in the BATSE data is controversial: one group (Norris et al. 1994) announced positive results, while other investigators (Rutledge et al. 1996) obtained a negative result using the same data.

Photons with energies ranging from 1 keV up to 20 GeV are associated with the main burst episodes of GRBs; and as noted above, the afterglows are identified in radio up to X-ray energies. In the bursts themselves, GRBs emit most of their power above 50 keV (Fishman & Meegan 1995). The extensive spectral diversity is revealed in the detailed study by Band et al. (1993) of GRB spectra observed with BATSE. Figure 2-3 shows examples of GRB energy spectra based on the spectral fits by Band et al. (1993). The shapes in this figure represent the average spectrum integrated over the burst; however, many GRBs show substantial spectral evolution, typically from hard to soft (Fishman & Meegan 1995).

Two measures of GRB intensity are in common use. The fluence in some energy

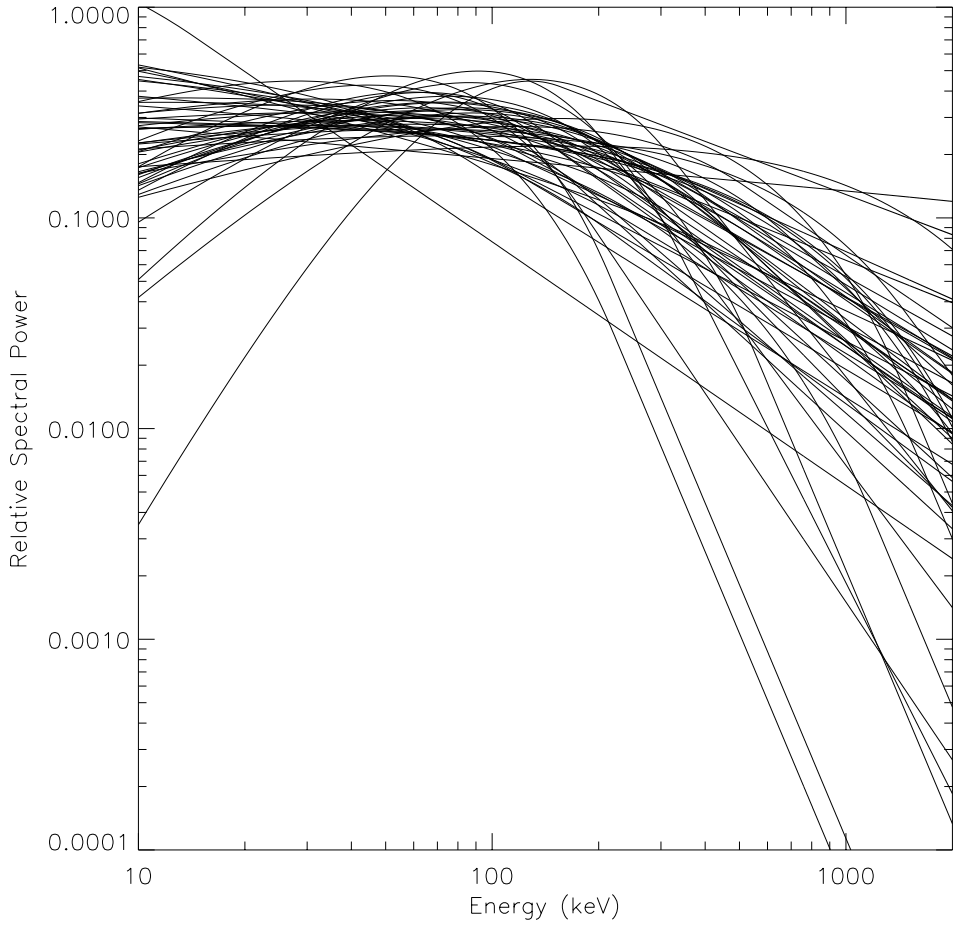

Figure 2-3 Relative spectral power versus energy for the GRBs studied by Band et al. (1993). The curves represent fits to the spectra of 54 relatively bright GRBs observed with the BATSE Spectroscopy Detectors. Since the point of this figure is to compare spectral shapes, the vertical axis expresses the (dimensionless) relative spectral power, defined as $E^2\ dN/dE$ divided by the total energy flux in the range 10–2000 keV. Here, E is photon energy and N is photon flux in $\mathrm{cm}^{-2}\ \mathrm{s}^{-1}$.

band is the total energy per unit area deposited in the detector by the burst. In the BATSE catalogs, measured fluences range from 1.3×10^{-8} erg cm^{-2} to 1.5×10^{-4} erg cm^{-2} in the 50–300 keV band (Meegan et al. 1998a). The peak photon flux in some energy band is the highest flux level measured during the burst, averaged over some time scale that must be specified. With BATSE, the reported peak photon fluxes are averaged over 64 ms, 256 ms, or 1024 ms. The peak photon flux is more directly related to the way bursts are detected (see Chapter 3) so most statistical studies of the GRB intensity distribution use peak fluxes. In the BATSE catalogs, the measured peak fluxes on the 1024 ms time scale range from 0.05 ph cm^{-2} s^{-1} to 163 ph cm^{-2} s^{-1} in the 50–300 keV band. The intensity distribution of GRBs will be discussed further in Chapter 6.

2.2 Soft Gamma-Ray Repeaters

Soft gamma-ray repeaters (SGRs) emit most of their energy in the range intermediate between GRBs (50–1000 keV) and the X-ray bursts (1–10 keV). The burst activity from SGRs consists of short (typically tens of ms but occasionally as long as 10 s) pulses of radiation separated by waiting times from seconds to years. A typical energy spectrum can be represented by an optically-thin thermal bremsstrahlung spectrum with an effective temperature $kT \sim 40$ keV (Hurley 1995).

Only 4 SGRs have been confirmed, and a fifth may have been detected; three of them are associated with supernova remnants (Kouveliotou et al. 1998b). Coherent X-ray pulsations have been detected from two, SGR 1806−20 (Kouveliotou et al. 1998a) and SGR 1900+14 (Kouveliotou et al. 1998b). The pulsation periods (7.47 s and 5.16 s, respectively) and spin-down rates are consistent with the sources being highly-magnetized neutron stars, or "magnetars." In the magnetar model, the intense bursts are produced when cracks produced by magnetic stresses in the neutron star crust lead to particle acceleration in the neutron star magnetosphere (Thompson & Duncan 1995). The more intense bursts from SGRs are easily detected with

BATSE (Kouveliotou et al. 1993; Kouveliotou et al. 1994; Kouveliotou et al. 1996).

2.3 Bursts and Flares from X-ray Binaries

X-ray bursts are fast, high-energy transients that emit most of their energy in the classical X-ray band, 1–10 keV. Credit for their discovery goes jointly to Grindlay et al. (1976), who in 1975 observed 2 bursts from the source 3U 1820−30 with the *Astronomical Netherlands Satellite*, and to Belian, Conner & Evans (1976), who reported on 10 bursts observed 6 years earlier with the *Vela* satellites. Comprehensive reviews of X-ray bursts and their properties are given in Lewin, van Paradijs, & Taam (1993; 1995b).

Two distinct types of X-ray burst are generally recognized. Type I bursts are by far the most commonly observed. They are the results of thermonuclear flashes on the surfaces of the neutron stars in X-ray binaries. A typical type I burst profile is a fast (1–10 s) rise followed by an approximately exponential decay on a time scale of 10 s to minutes. The type I burst spectra are well described by a blackbody (Planck) spectrum with blackbody temperatures (kT) of $\sim$ 1 keV to $\sim$ 3 keV. During the burst decay the blackbody temperature may decrease, for example, from a maximum of $kT \approx 3$ keV to $kT \approx 1$ keV; this spectral softening is a distinctive feature of the thermonuclear origin of type I bursts. Because the blackbody spectrum falls off exponentially with increasing photon energy, type I X-ray bursts (at distances typical of their sources in low-mass X-ray binaries) are not detectable in the energy range accessible to BATSE (> 20 keV).

The other type of X-ray burst, designated type II, shows temporal and spectral properties that are quite different from those of the type I bursts. Type II bursts have durations ranging from $\sim$ 2 s to $\sim$ 11 minutes and do not show the distinctive spectral softening during burst decay that accompanies type I bursts. The profiles of type II bursts range from spiky to flat-topped. Quasi-periodic oscillations are sometimes detected during the flat-top or decay portion of the burst. The energy spectra are

less well-fit by a blackbody; in some cases a power-law with an exponential cut-off provides better fits to the data (Lewin et al. 1993).

The cause of the type II X-ray bursts appears to be instabilities in the accretion flow onto the neutron star. While a half-dozen or so sources show occasional X-ray flares attributed to accretion instabilities (Lewin & Joss 1983), only 2 sources are universally associated with repetitive type II bursts. They are both low-mass X-ray binary systems. The first of these, the Rapid Burster (MXB 1730−335), shows both type I X-ray bursts and repetitive type II X-ray bursts. The type II bursts from this source show a rich and bewildering phenomenology. For example, the total energy released by a type II burst appears to be roughly proportional to the waiting time until the next type II burst occurs; this behavior is that of a "relaxation oscillator" (Lewin et al. 1993). The second type II burst source, GRO J1744−28, is an X-ray pulsar discovered with BATSE that has shown only repetitive type II X-ray bursts; it has never shown a type I burst (Kouveliotou et al. 1996). The easy detectability of the bursts from this source shows that some type II bursts are bright enough and spectrally hard enough to be detected in the BATSE energy range.

2.4 Solar and Terrestrial Phenomena

X-ray and gamma-ray detectors respond not only to photons from distant astronomical objects but also to more local sources of radiation. In particular, the Sun and the radiation belts of Earth produce transient events that can resemble GRBs and X-ray bursts. So, while solar and terrestrial phenomena are interesting in their own right, they nevertheless constitute a kind of interference for experiments primarily geared towards observations of extrasolar objects. For this reason, a few of these solar and terrestrial phenomena deserve mention.

2.4.1 Solar Flares

Solar flares are explosive outbursts that occur in the active regions of the Sun's atmosphere that overlay sunspots. Most flares release X-rays and gamma-rays with energies of 10–100 keV in pulses that last from milliseconds to minutes. This radiation is bremsstrahlung produced when electrons accelerated in magnetic loops interact with ambient ions (Doschek 1992). In experiments with uncollimated detectors that include the Sun in their field of view, solar flares can resemble X-ray bursts and GRBs. The time scales and erratic profiles are often like those seen in X-ray bursts and GRBs. X-rays with energies well above 50 keV are occasionally produced, though the bremsstrahlung spectrum cuts off more abruptly than is typical for the spectra of GRBs.

BATSE is the most sensitive instrument regularly available for the detection of hard X-ray solar flares. Dennis, Schwartz, & Tolbert (1998) maintain an ongoing project to identify and catalog solar flares observed in the continuous data from BATSE. Their data base is available electronically from the *Compton Gamma Ray Observatory* Science Support Center.

2.4.2 Radiation Belts

The Earth's geomagnetic field traps energetic electrons and ions in a pair of toroidal regions known as the inner and outer radiation belts, or the Van Allen belts (Hess 1965). Typical kinetic energies of the particles are upwards of 100 keV (Schulz & Lanzerotti 1974). The electrons and protons spiral around the Earth's (roughly dipole) longitudinal magnetic field lines in orbits that mirror the particles between conjugate magnetic field points. These orbits contain an azimuthal drift component that carries electrons eastward, and protons westward, as they mirror.

The toroidal inner radiation belt extends (very roughly) from an altitude of ~ 500 km to $\sim$ 1500 km at the equator, and between $+45°$ and $-45°$ magnetic latitude (Tascione 1994). The center of the Earth's dipole field is tilted by about 11° and

offset by about 400 km from its rotational axis. This results in a region of low field strength (for a given altitude above sea level) over the south Atlantic Ocean. In this region, called the South Atlantic Anomaly (SAA), trapped particles undergo mirror reflections at lower altitudes than anywhere else. Particles in the SAA are more susceptible to losing energy in interactions with the atmosphere. If they lose enough energy, or if the angle between the particle velocity and the local magnetic field direction exceeds a critical value, particles are released from their trapped orbits and they precipitate into the atmosphere.

Spacecraft in low-Earth orbit are typically at altitudes of 300–500 km, so they encounter radiation belt particles only when they pass through the SAA or when particles precipitate out of higher-altitude trapped orbits. The high-energy radiation belt particles have an adverse effect on astronomical detectors. Very high particle fluxes, such as those that exist in the SAA, can physically damage X-ray and gamma-ray detectors. Such instruments are therefore turned off during passages through the SAA. At lower fluxes, precipitating particles create a kind of interference because X-ray and gamma-ray detectors respond to particle as well as photon radiation. For this reason, the X-ray and gamma-ray detectors are shielded by charged-particle sensors that enable the instrument electronics to veto detector responses due to particles. Even so, precipitating particles can interact in the atmosphere or the outer skin of the spacecraft to produce secondary bremsstrahlung that is detected as high-energy photon radiation.

CGRO regularly encounters trapped electrons near the extreme geomagnetic latitudes reached by spacecraft. These encounters are more frequent during periods of increased magnetospheric activity (Horack et al. 1991). Electron precipitations are particularly frequent above certain geographic locations: along the line of (roughly) $-28°$ latitude between the southern tip of Madagascar and southwestern Australia, and along the line of $+28°$ latitude between the Baja peninsula and Florida in the southern United States.

Many of the precipitations encountered by *CGRO* are caused by high-powered

(1000 kW) VLF transmitters (Datlowe et al. 1995). The output from these stations resonantly scatters stably-trapped electrons from the inner radiation belt into quasi-trapped trajectories where the electrons drift for up to $\sim$ 90 minutes (up to $\sim$ 120° in longitude) before interacting with *CGRO*. BATSE is particularly sensitive to these events. A typical signature of a particle precipitation event in the BATSE data is a large (factor of 3–10) increase in the total counting rate of the detectors lasting for several minutes. Almost all of the count rate increase is observed in the lowest energy discriminator channel (25–50 keV), consistent with the bremsstrahlung spectrum expected from electrons impacting the outermost skin of the detector shielding. The transmitters that appear to be responsible for many of the precipitations detected with BATSE are NWC (on the western coast of Australia, at 114.2°E, 21.8°S) and UMC (about 400 km east of Moscow, Russian Federation, at 44.0°E, 56.0°N). Both stations produce precipitations to the east of their geographic coordinates, and to the east of their magnetically conjugate points in the opposite hemisphere (Datlowe et al. 1995).

2.4.3 Orbiting Nuclear Reactors

Unshielded nuclear reactors are a light and compact power source for artificial satellites, particularly those involved in military applications. Unfortunately they are also bright sources of gamma-rays and particle radiation. Astronomical gamma-ray detectors can respond to these reactors either directly or indirectly. Gamma-rays emitted from the unshielded reactors can be detected and imaged, as was shown in observations with a balloon-borne gamma-ray telescope (O'Neill et al. 1989). The indirect response occurs when positrons and electrons are pair-produced by reactor gamma-rays exiting the reactor's spacecraft skin. These particles enter quasi-trapped orbits in the geomagnetic field and create an artificial radiation belt. When an astronomical satellite passes through one of these artificial radiation belts, the electrons and positrons produce gamma-rays through annihilation or bremsstrahlung with the outermost skin of the detectors. These gamma-rays pass through any charged-particle

detectors and can appear to be astronomical gamma-ray transients with durations of tens of seconds (Rieger et al. 1989).

As early as 1977, the *SAS-3* satellite, operated by MIT, encountered burst-like events (Mayer 1976) that were apparently caused by a magnetospheric particle phenomenon. At the time, however, their exact cause was unknown. The MIT investigators were merely advised by Bill Priedhorsky, Bob Scarlett, and France Cordova of Los Alamos National Laboratory that the events were not of astronomical interest and should not be published (W. Lewin, private communication). The first published descriptions of artificial radiation belts created by orbiting nuclear reactors appeared in a special issue of *Science* (Primack 1989).

Transient gamma-ray phenomena due to orbiting nuclear reactors had serious impacts on the operations of the Gamma-Ray Spectrometer onboard the *Solar Maximum Mission* satellite and on the Gamma-Ray Burst Detector onboard *Ginga* (Primack 1989). Despite early concerns (Aftergood et al. 1991) no reactors appear to have been in operation in low-Earth orbit during the *CGRO* mission, so the operation of BATSE has been apparently unaffected by reactor events.

2.4.4 Terrestrial Gamma-Ray Flashes

Terrestrial gamma-ray flashes (TGFs) are extremely short pulses of radiation discovered with BATSE (Fishman et al. 1994a). Typical TGF durations are in the range $\sim$ 1 ms to $\sim$ 10 ms. Their profiles show from 1 to 4 distinct pulses, each with durations of 1 ms to 4 ms. Their energy spectra are not well-resolved with BATSE, but the data are consistent with a bremsstrahlung spectrum with a characteristic energy of 1 MeV. The cause of the TGFs appears to be high-altitude lightning discharges associated with strong thunderstorm activity; the typical energy release is on the order of 10^8 to 10^9 erg (Fishman et al. 1994a).

2.5 Unknown Phenomena

The various X-ray and gamma-ray transients mentioned above certainly comprise an incomplete list. In general transients are difficult to observe because one does not typically know when or where to look for them. All-sky monitoring instruments with good time coverage are therefore indispensable for observing fast transients. BATSE is one such instrument: with its combination of high sensitivity above 20 keV and nearly continuous all-sky coverage, one must be alert for hitherto unknown phenomena.

Gotthelf, Hamilton, & Helfand (1996) report the detection of 42 faint X-ray flashes in the 0.1–4 keV band of data from the *Einstein Observatory* that could not be attributed to an obvious instrumental or terrestrial origin. It is possible that these represent the X-ray emission of GRBs, but they could also represent some other (possibly instrumental) phenomenon. They occur at a rate roughly 10^3 times higher than known GRBs (Gotthelf et al. 1996).

Strohmayer et al. (1995) report the detection of an unusual X-ray transient with *Ginga* that was spectrally similar to emission from an SGR but with a duration that was more characteristic of a GRB. This event could represent a very soft GRB, an isolated flare from an X-ray binary, or a burst phenomenon that has not yet been identified.

2.6 Effects of High-Energy Transients on Earth

The brightest GRBs, flares from X-ray binaries, and bursts from SGRs produce immediate and measurable effects on the Earth's ionosphere. The high-energy photons produce additional ionization at altitudes of $\sim$ 20 km (for 150 keV gamma-rays) to $\sim$ 80 km (for 2 keV X-rays) that can be detected as an amplitude change or a phase shift of VLF radio transmissions (Weekes 1976; Fishman & Inan 1988). A typical energy requirement for a hard X-ray (5–25 keV) transient to make a measurable

ionospheric disturbance is that the energy flux at Earth be greater than a few times 10^{-5} erg cm^{-2} (Brown 1973; O'Mongain & Baird 1976).

Concurrent with the 1967 October 15 X-ray flare from Sco X-1 (Lewin et al. 1968) there was decrease in the field intensity of continuous VLF radio transmissions from Radio Tashkent, in what is now the Republic of Uzbekistan, received at Delhi, India (Ramanamurty et al. 1970). The steady X-ray emission of Sco X-1 was already known to affect the propagation of VLF radio waves between Tashkent and Ahmedabad, India during its sidereal transit (Ananthakrishnan & Ramanathan 1969).

The particularly intense gamma-ray burst of 1983 August 1, which had a total gamma-ray fluence of 2×10^{-3} erg cm^{-2} in the band from 5 keV to 7.5 MeV, was observed to reduce the amplitude of a VLF radio signal that was transmitted from Rugby, England and monitored at Palmer Station, Antarctica (Fishman & Inan 1988).

A particularly bright burst from SGR 1900+14 on 1998 August 27 was so powerful that it effectively changed night-time ionospheric conditions over the Pacific Ocean into day-time ones for a short time after the burst (G. J. Fishman, private communication).

Chapter 3

The Burst and Transient Source Experiment

3.1 The *Compton Gamma Ray Observatory*

The *Compton Gamma Ray Observatory* satellite, deployed by the space shuttle *Atlantis* on 1991 April 7, is in a nearly circular low-Earth orbit at an altitude of roughly 450 km and an inclination of 28.5°. It carries four astronomical instruments covering six decades of the gamma-ray energy range, from 20 keV to 30 GeV.

The Burst and Transient Source Experiment (BATSE) is a set of eight uncollimated detector modules that provide nearly continuous viewing of the entire celestial sphere not blocked by the Earth (Fishman et al. 1989). The Oriented Scintillation Spectrometer Experiment (OSSE) uses four collimated detectors with 3.8° by 11.4° fields-of-view to provide gamma-ray line and continuum detection in the 50 keV to 10 MeV range (Johnson et al. 1993). The Compton Telescope (COMPTEL) is sensitive to gamma-rays in the 1 MeV to 30 MeV range and provides a 1 sr field-of-view with angular resolution of 1°–2° (Schoenfelder et al. 1993). The Energetic Gamma Ray Experiment Telescope (EGRET) has a primary photon energy range extending from 20 MeV to 30 GeV and provides imaging capability using a spark chamber detector (Thompson et al. 1993). Figure 3-1 shows a diagram of the *CGRO* spacecraft

configuration.

The primary objective of BATSE is the detection and study of gamma-ray bursts (GRBs). As a nearly continuously operating all-sky monitor it serves several other objectives as well. The low-altitude, moderately inclined orbit of *CGRO* permits the use of the Earth as an occulting disk. This provides a long-term monitoring and crude imaging capability for persistent and transient X-ray sources (Zhang et al. 1993). The nearly continuous all-sky coverage with good sensitivity provides an unprecedented capability to study a large fraction of the known X-ray pulsars on time scales ranging from seconds to years (Chakrabarty 1996). BATSE is also the most sensitive instrument that is continuously available for the study of hard X-ray solar flares (Aschwanden et al. 1998).

This chapter summarizes the aspects of the BATSE instrumentation that are most relevant to the search for nontriggered GRBs and other fast transients. The discussion derives from the more detailed descriptions given in Fishman et al. (1989) and Horack (1991), with some additional information from Chakrabarty (1996).

3.2 BATSE Instrument Description

The eight detector modules of the BATSE instrument are arranged at the corners of the *CGRO* spacecraft (see Figure 3-1). They are numbered 0 through 7. The faces of the detector modules are parallel to the eight faces of a regular octahedron and together provide an unobstructed 4π sr field of view. Each detector module carries a Large Area Detector (LAD), a Spectroscopy Detector (SD), and a charged-particle detector (CPD). Figure 3-2 illustrates the configuration of the individual detector modules.

Each LAD contains a NaI(Tl) crystal that is 50.8 cm in diameter and 1.27 cm thick. The crystal is shielded by a 0.81 mm Al entrance window that strongly attenuates the detector's response to photons below 30 keV. The crystal absorbs incoming gamma-rays and charged particles. Some of this energy immediately reappears as a pulse of

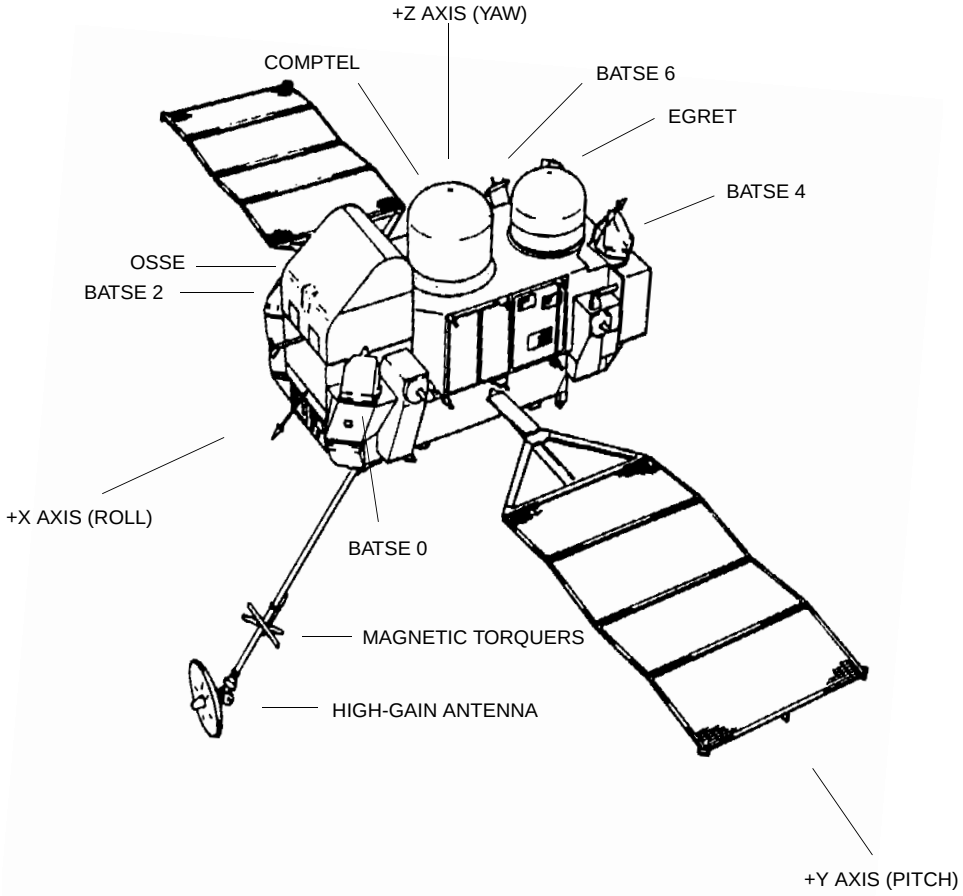

Figure 3-1 Diagram of the *Compton Gamma Ray Observatory* (*CGRO*).

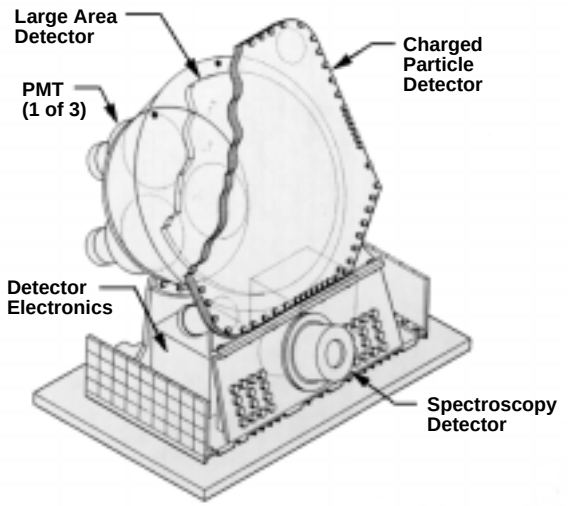

Figure 3-2 Diagram of a BATSE detector module.

light, or scintillation. The scintillation pulses are viewed by three 12.7 cm diameter photomultiplier tubes. The intensities of the scintillation pulses are proportional to the energies of the incoming photons; thus the charge liberated in the photomultiplier tubes provides a measure of the energy of the incoming gamma-ray or particle.

The electronics on each detector process the photomultiplier output pulses in parallel through a 4-channel discriminator circuit and a slower pulse-height analyzer. The pulse-pair resolution of the fast discriminator is approximately 300 ns. The pulse-height analyzer uses a monolithic charge-to-time converter to produce a logic-level output pulse whose duration is proportional to the charge contained in the photomultiplier output pulse.

The CPDs cover the fronts of the LADs. Each CPD contains a plastic scintillator viewed by two 5.08 cm diameter photomultiplier tubes. The detector module electronics use coincidences between scintillation pulses in the CPDs and in the LADs to veto the response of the LADs to charged particles.

The SDs operate similarly to the LADs. They consist of NaI(Tl) scintillating crystals 12.7 cm in diameter and 7.62 cm thick. They have no Al entrance window or anti-coincidence shield. Gamma rays enter the SD through a 8.3 cm diameter Be window which allows for effective observations at energies as low as 7 keV. The faces of the spectral detectors are offset by 18.5° from the octahedral aspects of the LADs because of mechanical constraints.

3.3 Onboard Data Processing and Burst Detection

Data from the detector modules is fed into the Central Electronics Unit (CEU) which is responsible for the onboard processing of data and for constructing the BATSE telemetry packets. The scientific data processing performed in the CEU includes real-time periodic folding of count rates for pulsar studies and real-time burst detection. The CEU makes extensive use of commandable parameters and the flight software

can be re-programmed after launch. These capabilities provide significant flexibility to respond to unforeseen conditions or new transient phenomena.

The onboard computer detects bursts by monitoring the count rates in the fast discriminator data from each of the eight LADs. For GRB studies the detection algorithm uses count rates from discriminator channels 2 and 3 (50–300 keV). The fiducial background count rates in each detector are recomputed at a commandable time interval, nominally every 17.408 s. The count rates in the detectors are continually monitored on three time scales: 64 ms, 256 ms, and 1024 ms. The computer signals a "burst trigger" when the count rates in at least two detectors simultaneously register a statistically significant count rate increase above the fiducial background levels. The magnitude of the increase required for a burst trigger is commandable separately for each time scale in terms of the standard deviations (σ) of the expected background fluctuations. It can be set in increments of 0.0625σ and is nominally set to 5.5σ.

In response to a burst trigger the onboard computer records high resolution data for a commandable time interval. This accumulation interval has been set to values ranging from 180 s to 573 s, during which further burst triggering is disabled. Immediately after the accumulation interval a "read out" interval begins, during which the burst memories are telemetered. During this read out time the burst trigger is disabled on the 256 ms and 1024 ms time scales, and the 64 ms threshold is set to the highest count rate measured for the burst being read out. If a brighter burst is detected during the read out period, a "burst overwrite" occurs in which data from the previous burst are discarded in favor of data from the brighter burst. The duration of the read out period depends on the intensity of the burst (the read outs of faint bursts omit high time resolution data) and on the schedule of telemetry contact with the ground stations and the *Tracking and Data Relay Satellite System* (*TDRSS*); but it is typically in the range 0.5 to 3 hours.

The science data from the detectors are collected into a variety of data types distinguished by their time and spectral resolution. The names of the data types used

in BATSE operations are the 3 to 6 letter abbreviations used in the flight software.

The data recorded in response to a burst trigger have the highest time and spectral resolution. Time Tagged Event (TTE) data record the time of occurrence, discriminator channel, and detector for 32,768 photons from the LADs, with 2 μs resolution. Spectroscopy Time-Tagged Event (STTE) data provide similar information for the SDs with a time resolution of 128 μs. Time-to-Spill (TTS) data provide the time required to accumulate a specified number of discriminator events from the LADs; the smallest time resolution is 1 μs. Medium Energy Resolution (MER) data record pulse-height analyzed events from the LADs at 16 ms time resolution for the first 32.768 s after the trigger and at 64 ms for the next 131.072 s. High Energy Resolution Burst (HERB) and Spectroscopy High Energy Resolution Burst (SHERB) data record 128 and 256 spectral channels (respectively) with a commandable time resolution.

The continuously recorded "background" data types have much lower temporal and spectral resolution. These data are continuously available subject only to certain technical limitations: the high voltage must be supplied to the photomultipliers, the telemetry schedule must allow transmission of the data to Earth, and the telemetry packets must be free of transmission errors. Discriminator data from the LADs (DISCLA) records count rates at 1.024 s time resolution from all 4 discriminator energy channels. The DISCLB data type, added after the failure of the onboard tape recorders, stores count rates at 1.024 s time resolution from the lower 3 discriminator channels. The combined DISCLA and DISCLB data have the most complete time coverage. The Continuous (CONT) data type records pulse-height analyzed count rates at 2.048 s time resolution with 16 energy channels. Discriminator data from the SDs (DISCSP) are available with 2.048 s time resolution.

There are four data types that are recorded only when a burst trigger is *not* being processed. High Energy Resolution (HER) and Spectroscopy High Energy Resolution (SHER) data record 128 and 256 energy channels, respectively, at commandable time resolutions of 16 s and 32 s, respectively, or longer. The pulsar data from the LADs

(PSRA) and SDs (PSRB) contain pulse profiles with 64 phase bins folded onboard at a commandable period; each profile is read out every 2 to 8 s with 4 to 16 energy channels.

3.4 Detector Characteristics

The calibration of the BATSE detectors is described in detail by Horack (1991) and Pendleton et al. (1995). The response of the detectors to incoming photons of different energies is summarized by means of a detector response matrix (DRM) associated with each detector. The DRMs are designed for use in converting background-subtracted source count rates into incident photon energy spectra. They are parameterized in terms of the incident photon energy, the angle between the source direction and the detector normal, and the discriminator (or pulse-height analyzer) output energy. The DRMs express the effective area of the detectors, that is, the number of counts expected in the output discriminator channels for a source flux of 1.0 ph cm^{-2} s^{-1} at the given input energy and source angle. The DRMs used for BATSE data analysis are the results of extensive Monte Carlo simulations of radiation transport in the detector and spacecraft geometry (Pendleton et al. 1995).

The DRMs are constructed on a finer grid of output energies than is available from the fast discriminators or the 16-channel pulse-height analyzed data. To determine the proper response in the fast discriminator channels requires that the DRMs be integrated over the appropriate output energy range. Although the gains of the LADs are automatically controlled by the onboard computer, the precise boundaries of the discriminator channels for each detector are determined from in-flight calibrations based on observations of the Crab Nebula. Table 3-1 lists the energy boundaries relevant to the DISCLA data that will be analyzed in later chapters. Only the lower channel boundaries are listed. The upper boundary of a channel is the lower boundary of the next, except for channel 4 which has no upper cut-off.

The Earth's atmosphere scatters incoming gamma-rays. Depending on the orien-

tation of the source with respect to the detectors and the Earth's limb, these scattered gamma-rays can enter the BATSE detectors along with gamma-rays incident directly from the source. Thus the atmosphere increases the effective area of the BATSE detectors. This effect can be modeled by a parameterized response matrix, an atmospheric response matrix (ARM). The ARM takes as input the same arguments as the DRM (input energy, output energy, and source angle) but with an additional parameter, the position of the Earth relative to the detector normal. The ARMs used for BATSE data analysis are the result of extensive Monte Carlo simulations (Pendleton et al. 1999).

The total response of the BATSE detectors to an astronomical source of gamma rays is the sum of the direct response and the atmospheric response. Figure 3-3 illustrates each of these contributions to the total response of the LADs, as a function of incoming photon energy. The four panels in the figure correspond to the four fast discriminator channels available in the DISCLA data. Vertical dotted lines show the nominal energy boundaries (or edges) associated with each channel. Note that the individual channels show some response to photons outside their nominal energy ranges, and that the atmospheric scattering contributes to the total response at the level of 5%–10% of the direct response. For this example the positions of the source and Earth are specifically chosen to provide a substantial atmospheric contribution.

The angular response of the BATSE detectors is *not* simply proportional to the cosine of the angle θ between the source direction and the detector normals. The geometry of the NaI(Tl) crystals and their shielding cause the angular response to fall more steeply than $\cos\theta$ for photons with energies less than ~ 100 keV and to fall less steeply for photons of higher energy. Figure 3-4 illustrates the angular response of one of the detectors to photons of various energies. The higher energy photons (260 keV and 600 keV in the figure) penetrate deeper into the crystal before producing a scintillation pulse. The increase in path length through the crystal offsets the $\cos\theta$ decrease in projected geometric area along the source direction; thus the resulting response is somewhat flatter than $\cos\theta$. In contrast, the lower-energy photons interact

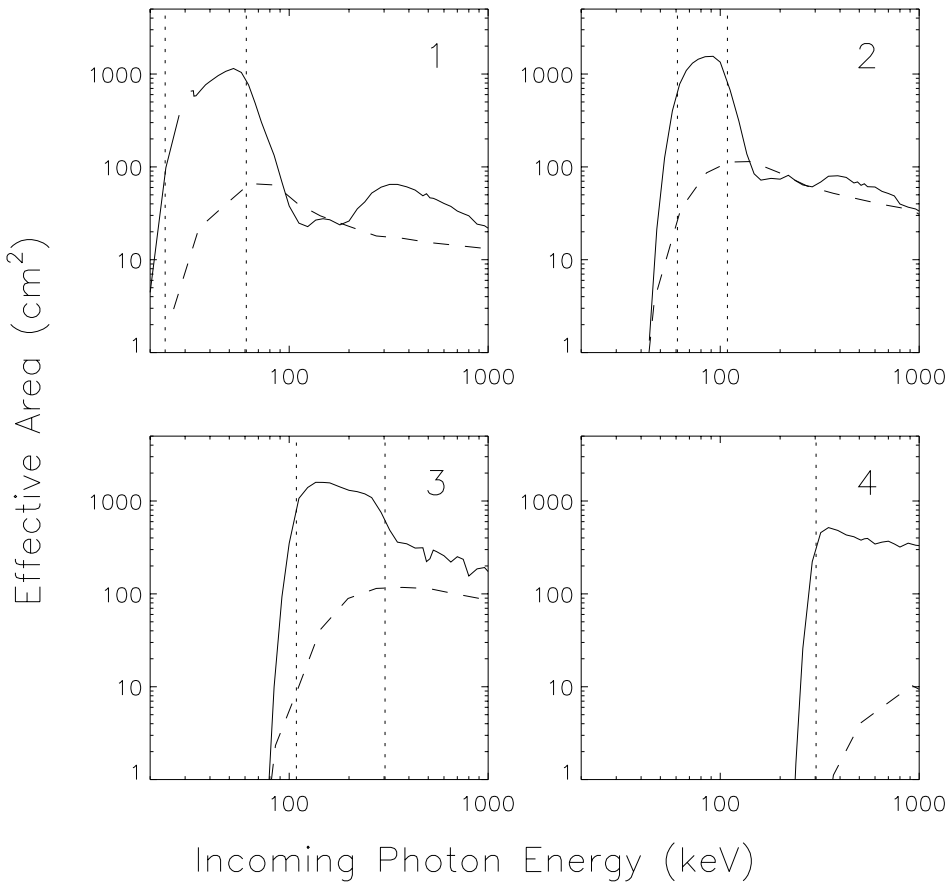

Figure 3-3 Response of the LADs as a function of incoming photon energy, for each of the 4 fast discriminator channels. Solid curves show the direct response of the detectors. Long-dashed curves show the additional response due to radiation scattered off the Earth's atmosphere. The total response is the sum of the two. This plot is for a source at normal incidence on detector 0 with a *CGRO* altitude of 450 km and the Earth's center 76° from the source direction. The smallest angle between the Earth's limb and the source direction is 7°. The atmospheric scattering increases the total effective area by 5% (channel 1) to 10% (channel 2). Vertical dotted lines indicate the nominal discriminator channel boundaries, except for channel 4 which has no well-defined upper cutoff.

near the surface of the crystal so its thickness is irrelevant. The path length through the shielding, however, increases with increasing θ, so the effective area for low-energy photons drops off more steeply than $\cos\theta$.

A consequence of the energy dependence of the angular and discriminator response functions is that the measured count rate from a source depends on its intrinsic photon spectrum. For example, if soft (low energy) photons dominate the source spectrum then the decrease in effective area due to the shielding will dominate the effective angular response. The expected count rates from a source with a given direction and photon spectrum are therefore determined by convolving the source spectrum with the energy-dependent response functions.

3.5 Detector Background

Typical total counting rates in the LADs are between 4000 and 7000 counts s^{-1}, of which between 3000 and 5000 are in discriminator channels 1 through 3. The rest are below the threshold of discriminator channel 1 or in discriminator channel 4. The dominant contribution to the rates below 100 keV is the diffuse cosmic gamma-ray background. The rates in the detectors therefore show a large variation at the spacecraft orbital period as the Earth occults a variable fraction of the sky that is visible to the detector. This effect is apparent in Figure 3-5, which shows a large modulation at the 92 minute orbital period of *CGRO*.

The contributions to the gamma-ray background in the BATSE detectors are discussed by Rubin et al. (1996). A general review of the gamma-ray background in low Earth orbit is given by Dean, Lei, & Knight (1991). Besides the diffuse cosmic gamma-rays, other significant sources of background include atmospheric gamma-rays, prompt gamma-ray emission from interactions of cosmic ray and magnetospheric particles with the detectors, and decays of radionuclides in the detectors activated by cosmic rays and trapped magnetospheric protons. The atmospheric gamma-rays in the BATSE energy range are bremsstrahlung from secondary and re-entrant albedo

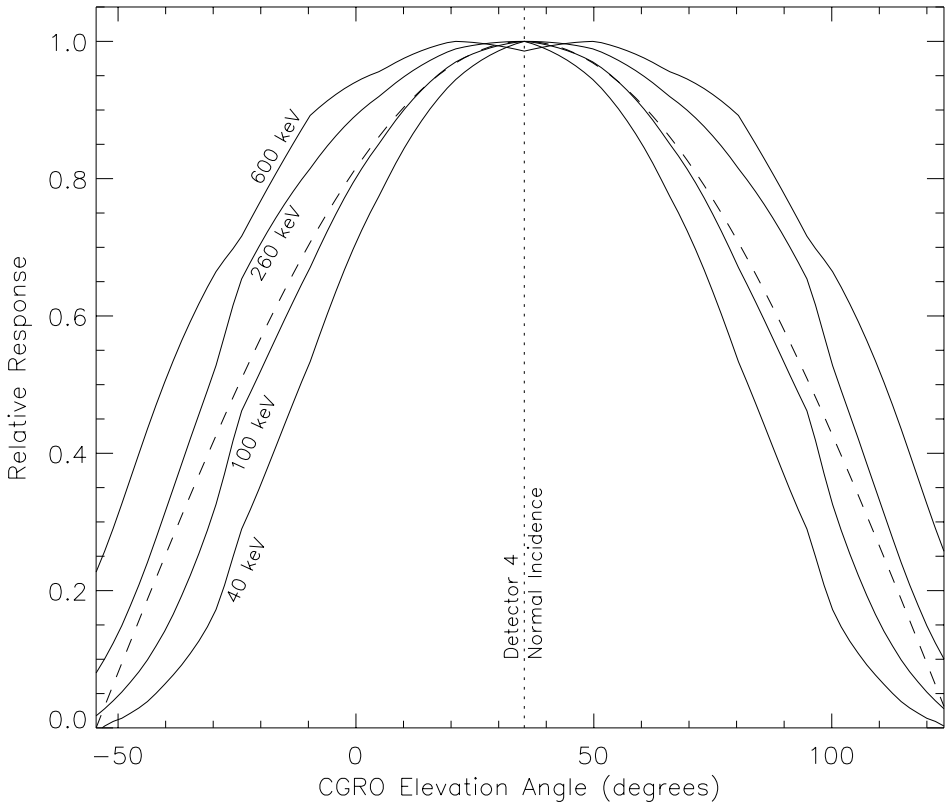

Figure 3-4 Angular response of the LADs to photons of different energies. The dashed curve indicates the ideal cosine response. This plot is for detector 4. The Earth is on the other side of the spacecraft in this example, so the atmospheric contribution to the response is negligible.

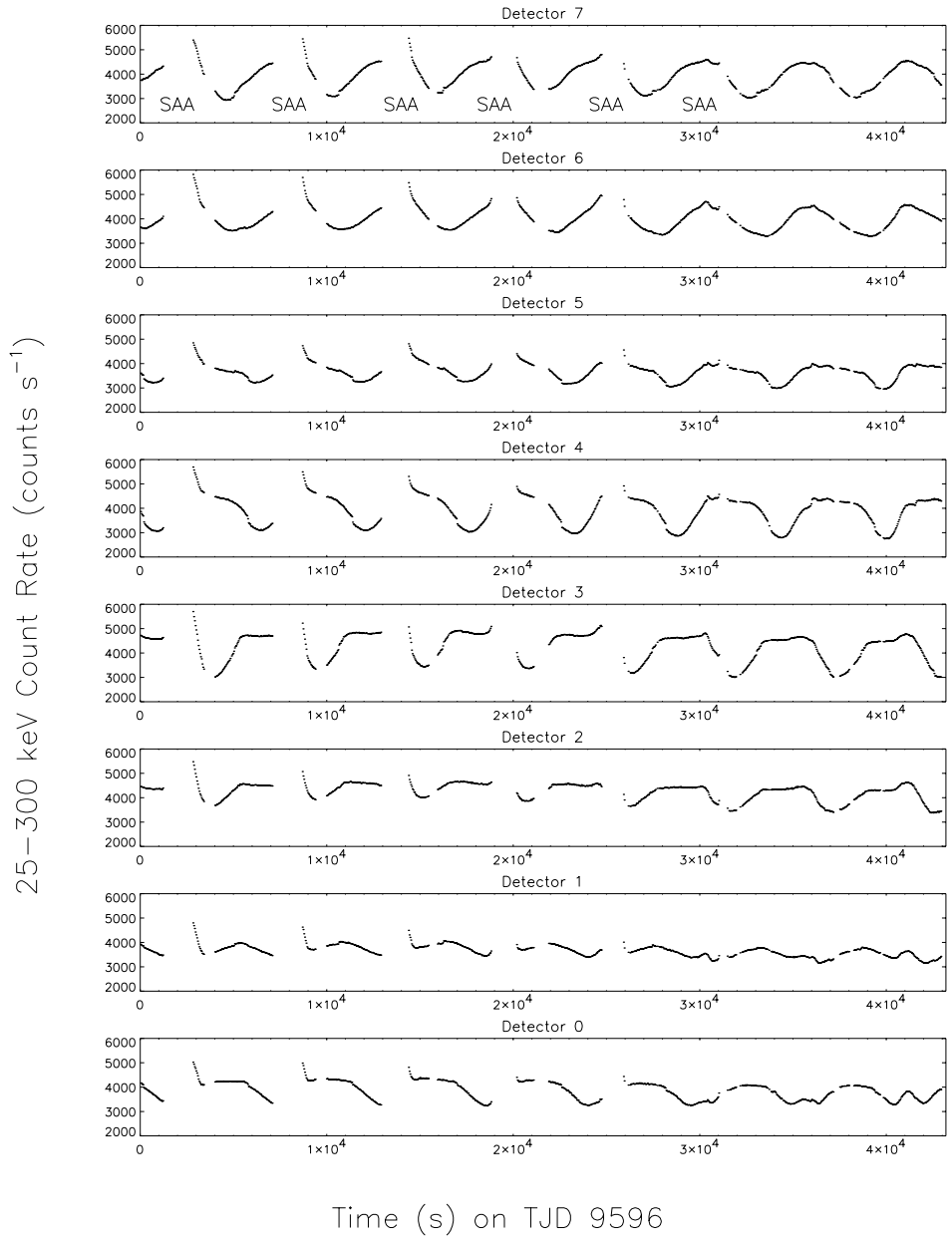

Figure 3-5 BATSE detector count rates over 12 hours. The modulation of the background at the 92 minute orbital period results from the varying fraction of the diffuse cosmic gamma-ray background that is blocked by Earth in the field of view of the detectors. As a result, the counting rates in detectors that face in opposite directions (0 and 7, 6 and 1, 5 and 2, 3 and 4) show a strong anti-correlation.

electrons which are products of cosmic ray interactions with the ambient gas. Cosmic ray interactions with the spacecraft materials produce a prompt "local" gamma-ray background (Dean et al. 1991).

Bombardment of the detector materials by cosmic rays and trapped magnetospheric particles (particularly in the SAA) produces radionuclides which decay with various lifetimes. An important contribution to the BATSE background of this kind comes from $_{53}I^{128}$ (Rubin et al. 1996). The activation of the detector materials during passages through the SAA is evident in Figure 3-5. Data gaps due to passages through the SAA (when the photomultiplier voltage is switched off) are marked in the top panel. The exponential decay of the counting rates upon exit from the SAA is evident following the data gaps, particularly for the first 3 orbits shown in the figure.

Table 3-1. Fast discriminator channel boundaries

Detector	Lower Boundaries (keV) Channel 1	Channel 2	Channel 3	Channel 4
0	23.8	60.9	108.7	303.3
1	23.3	53.2	112.6	300.1
2	23.8	57.1	110.4	323.4
3	21.8	63.0	131.3	320.0
4	20.2	58.4	110.0	313.5
5	26.4	52.4	112.2	348.5
6	21.5	59.1	116.1	306.1
7	20.2	57.8	110.9	351.6

Chapter 4

The Search for Nontriggered Events

This chapter describes a global search of the archival data from BATSE for gamma-ray bursts (GRBs) and other fast transients. Since the search is carried out with archival data, it is called the "off-line search" to distinguish it from the real-time data processing performed onboard the spacecraft. The transients detected exclusively with the off-line search are called "nontriggered" events.

The work described here is the successor of preliminary investigations carried out by Rubin et al. (1993), van Paradijs et al. (1993), and Kommers et al. (1996; 1997; 1998). Other searches for nontriggered events in the BATSE data are described by Skelton & Mahoney (1994) and Young et al. (1996), but these are more limited in scope and use techniques different from those described here.

The discussion in this chapter is very similar to that of Kommers et al. (1997), a paper which describes a preliminary off-line search of 345 days of archival data and which is reproduced in Appendix C. The present chapter is updated to reflect the improvements that were made to the preliminary off-line search before extending it to 6.0 years of the mission. Where necessary the search and analysis of the original 345 days of data was repeated to use the improved methods described in this chapter.

4.1 Motivations for the Off-line Search

A GRB or other transient may fail to activate the BATSE onboard burst trigger for any of several reasons:

1. it may be too faint;
2. it may occur while the onboard burst trigger is disabled for technical reasons;
3. it may have most of its counts in an energy range that is *not* being monitored by the onboard trigger; or
4. it may bias the onboard background estimate so that it artificially appears to be below threshold.

GRBs and other transients that go undetected onboard for any of these reasons are of scientific interest.

The bursts that are too faint to be detected onboard but that nevertheless leave a statistically significant signal in the continuous data can be recovered by a retrospective search. Because BATSE is the most sensitive GRB monitor to date, such bursts will be among the faintest ever detected. Depending on the cosmological evolution of the sources (in luminosity and burst rate) these faint bursts are likely to be the most distant. Chapter 6 discusses the scientific implications of the faint bursts detected by the off-line search.

GRBs that are not detected onboard for technical reasons may be of nearly any intensity, from very faint to very bright. As described in Chapter 3, the normal operation of the burst trigger requires that it be disabled for a limited time interval after a transient event is detected. The burst trigger is disabled entirely for the high-resolution data accumulation interval, and the thresholds are set to the maximum rate observed during the event while the high-resolution data are telemetered to the ground. A second burst that occurs during the accumulation interval is sure to be nontriggered; and a burst that occurs during the read-out interval will be nontriggered if it is fainter than the previous event.

The cause of an onboard trigger need not be a GRB. Solar flares, magnetospheric particle precipitations, variability from X-ray binaries, egress of bright persistent X-ray sources from behind the Earth, and other phenomena can activate the burst trigger. If such "false" (non-GRB) triggers are frequent—for example during periods of intense solar activity—then the live-time of the onboard trigger for detecting true GRBs can be seriously degraded. To avoid a high rate of non-GRB triggers due to magnetospheric particle precipitations, the onboard burst trigger is disabled while the spacecraft passes over certain geographic locations associated with a high rate of such events (see section 2.4.2). During outbursts of bright X-ray binaries, such as GRO J0422+32 (Nova Persei 1992), the onboard trigger thresholds are raised to avoid false triggers due to variability from the X-ray source or egress of the source from behind the Earth.

When the onboard trigger is optimized for detecting GRBs it monitors count rates from the 50–300 keV range (discriminator channels 2 and 3). Astronomically interesting transients occur that deposit most of their counts in lower energies, 25–50 keV (discriminator channel 1). Examples of such events include bursts and flares from X-ray binaries, activity from soft gamma-ray repeaters (SGRs), spectrally soft GRBs, and possibly so-far undiscovered burst phenomena. Such transients do not normally lead to an onboard burst trigger, so they require a retrospective search to find them. The exceptions are when the onboard burst trigger is changed to detect low-energy events, as was done for specific investigations of SGRs and the X-ray bursting pulsar GRO J1744−28.

The count rate thresholds of the onboard burst trigger depend on the current estimate of the expected background count rate (see section 3.3). The onboard computer finds a background count rate in each detector at a commandable time interval, nominally every 17.408 s, by averaging the count rates accumulated during the interval. Since many GRBs last longer than 17 s, it is possible that low-level emission from a burst may be included in the background estimate. Then the background estimate will be biased upwards, artificially raising the threshold required for a burst

trigger. If the burst profile rises very slowly, with no subsequent sharp count rate increases, then it may not activate the onboard burst trigger even though it would have been found to be of sufficient statistical significance for a trigger if more accurate background estimates were used. This so-called "slow-riser" bias has the effect of suppressing the detection of weak, long bursts that have a "slow-rising" time profile. Lingenfelter & Higdon (1996) suggested that as many as $19 \pm 6\%$ of all bursts above the "true" detection threshold were missed because of the slow-rising bias; however, based on results from the preliminary off-line search, it appears that the slow-rising bias causes the onboard trigger to miss only a few percent of GRBs that would have been otherwise detectable (see Section C.6.1).

The design goals of the off-line search of BATSE data are thus the following:

1. to detect GRBs that were too faint to activate the onboard burst trigger;
2. to detect GRBs that occurred while the onboard trigger was disabled;
3. to detect fast transients in the low-energy (25–50) keV range; and
4. to detect GRBs and other transients using a different background averaging scheme than the one used onboard.

The final products of the off-line search are a catalog nontriggered GRBs, a list of GRBs that were detected with both the off-line search and the onboard trigger, a list of bursts from SGRs, and a catalog of "astronomically interesting" low-energy (25–50 keV) transients that are not obviously associated with a solar flare, magnetospheric particle precipitation, or instrumental origin.

4.2 Data Selection and Scope

The data used for the off-line search are the DISCLA and DISCLB data types, which provide the count rates in the LADs with 1.024 s time resolution in 3 (DISCLB) or 4 (DISCLA) discriminator energy channels (see section 3.3). These data have some

advantages over the CONT data type, which provides 2.048 s time resolution in 16 energy channels. First, the 1.024 s discriminator data have the higher time coverage (live-time) and so permit a more comprehensive search. Second, the better time resolution of the DISCLA/DISCLB data provides better sensitivity to short duration events, such as short GRBs and bursts from SGRs.

The time period spanned by the search is 1992 December 9.0 to 1997 December 17.0, a total of 2200 days of the mission. The corresponding range of Truncated Julian Day (TJD) numbers is 8600.0 to 10800.0. The off-line search makes use of the archival data files available for 2178 of those days. Table 4-1 lists the TJDs for which an archival data file was *not* available at the *CGRO* Science Support Center at the time the search was performed. (Some of these files may be available presently or in the future, however.) The reason for not beginning the off-line search at the beginning of the mission is to avoid a high rate of off-line triggers due to interference from the Sun (*CGRO* was launched shortly after a maximum in the solar 11-year cycle) and from the X-ray binary Cygnus X-1 (which caused many false onboard triggers during the first year of the mission).

4.3 Off-line Search Algorithm

The basic strategy of the off-line search is the same as that of the onboard trigger: search the data sequentially to identify statistically significant count rate increases on a given time scale. A retrospective search can make use of burst detection schemes that would have been difficult or even impossible to implement in real-time onboard the spacecraft. The choice of transient detection scheme involves trade-offs between the sensitivity of the method to a given class of transients and the resources (computational and human) required to implement it. The off-line search described here uses lower thresholds in terms of statistical significance, detection criteria that provide more uniform sky coverage, and a background averaging scheme that is more sensitive to "slow-risers."

There are actually 7 separate off-line searches, each one using a different combination of discriminator channels and time resolution. Each search, in turn, uses 2 methods of background estimation.

The first step in each of the off-line searches is to combine the appropriate energy channels of the DISCLA/DISCLB data to form time series for each of the eight detectors. The next step is to search the eight time series sequentially with a moving window. For each time bin k where the count rates are available, two different procedures each yield an estimate of the background rate, $B_d(k)$, in detector d. The first background estimate uses the mean count rates observed during the 17.408 s preceding the time bin being tested. This estimate is much like that used onboard the spacecraft, except that it is continuously recomputed rather than being calculated in discrete 17.408 s blocks. An advantage of this method is that it can be performed on all the data except for those which follow within 17.408 s of a data gap.

The second method of background estimation takes advantage of the availability of data recorded after the time bin being tested. For the kth time bin of the time series, the expected number of background counts in detector d, $B_d(k)$, is obtained by interpolating a linear fit to data in time bins $k-N_b, \ldots, k-1$ and $k+1+N_b, \ldots k+2N_b$. The number of background bins, N_b, depends on the time scale of the search; if the data in time bins $k - N_b$ through $k + 2N_b$ are not temporally contiguous (e.g., if there is a data gap) then the background estimate is not formed. Note that the time bin being tested, k, is not centered in the gap of N_b bins that separates the fitted time intervals. This somewhat arbitrary choice is a result of trying various background schemes on 3 weeks worth of sample data; it gave satisfactory results. The use of a longer interval of data for the background fits means that this background estimate can be formed for fewer time bins than the 17.408 s background estimate.

Assuming the expected background rate $B_d(k)$ is obtained using at least one of the background estimates, the "significances" of the fluctuations in the detectors on

the 1.024 s time scale are defined from the measured count rates, $C_d(k)$, using

$$S_d(k) = \frac{C_d(k) - B_d(k)}{\sqrt{B_d(k)}}. \tag{4.1}$$

The definition of the "significances" for the longer time scales is a straightforward generalization:

$$S_d(k) = \frac{\sum_{i=0}^{n-1}[C_d(k+i) - B_d(k+i)]}{[\sum_{i=0}^{n-1} B_d(k+i)]^{1/2}} \tag{4.2}$$

Here n is the number of time bins in the time scale of the search. In the absence of signal, this definition of "significance" is intended to yield eight normally distributed random variables with zero mean and unit variance associated with time bin k. For $n > 1$ (time scales longer than 1.024 s) the "significances" are not independent between time bins that are separated by fewer than $1.024n$ s.

The off-line trigger criteria require that at least two of the $S_d(k)$ exceed a minimum value M and that the sum of the two greatest exceeds a minimum value Σ. Expressed another way, if s_1 and s_2 are the greatest and second greatest of the $S_d(k)$, then the off-line trigger is satisfied when $s_1 \geq s_2 \geq M$ and $s_1 + s_2 \geq \Sigma$. Figure 4-1 shows a diagram of the "phase space" formed by s_1 and s_2. The off-line trigger criteria are satisfied whenever the point (s_1,s_2) lies in the non-shaded area, labeled A in the figure.

The motivation for this trigger scheme is obtain more a more isotropic sensitivity than that of the onboard trigger. The onboard trigger's requirement that at least two detectors exceed a single threshold introduces an anisotropic sensitivity to faint transient events because of the cosine-like change in the detector's effective area with viewing angle (Brock et al. 1991). An event occurring directly in front of a detector that produces count rates $10\sigma_B$ above background in that detector would produce only a $3.5\sigma_B$ signal in the second-most brightly illuminated detector, and it would thus fail to activate the onboard burst trigger. The same event occurring along a direction midway between two detector normals would register approximately $7.1\sigma_B$ in both detectors and would comfortably cause an onboard burst trigger. The off-line

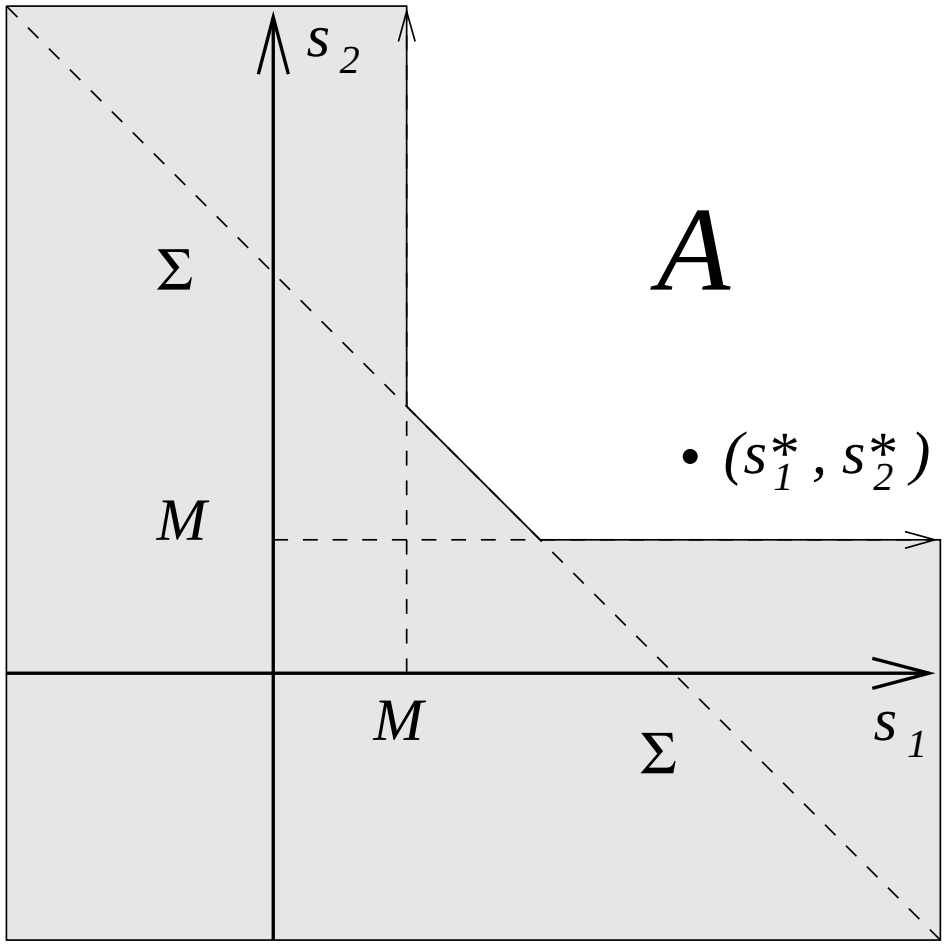

Figure 4-1 "Phase-space" representation of the off-line trigger criteria. An off-line trigger occurs only when the two greatest (s_1 and s_2) of the significances in the eight detectors lie in the non-shaded area A.

search procedure uses lower thresholds and combines the fluctuations in the detectors in a way that (partially) combats the directional anisotropy of the onboard trigger.

The parameters of the off-line searches for the 7 combinations of time resolution and energy range are listed in Table 4-2. Search A uses counts from the 25–50 keV range at 1.024 s time resolution, and it is expected to provide optimum sensitivity to short, low-energy transients such as bursts from SGRs (which typically last for $\sim$ 1 s or less). Search B uses counts from the nominal GRB energy channels (50–300 keV) with 1.024 s time resolution and provides sensitivity to short GRBs. Search C uses counts from all three lower discriminator channels (25–300 keV) to search for signals with a broad spectral range, such as faint GRBs with substantial low-energy emission.

The searches on the longer time scales (D through G) provide sensitivity to longer transients, including the "slow-rising" ones. The GRB duration distribution peaks between 20 s and 50 s (see Figure 2-2) so the statistical significance of most GRBs is expected to be higher on longer time scale searches than on the 1.024 s searches. Thus the longer time scale searches have lower peak flux thresholds. This is because the significance (as defined above) of a constant signal in an $1.024n$ s time bin is proportional to $\sqrt{n}$, assuming the burst lasts at least $1.024n$ s. The searches on the 4.096 s and 8.192 s time scales are thus expected to reach peak fluxes (averaged over the time scale of the search) that are lower by factors of (roughly) 2 and $2\sqrt{2}$, respectively, than can be reached on the 1.024 s time scale.

The specific time profile of each burst determines which of the three time scales in Table 4-2 is the most sensitive. Bursts detected on one time scale may or may not be detected on another. For this reason, each of these searches should be considered a separate experiment.

The ability of the off-line trigger to detect "slow-rising" GRBs is discussed in Kommers et al. (1997). The off-line trigger detects slow-risers better than does the onboard burst trigger because the off-line search is almost always able to use data from both before *and after* the time bin being tested. For further details see section C.4.2.

Table 4-1. Days for which no archival data were searched.

Missing Days (TJD)		
8947	10322	10330
9111	10323	10331
9112	10324	10332
9114	10325	10333
9153	10326	10334
9474	10327	10335
9827	10328	10336
	10329	

Table 4-2. Parameters of off-line searches

Search	Time Scale (s)	Discriminator Channels	N_b
A	1.024	1	30
B	1.024	2 and 3	30
C	1.024	1, 2, and 3	30
D	4.096	1	45
E	4.096	2 and 3	45
F	8.192	1	60
G	8.192	2 and 3	60

The parameters of the off-line trigger, M and Σ, are chosen to satisfy two requirements. First, they must at least be high enough to ensure that the null hypothesis of "no variability in excess of counting statistics in the time series of at least two of the eight detectors" is excluded with adequate statistical significance. The onboard burst trigger excludes the null hypothesis with very high confidence. The probability that at least 2 out of 8 samples from a normal distribution with zero mean and unit variance exceed 5.5 is 1.0×10^{-14}. (The counting rates in the BATSE detectors are high enough—over 1000 counts s^{-1} in each of discriminator channels 1 through 3—that the Poisson statistics of the counts in each bin can be treated to high accuracy in the Gaussian approximation.) On the other hand, M and Σ must not be so low that the number of detected events *due to real variability from astronomical and local photon sources* is unmanageable. In practice, it is this second requirement that sets the magnitudes of M and Σ.

The parameters of the off-line trigger listed in Table 4-2 are based on experience with a 3 week set of "trial" data (TJDs 9200–9221). For these data, $M = 2.5$ and $\Sigma = 8.0$ give a manageable number of off-line triggers, about 40–60 per day. When applied to the full data set, however, they can produce hundreds of off-line triggers per day during outbursts of bright X-ray sources such as Vela X-1, A0535+26, and GRO J0422+32, owing not to burst-like transients but to pulsations or aperiodic variability.

With $M = 2.5$ and $\Sigma = 8.0$ the rate of off-line trigger detections expected from statistical fluctuations (due to counting statistics alone) is quite small. The probability that a sample of eight significances drawn from the normal distribution with unit variance will satisfy the off-line trigger is estimated by first integrating the bivariate normal distribution (centered on the origin) over the allowed area A in the (s_1, s_2) plane (see Figure 4-1). The resulting probability is then multiplied by the number of ways to select two detectors out of eight:

$$P_{stat} = \left[\iint_A \frac{1}{2\pi} \exp\left(-\frac{s_1^2 + s_2^2}{2} \right) ds_1 \, ds_2 \right] \times \frac{8!}{6!\, 2!} \tag{4.3}$$

For $M = 2.5$ and $\Sigma = 8.0$ the value of P_{stat} is 2.1×10^{-7}. The accuracy of this calculation is verified by Monte Carlo simulations, which give a probability of $(2.0 \pm 0.5) \times 10^{-7}$. Thus the rate of "false triggers" on the 1.024 s search due to statistical fluctuations alone is about 0.012 per day of data searched (assuming 70% live-time). Monte Carlo simulations of the 4.096 and 8.192 s searches (which are not independent of the 1.024 s searches) give "false triggers" at about the same rate.

In practice the off-line trigger detects many more events than can be expected based on statistical fluctuations. This is because the time series being searched are not Poissonian. They are dominated by the activity of real sources. Variable astronomical sources, the Sun, terrestrial photon sources, and the interaction of cosmic-ray particles in the detectors all contribute to the count rates. Figure C-2 shows an integral distribution of $S_d(k)$ for a single detector ($d = 0$) taken from a search of a "quiet" day in which no off-line triggers were found in the detector. For comparison, the expectation from a normal distribution with zero mean and unit variance is also shown. The excess of high-significance measurements over what is expected from a normal distribution reflects both deficiencies in the background subtraction and the activity of real sources.

4.4 Detection Efficiency and Sky Exposure

The "trigger efficiency" is the probability that a transient with given physical characteristics (time profile, photon flux, energy spectrum, and source direction) occurring under given instrumental conditions (background rates and spacecraft orientation) will be detected by the off-line trigger. In the BATSE catalogs, the trigger efficiency is expressed as function of intensity only, by averaging over the other relevant quantities. Similarly, the sky exposure is the detection probability as function of source direction only.

The first step in computing the trigger efficiency is to estimate the probability $E_1(P, \nu, \alpha, \delta, t)$ that a burst that occupies exactly one time bin will be detected. The

burst is parameterized by its peak flux on the time scale of the search (P), its power-law photon spectral index (ν), its source direction (right ascension, declination) in celestial coordinates (α, δ), and time of occurrence during the mission (t). The time during the mission determines the background rates and spacecraft orientation, both of which are obtained from the data files being searched. If no data are available at the specified time or if the source direction is occulted by the Earth, the trigger efficiency is trivially zero. Otherwise, the expected count rates in the detectors are obtained using the instrument and atmospheric response matrices described in Section 3.4. The expected count rates are multiplied by the duration of the time bins to obtain the expected number of counts above background in the detectors, denoted here by C_d^*. The expected background counts, $B_d^*(k)$ are obtained from the measured count rates at time t during the mission. The expected significances in the detectors are $S_d^* = C_d^*/\sqrt{B_d^*}$.

Let s_1^* and s_2^* denote the greatest and second greatest of the S_d^*, respectively. The trigger efficiency $E_1(P, \nu, \alpha, \delta, t)$ is estimated by integrating the bivariate normal distribution centered on the point (s_1^*, s_2^*) over the area A in which the off-line trigger criteria are satisfied (see Figure 4-1):

$$E_1(P,\nu,\alpha,\delta,t) = \iint_A \frac{1}{2\pi} \exp\left[-\frac{(s_1 - s_1^*)^2}{2}\right] \exp\left[-\frac{(s_2 - s_2^*)^2}{2}\right] ds_1\, ds_2. \qquad (4.4)$$

This expression can be reduced to a one-dimensional quadrature for more efficient numerical evaluation:

$$E_1(P,\nu,\alpha,\delta,t) = \frac{1}{4}\mathrm{erfc}\left(\frac{\Sigma - M - s_1^*}{\sqrt{2}}\right)\mathrm{erfc}\left(\frac{M - s_2^*}{\sqrt{2}}\right) + \frac{1}{2\sqrt{\pi}} \int_{\frac{M-s_1^*}{\sqrt{2}}}^{\frac{\Sigma-M-s_1^*}{\sqrt{2}}} e^{-x^2}\mathrm{erfc}\left(\frac{\Sigma - x\sqrt{2} - s_1^* - s_2^*}{\sqrt{2}}\right) dx, \qquad (4.5)$$

where $\mathrm{erfc}(x)$ is the complementary error function.

Equation 4.5 must be evaluated on a grid of peak fluxes, source directions, spectral indices, and times during the mission. To adequately sample the ranges of possible

burst characteristics for every time bin checked in the off-line search is computationally infeasible. To obtain a reasonable answer, the efficiency is evaluated on a grid of 9 peak fluxes, 252 source directions, and a set of times that sample background rates every 8 minutes on 110 quasi-randomly chosen days of the mission. The power-law index ν of the photon energy spectrum ($\phi(E) \propto E^{-\nu}$) is fixed at a single typical value, $\nu = 2.0$. The peak fluxes span a range where the detection efficiency is expected to vary significantly between 0 and 1. The source directions are nearly isotropically distributed on the celestial sphere (Tegmark 1996).

The choice of times at which to compute $E_1(P, \nu, \alpha, \delta, t)$ balances two opposing considerations. For a given burst, the efficiency as a function of intensity depends on the background rates. The variations in background are dominated by orbital modulation, so there is little need to sample densely in time to get adequate phase coverage for the distribution of background rates. On the other hand, to adequately estimate anisotropies in the sky exposure requires sampling on a time scale finer than the durations of typical data gaps due telemetry drop-outs and passages through the SAA. The compromise used here is the following. The first 110 numbers of a Sobol quasi-random sequence (Press et al. 1995) provide 110 mission days that uniformly sample the full 2200 days of the off-line search. On each of the 110 days, $E_1(P, \nu, \alpha, \delta, t)$ is sampled at time intervals of 8 minutes. This scheme should adequately sample the spacecraft orbital precession period (≈ 51 days) and the orbital modulation of background rates (≈ 92 minutes), while providing a dense sampling to evaluate the effects on sky exposure of regular data gaps due to the SAA and telemetry schedule.

The single-time-bin off-line trigger efficiency as a function of peak flux only, $E_1(P)$, is obtained by averaging $E_1(P, \nu, \alpha, \delta, t)$ over the quantities α, δ, and t (ν has the single value 2.0). This efficiency underestimates the probability of detecting most GRBs, however, because most bursts last longer than a single time bin and so have more than one statistical chance to be detected. The method for taking the time profiles of the bursts into account is discussed further in Section 6.3.1, where approximation formulas for the trigger efficiency are given.

The sky exposure of the off-line search is given by averaging $E_1(P, \nu, \alpha, \delta, t)$ over time (t) to obtain $E_1(\alpha, \delta)$. Figure 4-2 shows $E_1(\alpha, \delta)$ plotted in equatorial and Galactic coordinates. The maximum exposure is 70.0% owing to the presence of data gaps. The minimum exposure is found around the celestial equator, $\delta = 0$, owing to blockage by the Earth. The Southern Hemisphere has an overall lower exposure than the Northern Hemisphere owing to data gaps during passages through the SAA. Over long time periods, the dependence on right ascension averages out, so that the sky exposure is effectively a function of declination only. Figure 4-3 shows the sky exposure as a function of equatorial declination. The dipole and quadrupole moments of the sky exposure (in equatorial and Galactic coordinates) are listed in Table 4-3.

4.5 Classification of Off-line Triggers

The off-line search identifies a variety of statistically significant count rate fluctuations, not all of which correspond to phenomena that are interesting in the context of this search. The "interesting" events are GRBs, bursts from SGRs, and bursts and flares from X-ray binaries. The other phenomena that are detected—such as solar flares, magnetospheric particle precipitations, and aperiodic variability from X-ray binaries—are of scientific interest but they are not the targets of this search. The off-line triggers must therefore be sorted into useful categories.

The first step in the classification process is to visually inspect the count rates as a function of time for each off-line trigger. An examination of the count rates in the eight detectors, summed over the appropriate energy channels, provides immediate information about whether an off-line trigger is associated with a point source of photons. The majority of off-line triggers can be rejected as "uninteresting" based on this information alone. Next, examination of the count rates in the different energy channels allows transients to be distinguished based on their spectral characteristics. This section describes the most common causes of off-line triggers and how they can be confidently identified. The general strategy is to first ask if the event resembles

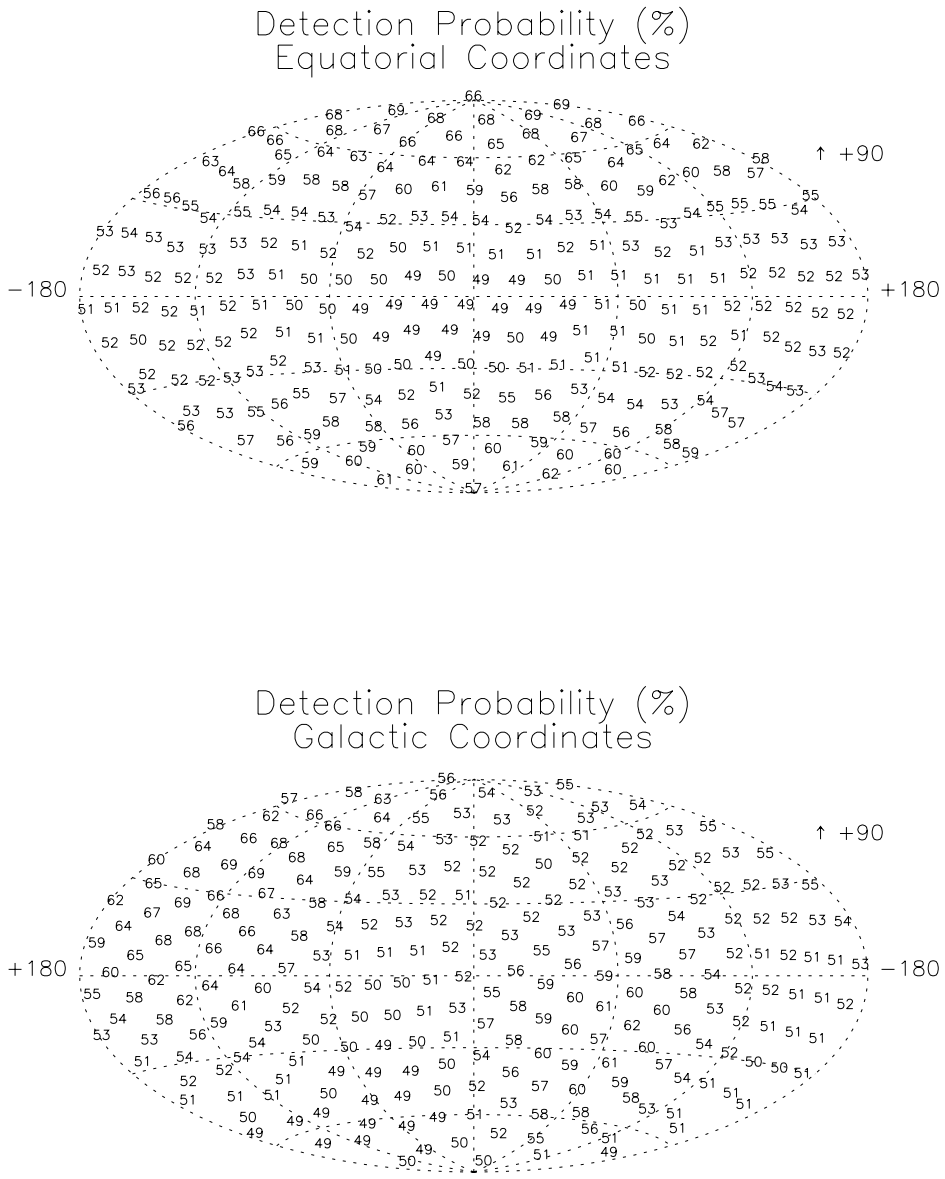

Figure 4-2 The sky exposure of the off-line trigger, expressed as percentage of elapsed time. The upper figure shows the exposure plotted in equatorial coordinates. The lower figure shows the exposure plotted in Galactic coordinates (the plane of the Galaxy runs across the equator). The maximum exposure is 70.0% owing to gaps in the DISCLA data.

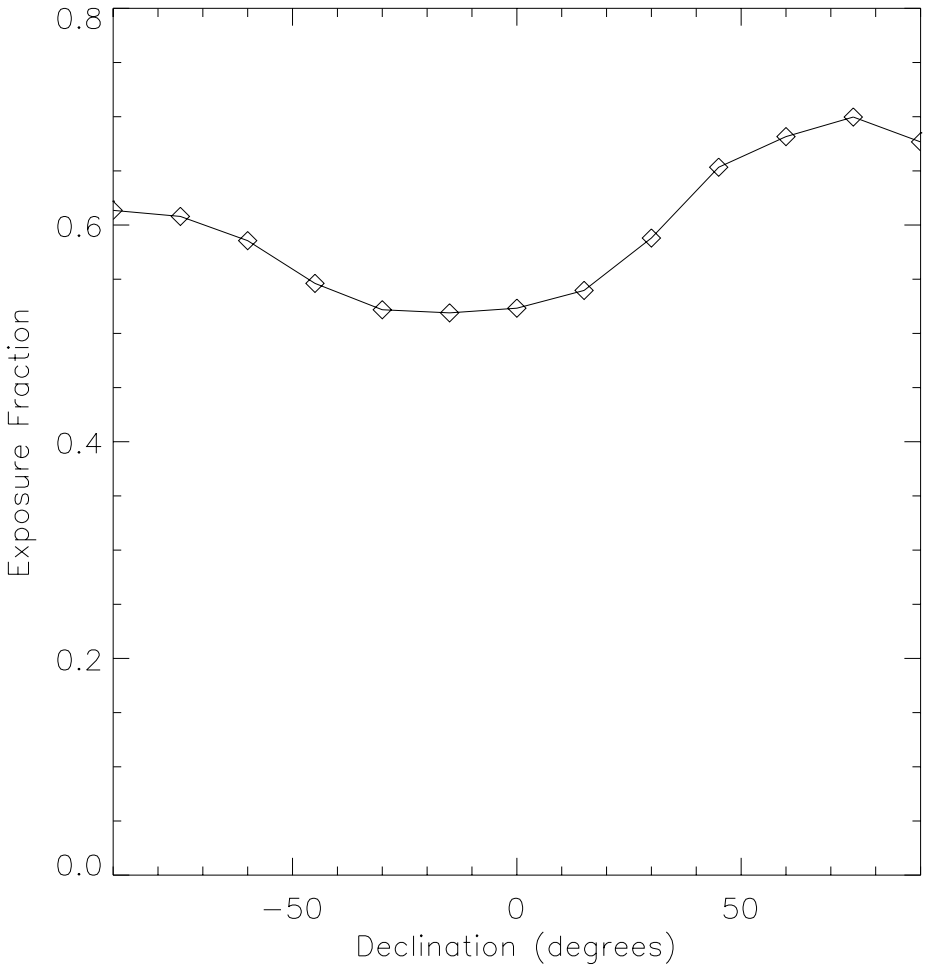

Figure 4-3 The sky exposure of the off-line trigger, as a function of declination. Over long viewing times, the dependence on right ascension averages out leaving only the dependence on declination.

an "uninteresting" cause of off-line triggers, and if it does not, then try to classify it as a GRB, SGR burst, or low-energy transient with an "unknown" origin.

4.5.1 Occultation Steps and Aperiodic Variability

When a bright X-ray source such as Cyg X-1 egresses from behind the Earth there is a significant increase in the count rates in the detectors facing the source. This increase takes place over 8 s to 25 s and is useful for monitoring the long-term intensity bright of X-ray sources (Zhang et al. 1993). Likewise, when the source subsequently goes behind the Earth there is a decrease in the count rates. Examples of the egress and ingress of the Crab Nebula and Cyg X-1 are shown in Figure 4-4. Off-line triggers caused by the egress and ingress of bright sources can be readily identified by their appearance as an "occultation step" in a plot like this.

Like all X-ray binaries, Cyg X-1 shows rapid aperiodic variability (sometimes called "shot-noise," though individual shots are not necessarily responsible) on a wide range of time scales (van der Klis 1995). This variability causes an increase in the amplitude of count rate fluctuations in the detectors viewing the source. Large fluctuations can cause off-line triggers, even though the source of the variability is more like a stationary stochastic process than a (non-stationary) impulsive transient. Off-line triggers caused by such variability are not interesting in the context of the off-line search, although they are due to real source activity. Fortunately the vast majority of them are easy to identify based on an examination of a plot like Figure 4-4 because they occur in the detectors facing a known "noisy" source and they show no particular burst-like structure. The increased fluctuations clearly accompany the rise of Cyg X-1 and then subside when Cyg X-1 sets. In contrast, the Crab Nebula is a steady source, and shows no increase in count rate fluctuations (beyond what is expected based on counting statistics) when it is visible.

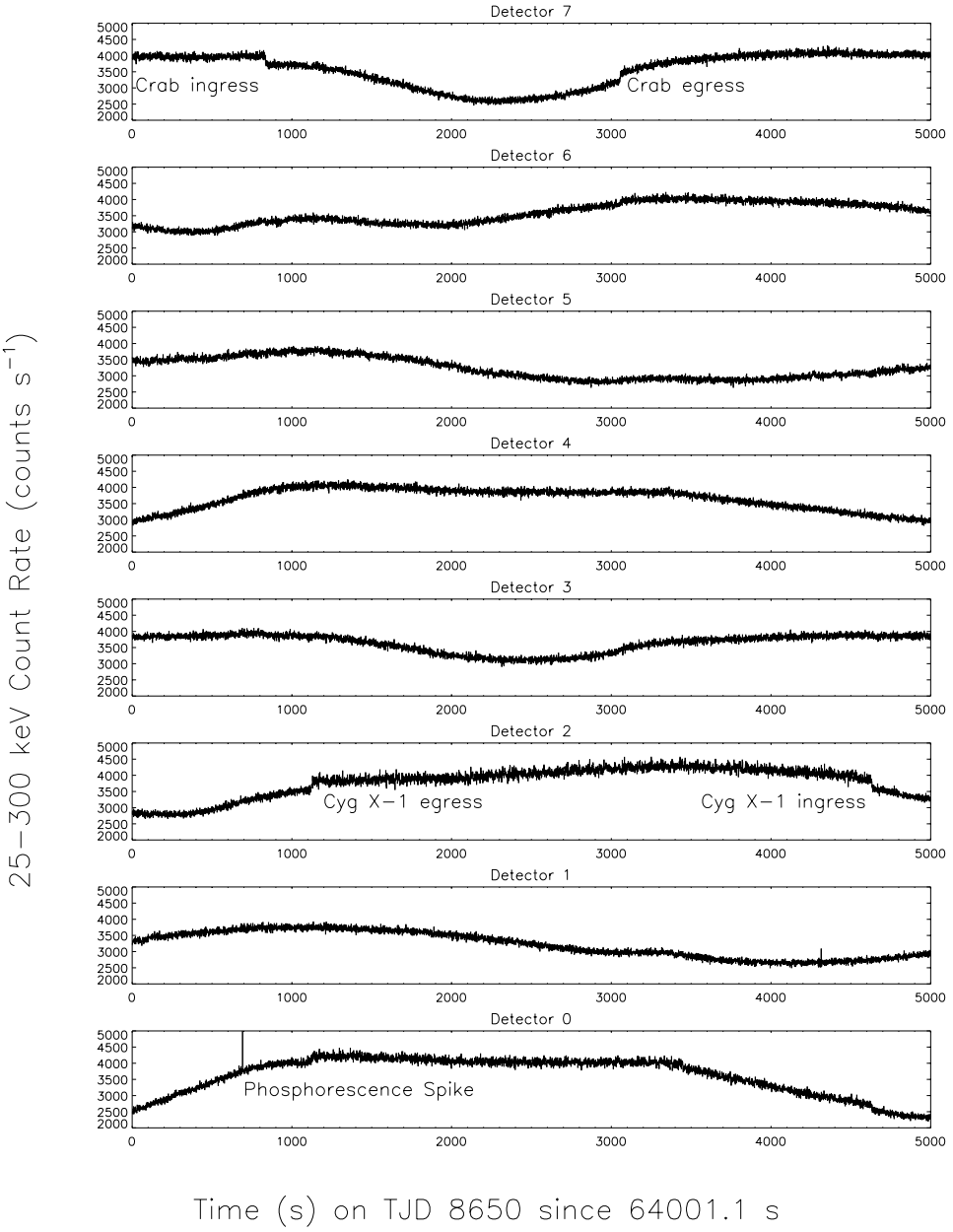

Figure 4-4 The ingress and egress of bright X-ray sources. The ingress and egress of the Crab Nebula is illustrated in the top panel (detector 7). The egress and ingress of Cyg X-1 is illustrated in detector 2. Note the increased amplitude of fluctuations in the detector 2 count rates due to aperiodic variability from Cyg X-1.

4.5.2 Phosphorescence Spikes

When a high energy cosmic ray particle interacts in one of the LAD crystals it produces a short (< 1.024 s), intense increase in the count rates in the lowest discriminator channel (25–50 keV). This signal is due to activation of energy levels in the NaI(Tl) crystal that decay on time scales longer than the time scale of the veto signal from the CPD. These events can be easily identified by the presence of an intense signal in just one detector. An example is shown in the bottom panel of Figure 4-4. Even though the off-line trigger requires a significant signal in more than one detector, occasionally a phosphorescence spike can occur simultaneously with an unrelated fluctuation in a second detector to produce an off-line trigger.

4.5.3 Magnetospheric Particle Precipitations

As described in Section 2.4.2, electrons and protons from Earth's radiation belts can precipitate out of their magnetically trapped orbits. The LADs detect bremsstrahlung when these particles interact in the atmosphere or in the spacecraft materials. These events typically produce one of three kinds of signatures in the archival data (Horack et al. 1991). The first is a smooth rise and decay with comparable count rates in opposite-facing detectors. This signature is clearly inconsistent with a point source of photons; it indicates that the spacecraft has encountered a cloud of electron flux from all directions. The electron flux is not isotropic, as detectors with normal vectors perpendicular to local magnetic field lines will register higher count rates (Horack et al. 1991). The second kind of event shows a smooth rise and decay in the count rates of detectors on only one side of the satellite. This indicates the photons are produced in the atmosphere at some distance from the spacecraft. Since the source of radiation is relatively nearby, however, the orbital motion of *CGRO* causes the event to have different intensity profiles in different detectors; this is clearly inconsistent with an astronomical point source. The third class of events shows complex time profiles with variability on time scales as short as the data provide (1.024 s). Such

events can closely mimic a GRB or other astronomical transient, although in practice they can often still be identified as terrestrial because they show some characteristics of the previous two categories (appearance in opposite-facing detectors, inconsistent time profiles between detectors).

Two other characteristics are common for particle precipitation events. First, they tend to occur when the spacecraft is near its extreme geographic latitudes, where the spacecraft orbit enters higher geomagnetic L-shells (Tascione 1994). Second, the bremsstrahlung character of the radiation spectrum is often evident in the very high ratios of count rates in the lowest discriminator channel (20–50 keV) to those in the higher channels (50–300 keV). Figure 4-5 shows an example of a particle precipitation that is easily identified by its appearance in all eight detectors with comparable intensities.

4.5.4 Solar Flares

The time profiles of solar X-ray flares can easily resemble those of GRBs and other extra-solar astronomical transients. Their distinguishing features are their spectral characteristics, source direction, and association with other solar flares on the same day. Figure 4-6 is a plot of the count rates in the eight detectors showing two solar flares and GRB. Both kinds of event are impulsive transients that appear in detectors on a single side of the spacecraft, with relative intensities that are consistent with a point source. An examination of the count rates in the four discriminator energy channels, however, shows a difference. As seen in Figure 4-7, solar flares typically have soft energy spectra. Most of the counts are in the lowest energy channel (below 50 keV) and almost none are above 100 keV (discriminator channels 3 and 4). This is occasionally unreliable, though, as spectrally hard solar flares are observed (having been identified as such based on other observations with dedicated solar experiments such as those onboard the *GOES* missions). If necessary, a further check on a solar origin can be made using the source direction, estimated crudely based on knowledge of which detectors are facing the Sun or using the more precise techniques described

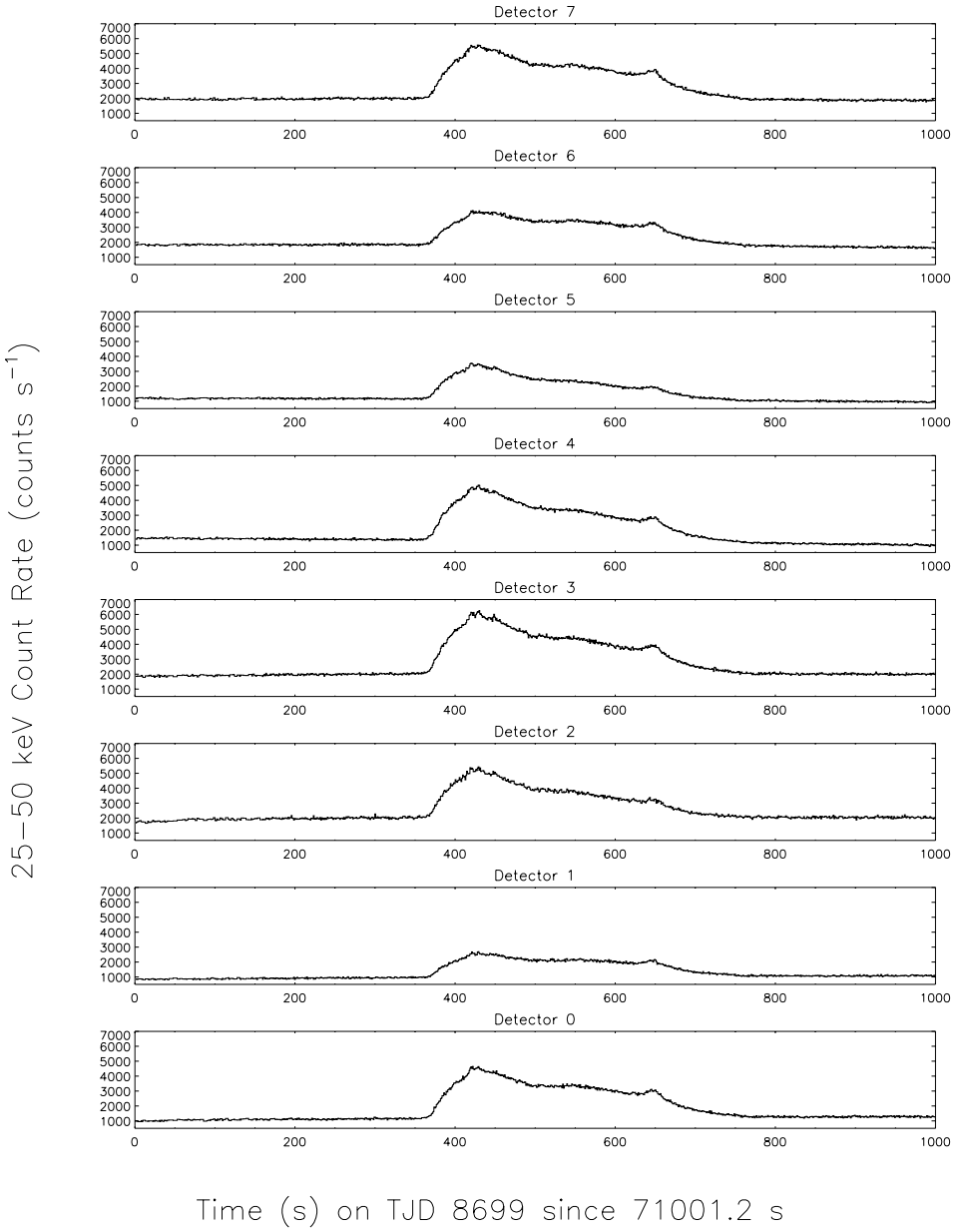

Figure 4-5 Precipitation of magnetospheric electrons. The electrons interact in the outer skin of the detectors to produce bremsstrahlung. The electron flux is approximately isotropic, so detectors facing in opposite directions (7 and 0, 6 and 1, 5 and 2, 4 and 3) show comparable count rate increases.

in section 5.3.1. Solar flares tend to be observed rather frequently during periods of solar activity, so it is often possible to see from a plot like that in Figure 4-6 that a given event is just one in a sequence of repetitive solar X-ray flares.

4.5.5 Terrestrial Gamma-Ray Flashes

Because of their short durations, TGFs (see Section 2.4.4) rarely have adequate statistical significance in the DISCLA data to cause an off-line trigger. When they do, however, they are distinguished by their hard spectra and source directions that are usually below the limb of the Earth. This signature is clearly inconsistent with an astronomical source.

4.5.6 Gamma-Ray Bursts

The identification of GRBs in the data is based on their spectral characteristics. Figure 4-8 shows the count rates from a GRB in the 4 discriminator energy channels (this is the same GRB seen in Figure 4-6). Of the known high-energy transient phenomena (see Chapter 2) only GRBs, TGFs, and hard solar X-ray flares generally have their peak energy output at energies above $\sim$ 50 keV. The TGFs are already distinguished in the DISCLA data by locations below the satellite horizon, and solar flares are already identified with adequate accuracy using the techniques already discussed. Magnetospheric particle precipitations sometimes produce significant count rates above 50 keV, but such events typically have the characteristics discussed previously that allow them to be identified as local events.

Any transient is a candidate for being a GRB if it

1. shows significant emission above 100 keV,
2. appears to be consistent with a point-source origin above the horizon, and
3. does not appear to be a TGF, hard solar flare or magnetospheric particle precipitation.

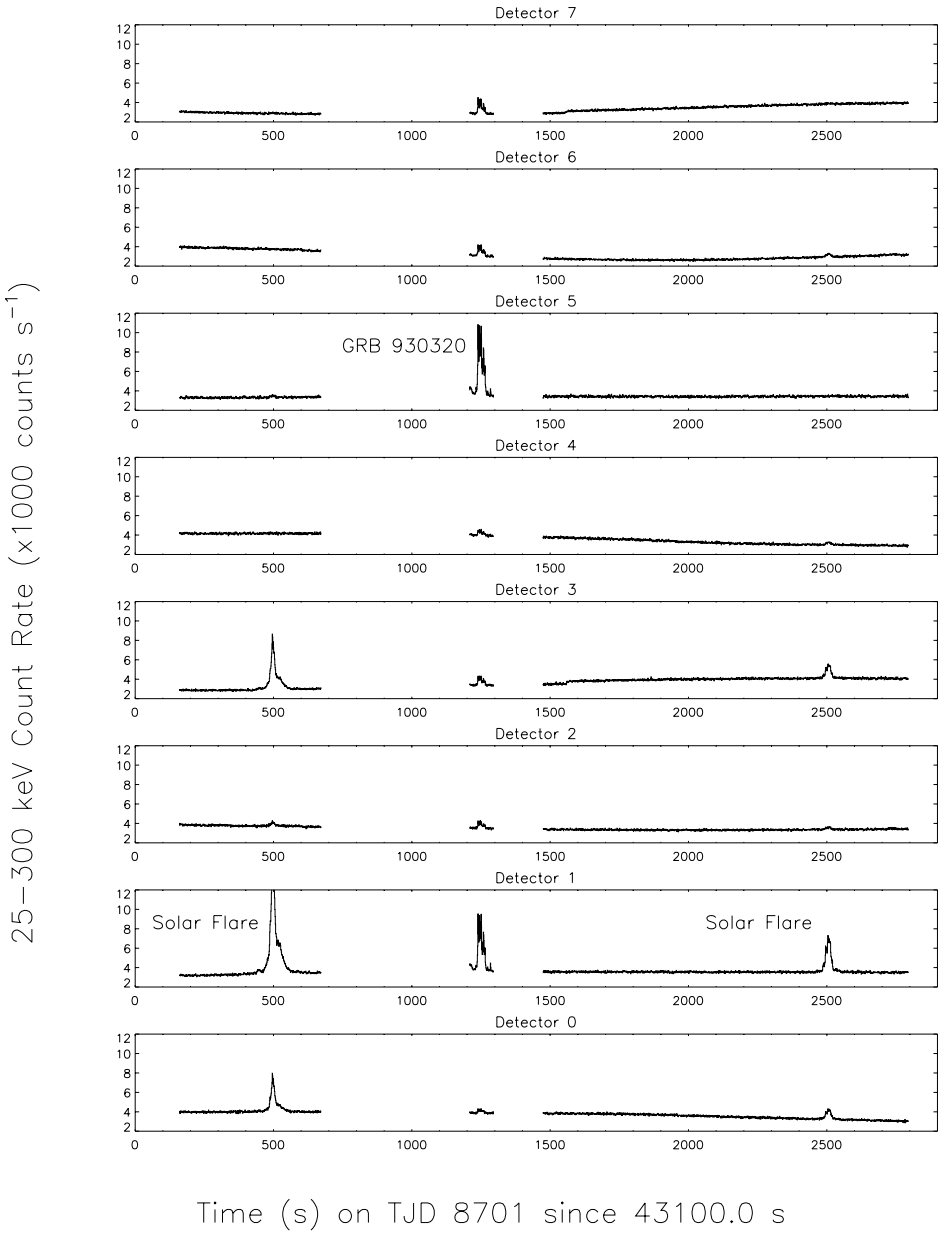

Figure 4-6 Two solar flares and a GRB. Both show an impulsive burst-like shape and are consistent with emission from a point source.

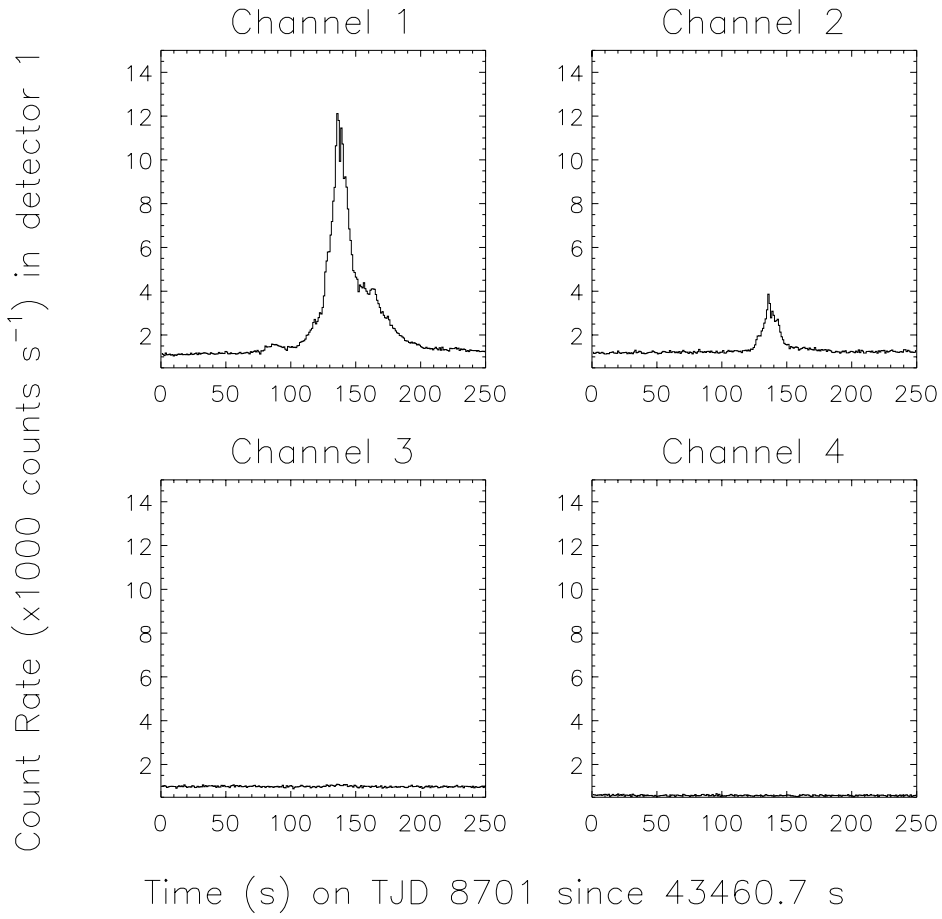

Figure 4-7 Solar flare count rates in the 4 discriminator energy channels. Most of the counts are in the low-energy (25–50 keV) channel, with none apparent in channel 3 (100–300 keV).

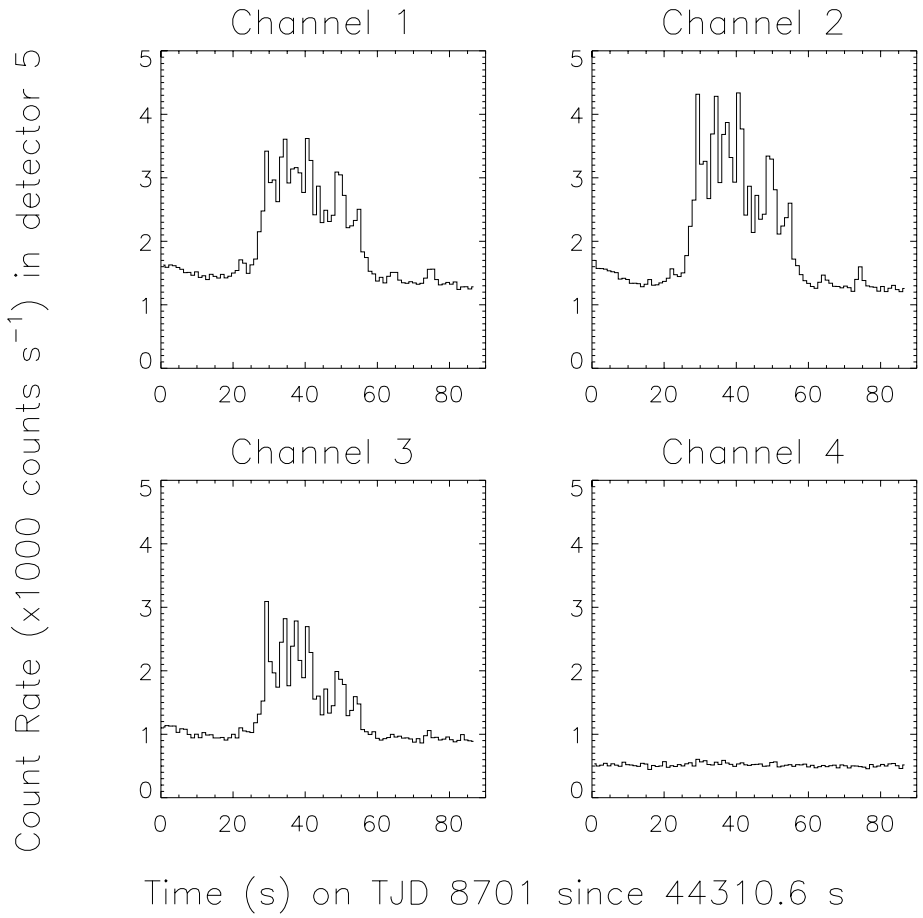

Figure 4-8 Gamma-ray burst in the 4 discriminator energy channels. The GRB shows significant signal in channels 2 and 3 (50–100 and 100–300 keV). The ratios of count rates in channel 1 (25–50 keV) to those in channels 2 and 3 are much smaller than is typical for a solar flare.

4.5.7 Bursts and Flares Associated with Known Sources in Outburst

Some X-ray binaries occasionally show periods of bursting activity lasting from days to months. A dramatic example is the behavior of GRO J1744−28, a transient low-mass X-ray binary pulsar discovered with BATSE (Fishman et al. 1995; Kouveliotou et al. 1996). Over 6000 bursts from this source have been detected with BATSE during the course of two major outbursts in 1995–1996 and 1996–1997. So far this source and 4U 1700−37 (Rubin et al. 1996) are the only X-ray binaries to produce bursts with sufficient brightness, spectral hardness, and frequency to be easily identified in the BATSE data. Occasional "giant pulsations" from Vela X-1 can have a flare-like time profile; but these can be identified based on their pulse profile, source direction, and occurrence during brief intensity outbursts of this source.

An example of a burst from GRO J1744−28 is shown in Figure 4-9. It appears almost exclusively in the lowest discriminator energy channel (25–50 keV). The bursts from this source can be identified based on their soft spectra, source direction, and their occurrence during the known outbursts.

4.5.8 Soft Gamma-Ray Repeaters

Typical bursts from SGRs have durations less than ~ 1 s, so their time profiles are not resolved in the DISCLA data. A burst from a SGR appears as an intense spike occupying one or two 1.024 s time bins with most of its counts in the 25–50 keV channel and no significant signature in the 100–300 keV channel. Figure 4-10 shows how a burst from SGR 1806−20 appears in discriminator channels 1 through 3. Any event that has these spectral characteristics and a source direction consistent with the position of one of the known SGRs is classified as an SGR event. Since SGRs tend to show bursts during periods of activity lasting from days to weeks, more confidence in the association of a given event with a particular SGR can be obtained if it occurs during such a known outburst.

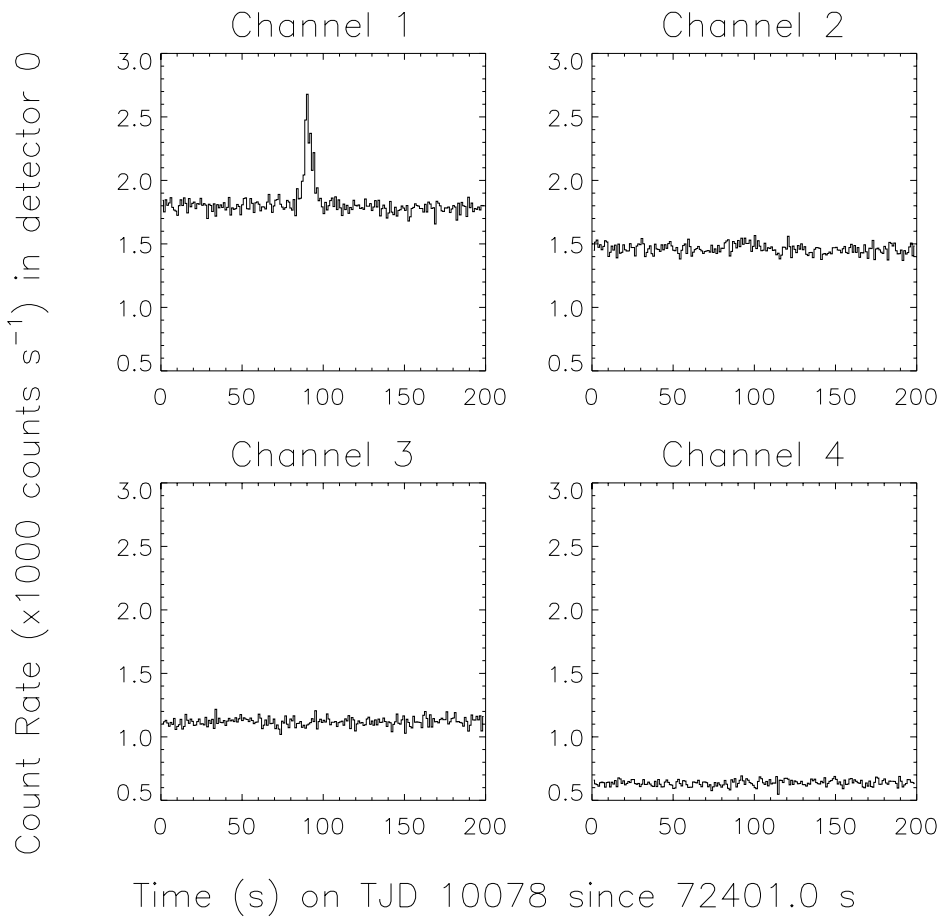

Figure 4-9 X-ray burst from the low-mass X-ray binary pulsar GRO J1744−28.

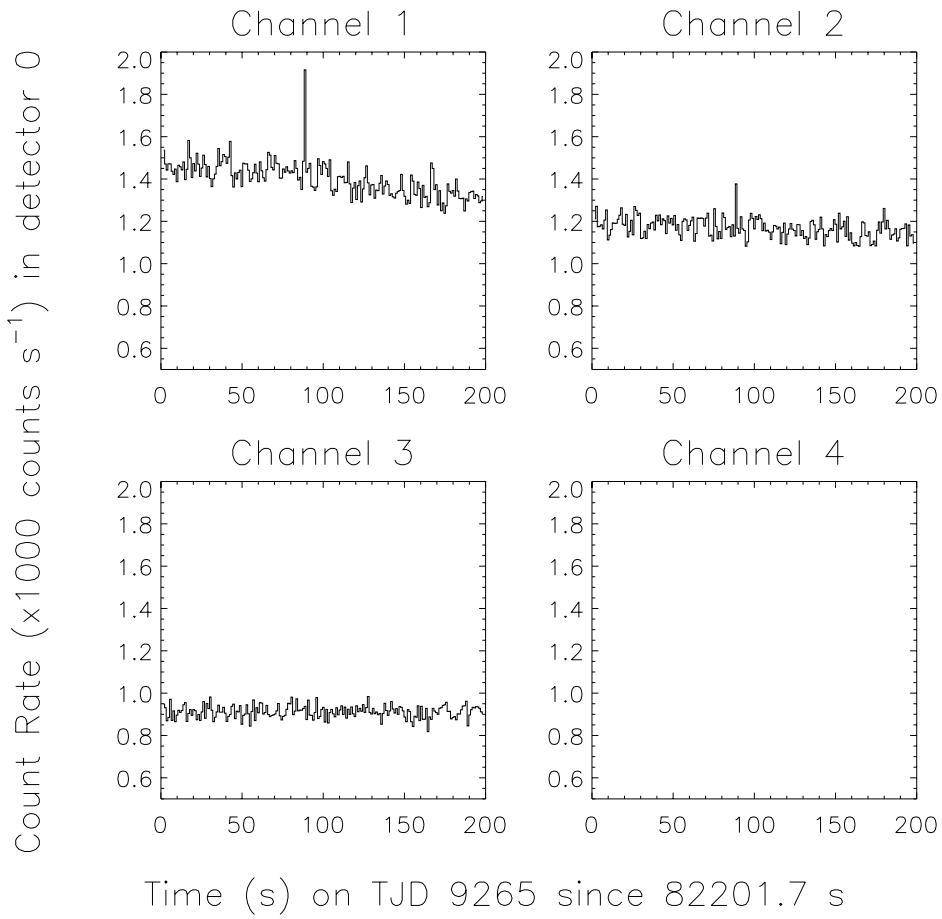

Figure 4-10 A burst from the soft gamma-ray repeater SGR 1806−20. This is DISCLB data, so no count rates are available for discriminator channel 4. The direction of this event is consistent with the SGR, and it occurred during a known outburst of this source.

4.5.9 "Unknown" Low-Energy Events

The off-line search detects a variety of other transients that

1. are not obviously due to magnetospheric particles,
2. appear in the lowest energy channels (25-100 keV),
3. have directions inconsistent with the sun,
4. do not appear to be large fluctuations in the aperiodic variability of a known bright X-ray source, and
5. are not consistent with flares or bursts from SGRs or known X-ray binaries in outburst, such as GRO J1744−28, Vela X-1, and 4U 1700−37.

These low-energy transients constitute a class of events called "unknown low-energy events" because their origin is not clear. They could represent hard-to-classify magnetospheric particle events, bursts and flares from X-ray binaries, the low-energy tail of the GRB spectral distribution, or some as yet unknown burst phenomenon. In fact, it is likely that this class of events represents a combination of all these causes.

Table 4-3. Dipole and quadrupole moments of sky exposure

Statistic[a]	Coordinate System	Moment	Value[b]
$\langle \cos\theta \rangle$	Galactic	Dipole	−0.0100
$\langle \sin^2 b - \frac{1}{3} \rangle$	Galactic	Quadrupole	−0.0049
$\langle \sin\delta \rangle$	Equatorial	Dipole	0.0219
$\langle \sin^2 \delta - \frac{1}{3} \rangle$	Equatorial	Quadrupole	0.0240

[a] θ is the angle between the source direction and the Galactic center, b is the Galactic latitude, and δ is the declination.

[b] Uncertainties in the moments (owing to uncertainties in the sky exposure calculation) are estimated to be ± 0.0002.

Chapter 5

The Nontriggered Event Catalogs

The search described in Chapter 4 yields a database of off-line triggers and their causes as assigned by visual inspection. All of these events are of potential scientific interest, but the focus of the off-line search is to find three particular kinds of events: gamma-ray bursts (GRBs), activity from soft gamma-ray repeaters (SGRs), and low-energy bursts and flares of unknown origin. This chapter discusses the global characteristics of the events that were classified into these three categories.

The catalog tables are found in Appendix A (nontriggered GRBs) and Appendix B (SGR and low-energy events). The bulk of this chapter is devoted to the properties of the GRBs detected by the off-line search. The discussion of the SGR events is brief, because these events can be better studied in detail with other instruments. The catalog of low-energy events of unknown origin shows no clear evidence for any new phenomenon; it is consistent with representing the low-energy tail of the GRB spectral distribution.

5.1 Off-line Triggers

The total number of off-line triggers detected in the search of 6 years of archival data is 371,474. This large number does not directly reflect the number of individual transients that are responsible for the off-line triggers, however. A single transient

can cause from one to hundreds of off-line triggers. For example, a typical $\sim$ 10 s duration GRB may cause 2 to 20 off-line triggers, while a magnetospheric particle precipitation lasting several minutes may cause several hundreds of off-line triggers.

The number of time bins in the DISCLA data for which the 17.408 s background estimate could be formed (for the 1.024 s time scale search) is 133,029,944. The number of bins for which the background could be estimated using information from before and after the time bin being tested is 119,346,281. Thus the total live-time of the search is 1.33×10^8 s. This is 70.0% of the total 1.90×10^8 s spanned by the observations (1991 December 9.0 to 1997 December 17.0).

The rate of off-line triggers varies dramatically according to the activity of the Sun and certain bright X-ray binaries. Figure 5-1 shows ten-day averages of the rate of off-line triggers. The prominent features have been labeled according to the sources responsible for most of the detections. The time period used to experiment with different off-line trigger algorithms and thresholds (TJD 9200–9221) is unfortunately one of the "quietest" time periods in the data. Higher thresholds might have been chosen if this had been known in advance.

The vast majority of off-line triggers are not associated with transients of the sort that are the targets of the off-line search. Most of the off-line triggers are associated with aperiodic variability from bright X-ray binaries in outburst and atmospheric particle precipitations. Table 5-1 shows a breakdown of the causes of off-line triggers as determined from the visual inspection described in section 4.5. This table shows that only about 17% of the off-line triggers are associated with burst-like astronomical transients: GRBs, solar flares, bursts from the X-ray binary GRO J1744−28, bursts from SGRs, and low-energy transients of unknown origin.

5.2 Nontriggered GRB Candidates

There are 2265 bursts (corresponding to $\sim$ 22,000 off-line triggers) that were classified by visual inspection as GRB candidates. Of these, 1392 are onboard triggers that

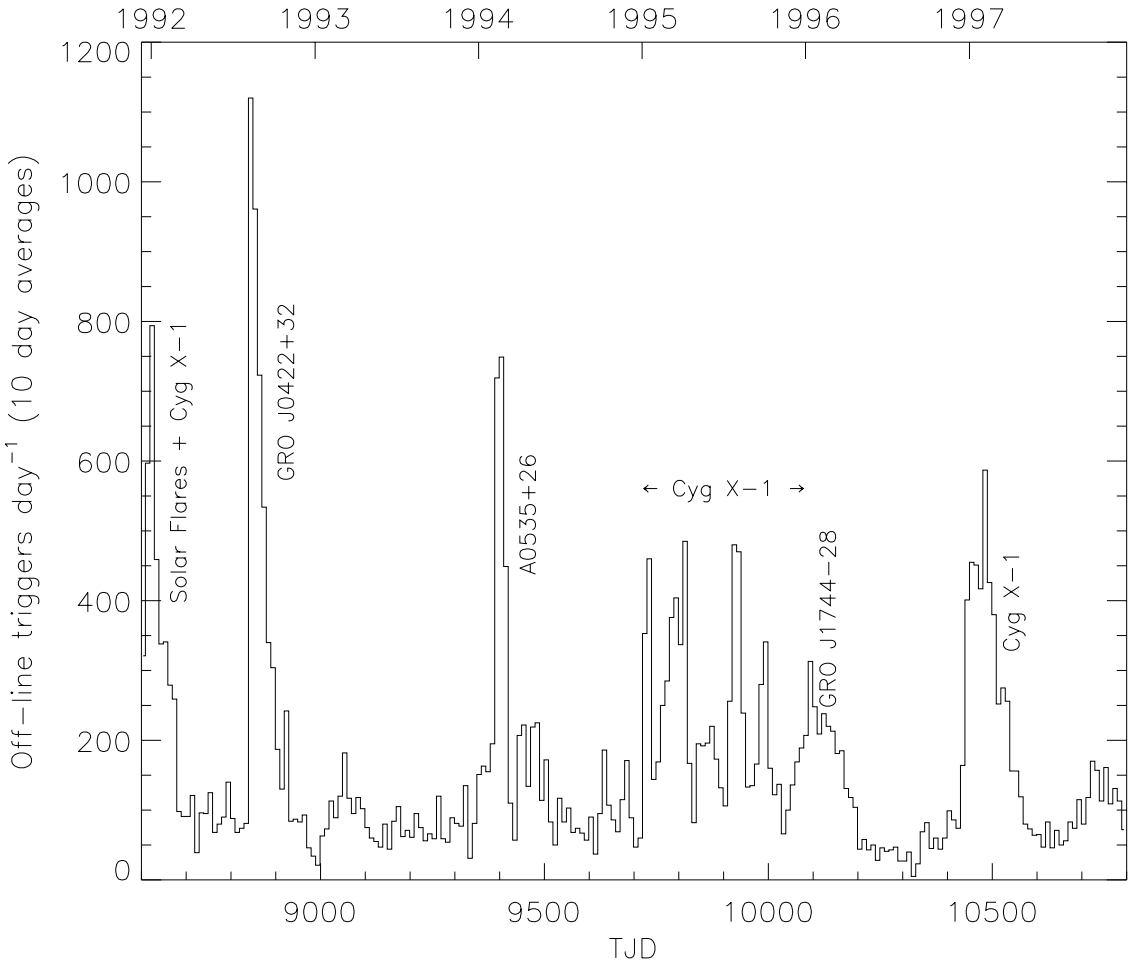

Figure 5-1 The total rate of off-line triggers, shown as 10-day averages. Aperiodic variability from X-ray binaries in outburst is responsible for the most prominent peaks. Selected features are labeled according the source responsible.

are already listed as GRBs in the BATSE trigger catalog (W. Henze, private communication). The onboard trigger numbers for these events are listed in Table A-1. The remaining 873 events that did not activate the onboard burst trigger are the nontriggered GRB candidates. The times, source directions, durations, peak fluxes, and fluences for these events are listed in Table A-2. The union of the 1392 onboard triggered bursts with the 873 nontriggered bursts constitutes a well-defined sample of GRBs found with homogeneous detection criteria.

During the time period covered by the off-line search (TJD 8600.0 through TJD 10800.0) the onboard burst trigger detected 1815 events that are listed in the BATSE trigger catalog as GRBs. The off-line search did *not* detect 423 of these onboard triggers owing to gaps in the DISCLA/DISCLB data and the fact that the 1.024 s time resolution reduces the statistical significance of bursts with durations shorter than about 1 s.

5.3 Estimation of Physical Parameters

The nontriggered GRB catalog (Table A-2) is a supplement to the regular BATSE burst catalogs. The physical parameters listed in it are therefore those that the BATSE team reports for onboard-triggered GRBs (Fishman et al. 1994; Meegan et al. 1996; Paciesas et al. 1999; Meegan et al. 1998a). These quantities are source direction, duration, peak photon flux, fluence, and the ratio of the maximum count rate observed during the burst to the minimum count rate required for detection. This section describes how these parameters are estimated in the off-line search, and it compares the results obtained with the off-line techniques to those obtained by the BATSE team for a suite of 80 onboard-triggered bursts.

The first step in estimating the physical parameters of a burst is to determine background count rates. Using interactive plotting and analysis software, background time intervals are selected from before and after the burst. The data in the selected intervals are used to determine a linear least-squares best-fit polynomial. The back-

ground during the burst is assumed to be the interpolation of this polynomial to the times between the selected intervals. The degree of the polynomial depends on how the background appears to be changing on the time scale of the burst. Typically a polynomial of order 4 or less provides both a good fit to the selected background data and shows reasonable behavior in the intermediate interval where the burst occurs. This procedure is the same as the one used by the BATSE analysis team.

5.3.1 Source Directions

To estimate the source direction, a time interval containing the "main" part of the burst is selected by hand. The purpose of this selection is to obtain optimum signal-to-noise ratios for the average count rates during the burst. The average background-subtracted count rates obtained from the main section of the burst are used to derive a best-fit source direction. The software for this purpose uses the detector and atmospheric response matrices to predict the count rates expected from an event with given physical parameters. Those parameters are the intensity P measured in ph cm^{-2} s^{-1} in a given energy range, the power-law photon spectral index ν (where the photon spectrum is of the form $\phi(E) \propto E^{-\nu}$), and the source direction in terms of the azimuthal and elevation angles (ψ, θ) in *CGRO* coordinates. The best-fit values for these quantities are determined by minimizing the following measure of goodness-of-fit:

$$\chi^2 = \sum_d \sum_i \left[\frac{C_d^i - \tilde{C}_d^i(P, \nu, \psi, \theta)}{\sigma_d^i} \right]^2 , \tag{5.1}$$

where C_d^i denotes the measured count rates in detector d and discriminator channel i, σ_d^i denotes the uncertainties in the measured count rates, and $\tilde{C}_d^i(P, \nu, \psi, \theta)$ denotes the count rates predicted by the response matrices. The sum over detectors is restricted to the 4 detectors that face the given source direction. The sum over energy channels is generally restricted to DISCLA channels 2 and 3 (50–300 keV) for GRB candidates and to channels 1 and 2 (25–100 keV) for bursts from SGRs and other low-energy transients.

The geometry of the BATSE detectors can allow for multiple, widely separated local minima in the χ^2 parameter space. This is especially true for weak bursts that have little or no signal in the third and fourth most brightly illuminated detectors. When most of the counts are in just two detectors, the data can be equally consistent with between 2 and 4 source directions depending on the choice of the third and fourth most brightly illuminated detectors. In the absence of strong signal this choice can be strongly influenced by fluctuations in the count rates due to counting statistics or variability from unrelated background sources. For this reason, the uncertainties in the source directions are determined using a boot-strap Monte Carlo approach. A set of 50 synthetic count rates is generated by sampling from Poisson distributions with the same means and variances as the measured count rates. The best fit locations are determined for these synthetic count rates. The uncertainty in the source direction is the radius (arclength) of the circle on the unit sphere that encloses 34 (68%) of the synthetic best-fit source directions.

5.3.2 Durations

The durations of events are measured using the T_{50} and T_{90} statistics (Kouveliotou et al. 1993). These duration measures are the time intervals during which the total number of counts in the burst increases from 25% to 75% and from 5% to 95%, respectively, of the total counts. They are the same duration measures reported in the BATSE catalogs. The algorithm for computing them and an evaluation of the systematic errors arising from the background modeling is given in Koshut et al. (1996). The intervals chosen for the background fit and the order of the polynomial used to interpolate the background during the burst are subjective, so systematic errors arise depending the burst profile. A particularly problematic case arises for bursts that have extended, low level emission that is difficult to distinguish from background variations. The magnitudes of the systematic errors in the T_{90} duration measure can then be as large as $\sim 20\%$ (Koshut et al. 1996).

For some events, particularly faint ones, background fluctuations cause the dura-

tions estimated by the T_{50}/T_{90} algorithm to be obviously unreliable. These cases are easily identified by visual inspection of the count rate plots that have the boundaries of the duration measures superimposed. In cases where the algorithm fails, estimates of T_{90} and its associated uncertainty are made by visual inspection of the burst profile.

5.3.3 Peak Photon Fluxes

The photon spectrum of an event is assumed to be a simple power-law over the energy range of interest (50–300 keV for GRB candidates, 25–100 keV for low-energy events). The best-fit peak photon flux is determined by minimizing equation 5.1 with respect to P and ν. The count rates used for the minimization are the count rates observed in the detectors during the 1.024 s time bin for which the summed count rate (above background) in the two most brightly illuminated detectors is a maximum. The source direction is fixed at the best-fit value found previously using the more precise count rates averaged over the "main" portion of the burst.

This procedure is somewhat different from that used to derive the peak fluxes listed in the BATSE catalogs. For bursts that caused an onboard trigger, data types are available with time resolution better than 1.024 s. The peak fluxes in the BATSE catalogs make use of data with 64 ms time resolution to find the optimum placement of a 1.024 s window that yields the highest count rate averaged over that window (Pendleton et al. 1996b). In contrast, the DISCLA data used for the off-line analysis do not allow the freedom to choose the phase of the 1.024 s window that contains the most counts from the burst. In the worst case, the 1.024 s window used by the BATSE team may get split into two DISCLA time bins, so the peak flux determined with the off-line search will be lower by a factor of ~ 2. The BATSE catalogs also use a more sophisticated model of the GRB photon spectrum when estimating peak fluxes and fluences (Pendleton et al. 1996b).

5.3.4 Fluences

The estimates of burst fluence make use of the count rates (above background) from the T_{90} interval. The fluence F is estimated by the formula $F = cTP\langle E\rangle$, where $c = 1.602 \times 10^{-9}$ erg keV^{-1} is a conversion factor from keV to erg, T is the duration of the time interval over which the fluence is estimated (usually $T_{90}/0.9$), P is the average photon flux over the time interval T, and $\langle E\rangle$ is the mean photon energy of the (best-fit power-law) photon spectrum in the energy range of interest. GRBs often show some degree of spectral softening over their duration, so events with T_{90} longer than 4.096 s are partitioned into 4.096 s sub-intervals and the total fluence is obtained by summing the fluences estimated for each sub-interval. For bursts with T_{90} less than 4.096 s, the T_{90} interval itself is used.

5.3.5 $C_{\max}/C_{\min}$

The ratio of the maximum count rate detected during the burst to the minimum count rate required for detection is more complicated for the off-line trigger than for the onboard trigger. The conditions for an onboard trigger depend on the count rates in a single detector: the one with the second highest number of counts above the background estimate. In contrast, the off-line trigger depends not only on the values of the count rates in two detectors but on their ratio. Let s_1 and s_2 denote the significances of the most significant and second most significant detector, respectively. As can be seen from Figure 4-1 the source intensity required for detection could be determined either by the point at which s_2 falls below M or the point at which the sum $s_1 + s_2$ falls below Σ; which of these alternatives is chosen is determined by the ratio of s_1 to s_2.

5.3.6 Accuracy of Off-line Burst Parameters

A sample of 80 onboard-triggered GRBs that were also detected with the off-line search provides a basis for evaluating the accuracy of the physical burst parameters

derived using the techniques described above. The source directions, peak fluxes, fluences, and durations derived using the off-line search techniques can be compared to the values derived by the BATSE team and published in the current BATSE catalog (Meegan et al. 1998a).

A measure of the disagreement between the estimates produced by each method is provided by the difference in best-fit values divided by the uncertainty in the difference, as given by the statistical error estimates associated with each measurement. The formula for the "measurement disagreement" Δ is:

$$\Delta = \frac{X_B - X_O}{\sqrt{\sigma_B^2 + \sigma_O^2 + \sigma_{\rm sys}^2}}, \tag{5.2}$$

where X_B and X_O denote the values of a physical quantity estimated by the BATSE team and by the off-line search methods, respectively; σ_B and σ_O denote the estimates of the statistical uncertainties in each estimate; and $\sigma_{\rm sys}$ denotes estimated contributions to the uncertainties from random systematic errors. In the case of source directions, the arclength on the unit sphere is used as the "difference" between the source directions. Figure 5-2 shows histograms of the measurement disagreement for the 80 onboard-triggered bursts used in the comparison. Dotted histograms do not include any contribution from random systematic errors ($\sigma_{\rm sys} = 0$), while solid histograms do. The figure shows that the physical quantities estimated with the off-line search methods agree reasonably well with those estimated by the BATSE team.

The direction estimates in the BATSE catalog are estimated to contain a systematic uncertainty of $\sigma_{\rm sys} = 1.6^\circ$ to be added in quadrature to the quoted statistical uncertainties; that is, the uncertainty the direction to a burst with a 2.0° statistical error is $\sigma = \sqrt{(1.6^\circ)^2 + (2.0^\circ)^2} = 2.6^\circ$ (Paciesas et al. 1999). The magnitudes of the systematic errors are estimated by finding directions for transients from sources with well-known coordinates, such as Cyg X-1, the Sun, and GRBs localized by arrival-time triangulation with the Interplanetary Network. Using a suite of solar flares and X-ray

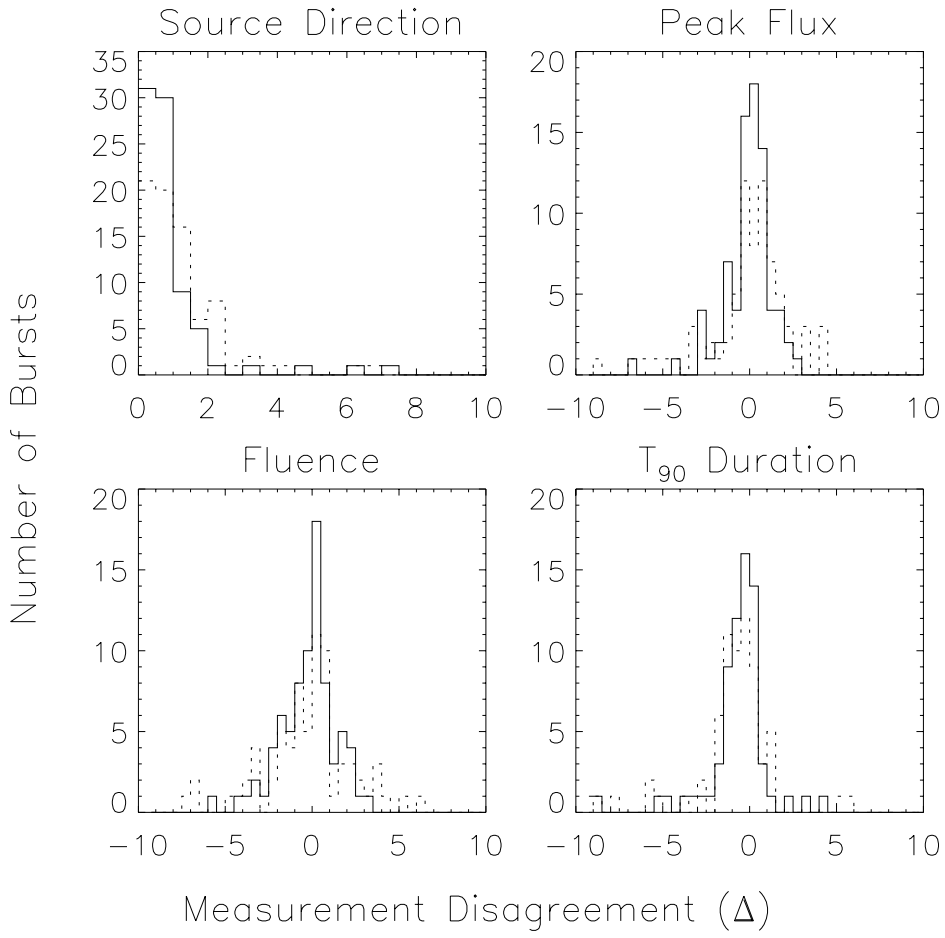

Figure 5-2 Histograms of the relative disagreement in measurements of burst properties. The measurement disagreement (Δ) is defined as the difference between the off-line estimate and the BATSE team's estimate divided by the uncertainty in the difference. The uncertainty in the difference combines the statistical uncertainties of each measurement in quadrature with an estimate of random systematic uncertainties.

bursts from GRO J1744−28 the systematic uncertainty in the off-line search source directions is estimated to be approximately 4°, to be added in quadrature to the statistical uncertainties reported in the catalog. The systematic error contributions used to make the solid histogram for the source direction comparison in Figure 5-2 contain both the 1.6° and the 4° contributions to $\sigma_{\rm sys}$. With systematic uncertainties included, 76% of the measurement disagreements are less than $\Delta = 1.0$, and 94% are less than $\Delta = 2.0$.

The peak fluxes listed in the BATSE catalogs have systematic uncertainties on the order of 20% (Paciesas et al. 1999). If a 20% random systematic uncertainty is added in quadrature to the statistical uncertainties of the off-line peak fluxes, then 76% of the bursts have measurement disagreements less than $\Delta = 1.0$ and 93% have disagreements less than $\Delta = 2.0$.

The fluences are particularly prone to systematic errors. They depend on the duration of the burst, which may be hard to determine if there are long "tails" of low level emission that could be confused with background. They depend on the model of the photon spectrum, and the simple power-law that is used in the off-line analysis may be inadequate in some bursts. With a 20% uncertainty added in quadrature to the statistical uncertainties in the off-line fluences, 55% of the bursts have measurement disagreements less than $\Delta = 1.0$ and 79% have disagreements less than $\Delta = 2.0$.

The durations are also prone to systematic errors related to the choice of background intervals. For many bursts it is difficult to distinguish low-level emission from background variations. If a 20% uncertainty is added in quadrature to the statistical uncertainties of the off-line durations, 56% of the durations have measurement disagreements less than $\Delta = 1.0$ and 73% have disagreements less than $\Delta = 2.0$.

5.4 Classification Accuracy

The classification of the off-line triggers is subjective in cases where there is not a clear indication of the nature of the event. Furthermore, with over 370,000 off-line triggers to classify, human error is inevitable. The ambiguous cases are fortunately relatively rare. A comparison of event classifications assigned in the present investigation with those assigned by the BATSE team is discussed in section C.5. For the work described there, covering TJD 9000 through 9345, all events were classified without knowledge of what classifications the BATSE team assigned to the onboard triggers. The results show that 89% of the classifications assigned in the off-line search agree with those assigned by the BATSE team. The two dominant sources of disagreements are hard (GRB-like) events that occur in the direction of the Sun and events that were difficult to classify (using DISCLA data alone) because they showed very little signal, owing to duration shorter than the time resolution of the data. In these ambiguous cases the classifications assigned in the off-line search tended to prefer a non-GRB origin.

This section re-examines the extent to which two kinds of classification errors have affected the catalog of nontriggered GRBs. The first possible error is the classification of an event as a GRB when it is really caused by something else (such as a solar flare or particle precipitation). This produces contamination in the catalog of GRBs. The second possible error is the rejection of a genuine GRB as some other phenomenon. This may occur owing to human error or ambiguity in the characteristics of the event, and it produces incompleteness in the catalog of GRBs.

5.4.1 Contamination by Non-GRB Events

The class of events identified as nontriggered GRBs can be examined for contamination by solar flares and magnetospheric particle precipitation events. Figure 5-3 shows the histogram of angles between the Sun and the source direction for the nontriggered GRBs. The solid line shows the expectation for GRB directions distributed randomly with respect to the solar direction. This histogram shows no evidence for an excess of

events in the direction of the Sun, nor for a substantial deficit. It appears that there is no significant contamination by solar flares, nor is there a dramatic "blind spot" for nontriggered GRBs in the direction of the Sun (but see section 5.5).

Significant contamination of the nontriggered GRB sample by auroral X-rays (magnetospheric particle precipitation events occurring at some distance from the spacecraft) is expected to appear as an excess of events detected from directions near the limb of the Earth. Figure 5-4 shows the histogram of angles between the direction of the center of the Earth and the source directions of the nontriggered GRB candidates. The dotted line shows the approximate location of the Earth's limb (the exact angle varies with the altitude of the spacecraft). The distribution of angles does not cut off sharply at the Earth's limb because of the smearing effect of occasionally large direction uncertainties. There is no evidence in this figure for a significant contribution from auroral X-ray events in the nontriggered GRB sample.

Contamination of the nontriggered GRB sample by particle precipitations in the vicinity of the spacecraft would appear as an excess of events detected while the satellite is at geographic locations where particle precipitations are more frequent. Local particle precipitation events typically occur at the extreme geographic latitudes of the orbit where the spacecraft enters a higher geomagnetic L-shell. There are certain other geographic locations where VLF transmitters cause an excess frequency of particle precipitation events (see section 2.4.2), and the onboard trigger is disabled while the spacecraft passes over these regions. Figure 5-5 shows the geographic locations of *CGRO* at the times when the nontriggered GRBs were detected. The nontriggered GRBs occur more frequently at the extreme latitudes of the orbit, but this is to be expected because the spacecraft spends most of its time at extreme latitudes. Also, the sample of nontriggered GRBs is expected to show some excess of bursts detected while the spacecraft is above the geographic locations where the onboard burst trigger is temporarily disabled.

Figure 5-6 compares a histogram of the geographic latitudes of *CGRO* when the nontriggered GRBs were detected (upper panel) with the relative amount of time

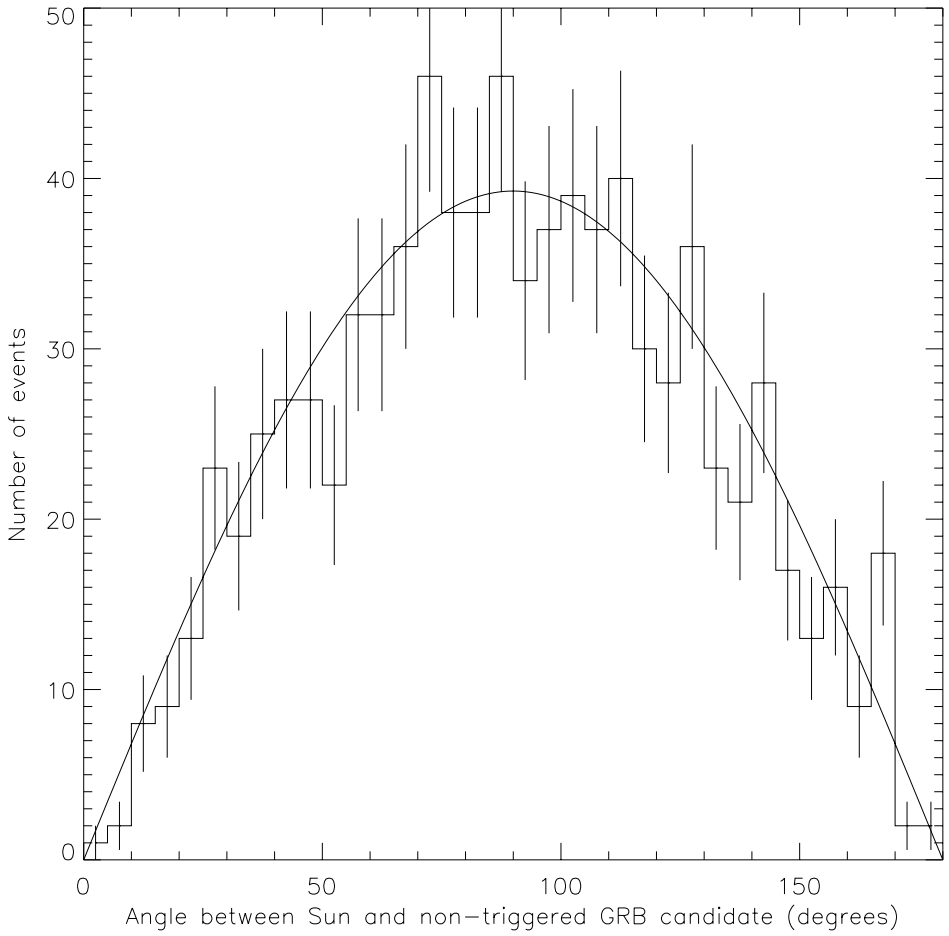

Figure 5-3 Histogram of angles between nontriggered GRB sources and the Sun. The solid line shows the expectation for direction distributed randomly with respect to the direction of the Sun, as is expected for GRBs. There is no evidence for an excess or large deficiency of nontriggered GRB candidates in the direction of the Sun.

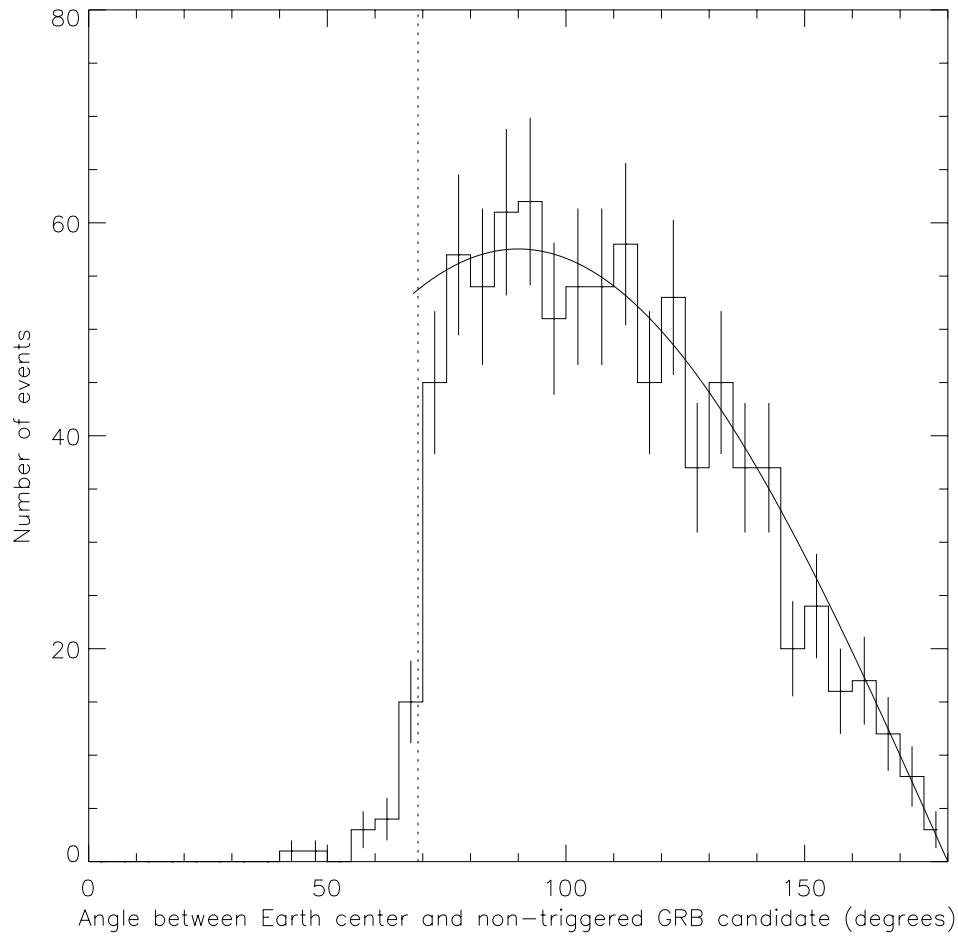

Figure 5-4 Histogram of angles between nontriggered GRB sources and the Earth's center. The solid line shows the expectation for direction distributed randomly with respect to the direction of the Earth's center, as is expected for GRBs. There is no evidence for a large excess of directions near the Earth's limb, as would be expected if there were substantial contamination from auroral X-rays.

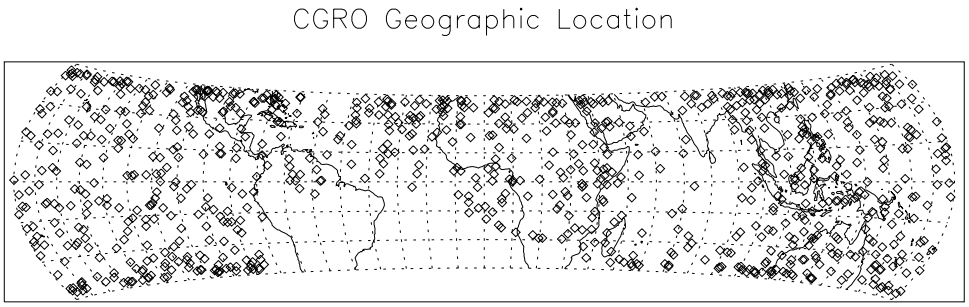

Figure 5-5 Geographic location of *CGRO* at the times when the nontriggered GRB candidates were detected. The excess of events at the extreme latitudes of the orbit is expected because that is where the spacecraft spends most of its time. There is an absence of bursts detected over the South Atlantic Ocean because the high voltage supply to the detectors is turned off while the spacecraft travels through the SAA. The paucity of bursts detected over the Indian Ocean is due to telemetry gaps that occur in between contacts with the *TDRSS* satellites.

spent by the spacecraft at a given latitude (lower panel). The qualitative agreement suggests there is no great contamination of the nontriggered GRB sample by local particle precipitation events. Precise quantitative agreement cannot be expected because of the many reasons why a GRB might be nontriggered, which make it difficult to estimate an appropriate "live-time" for sensitivity to *strictly nontriggered* GRBs.

5.4.2 Incompleteness by Misclassification of GRBs

Even if it is rare that an event gets classified as a GRB when it is in fact something else, the converse possibility still exists: that some fraction of genuine GRBs get classified as some other kind of phenomenon (such as solar flares or particle precipitations). In the absence of an independent set of event classifications, one way to estimate how many GRBs have been classified as something else is to review the off-line triggers and their classifications to look for ambiguous cases or examples of simple human error.

For 77 days of data distributed throughout the mission, a secondary review of the off-line triggers reveals 3 events that are likely to be GRBs, but that were classified as something else (owing to human error or to ambiguity in the characteristics of the event). The total live-time of the search during these 77 days is 4.6×10^6 s. To estimate the number of GRBs missed (due to misclassification) in the entire 6 years of the search, it is assumed that the rate of misclassified bursts is constant and that the number of bursts that are misclassified in a given time interval is distributed according to the Poisson distribution. Then the likelihood function (Loredo 1992) for the rate of missed bursts when 3 events are observed in 4.6×10^6 s has a maximum at 6.5×10^{-7} s^{-1}. This corresponds to a most likely value of 86 genuine GRBs that have been classified as non-GRB phenomena in the entire off-line search. The limits of the central 90% confidence interval indicate that between 50 and 200 bursts have been misclassified. This corresponds to a "loss rate" for GRBs of between 2% and 8% (most likely 4%) of the total 2265 detected.

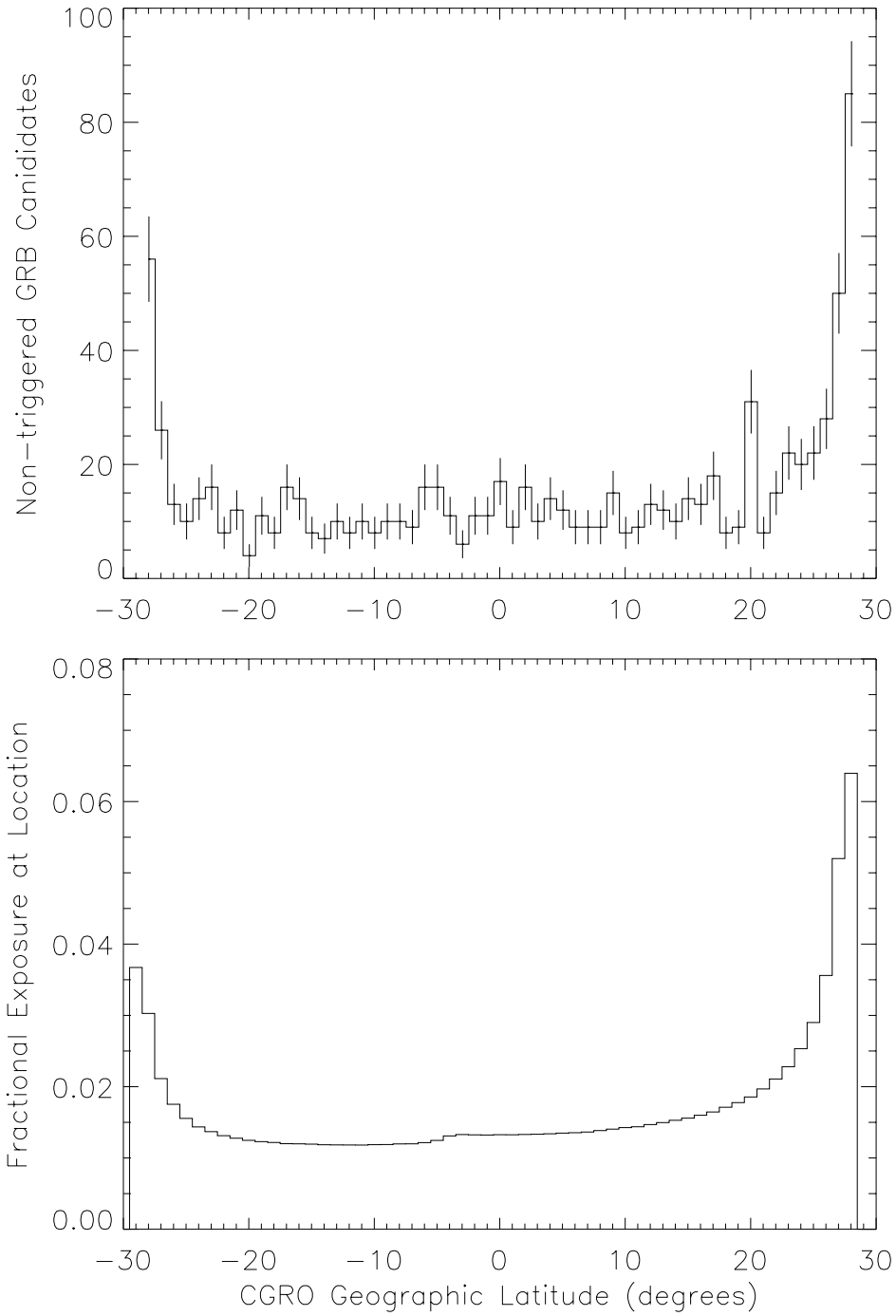

Figure 5-6 Histograms of *CGRO* geographic latitudes. The upper panel shows the histogram of latitudes where nontriggered GRBs were detected. The lower panel shows the relative amount of time that *CGRO* spends at a given latitude. The qualitative agreement shows no evidence for significant contamination of the nontriggered GRB sample by particle precipitation events at extreme latitudes.

5.5 GRB Direction Distribution

The direction distribution of the nontriggered GRB candidates is shown in Figure 5-7. There are a number of statistics to test the hypothesis that these directions are isotropic (Briggs et al. 1996). Table 5-2 lists the dipole and quadrupole moments in equatorial and Galactic coordinates for the nontriggered GRB candidates alone and for the combined sample of triggered and nontriggered GRBs that were detected by the off-line search. The moments in the table have been corrected for the sky exposure shown in Figure 4-2. The dipole and quadrupole moments in Galactic coordinates are sensitive to concentrations towards the Galactic center and the Galactic plane, respectively. The dipole and quadrupole moments in equatorial coordinates are sensitive to concentrations towards Earth's North pole and towards Earth's poles, respectively (Briggs et al. 1996). There is no significant evidence for anisotropy in these samples.

The faintest bursts detected with the off-line search are those below the onboard detection threshold. A "faint" sample of GRBs can be defined by taking only those bursts with peak fluxes (on the 1.024 s time scale in 50–300 keV) that are less than 0.3 ph cm^{-2} s^{-1}, the approximate onboard threshold for 50% detection probability (Paciesas et al. 1999). In this sample there are 669 bursts, of which 551 are strictly nontriggered GRBs and 118 were also detected with the onboard trigger. The dipole and quadrupole moments for this sample are given in Table 5-2. They show marginal (2σ) evidence for clustering near the poles of the equatorial coordinate system. This is almost certainly due to systematic classification errors. There is a tendency to classify events that arrive from source directions consistent with the Sun as solar flares (see section C.5). A faint GRB arriving from a direction near the Sun is more likely to have characteristics such that it would be difficult to argue that it is *not* a solar flare; thus the event would likely be assigned to the solar flare category. In such cases, some GRBs will be "lost" from the nontriggered GRB catalog because they are classified as solar flares (as previously discussed in section 5.4).

Table 5-1. Some causes of off-line triggers

Cause of Off-line Trigger	% of Off-line Triggers
Aperiodic variability from X-ray binaries and particle precipitations	70
Occultation steps	13
GRBs	6
Solar flares	4
GRO J1744−28	6
Other (including SGRs, low-energy unknown events)	1

Table 5-2. Dipole and quadrupole statistics for nontriggered GRBs

Statistic[a]	Sample	Coordinate System	Moment Tested	Value[b]
$\langle \cos\theta \rangle$	Nontriggered	Galactic	Dipole	-0.0029 ± 0.0195
$\langle \sin^2 b - \frac{1}{3} \rangle$	Nontriggered	Galactic	Quadrupole	-0.0015 ± 0.0101
$\langle \sin\delta \rangle$	Nontriggered	Equatorial	Dipole	0.0087 ± 0.0195
$\langle \sin^2 \delta - \frac{1}{3} \rangle$	Nontriggered	Equatorial	Quadrupole	0.0191 ± 0.0101
$\langle \cos\theta \rangle$	Combined	Galactic	Dipole	-0.0063 ± 0.0121
$\langle \sin^2 b - \frac{1}{3} \rangle$	Combined	Galactic	Quadrupole	0.0018 ± 0.0063
$\langle \sin\delta \rangle$	Combined	Equatorial	Dipole	0.0077 ± 0.0121
$\langle \sin^2 \delta - \frac{1}{3} \rangle$	Combined	Equatorial	Quadrupole	0.0085 ± 0.0063
$\langle \cos\theta \rangle$	$P < 0.3$ ph cm^{-2} s^{-1}	Galactic	Dipole	-0.0352 ± 0.0223
$\langle \sin^2 b - \frac{1}{3} \rangle$	$P < 0.3$ ph cm^{-2} s^{-1}	Galactic	Quadrupole	0.0011 ± 0.0115
$\langle \sin\delta \rangle$	$P < 0.3$ ph cm^{-2} s^{-1}	Equatorial	Dipole	0.0526 ± 0.0223
$\langle \sin^2 \delta - \frac{1}{3} \rangle$	$P < 0.3$ ph cm^{-2} s^{-1}	Equatorial	Quadrupole	0.0293 ± 0.0115

[a] θ is the angle between the source direction and the Galactic center, b is the Galactic latitude, and δ is the declination.

[b] Moments are corrected for sky exposure.

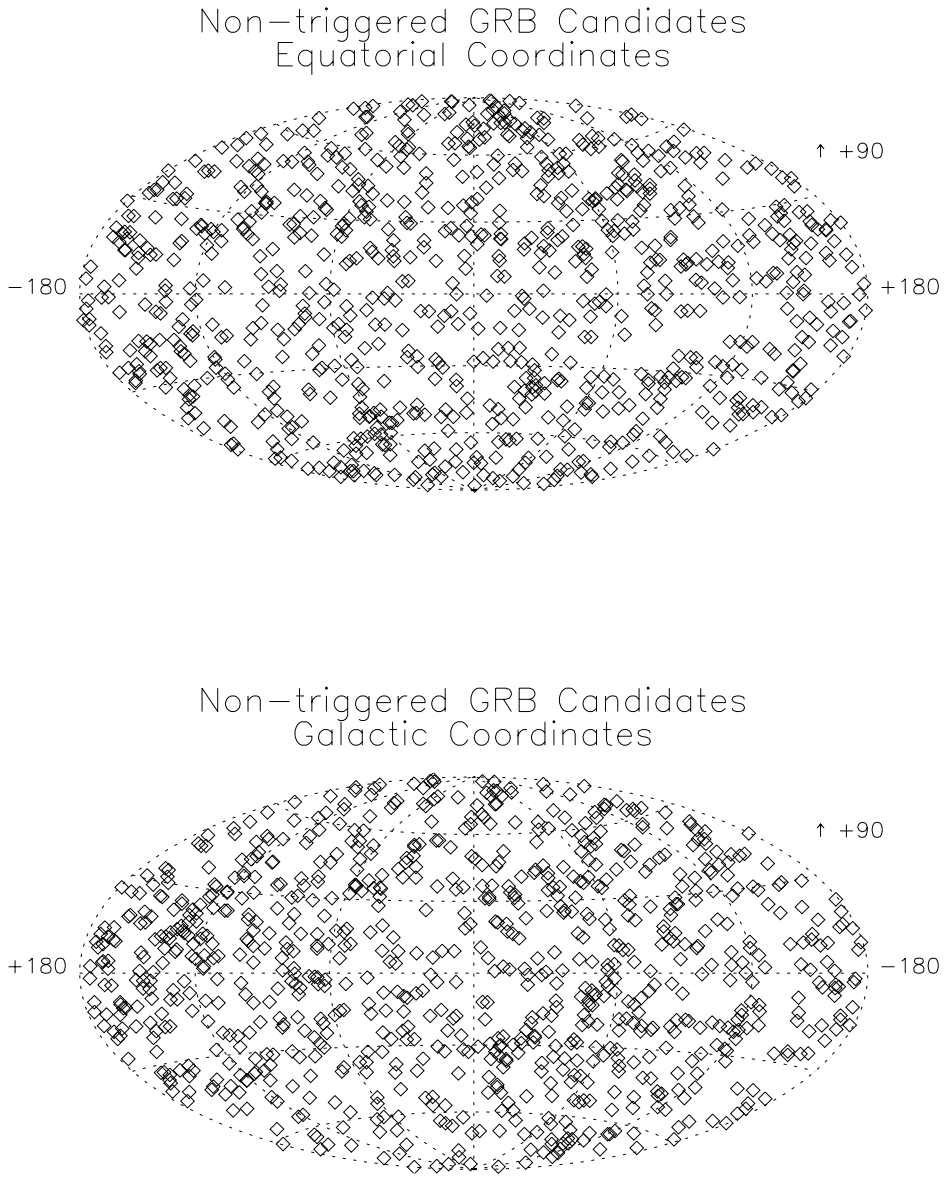

Figure 5-7 The best-fit source directions for the nontriggered GRB candidates. The median direction uncertainty is 6°.

5.6 GRB Duration Distribution

The T_{90} durations of the nontriggered GRB candidates range from 1.024 s (the minimum that can be measured with DISCLA data) to 280 s. The longest burst detected with the off-line search is one that caused an onboard trigger and has $T_{90} = 674$ s (Meegan et al. 1998a). Figure 5-8 shows the duration distributions of the nontriggered GRB candidates only (solid histogram) and of the onboard-triggered bursts that were detected with the off-line search (dashed histogram). The similar shapes of the two curves above durations of $T_{90} = 2.048$ s indicates that the bursts detected with the off-line search have approximately the same duration distribution as those detected onboard. The figure also shows that the off-line search has difficulty detecting bursts with durations less than $T_{90} \approx 1.024$ s. Evidently the off-line search is not detecting any new burst population based on duration.

5.7 GRB Rate

The rate at which the off-line search detects GRBs is shown as a function of time in Figure 5-9. The upper panel shows the raw histogram of GRB arrival times. The corresponding GRB rates, corrected for live-time and sky exposure, are shown in the lower panel. These rates are *not* corrected for variations in sensitivity owing to long-term variations in the particle and cosmic background rates due to the decay and re-boost of the spacecraft orbit. These rates also do not completely reflect the contribution of the "short" ($T_{90} < 1$ s) GRBs because of the difficulty in detecting such events in the DISCLA data.

The mean all-sky GRB rate for the off-line search is 2.13 ± 0.07 day^{-1}. Although the rate is fairly constant over the course of the off-line search, there are variations. The data are only marginally consistent with a constant GRB rate. Assuming that the mean rate is the "true" rate, the value of the reduced χ^2 statistic for the data in the figure is 1.54 for 43 degrees of freedom; the probability of exceeding this value

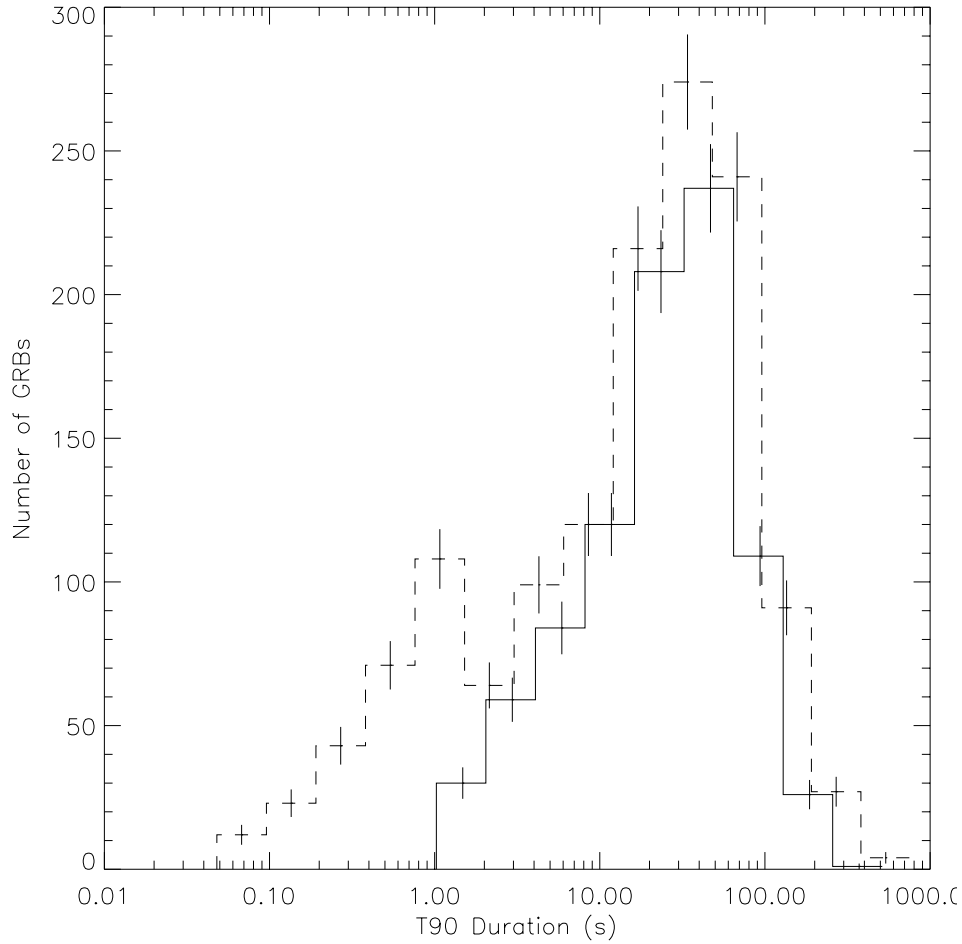

Figure 5-8 The duration distribution of GRBs detected with the off-line search. The dashed line indicates the duration histogram for GRBs that also triggered onboard; the durations are the values measured from the high-resolution triggered data types as listed in the 4B catalog (Paciesas et al. 1999). The solid line indicates the duration distribution of the nontriggered GRB candidates. The shapes are very similar at durations greater than $\sim$ 2 s. This shows that the off-line search is not detecting a population of bursts with durations significantly different from those detected onboard.

by chance is 0.013. The deviations from the mean rate likely reflect variations in observing conditions (owing to changes in the background rates and the activity of bright X-ray sources) and occasional inconsistencies in the visual classifications.

5.8 SGR Events

The SGRs that have caused onboard burst triggers during the time period of the off-line search are SGR 1900+14 (Kouveliotou et al. 1993) and SGR 1806−20 (Kouveliotou et al. 1994; Kouveliotou et al. 1996). The bursts from these sources exhibit short durations (< 1.024 s) and show a very intense (> 500 counts s^{-1}) signal in the 25–50 keV and 50–100 keV discriminator channels, with no significant signal in the 100–300 keV channel. The bursts tend to arrive with separations of hours to weeks as part of outbursts that are separated by months to years.

There are 25 nontriggered events that clearly appear to have characteristics typical of bursts from SGRs: short duration, soft spectrum, and > 500 counts s^{-1} in discriminator channels 1 and 2. They are listed in Table B-1. All but two have source directions consistent with SGR 1806−20. Figure 5-10 shows a sky map of the source directions. The 23 bursts that are directionally consistent with SGR 1806−20 have arrival times during known periods of activity from this source. One of the bursts that is directionally inconsistent with this source, the one with a best fit location at Galactic longitude $l = 32°$ and latitude $b = -40°$, also occurred during a period of known activity from SGR 1806−20; thus this event probably originates from SGR 1806−20 and represents a poor estimation of the source direction.

The remaining event that has a source direction inconsistent with SGR 1806−20 did not occur during a known outburst of that source and could represent emission from a previously unknown SGR source. This event, NTB 941022.58, has a position that is clearly inconsistent with any of the known SGR sources. The large uncertainty in its source direction makes any definitive identification impossible, however. The GRB monitor onboard *Ulysses* has complete data for 1000 s before and after these,

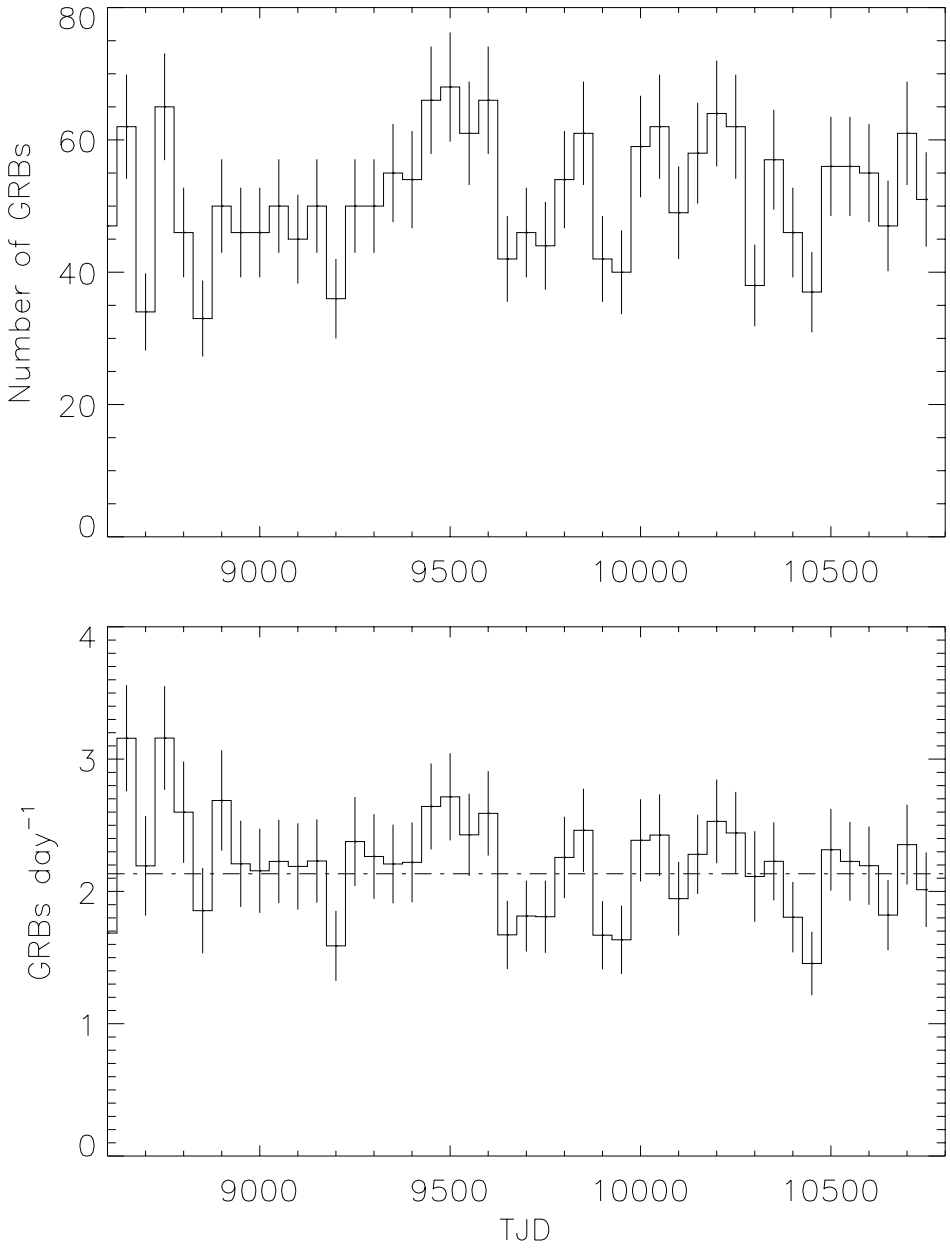

Figure 5-9 The detection rate of GRBs in the off-line search. The upper panel shows the histogram of GRB arrival times. The lower panel shows the number of GRBs detected in a 50-day time bin divided by the exposure during that time. The exposure is the live-time of the search divided by the fraction of the sky visible to the detectors. The mean GRB rate is 2.13 ± 0.07 day^{-1}.

but no burst is detected. It is possible that this event is a short, soft-spectrum GRB or an unusual magnetospheric particle event.

5.9 "Unknown" Low-Energy Events

Events that do not have the obvious signatures of terrestrial phenomena, instrumental effects, solar flares, GRBs, bursts from SGRs, or bursts from X-ray binaries are put into the "unknown" category. Membership in this category does not rule out any of these causes, however. It just means that there is not enough information to make a confident identification. Thus the unknown category is almost certainly a mix of events from a variety of sources. In fact, of the 125 events that originally constituted this class, only 50 remain listed. The 75 discarded events appear in retrospect (upon closer examination) to be due to magnetospheric particle precipitations or to aperiodic variability from known X-ray binaries in outburst. This kind of revision shows that the "unknown" low-energy events are identified less reliably than those classified as GRBs and SGRs.

The 50 "unknown" low-energy events are listed in Table B-2. As discussed in the following sections, it is likely that a variety of burst phenomena are represented in this class of events. Their directional isotropy and spectral characteristics are consistent with the hypothesis that some or all of them represent the low-energy tail of the GRB spectral distribution. The fact that their arrival times are not consistent with a constant rate could indicate the presence of sporadic burst phenomena or it could simply be the result of variations in observing conditions.

5.9.1 Direction Distribution

The direction distribution of the 50 low-energy events is consistent with isotropy. Figure 5-11 shows sky maps of the best-fit source directions in equatorial and Galactic coordinates. There is no obvious clustering of burst directions. Table 5-3 gives the values of the dipole and quadrupole statistics for these events.

The distribution of geocenter angles (the angles between the source directions and the center of the Earth) is consistent with a sample of transients from astronomical sources. Figure 5-12 shows the cumulative distribution of the geocenter angles along with the cumulative distribution expected from an isotropic population of astronomical sources. The Kolomogorov-Smirnov (K-S) statistic D (Press et al. 1995) for these angles is $D = 0.11$ using the null hypothesis that the distribution of source directions is proportional to the solid angle of sky not blocked by the Earth. The probability that this value or a larger one is obtained is 0.57, indicating that the data are consistent with the null hypothesis.

Like the distribution of geocenter angles, the distribution of angles between the Sun and the directions of the "unknown" events is consistent with an astronomical origin. The K-S statistic is $D = 0.13$ using the null hypothesis that the distribution of source directions is isotropic. The corresponding probability is 0.38, showing that the data are compatible with the null hypothesis.

5.9.2 Spectral Hardness

The distribution of instrumental hardness ratios for the unknown events is a function of the classification process. The unknown events are selected to be those events that appear to be spectrally softer than is typical for GRBs but that cannot be obviously assigned to some other cause, such as a magnetospheric particle precipitation or solar flare. A crude way to characterize the spectral characteristics of these events is with an instrumental hardness ratio, the ratio of the mean count rates in two energy bands. Figure 5-13 shows hardness ratios for the nontriggered GRB candidates (points) and for the "unknown" events (diamonds with error bars). The horizontal axis shows the ratio of mean count rates in discriminator channel 1 to those in the sum of channels 1 and 2. Likewise, the vertical axis shows the ratio of mean count rates in discriminator channel 3 to the sum of those in channels 2 and 3. The "unknown" events are spectrally softer because they were chosen to be. The large uncertainties associated with their position on this diagram is a symptom of the fact that they are

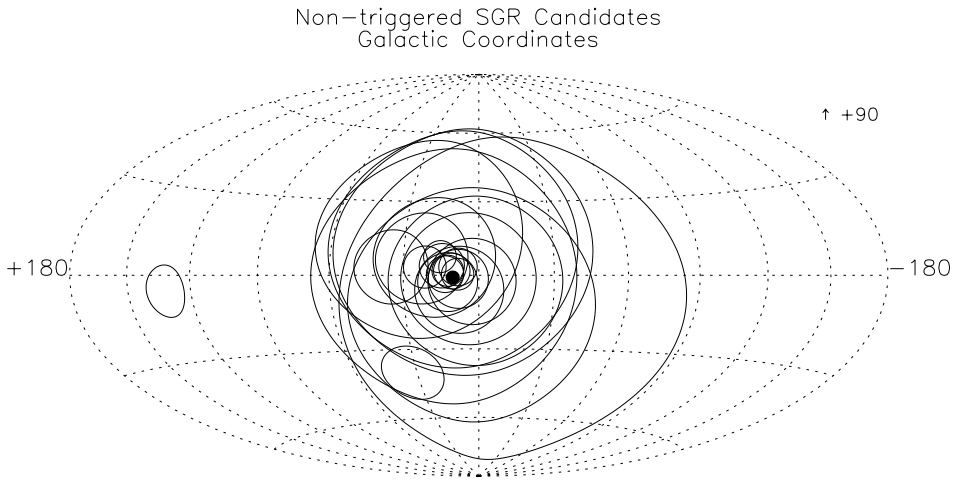

Figure 5-10 Sky map of nontriggered SGR events, shown as 1.0σ error circles. The position of SGR 1806−20 is marked with a filled circle.

Table 5-3. Dipole and quadrupole statistics for low-energy "unknown" events

Statistic[a]	Coordinate System	Moment Tested	Value[b]
$\langle \cos\theta \rangle$	Galactic	Dipole	-0.039 ± 0.082
$\langle \sin^2 b - \frac{1}{3} \rangle$	Galactic	Quadrupole	0.015 ± 0.043
$\langle \sin\delta \rangle$	Equatorial	Dipole	0.010 ± 0.082
$\langle \sin^2 \delta - \frac{1}{3} \rangle$	Equatorial	Quadrupole	-0.002 ± 0.043

[a] θ is the angle between the source direction and the Galactic center, b is the Galactic latitude, and δ is the declination.

[b] Moments are corrected for sky exposure.

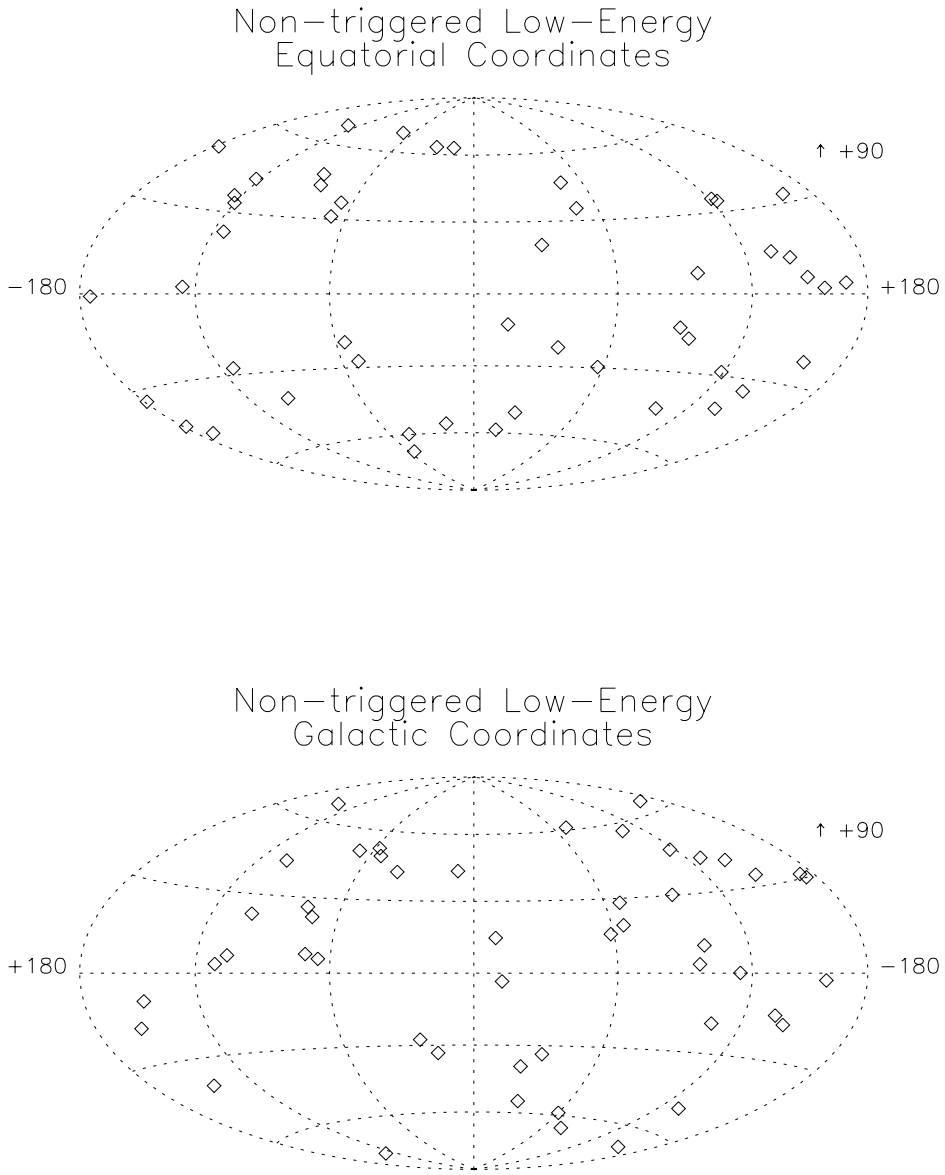

Figure 5-11 The best-fit source directions for the "unknown" low-energy bursts. The median direction uncertainty is 16°.

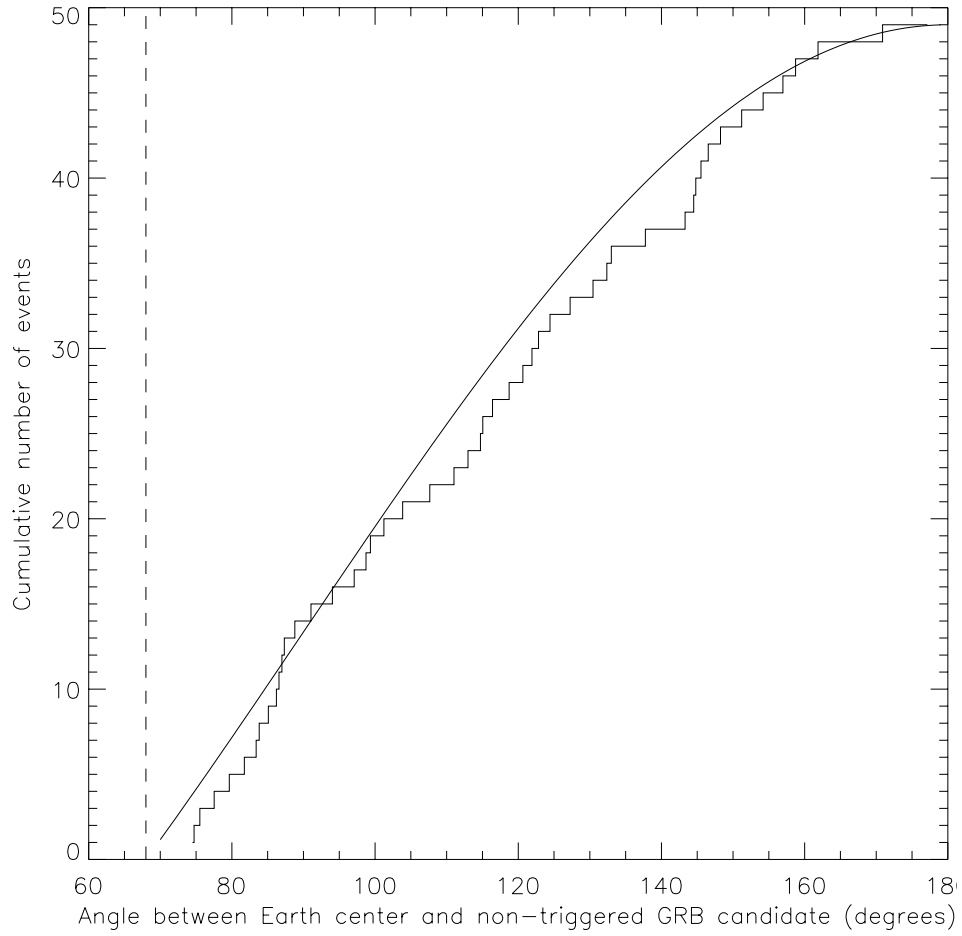

Figure 5-12 Cumulative distribution of angles between "unknown" events and the Earth's center (histogram). The solid curve shows the expectation for a direction distributed randomly with respect to the direction of the Earth's center, as is expected for GRBs. There is no evidence for a large excess of directions near the Earth's limb (dashed line) as would be expected if there were substantial contamination from auroral X-rays.

typically too faint to classify with confidence.

5.9.3 Event Rate

The arrival times of the "unknown" events are somewhat irregular. A K-S test rejects with high confidence the null hypothesis that "unknown" events arrive at the detector at a constant rate. Assuming the null hypothesis that the rate of detected "unknown" events is proportional to the live-time of the search (as would be expected if they arrive with a constant rate), the probability of getting a higher value of the K-S statistic ($D = 0.28$) is 6×10^{-4}. Figure 5-14 shows the detection rate of the "unknown" events. The highest points in the histogram correspond to 5 events detected in 50 days of mission time; they indicate different rates because of variations in the live-time of the search. The irregularities in the rate of these events are most likely due to a combination of variations in observing conditions, inconsistencies in the classification of events, and irregular bursting or flaring activity from the sources contributing to this class.

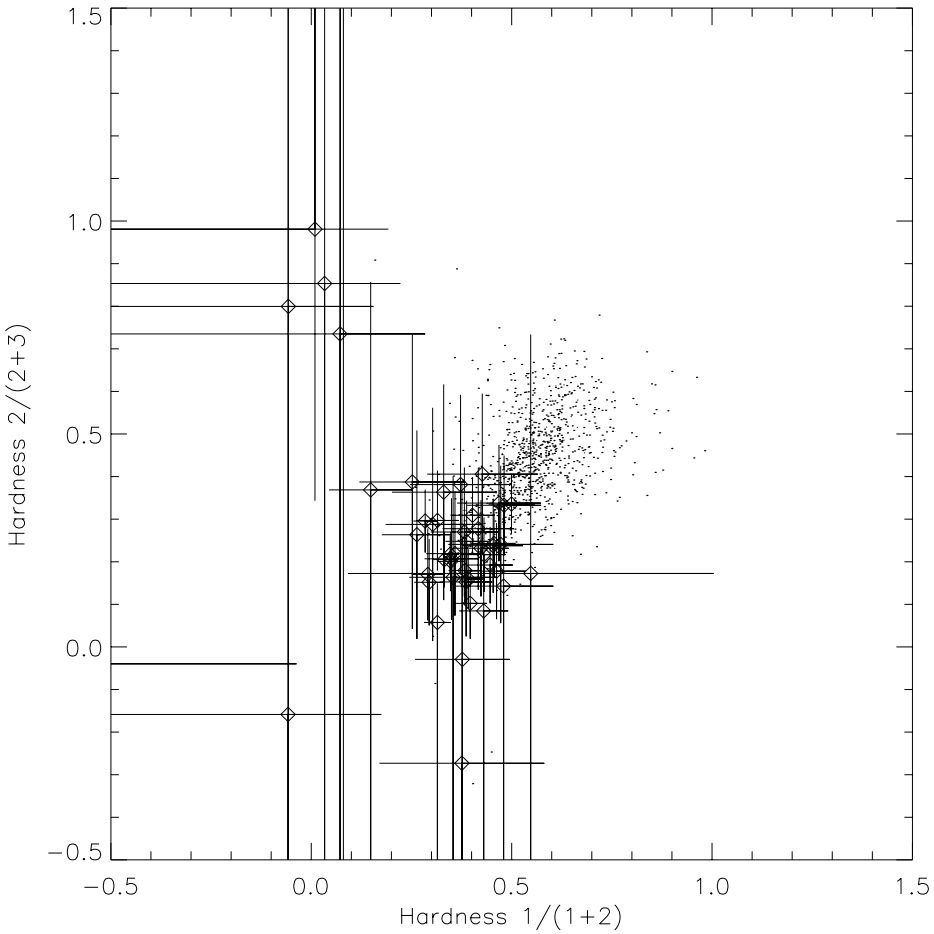

Figure 5-13 Hardness ratios of "unknown" events (diamonds with error bars) and nontriggered GRBs (points). The "unknown" events are selected to be softer than GRBs, but they are not far separated from the population of GRB hardness ratios. For clarity, error bars are not shown for the GRBs.

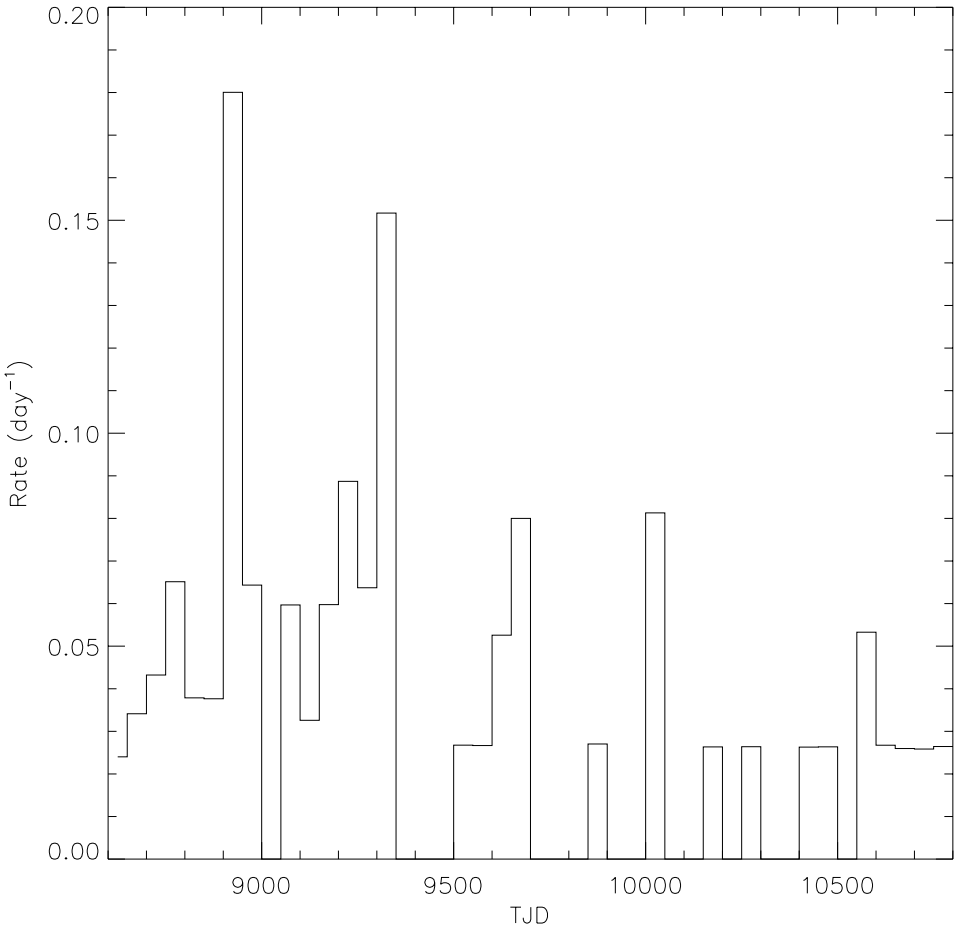

Figure 5-14 Rate of "unknown" events as a function of time.

Chapter 6

Gamma-Ray Burst Intensity Distribution

This chapter is a self-contained paper entitled, "The Intensity Distribution of Faint Gamma-ray Bursts Detected with BATSE," submitted to the *Astrophysical Journal* (Kommers et al. 1999a).

6.1 Abstract

We have recently completed a search of 6 years of archival BATSE data for gamma-ray bursts (GRBs) that were too faint to activate the real-time burst detection system running onboard the spacecraft. These "nontriggered" bursts can be combined with the "triggered" bursts detected onboard to produce a GRB intensity distribution that reaches peak fluxes a factor of ~ 2 lower than could be studied previously. The value of the $\langle V/V_{max} \rangle$ statistic (in Euclidean space) for the bursts we detect is 0.177 ± 0.006. This surprisingly low value is obtained because we detected very few bursts on the 4.096 s and 8.192 s time scales (where most bursts have their highest signal-to-noise ratio) that were not already detected on the 1.024 s time scale. If allowance is made for a power-law distribution of intrinsic peak luminosities, the extended peak flux distribution is consistent with models in which the redshift distribution of the

gamma-ray burst rate approximately traces the star formation history of the Universe. We argue that this class of models is preferred over those in which the burst rate is independent of redshift. We use the peak flux distribution to derive a limit of 10% (99% confidence) on the fraction of the total burst rate that could be contributed by a spatially homogeneous (in Euclidean space) subpopulation of burst sources, such as type Ib/c supernovae. These results lend support to the conclusions of previous studies predicting that relatively few faint "classical" GRBs will be found below the BATSE onboard detection threshold.

6.2 Introduction

The origin of some, and possibly all, gamma-ray bursts (GRBs) at cosmological distances has been firmly established with the identification of X-ray, optical, and radio afterglows (Costa et al. 1997; van Paradijs et al. 1997; Frail et al. 1997) and the subsequent measurement of cosmological redshifts for three of the optical afterglows and/or their host galaxies (Metzger et al. 1997; Kulkarni et al. 1998; Djorgovski et al. 1998). The objects responsible for producing the majority of GRBs, the gamma-ray bursters themselves, have yet to be understood, however. To obtain an understanding of the spatial distribution of sources and the distribution of their burst luminosities is a crucial step towards identifying the physical processes that produce GRBs.

Before the rapid follow-up of GRB afterglows was made possible by the *BeppoSAX* satellite, the only way to test hypotheses about the spatial and luminosity distributions was to fit parametric models to the measured characteristics of the bursts themselves. For this purpose the distribution of GRB intensities was used (Fenimore et al. 1993; Rutledge et al. 1995; Fenimore & Bloom 1995; Cohen & Piran 1995; Hakkila et al. 1996). The effects of cosmological time dilation on the time profiles of bright versus faint bursts were also studied (Norris et al. 1995). Since redshifts are so far associated individually with only three (possibly four) bursts[1], number counts

[1]The proposed association of GRB 980425 with SN 1998bw (z = 0.008; Galama et al. 1998)

as a function of intensity remain an important tool for exploring the possible spatial and luminosity distributions of GRBs.

Several recent papers (Totani 1997; Totani 1998; Wijers et al. 1998; Krumholz et al. 1998; Mao & Mo 1998) have used the observed GRB intensity distributions to investigate the possibility that the redshift distribution of gamma-ray bursters traces the global star formation history of the Universe. The motivation for this hypothesis is a collection of theoretical models in which GRBs are produced by stellar objects that evolve from their formation to their bursting phase on a time scale of ~ 100 Myr or less. This group of models includes the merging of a neutron star with another neutron star or a black hole, the collapse of a massive star, and the collapse of a Chandrasekhar-mass white dwarf (Wijers et al. 1998). In these scenarios, the cosmological redshift distribution of the GRB rate should approximately follow the redshift distribution of the formation rate of stellar objects; in other words, the GRB rate should trace the global star formation history of the Universe. This hypothesis appears to solve some puzzling aspects of the observations, such as the "no host" problem (Schaefer et al. 1997; Wijers et al. 1998).

The star formation rate (SFR) as a function of redshift has been studied by Lilly et al. (1996), Fall, Charlot, & Pei (1996), Madau, Pozzetti, & Dickinson (1998b), and Hughes et al. (1998). The principal result of these studies is that the SFR was substantially higher in the past. Between the present and $z \approx 1$ the SFR increases by a factor of ~ 10; it peaks somewhere in the range $z \approx 1$ to $z \approx 3$; and it decreases to a rate comparable to the present by $z \approx 4$–5.

Totani (1997), Wijers et al. (1998), Krumholz et al. (1998), and Mao & Mo (1998) all find that the GRB peak flux number counts can accommodate the hypothesis that the GRB rate follows the SFR. Among the important conclusions that these authors derive from this interpretation of the data are the following: 1) that the faintest gamma-ray bursts observed with the Burst and Transient Source Experiment

may indicate a separate class of GRBs (Bloom et al. 1998). We will therefore consider that event separately. See section 3.2.

(BATSE) onboard the *Compton Gamma Ray Observatory* (*CGRO*) are already produced at redshifts of $z \approx 3$ to $z \approx 6$ (Wijers et al. 1998) (but see Section 6.5); and 2) that more sensitive experiments are unlikely to discover large numbers of faint GRBs (of the "classical" kind that are detected with current instruments) below the BATSE onboard detection threshold. The latter conclusion has important implications for the design and operation of future GRB detectors, which will test the behavior of GRB number counts at intensities well below the BATSE threshold.

We have recently completed a search of 6 years of archival data from BATSE for GRBs and other transients that did *not* activate the real-time burst detection system (or "trigger") running onboard the spacecraft. A GRB or other transient may fail to activate the BATSE onboard burst trigger for any of several reasons. The burst may be too faint to exceed the onboard detection threshold, it may occur while the onboard trigger is disabled for technical reasons, it may occur while the onboard trigger is optimized for detecting non-GRB phenomena, or it may artificially raise the onboard background estimate and be mistaken for a below-threshold event. Our search of the archival data is sensitive to GRBs with peak fluxes (measured over 1.024 s in the 50–300 keV energy range) that are a factor of ~ 2 lower than can be detected with the onboard trigger in its nominal configuration. Thus our search constitutes an experiment that is ~ 2 times more sensitive than those reported in the BATSE catalogs (Fishman et al. 1994; Meegan et al. 1996; Paciesas et al. 1999; Meegan et al. 1998a).

In this paper we present results regarding the peak flux distribution of the GRBs detected with our "off-line" search of archival data. In section 6.3 we summarize some important aspects of our off-line search and we discuss the $\langle V/V_{max} \rangle$ statistic for the bursts we detected. We show that surprisingly few bursts are found on the 4.096 s and 8.192 s time scales that were not already detected on the 1.024 s time scale. In section 6.4 we fit parametric cosmological models to the observed differential peak flux distribution to compare scenarios in which the GRB rate follows the SFR with the model in which the co-moving GRB rate is independent of redshift. We also examine

the possibility that a homogeneous (in Euclidean space) population of bursting objects could be contributing to the observed sample of GRBs. In section 6.5 we show how our results provide two independent arguments that favor models in which the GRB rate follows the SFR over models in which the GRB rate is independent of redshift.

6.3 The Search for Nontriggered GRBs

The details of our off-line search of the BATSE data are discussed in Kommers et al. (1997). We have merely extended the search from covering 345 days of the mission to covering 2200 days. We have also made minor modifications to our peak flux estimation procedure in order to secure better relative calibration between our peak fluxes and those in the 4B catalog (Paciesas et al. 1999). The extended catalog of nontriggered events will be provided and discussed in the Nontriggered Supplement to the BATSE Gamma Ray Burst Catalogs (Kommers et al. 1999b). Here we address only those aspects of the search that are relevant to the GRB intensity distribution analysis.

We use the data from the Large Area Detectors that provide count rates in 4 energy channels with 1.024 s time resolution, the data type designated "DISCLA" in the flight software (Fishman et al. 1989). These data are searched for statistically significant count rate increases to identify candidate burst events. The many candidate events ("off-line triggers") are then visually inspected to separate astronomically interesting transients from instrumental and terrestrial effects. To be considered a GRB, a candidate must exhibit significant signal in the 50–300 keV range (DISCLA channels 2 and 3) and it must *lack* any characteristics that would associate it with a solar flare, Earth magnetospheric particle precipitation, or other non-GRB origin. Since the DISCLA data are (nearly) continuously recorded, our search detects some bursts that already activated the onboard burst trigger; we call these events "onboard-triggered bursts." Bursts that were detected *exclusively* by our search of archival data are called "nontriggered bursts."

In addition to searching at the 1.024 s time resolution of the DISCLA files, we also search the data binned at 4.096 s and 8.192 s time resolution. The longer time bins provide greater sensitivity to faint bursts that have durations longer than ~ 4 s or ~ 8 s. The specific time profile of each burst determines which of these three time scales is the most sensitive. For this reason the searches on each time scale should be considered separate experiments.

Our search so far covers 1.3×10^8 s of archival data spanning the time from 1991 December 9 to 1997 December 16. In these data we detected 2265 GRBs, of which 1392 activated the onboard burst trigger and 873 did not. We will refer to these 2265 GRBs as the "off-line GRB sample." During the same time period, the onboard burst trigger detected 1815 GRBs. The $1815 - 1392 = 423$ bursts that were detected by the onboard burst trigger but that were *not* detected by our search either occurred during gaps in the archival DISCLA data or had durations much less than the 1.024 s time resolution (so they did not achieve adequate statistical significance in the archival data).

Note that because the best time resolution available to our retrospective search is 1.024 s, all results in this paper pertain to bursts with durations longer than about 1 s. Thus, the population of "short" (duration less than ~ 2 s) bursts that contributes to the bimodal GRB duration distribution (Kouveliotou et al. 1993) is not well represented in the off-line sample. An estimate for the fraction of bursts that our search is likely to miss because of our time resolution can be obtained from the 4B catalog. Although 21% of GRBs for which both durations and fluences were available had $T_{90} < 1.024$ s, only 7% had both $T_{90} < 1.024$ s and fluences too small to create adequate statistical significance in the 1.024 s data (Paciesas et al. 1999).

For each of the 873 nontriggered GRBs we have estimated a peak flux in the 50–300 keV range based on the time bin with the most counts above background. For 1288 of the 1392 onboard-triggered GRBs, we used the peak fluxes from the current BATSE GRB catalog (Meegan et al. 1998a). For the remaining 104 onboard-triggered bursts, peak fluxes were not available from the current burst catalog; we estimated

peak fluxes for them using our own techniques as we did for the nontriggered bursts.

Since the onboard trigger criteria were changed for a variety of reasons during the time spanned by our search, we adopt for the nominal onboard detection threshold the value 0.3 ph cm^{-2} s^{-1} in the 50–300 keV range. At this peak flux the onboard trigger efficiency is ≈ 0.5 (Paciesas et al. 1999). With this estimate, 551 of our 873 nontriggered bursts were below the nominal onboard detection threshold. The rest were not detected onboard for the reasons cited previously.

6.3.1 Trigger Efficiency

To determine the peak flux threshold of the off-line GRB sample, the trigger efficiency $E_1(P)$ of our off-line search has been calculated using the techniques described in Kommers et al. (1997). This quantity is the probability that a burst that occupies exactly one 1.024 s time bin with a peak flux P will be detected by the off-line search algorithm. $E_1(P)$ is well represented (within the uncertainties of the calculation owing to variations in the background rates) by the following function:

$$E_1(P) = \frac{1}{2}\left[1 + \mathrm{erf}(-3.125 + 16.677P)\right], \tag{6.1}$$

where $\mathrm{erf}(x)$ is the standard error function and P is given in units of photons cm^{-2} s^{-1} in the 50-300 keV band. This equation is plotted as the dashed line in Figure 6-1. Error bars on the grid points of the calculation (diamonds) represent the sample standard deviation of the calculated probabilities owing to variations in the background rates. For comparison, the BATSE trigger efficiency from the 4B catalog (Paciesas et al. 1999) is plotted as the dotted line (grid points are indicated by open squares). Equation 6.1 tends to *underestimate* the probability that a typical GRB will be detected, however. This is because many GRBs in our sample last longer than 1.024 s; therefore, these bursts have more than one statistical chance to be included in the sample.

Suppose the peak of a burst occupies N time bins, so that the burst has effectively

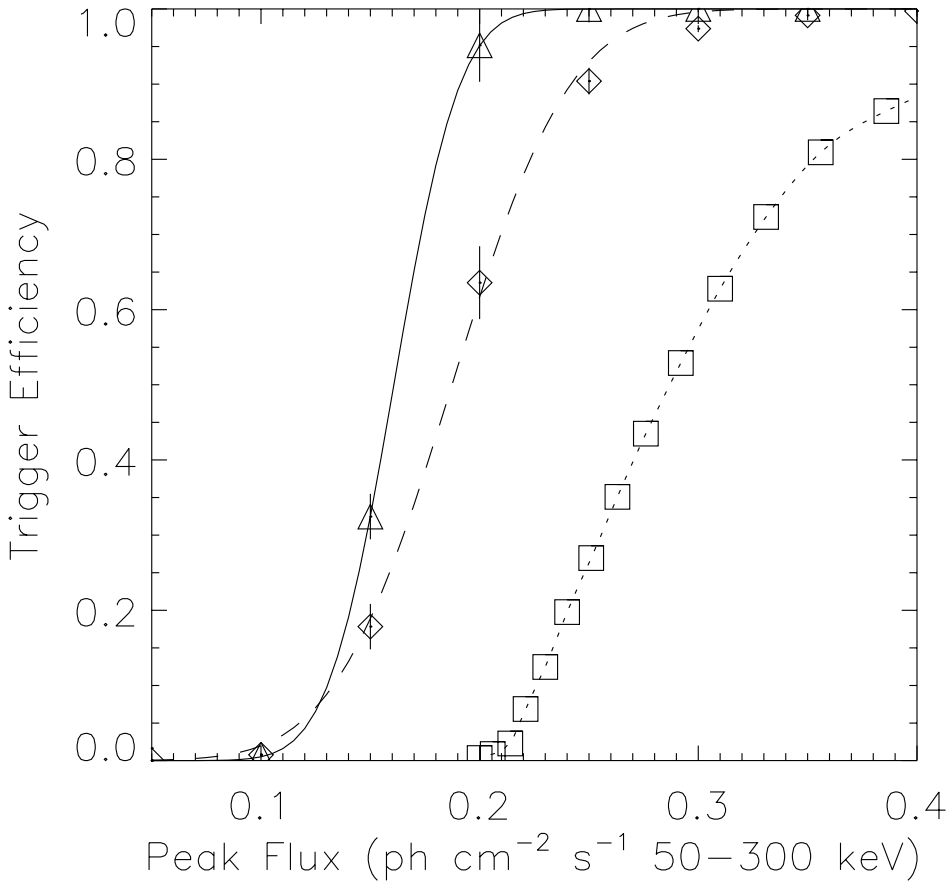

Figure 6-1 The trigger efficiency for the off-line search. The grid points of the calculations are plotted as individual symbols. Error bars represent the standard deviations of the calculated probabilities owing to variations in the background rates. The dashed line (equation 6.1) shows the probability that a burst occupying a single time bin is detected by our search. The solid line (equation 6.4) shows the marginal probability that a burst is detected by our search, given that some bursts longer than 1.024 s have more than one statistical chance to be detected. For comparison, the dotted line shows the trigger efficiency from the 4B catalog; no uncertainties are available for the grid points (squares).

N statistical chances to be detected. Then the probability that the burst is detected can be approximated as unity minus the probability that the burst *fails* to be detected in all N trials:

$$E_N(P) = 1 - [1 - E_1(P)]^N . \tag{6.2}$$

Since the number of chances N is not known for GRBs *a priori*, the actual probability of detection $E(P)$ is obtained by marginalizing $E_N(P)$ over the distribution of N for bursts with peak fluxes near P:

$$E(P) = \frac{\sum h(N,P)\, E_N(P)}{\sum h(N,P)}. \tag{6.3}$$

Our estimate for $h(N,P)$, the histogram of the various integer values of N for bursts with peak fluxes near P, was obtained from the detected sample of bursts by counting, for each burst, the number of time bins with count rates that were within one standard deviation of the peak count rate. For purposes of illustration, Figure 6-2 shows the histogram of N for bursts with peak fluxes in the range 0.1–0.4 ph cm^{-2} s^{-1}. The resulting function $E(P)$ is well represented (to within the uncertainties of the calculation) by the formula

$$E(P) = \frac{1}{2}\left[1 + \mathrm{erf}(-4.801 + 29.868P)\right]. \tag{6.4}$$

This equation expresses our best estimate of the trigger efficiency of our off-line search on the 1.024 s time scale. It is plotted as the solid line in Figure 6-1. The efficiency of our search falls below 0.5 at a peak flux of 0.16 ph cm^{-2} s^{-1}.

If we had not made some correction for the effect of time profiles on the single-time-bin burst detection probabilities, we would have substantially underestimated our trigger efficiency near the detection threshold (~ 0.2 ph cm^{-2} s^{-1}). We note that this type of correction to the single-time-bin trigger efficiency should also be applied when using the trigger efficiencies given in the 1B, 2B, 3B, and 4B catalogs (Fishman et al. 1994; Meegan et al. 1996; Paciesas et al. 1999). Similar considerations are

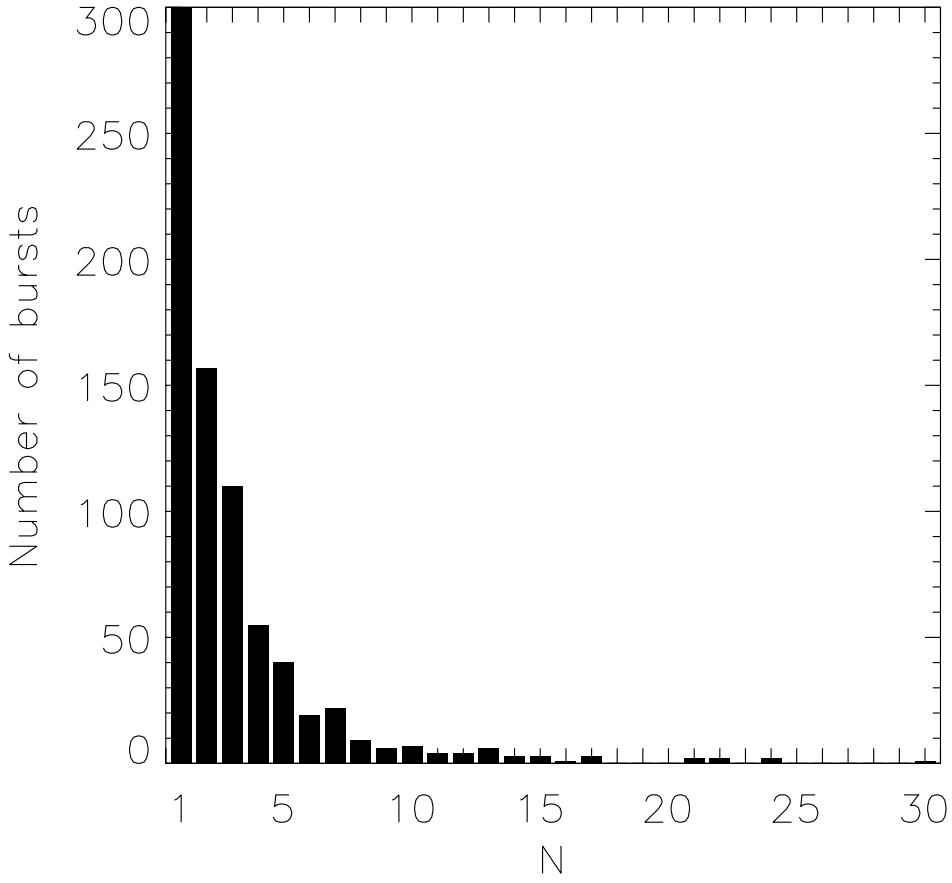

Figure 6-2 Histogram of N, the number of time bins within one standard deviation of the peak count rate, for bursts with peak fluxes in the range 0.1–0.4 ph cm^{-2} s^{-1}.

addressed by in't Zand & Fenimore (1994) and Loredo & Wasserman (1995).

6.3.2 $(C_{min}/C_{max})^{3/2}$ Distribution

As successively more sensitive instruments have been used to produce GRB catalogs, it has been customary to give the value of the $\langle V/V_{max} \rangle$ statistic for the detected bursts (Schmidt et al. 1988). For photon counting experiments like BATSE, it is not strictly $\langle V/V_{max} \rangle$ that is typically calculated, but rather $\langle (C_{min}/C_{max})^{3/2} \rangle$, where C_{min} is the threshold count rate and C_{max} is the maximum count rate measured during the burst. The departure of $\langle (C_{min}/C_{max})^{3/2} \rangle$ from the value of $\frac{1}{2}$ expected for a population of bursters distributed homogeneously in Euclidean space (with a well-behaved, but otherwise arbitrary luminosity distribution) has been firmly established (Meegan et al. 1992; Meegan et al. 1996). Since the discovery that most GRBs originate at cosmological distances, the quantity $\langle (C_{min}/C_{max})^{3/2} \rangle$ can no longer be interpreted as $\langle V/V_{max} \rangle$. Nevertheless, it is useful to compare the values of $\langle (C_{min}/C_{max})^{3/2} \rangle$ obtained by successively more sensitive experiments, including the value obtained for the bursts detected with our search.

Table 6-1 lists various missions and the values they obtained for $\langle (C_{min}/C_{max})^{3/2} \rangle$. The trend towards lower values of $\langle (C_{min}/C_{max})^{3/2} \rangle$ with more sensitive experiments indicates that increasing the accessible survey volume by decreasing the flux threshold does not lead to the detection of large numbers of faint bursts.

The value of $\langle (C_{min}/C_{max})^{3/2} \rangle$ for the 2265 GRBs detected by our search[2] is 0.177 ± 0.006. *This is the lowest value ever obtained for a sample of GRBs.* The cumulative distribution of $(C_{min}/C_{max})^{3/2}$ for our GRBs is shown in Figure 6-3. The flattening of this curve in the range $0.5 < (C_{min}/C_{max})^{3/2} < 1.0$ shows that over 90% of the GRBs we detect are above threshold (on at least one of the 3 time scales) by a factor of at least $(0.5)^{-3/2} = 1.6$.

[2]This value supersedes the ones given in Kommers et al. (1996, 1997, 1998), which are incorrect due to a programming error. An erratum has been submitted (Kommers et al. 1999c).

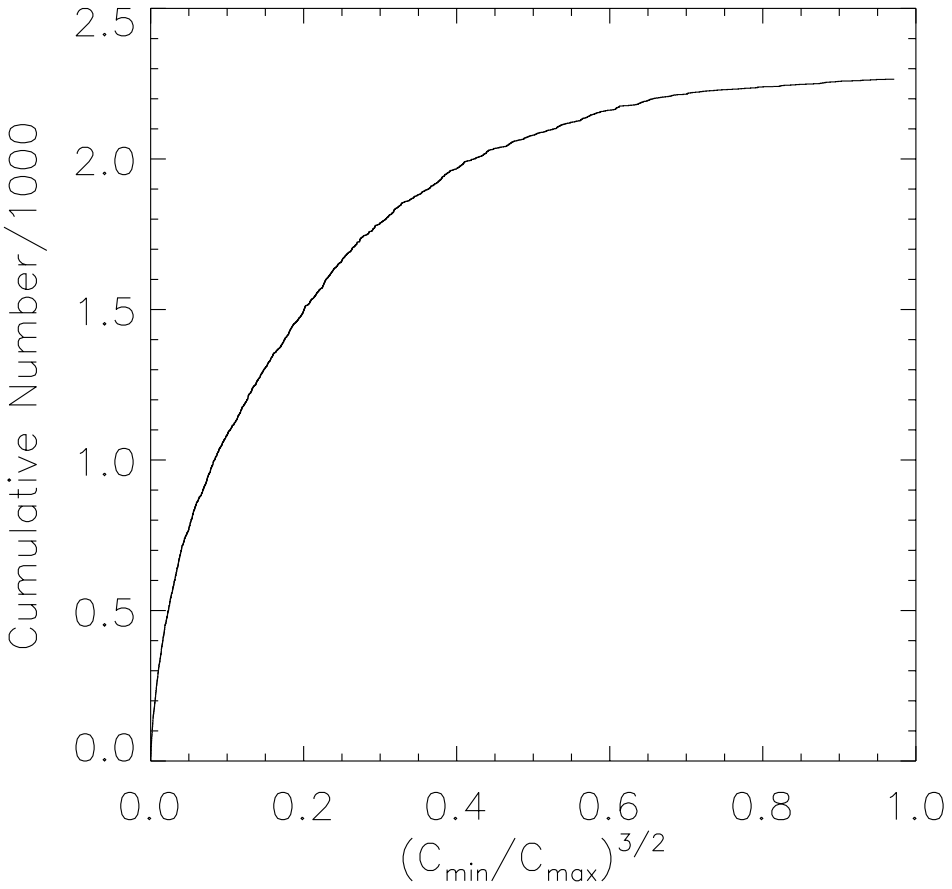

Figure 6-3 Cumulative distribution of $(C_{min}/C_{max})^{3/2}$ for the off-line GRB sample. The dramatic flattening of the curve above $(C_{min}/C_{max})^{3/2} = 0.5$ shows that few of the GRBs detected in our search are just barely above the detection threshold on all 3 time scales (1.024 s, 4.096 s, and 8.192 s).

The reason for this low value of $\langle (C_{min}/C_{max})^{3/2} \rangle$ is the fact that most of the bursts we detected had their maximum signal-to-noise ratios on the 4.096 s and 8.192 s time scales, yet surprisingly few bursts were detected *only* on these longer time scales. For each burst we compute the values of $(C_{min}/C_{max})^{3/2}$ on each of the 3 time scales. The largest of the three values for each burst is used in taking the average. In Euclidean space this corresponds to taking for each burst the *smallest* value of $\langle V/V_{max} \rangle$. Since 72.0% of the bursts we detected have T_{90} durations (Koshut et al. 1996) longer than 8 s, we expect the average $\langle (C_{min}/C_{max})^{3/2} \rangle$ to be dominated by values measured on the 8.192 s time scale.

In fact, the average $\langle (C_{min}/C_{max})^{3/2} \rangle = 0.177 \pm 0.006$ includes 520 values measured on the 1.024 s time scale, 491 values measured on the 4.096 s time scale, and 1254 values measured on the 8.192 s time scale. Yet only 105 bursts were detected *exclusively* on either of the 4.096 or 8.192 s time scales (or both). Many of the bursts that are barely above the detection threshold on the 1.024 s time scale are well above the detection threshold on the longer time scales. Thus very few bursts are found to be just barely above our detection threshold on all 3 time scales, and this accounts for the low value of $\langle (C_{min}/C_{max})^{3/2} \rangle$. Restricting our calculation to use *only* count rates measured on the 1.024 s time scale (and bursts detected on the 1.024 s time scale) gives a larger value, $\langle (C_{min}/C_{max})^{3/2} \rangle = 0.247 \pm 0.006$.

Roughly, the 4.096 s search should be ~ 2 times more sensitive than the 1.024 s search for bursts that maintain their peak flux for at least ~ 4 s, and the 8.192 s search should be yet more sensitive. Therefore our lack of GRB detections exclusively on the longer time scales indicates either 1) a substantial paucity of faint, long bursts below the threshold of our 1.024 s search, or 2) that during our visual inspection of the off-line triggers we have tended to classify a substantial number of faint, long GRBs as other (non-GRB) phenomena. We feel that both alternatives must be present at some level. Our review of the non-GRB off-line triggers suggests that events resembling faint, long GRBs that illuminate the same detectors as a known, bright, variable X-ray source are more likely to be attributed to variability from the X-ray source

than to be classified as GRBs. A secondary evaluation of the event classifications indicates that between 50 and 200 (with a most likely value of 86) GRBs have been misclassified in this way. This is not enough to fully explain, as experimental error, the dearth of faint, long bursts below our 1.024 s threshold.

6.3.3 Peak Fluxes

Detailed comparisons of cosmological models with the data require intensity distributions in physical units. We have chosen to do the analysis in terms of the burst rate as a function of peak photon flux measured over 1.024 s in the energy range 50–300 keV. Compared with the fluence (total energy per unit area deposited in the detector by the burst) we prefer peak photon flux for the purposes of intensity analysis. The peak photon flux can be obtained more reliably from the raw count data and it is more directly related to our ability to detect bursts.

Of the 2265 GRBs detected by our search, we chose to include in our peak flux analysis only those that were detected on the 1.024 s time scale, so that equation 6.4 gives the detection efficiency. We also chose to use only those bursts with peak fluxes in the range 0.18–20.0 ph cm^{-2} s^{-1}. The lower limit ensures that the off-line trigger efficiency exceeds 0.8 for the range of intensities used in the analysis, and the upper limit excludes very bright bursts which are too rare to provide adequate counting statistics in narrow peak flux bins. With these cuts on the data, we are left with 1998 peak flux measurements. To fit the differential intensity distribution, we bin the 1998 bursts into 25 peak flux intervals that were chosen to be approximately evenly spaced in the logarithm of P. The spacing is $\Delta \log P \approx 0.05$ in the range $0.18 < P < 1.0$, $\Delta \log P \approx 0.1$ in the range $1.0 < P < 7.9$, and there is a final broad bin for the range $7.9 < P < 20.0$. Uncertainties in the number of bursts ΔN_{obs} in each bin are taken to be $\pm\sqrt{\Delta N_{obs}}$. The burst rate is computed by dividing the number of bursts in each bin by the live time of the search (1.33×10^8 s = 4.21 yr) and the mean solid angle visible to the BATSE detectors ($0.67 \times 4\pi$). Table 6-2 gives the peak flux intervals, number of bursts, and burst rate for each bin.

6.4 Cosmological Model Comparison

Many investigators, in scores of papers, have shown the consistency of the GRB peak flux distribution with various cosmological models; see, for example, (Wijers et al. 1998; Loredo & Wasserman 1998b; Hakkila et al. 1996; Horack et al. 1996; Rutledge et al. 1995; Fenimore & Bloom 1995) and references therein. As shown in the previous section, the off-line GRB sample extends the observed GRB intensity distribution to peak fluxes that are lower by a factor of ~ 2 than could be studied previously. While it is unlikely that a factor of ~ 2 will yield stringent new model constraints, it remains of interest to note a few cosmological models that provide good fits to the extended GRB peak flux distribution. These can be used to set limits on the rate of GRBs that may come from a nearby, homogeneous subpopulation of burst sources.

6.4.1 Purely Cosmological Models

To limit the number of free parameters that must be considered, our choice of cosmological world model is the Einstein-de Sitter model: $\Omega = 1$, $\Lambda = 0$, $q_0 = \frac{1}{2}$ (Wienberg 1972). This cosmology has been used by many other investigators so it allows easy comparison of results. Where needed, we assume a Hubble constant $H_0 = 70h_{70}$ km s^{-1} Mpc^{-1}. We also assume that bursters are distributed isotropically, so the only interesting parameter in the burster spatial (redshift) distribution is the radial coordinate $r(z)$ from Earth. The following derivation of the expected observed peak flux distributions follows the discussions in Fenimore & Bloom (1995) and Loredo & Wasserman (1997).

In general the rate of bursts R per unit interval in peak flux P observable at Earth is given by

$$\frac{dR}{dP} = \int dL \int dz \; \frac{d^2R}{dL\,dz} \; \delta(P - \Phi(L,z)), \tag{6.5}$$

where L is the equivalent isotropic peak luminosity of the burst at the source, z is the redshift parameter, $d^2R/dLdz$ is the rate of bursts per unit L per unit redshift

interval, $\delta(x)$ is the Dirac delta function, and $\Phi(L,z)$ is the peak photon flux measured at Earth for a burst with peak luminosity L located at redshift z. We will assume that the redshift and luminosity distributions are independent, so that the burst rate as a function of L and z is given by

$$\frac{d^2R}{dL\,dz} = \frac{4\pi c R_0}{H_0}\ \psi(L)\rho(z)\ \frac{r^2(z)}{(1+z)^2\ \sqrt{1+z}} \tag{6.6}$$

where R_0 is an overall normalization, $\psi(L)$ is the distribution of burst luminosities (normalized to unity), $\rho(z)$ is the distribution of the co-moving burst rate as a function of redshift (normalized to unity on the interval $0 < z < 10$), and $r(z) = (2c/H_0)(1 + z - \sqrt{1+z})/(1+z)$ is the co-moving radial coordinate.

The peak flux $\Phi(L,z)$ observed at Earth in the 50–300 keV energy range, where the BATSE burst trigger is sensitive, depends on the intrinsic spectrum of the GRB. We write it as

$$\Phi(L,z) = \frac{L\ K(z)}{4\pi\ (1+z)\ r^2(z)}. \tag{6.7}$$

The spectral correction function $K(z)$ depends on the shape of the burst photon energy spectrum at the source. The observed GRBs have a variety of spectral shapes, and in the cosmological scenario these observed spectra have been redshifted according to the (unknown) redshifts of the sources.

To account for the spectral variety of GRBs we use the spectral fits of Band et al. (1993). To account for the unknown redshift factors for these spectra, we use the procedure described in Fenimore & Bloom (1995). The peak fluxes of the bursts for which Band et al. (1993) derived spectral fits are used in conjunction with the cosmological model under consideration to self-consistently estimate the redshift factors for the fitted spectra. We assume that the ith burst fitted by Band et al. (1993) has exactly the mean intrinsic peak luminosity in the cosmological model being considered: $L_i = \int dL'\ L'\psi(L')$, where the shape of $\psi(L)$ depends on the parameters of the cosmological model. We then solve for the redshift z_i which the fitted burst i must have had to produce the peak flux listed for it in the current BATSE GRB

catalog (Meegan et al. 1998a). Fifty-one of the bursts fitted by Band et al. (1993) had peak fluxes available. For each of their spectral shapes $\phi_i(E)$ the spectral correction function takes the form

$$K_i(z) = \frac{\int_{50(1+z)/(1+z_i)}^{300(1+z)/(1+z_i)} dE\ \phi_i(E)}{(1+z_i)\ \int_{30/(1+z_i)}^{2000/(1+z_i)} dE\ E\phi_i(E)}. \tag{6.8}$$

The integrals in the denominator and numerator convert the model parameter L, which represents the peak luminosity in the 30–2000 keV range at the source, to the observed photons cm^{-2} s^{-1} in the 50-300 keV band at Earth. The burst rate expected in the BATSE band pass for the ith spectral shape $\phi_i(E)$ is then (from equation 6.5)

$$\left(\frac{dR}{dP}\right)_i = \frac{16\pi^2 c R_0}{H_0} \int dz\ \frac{\rho(z)\ r^4(z)}{(1+z)\ \sqrt{1+z}\ K_i(z)}\ \psi\left(\frac{4\pi\ (1+z)\ r^2(z)\ P}{K_i(z)}\right). \tag{6.9}$$

The limits on the integral are determined by the range of z for which the luminosity distribution $\psi(4\pi(1+z)r^2(z)P/K_i(z))$ is non-zero at the given P.

To estimate the observed distribution of bursts, which includes a variety of spectral shapes, we average Equation 6.9 over the 51 spectral correction functions $K_i(z)$. This procedure is equivalent to marginalizing the unknown spectral parameters of the observed bursts (i.e., those in the off-line sample) to obtain the posterior rate distribution. The 51 spectra from Band et al. (1993) are furnishing estimates of the prior distributions of the spectral parameters. The expectation value of the observed burst rate for peak fluxes between P_1 and P_2 is then

$$\Delta R(P_1, P_2) = \int_{P_1}^{P_2} dP\ E(P)\ \left\langle \frac{dR}{dP} \right\rangle, \tag{6.10}$$

where $\langle dR/dP \rangle$ is the mean rate estimated from the 51 observed spectra and $E(P)$ is the detection efficiency.

The use of the Band et al. spectra increases the computational cost of the rate model by a factor of ~ 50 over using a single "universal" burst spectrum. We found that a simple power-law form for the GRB photon energy spectrum—as has been

used by many previous studies—predicts significantly different burst rates at low peak fluxes than does equation 6.10. Since we are interested in the behavior of the burst rate at low peak fluxes, we felt that the analysis based on the full 51 Band et al. spectra would be more reliable. Similar conclusions are reached by Fenimore & Bloom (1995) and Mallozzi, Pendleton, & Paciesas (1996).

For comparison with the results of previous studies, we chose two forms for the luminosity distribution. The first is a monoluminous (standard candle) distribution. The second is a truncated power-law,

$$\psi(L) = \begin{cases} \frac{1}{L \log(L_{max}/L_{min})} & \beta = 1 \\ \frac{(1-\beta)\ L^{-\beta}}{L_{min}^{1-\beta} - L_{max}^{1-\beta}} & \beta \neq 1 \end{cases} \tag{6.11}$$

with $\psi(L) = 0$ if $L < L_{min}$ or $L > L_{max}$. The normalization factors ensure that $\int dL\ \psi(L) = 1$.

The standard candle distribution, though useful for comparison with other results, is ruled out by the observed peak fluxes of the 3 bursts for which redshifts have been measured. For GRBs 970508, 971214, and 980703 the inferred equivalent isotropic peak luminosities in the 30–2000 keV energy range are $(0.6 \pm 0.1)\ 10^{51} h_{70}^{-2}$ erg s^{-1}, $(37 \pm 16)\ 10^{51} h_{70}^{-2}$ erg s^{-1}, and $(2.2 \pm 0.4)\ 10^{51} h_{70}^{-2}$ erg s^{-1} respectively. In calculating each of these peak luminosities, we have used the observed peak flux (Meegan et al. 1998a) in combination with the observed redshift (Metzger et al. 1997; Kulkarni et al. 1998; Djorgovski et al. 1998) to find the expectation value of the intrinsic luminosity averaged over the 51 Band et al. spectra. This procedure is the one used in our modeling, so it was used on these 3 bursts as well to facilitate comparisons with the models (see section 6.5). The peak luminosities estimated here are somewhat higher by factors of ~ 3 to ~ 6 than those reported elsewhere (Krumholz et al. 1998). This is because the spectral shapes fitted by Band et al. (1993) generally become steeper at high energies, so a source at high redshift must be more luminous to produce the flux observed at Earth than it would have to be if the spectrum did not fall off so rapidly at higher energies. These differences illustrate the importance

of using the most realistic spectral models available rather than simple power-laws when analyzing the GRB intensity distribution.

A variety of spatial, or rather redshift, distributions for the bursters have been used in previous studies of the GRB intensity distribution. With up to 4 free parameters already incorporated into our burst rate models (the overall normalization R_0, and the parameters of the power-law luminosity function β, L_{min}, and L_{max}) there is little hope of constraining any additional free parameters in the redshift distribution. Here we explore 3 specific models of the redshift distribution that contain no free parameters. The two physical scenarios we examine are 1) that the co-moving burst rate is independent of redshift between $z = 0$ and $z = 10$, and 2) that the co-moving GRB rate is proportional to the star formation rate (SFR).

For the GRB rate model that is independent of redshift, $\rho(z) = 0.1$ for $0 < z \leq 10$ and $\rho(z) = 0$ for $z > 10$. We refer to this redshift distribution as "model D1."

For the case where the burst rate follows the star formation history of the Universe, we use two slightly different parameterizations of the SFR. The first is the SFR deduced from the rest-frame ultraviolet luminosity density, with the functional form given in footnote 1 of Madau, Della Valle, & Panagia (1998a). In this estimation the SFR peaks around z =1–1.5. A SFR of roughly this form has been used by several previous studies of the GRB intensity distribution (Totani 1997; Wijers et al. 1998; Krumholz et al. 1998). We refer to this redshift distribution as "model D2."

The second SFR parameterization assumes that the SFR—and thus the GRB rate—tracks the total output of radio-loud AGN. In this scenario the SFR peaks at z =2–3 (Hughes et al. 1998; Dunlop 1998). This form of the SFR appears to be more consistent with recent results from SCUBA (Hughes et al. 1998) which are not susceptible to the same problems of dust obscuration as the determination by Madau et al. (1998a). The specific functional form we use is a best-fit analytic model to points measured by hand from Figure 6 of Hughes et al. 1998: $\rho(z) \propto 0.00360 + 0.0108 \exp(2.76z - 0.573z^2)$. This approximation appears to be accurate to within 5% for the redshift range $1 < z < 4$. (At lower and higher redshifts the

formula likely underestimates the actual rate of star formation; but this is no great concern as it is the redshift of the peak SFR that is of primary interest.) We refer to this redshift distribution as "model D3."

Figure 6-4 plots the normalized GRB rate $\rho(z)$ for the three models of the star-formation rate as a function of redshift.

With choices for $\psi(L)$ and $\rho(z)$ as discussed, we fit equation 6.10 to the data in Table 6-2 by minimizing the χ^2 statistic. In all cases, we found that the parameter L_{max} was not well constrained: variations in L_{max} did not change the minimum χ^2 by a significant amount. The (mathematical) reason for this is that the integrand in equation 6.9 is a decreasing function of z for plausible values of β, so that varying the upper limit (z_{max} corresponding to L_{max} for the given P) causes only small changes in the value of the integral. Accordingly, all the results reported here set $L_{max} \equiv 1000 L_{min}$. The free parameters are thus R_0 and L_0 in the cases of the standard candle models, and R_0, β, and L_{min} in the cases of the power-law luminosity distribution models. The results of the fits are listed in Table 6-3 and Table 6-4. Uncertainties on the fitted parameters correspond to 68% confidence limits for 2 ($\Delta\chi^2 = 2.3$) or 3 ($\Delta\chi^2 = 3.5$) interesting parameters, respectively (Avni 1976).

Model D1 (constant burst rate density as a function of redshift) produces an acceptable fit for the standard candle luminosity distribution. The probability of getting $\chi^2 > 32.3$ for 23 degrees of freedom is 0.094. Adding one more free parameter (β) for the power-law luminosity distribution produces an insignificant change in the minimum χ^2. Furthermore, the high value of β in the best-fit power-law distribution indicates a very narrow range of peak luminosities.

Model D2 (burst rate density follows the SFR as determined by Madau et al. [1998a]) produces a formally unacceptable fit in the monoluminous case. But it achieves an excellent fit (χ^2 per degree of freedom = 0.81) for the power-law luminosity distribution. The F-test estimates that the probability that the improvement in χ^2 is due to chance is 1.5×10^{-7}, justifying the inclusion of the additional parameter in the power-law luminosity function model. The value of β in this model is remarkably

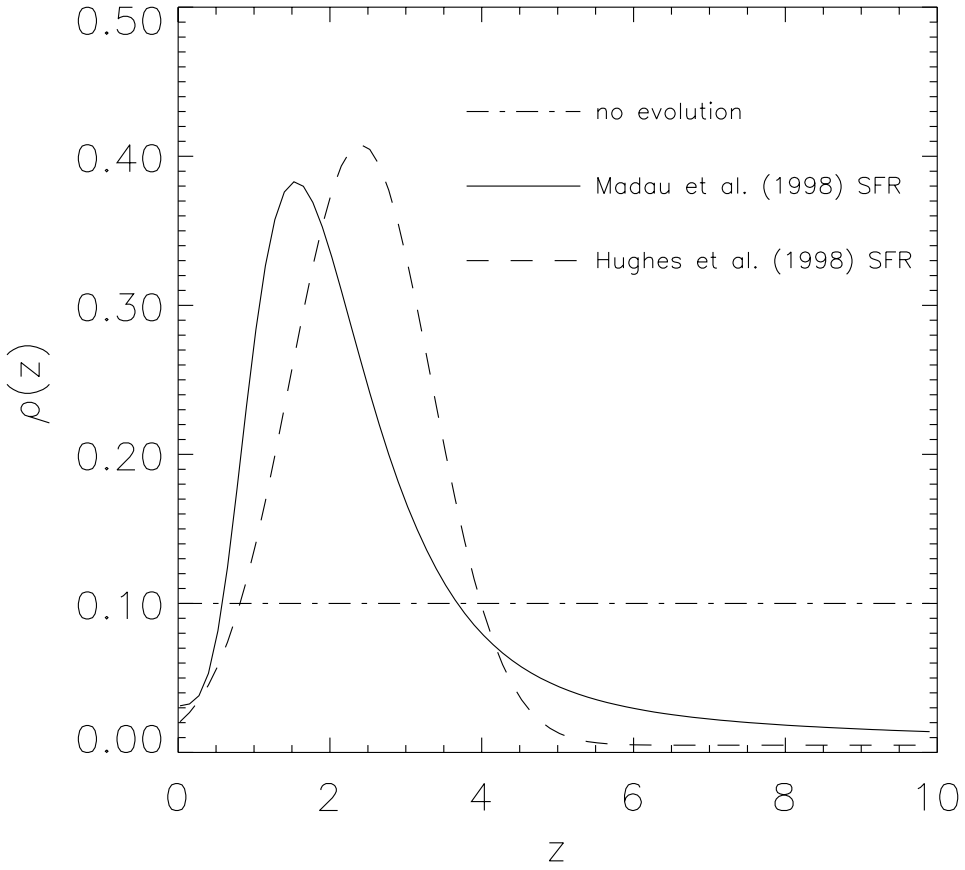

Figure 6-4 Normalized redshift distributions of the star-formation history of the Universe. These functions are used as the models for the evolution of the GRB rate as a function of redshift.

well-constrained. If the other fit parameters are regarded as "uninteresting" then the 90% ($\Delta\chi^2 = 2.7$) and 99% ($\Delta\chi^2 = 6.6$) confidence intervals (Avni 1976) on β are 2.0–2.3 and 1.8–2.6, respectively.

Model D3 (burst rate density follows the output of radio-loud AGN) produces formally acceptable fits with both the standard candle and power-law luminosity distributions. The power-law luminosity distribution achieves a significantly lower χ^2, however. The F-test estimate of the probability that the improvement is due to chance is 1.5×10^{-3}.

Figure 6-5 plots the differential peak flux distributions for the best-fit models with power-law luminosity distributions. For all three best-fit models the value of $\langle (P_{min}/P)^{3/2} \rangle$ is consistent with the value of $\langle (C_{min}/C_{max})^{3/2} \rangle$ measured for the sample (see section 6.3.2). Extrapolating the best-fit models to peak fluxes lower than those included in our data shows very different behaviors. Model D1 (dot-dashed lines) predicts a dramatically higher burst rate at low peak fluxes than do models D2 (solid line) and D3 (dashed line).

In each model the best-fit parameters for the power-law luminosity function yield our best estimate of the parameters of the *intrinsic* distribution of GRB peak luminosities. The distribution of peak luminosities of the *observed* bursts is different, however, because the most luminous bursts are sampled from a much larger volume than are the least luminous bursts. Even though high luminosity bursts are infrequent, the geometrical advantage of sampling them from a larger volume means that they will be over-represented in a sample of bursts observed over a fixed time interval. The distribution of peak luminosities for the observed bursts is the "effective luminosity function" (Loredo & Wasserman 1997). For the best-fit parameters of model D1 the effective luminosity function is a power-law that is less steep than that of the intrinsic luminosity function. We find $\beta_{\rm eff}^{\rm D1} = 2.8$ for the effective luminosity function versus $\beta = 4.6$ for the intrinsic one. The power-law slopes of the effective luminosity functions for models D2 and D3 are $\beta_{\rm eff}^{\rm D2} = 1.6$ and $\beta_{\rm eff}^{\rm D3} = 1.9$, respectively.

Similarly, the distribution of the GRB rate as a function of redshift for the observed

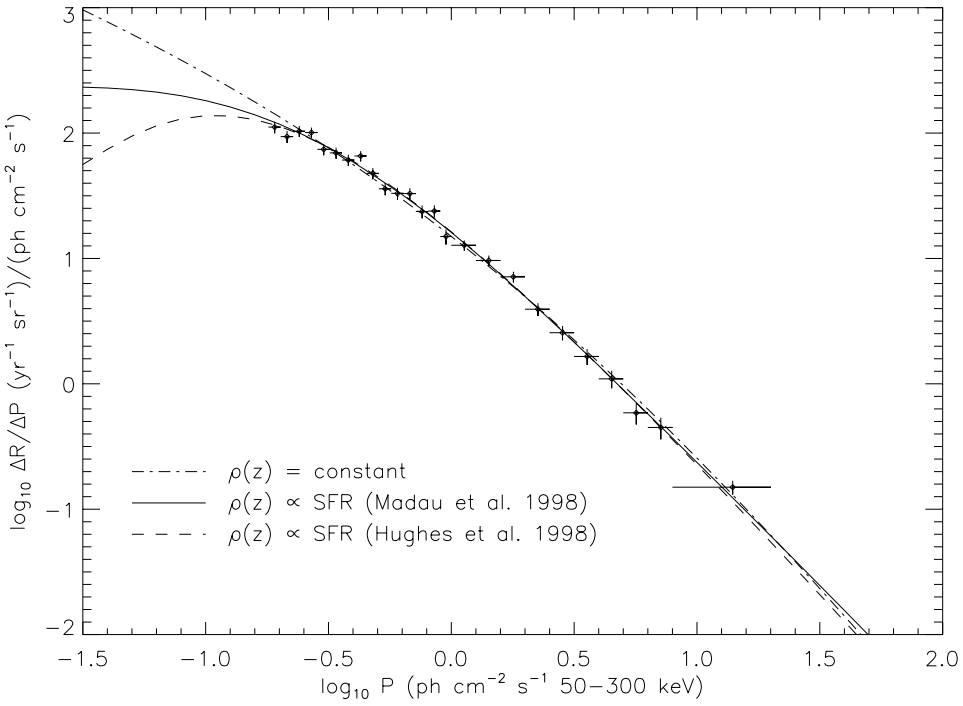

Figure 6-5 Best-fit cosmological models with power-law luminosity distributions. Units of R are bursts yr^{-1} sr^{-1}, and those of P are ph cm^{-2} s^{-1} in 50–300 keV. The dot-dashed line corresponds to model D1 (co-moving burst rate is independent of redshift). The solid line shows model D2 (burst rate follows the rest-frame ultraviolet luminosity density) and the dashed line shows model D3 (burst rate follows the output of radio-loud AGN). Measured rates are shown with 1σ vertical error bars; horizontal error bars indicate the bin widths. The best-fit model curves displayed here have not been corrected for detection efficiency.

bursts is not identical to the intrinsic redshift distribution given by $\rho(z)$ (Loredo & Wasserman 1997). Figure 6-6 shows the effective redshift distributions for the best-fit models D1, D2, and D3. In all 3 models the effective redshift distribution cuts off at a lower redshift than does the corresponding intrinsic redshift distribution. The mean redshifts of the observed bursts in the best-fit models D1, D2, and D3 are $\langle z \rangle^{D1} = 0.86$, $\langle z \rangle^{D2} = 1.4$, and $\langle z \rangle^{D3} = 1.9$, respectively. The maximum redshifts of the bursts in models D1, D2, and D3 are not precisely determined, but the observed redshift distributions cut off around $z_{\rm max}^{\rm D1} \approx 1.5$, $z_{\rm max}^{\rm D2} \approx 2$, and $z_{\rm max}^{\rm D3} \approx 3$, respectively (see Figure 6-6).

It is interesting to compare the rate of bursts that are seen with the off-line search to the total rate of bursts that occur in the Universe, subject to the cosmological rate models we are considering. The fraction of bursts that are detected with BATSE is given by the integral of the effective redshift distribution for the off-line search (over the range $0 < z < 10$) divided by the integral of the effective redshift distribution that would be visible to a "perfect detector" which can detect infinitely faint bursts, multiplied by the live-time (0.70) and sky exposure (0.67) fractions. In the best-fit models D1, D2, and D3, it follows that the off-line search detects $\sim 14\%$, $\sim 30\%$, and $\sim 37\%$, respectively, of the bursts that occur in the Universe. Of course, these estimates can apply only to bursts with spectra and durations of the kind that are accessible to the off-line search. If BATSE had 100% live-time and no Earth blockage, then in model D1 30% of the bursts that occur could be detected with the off-line search. In models D2 and D3, 65% and 78%, respectively, of the bursts that occur could be detected with the off-line search.

It is customary to quote the rate of GRBs as the co-moving rate per unit volume at $z = 0$, a quantity often denoted by ρ_0 with units of Gpc^{-3} yr^{-1} (Fenimore & Bloom 1995; Wijers et al. 1998). The model parameter R_0 is related to ρ_0 by $\rho_0 = 4\pi R_0 \rho(0)$. Table 6-5 lists the values of ρ_0 corresponding to the best-fit values of R_0 for the standard-candle GRB models. Table 6-6 does the same for the GRB models with a power-law luminosity function. This burst rate can be converted into an event

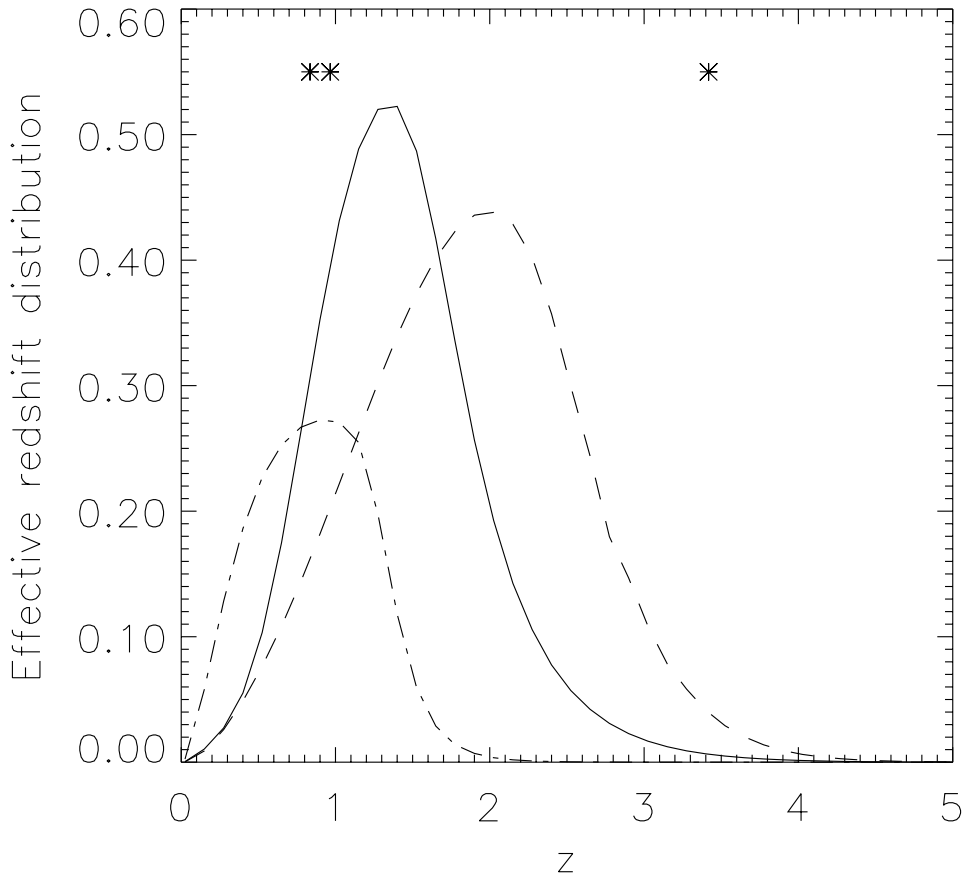

Figure 6-6 Redshift distribution of the burst rate for observed bursts (i.e., the effective differential burst rate as function of redshift). The distributions are normalized so that the number of bursts visible to a perfect detector (one with no sensitivity limit) is unity; thus in models D2 and D3 there is a greater fraction of bursts that could be seen with BATSE than in model D1. These distributions peak at lower redshifts than do the intrinsic burst rate distributions. The dot-dashed line corresponds to a constant burst rate as a function of redshift (model D1). The solid line corresponds to the model (D2) where the burst rate traces the SFR as determined by Madau et al. (1998a). The dashed line corresponds to the model (D3) where the burst rate traces the output of radio-loud AGN (Hughes et al. 1998). The redshifts of GRBs 970508 ($z = 0.835$; Metzger et al. 1997), 971214 ($z = 3.418$; Kulkarni et al. 1998a), and 980703 ($z = 0.966$; Djorgovski et al. 1998) are marked with asterisks.

rate per "typical" galaxy using the space density of such galaxies. Here, a "typical" galaxy is taken to be one with a luminosity L^* equal to the characteristic luminosity of galaxies in the Schechter function (Schechter 1976). Loveday et al. (1992) report the mean space density of L^* galaxies to be $(4.8 \pm 0.6)\ 10^{-3}\ h_{70}^3$ Mpc^{-3}. With this conversion, the co-moving rate of GRBs at $z = 0$ can be expressed in GEM (Galactic Events per Million years), which is the rate of GRBs in an L^* galaxy. This quantity is also listed in Tables 6-5 and 6-6.

6.4.2 Limits on a Possible Homogeneous Sub-population

The discovery of the unusual Type Ib/c supernova SN 1998bw in the X-ray error box of GRB 980425 has fueled speculation that the supernova (SN) produced the GRB (Galama et al. 1998; Iwamoto et al. 1998; Kulkarni et al. 1998). It has been suggested that such events (the supernova-GRBs, or "S-GRBs") may constitute a subclass of all GRBs (Bloom et al. 1998). In this subsection we discuss what fraction of all GRBs could belong to such a subclass assuming that the remaining bursts come from the "reasonable" cosmological scenarios discussed previously.

If the inferred peak luminosity of GRB 980425, assuming a distance corresponding to the redshift $z = 0.0085$ of SN 1998bw (Tinney et al. 1998) is typical of S-GRBs, then the bursts in this subclass are detectable within a volume of radius ~ 100 Mpc (Bloom et al. 1998). Within this volume, we assume the distribution of Type Ib/c SNe to be approximately homogeneous. Thus the cumulative intensity distribution of S-GRBs can be expected to follow a $-3/2$ power-law. This conclusion follows for any well-behaved distribution of intrinsic luminosities as long the spatial distribution does not deviate from homogeneity within the volume sampled by our detectors. Since the observed intensity distribution of all GRBs deviates strongly from the $-3/2$ power-law, it can be used to set an upper limit on the fraction of all GRBs that can come from a subclass which obeys the $-3/2$ power-law. In this respect, the faint end of the peak flux distribution (as explored by our off-line search) provides the most stringent

constraints.

A model-independent limit on the fraction of bursts that might come from a nearby homogeneous population can be obtained from the histogram of $(C_{min}/C_{max})^{3/2}$ for the observed bursts. Any homogeneous subpopulation is expected to contribute a constant number of bursts to each bin in the histogram. Thus the bin with the fewest number of bursts sets an upper limit on the total number of bursts that could come from the subpopulation. The bursts detected with our search have already been used to set an upper limit of 5–6% on the fraction of bursts that could come from a homogeneous subpopulation; this limit is therefore an upper limit on the fraction of bursts that could be associated with nearby Type Ib/c SNe (Kippen et al. 1998). Though model-independent, this limit depends on how coarsely the histogram is binned. It also assumes than an arbitrary distribution of intensities is acceptable for bursts that do *not* come from the homogeneous subpopulation. This is too much freedom, because physically plausible distributions occupy only a subset of all arbitrary intensity distributions.

Here we assume that the bulk of GRBs come from the cosmological distributions discussed in section 6.4.1. An upper limit on the rate of all GRBs that might come from Type Ib/c SNe (or any nearby homogeneous distribution) is then fixed by determining the maximum rate of bursts that can come from a (differential) distribution proportional to $P^{-5/2}$ before the model becomes inconsistent with the data. We thus fit a model of the form

$$\Delta R(P_1, P_2) = R_H \int_{P_1}^{P_2} dP \; E(P) \; P^{-5/2} \; + \; \int_{P_1}^{P_2} dP \; E(P) \; \left\langle \frac{dR}{dP} \right\rangle . \qquad (6.12)$$

The fractional burst rates corresponding to the 90% and 99% confidence upper limits on the normalization R_H in each model are given in Table 6-7. The upper limits were determined by finding the value of R_H for which $\Delta\chi^2 = 2.7$ and $\Delta\chi^2 = 6.6$, respectively, when χ^2 is minimized with respect to the other fit parameters (Avni 1976). In all cases, only a modest fraction, 5–10%, of the observed GRBs could come from

a homogeneous subpopulation (and thus from nearby SNe). These upper limits are comparable to the model-independent result found in the previous paragraph. They are slightly less constraining because of the fact that our peak flux distribution refers only to the 1.024 s time scale, so it takes no account of the paucity of faint bursts found on the 4.096 s and 8.192 s time scales (see section 6.3.2).

These results were to be expected from the facts that 1) models D1, D2, and D3 with power-law luminosity distributions already gave excellent fits to the data without the presence of the homogeneous ($P^{-5/2}$) term, which is sharply peaked at low peak fluxes, and 2) the fractional uncertainties on the rates in each bin are on the order of 10%. The upper limits discussed here would be further reduced if a given GRB must exhibit certain characteristics (e.g., single-peaked time profile, lack of emission above 300 keV) in order to be considered a candidate S-GRB (Bloom et al. 1998). Norris, Bonnell, & Watanabe (1998) have found that only 0.25–0.5% of BATSE GRBs have temporal and spectral characteristics similar to GRB 980425.

6.5 Discussion

The GRB peak flux distribution alone (on the 1.024 s time scale) only weakly distinguishes between the non-evolving model $\rho(z)$ = constant (D1) and the evolving models where $\rho(z)$ is proportional to an estimate of the star formation history (D2 and D3). (In this section we restrict our attention to models that include a power-law distribution of intrinsic peak luminosities.) A similar conclusion has been reached previously by Krumholz et al. (1998), who analyze the BATSE catalog data and find that to reliably distinguish the non-evolving and evolving models requires data from more sensitive GRB detectors and/or the measurement of more individual GRB redshifts.

The off-line sample of GRBs constitutes a more sensitive experiment than the one analyzed by Krumholz et al. (1998). Here we argue that models similar (or identical) to D2 and D3, in which the GRB rate has a significant peak in the redshift range $1 < z < 3$, *are modestly preferred over the constant rate density model.* Two

independent lines of reasoning serve to denigrate the $\rho(z) = \text{constant}$ ("non-evolving") models in favor of the evolving ones.

First, our search on the 1.024 s time scale can reach peak fluxes as low as 0.16 ph cm^{-2} s^{-1} in the 50–300 keV band (50% detection efficiency). But our searches on the 4.096 and 8.192 s time scales are sensitive to peak fluxes (averaged over the matching time scale) that are lower by factors of ~ 2 and $\sim 2\sqrt{2}$, respectively, than the 1.024 s threshold. In fact, most of the bursts we detect have their highest signal-to-noise ratio in the 8.192 s search. Yet surprisingly few bursts are detected *exclusively* on the longer 4.096 s and 8.192 s time scales. This suggests that there are relatively few faint GRBs waiting to be detected by a search that is more sensitive than the one we carried out. In this respect, the evolving models (D2 and D3) appear to be more accurate. They predict that the number of bursts per logarithmic peak flux interval will level off towards lower peak fluxes, and may even start to decline (see Figure 6-5). The non-evolving model, on the other hand, predicts that the number of bursts observed per logarithmic peak flux interval will continue to increase towards lower peak fluxes.

Since we have not derived peak fluxes on the 4.096 and 8.192 s time scales in order to repeat the analysis of section 6.4.1, we offer the following quantitative evidence that the paucity of bursts detected on the longer time scales favors the evolving models D2 and D3 over the non-evolving model D1. On the 1.024 s time scale, the measured value of $\langle (C_{min}/C_{max})^{3/2} \rangle = 0.247 \pm 0.006$ is trivially consistent with the values of $\langle (P_{min}/P)^{3/2} \rangle$ found for the best-fit models in section 6.4.1. But the value of $\langle (C_{min}/C_{max})^{3/2} \rangle = 0.177 \pm 0.006$ found for *all* bursts detected by our search contains information on the paucity of faint bursts on the 4.096 and 8.192 s time scales. We can compare it with the value of $\langle (P_{min}/P)^{3/2} \rangle$ obtained by extrapolating the best-fit models of section 6.4.1 to the peak flux threshold associated with the 8.192 s search. Taking $0.18/(2\sqrt{2}) = 0.06$ ph cm^{-2} s^{-1} as the approximate P_{min} for the 8.192 s search, we obtain the following values for $\langle (P_{min}/P)^{3/2} \rangle$: 0.221 in model D1, 0.169 in model D2, and 0.147 in model D3. Thus model D2 produces a value of $\langle (P_{min}/P)^{3/2} \rangle$ that

is the most consistent with the value of $\langle (C_{min}/C_{max})^{3/2} \rangle$ found for our full sample, and model D1 produces the most inconsistent value.

Second, the inferred equivalent isotropic peak luminosities (in the 30–2000 keV range) of the 3 bursts for which associated redshifts have been measured can be compared with the effective luminosity distributions of the best-fit models. The best-fit non-evolving model (D1) predicts that 90% of all GRBs should come from the narrow range of intrinsic peak luminosities (0.29–0.66) $10^{51} h_{70}^{-2}$ erg s^{-1} (a factor of ~ 2). The range from which 90% of the *observed* GRBs in this model are drawn is somewhat broader, however: (0.29–1.5) $10^{51} h_{70}^{-2}$ erg s^{-1} (a factor of ~ 5). In contrast, the intrinsic luminosities inferred from the 3 bursts with associated redshift information span a much broader peak luminosity range, (0.6–37) $10^{51} h_{70}^{-2}$ erg s^{-1} (a factor of ~ 62). Bursts with peak luminosities as high as those inferred for GRB 971214 ((37 ± 16) $10^{51} h_{70}^{-2}$ erg s^{-1}) and GRB 980703 ((2.2 ± 0.4) $10^{51} h_{70}^{-2}$ erg s^{-1}) are extremely rare events if the (non-evolving) model D1 is correct. On the other hand, the best-fit (evolving) models D2 and D3 allow a much broader (and uniformly higher) range of luminosities. The best-fit model D2 predicts that 90% of all GRBs are drawn from the intrinsic peak luminosity range (0.50–7.3) $10^{51} h_{70}^{-2}$ erg s^{-1} (a factor of ~ 15) and that 90% of the observed GRBs are drawn from the range (0.53–72) $10^{51} h_{70}^{-2}$ erg s^{-1} (a factor of ~ 130). Likewise, the best-fit model D3 predicts that 90% of all GRBs are drawn from the range (1.5–9.3) $10^{51} h_{70}^{-2}$ erg s^{-1} (a factor of ~ 6) and 90% of the observed GRBs are drawn from the range (1.5–40) $10^{51} h_{70}^{-2}$ erg s^{-1} (a factor of ~ 25). In the context of models D2 and D3, the GRBs 970508, 971214, and 980703 constitute a much more likely sample of detected bursts than in model D1.

The effective redshift distributions (the rates of observed bursts as a function of redshift) furnish another point of comparison with GRBs 970508, 971214, and 980703. As shown in Figure 6-6 the model D1 predicts a vanishingly small rate of observed bursts from the redshift $z = 3.418$ measured for GRB 981214 (Kulkarni et al. 1998). If model D1 were correct, then it would be remarkable that BATSE and *BeppoSAX* detected such a rare burst: only 1×10^{-6} of the rate distribution comes from higher

redshifts. On the other hand, the evolving models D2 and D3 predict much higher rates of observed bursts from $z = 3.418$. Even in these models, however, such a high redshift is exceptional: in model D2 only 0.4% of the burst rate distribution lies beyond $z = 3.4$, and in model D3 only 1.8% does. Still, as in the case of the inferred luminosity distributions, the 3 bursts with associated redshifts are a much more likely sample in models D2 and D3, where the GRB rate follows an estimate of the star formation history.

These results certainly do not prove that the GRB rate traces the star formation rate. The peak flux distributions alone fail to exclude the non-evolving rate density model (D1) with high confidence, especially in view of the unknown cosmological parameters which can be varied to improve the fit. Furthermore, until many more redshifts are associated with specific GRBs and/or more sensitive GRB detectors go on-line, the data will not be able to distinguish qualitatively similar SFR evolution models such as D2 and D3. Any evolution that specifies a significant peak in the burst rate in the redshift range $1 < z < 3$ is likely to be consistent with current data. The reasoning regarding the paucity of faint bursts detected *only* on the 4 s and 8 s time scales should be addressed more quantitatively in the context of the models; but this is difficult owing to our poor understanding of the diverse time profiles of GRBs and of the correlations between time profiles and peak fluxes. Finally, we have considered only 3 very specific "straw-man" models, and it may be that none of them are particularly accurate representations of the true GRB rate density and peak luminosity distributions. For example, a previous episode of star formation at high redshift could contribute a hitherto undetected population of very faint GRBs.

Nevertheless, the results of our search appear to support the conclusions reached by Totani (1997), Wijers et al. (1998), and Krumholz et al. (1998), who showed that if the GRB rate traces the SFR then relatively few faint "classical" GRBs are to be found below the BATSE onboard detection threshold. This information should be useful to the designers and operators of future GRB detectors.

In Figure 6-7 we plot the cumulative rate distribution of the off-line sample of

GRBs, along with the extrapolations of the best-fit models. At least some, and possibly all, of the discrepancy between the data and the models at high peak fluxes is due to the fact that BATSE has not operated long enough to detect the very bright (but rare) bursts; therefore this discrepancy is not significant. The GRB detector onboard *Pioneer Venus Orbiter* (*PVO*) operated for a much longer mission, so it has more completely sampled the rate of very bright bursts. When the peak fluxes of the GRBs detected with *PVO* are calibrated to match the BATSE peak fluxes, it would be of interest to see if the best-fit models found in this paper are also consistent with the very bright burst population. Figure 6-7 shows that the slopes of the best-fit models approach the $-3/2$ slope reported to be consistent with the brightest *PVO* bursts (Fenimore et al. 1993).

The results of the best-fit models are generally consistent with previous studies of the BATSE data. In particular we find that while we cannot constrain the full width of the power-law luminosity function in any of the scenarios we considered, the best-fit models yield intrinsic peak luminosity functions that contain 90% of all GRBs within a factor of 10–20. This result (or a similar one) has been previously obtained by Ulmer, Wijers, & Fenimore (1995), Woods & Loeb (1995), Hakkila et al. (1996), and Horack et al. (1996). We find that the peak luminosity distribution of the observed bursts, however, is wider: in model D2, 90% of the observed bursts come from a peak luminosity range that spans a factor of ~ 100 or more. A similar result was discussed by Loredo & Wasserman (1998).

The effective redshift distributions we obtain (see Figure 6-6) are reasonably consistent with those obtained by Krumholz et al. (1998) and Mao & Mo (1998) using the BATSE catalog data. They are also consistent with limits on the redshifts of GRB sources set by the non-detection of any gravitationally lensed GRBs in the BATSE catalogs (Marani et al. 1998). Holz, Miller, & Quashnock (1998) derive upper limits of $\langle z \rangle = 2.3$ (68% confidence) and $\langle z \rangle = 5.3$ (95% confidence) for the average redshift of GRB sources in the Einstein-de Sitter cosmology. The values of $\langle z \rangle$ we obtain for our best fit models (see Section 6.4.1) are well within these limits. The effective red-

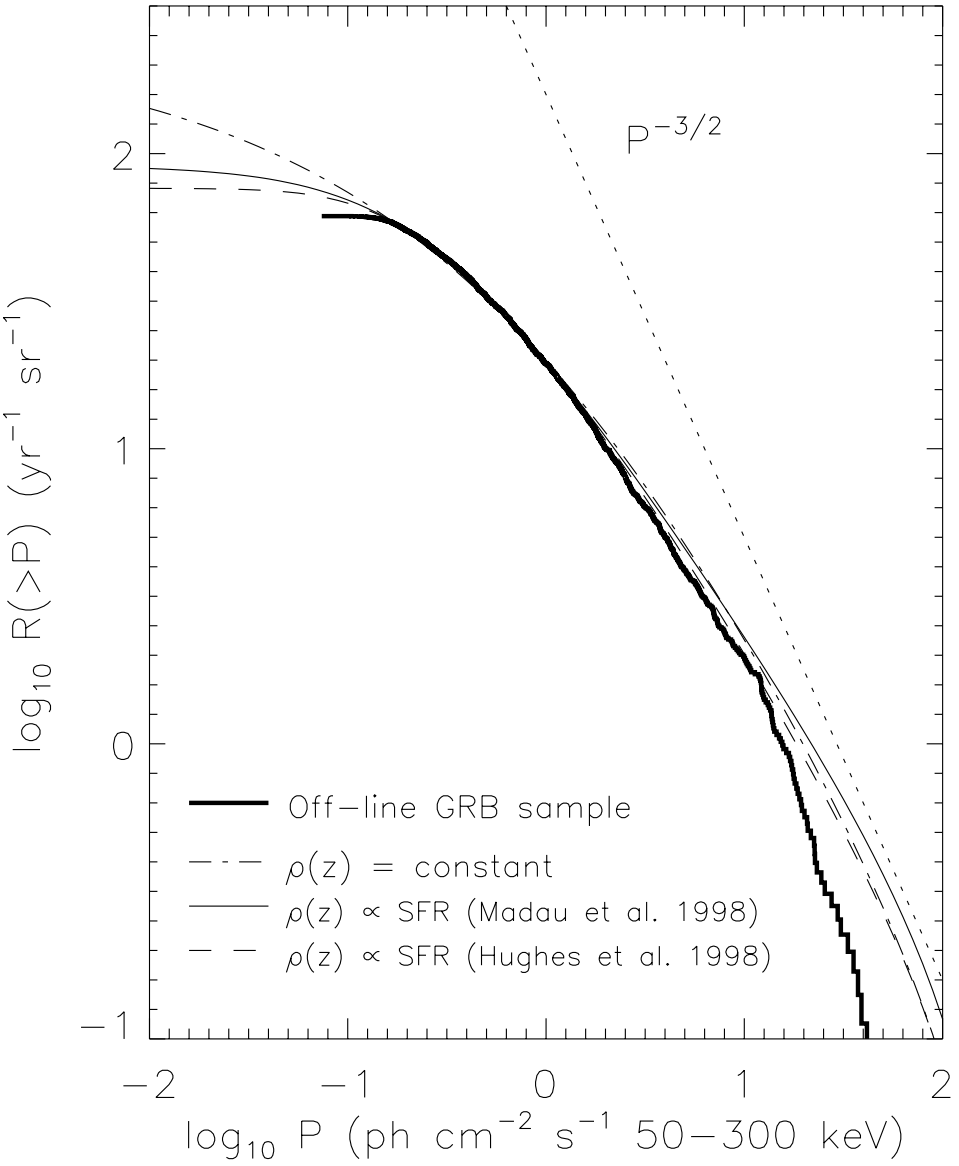

Figure 6-7 Cumulative rate distributions for best-fit models. The units of R are bursts yr^{-1} sr^{-1}. The observed peak flux distribution is shown as the solid histogram. The best-fit model D1 is shown as the dot-dashed line. Model D2 is shown as the solid line. Model D3 is shown as the dashed line. The discrepancy at high peak fluxes is not significant, since BATSE has not operated long enough to adequately sample the rate of the brightest bursts.

shift distributions are also consistent with the disparity found by Norris et al. (1995) between the duration distributions of bright and dim GRBs, which they interpret as the signature of cosmological time dilation for a GRB source distribution with the dimmest bursts at $z \approx 2$.

On the other hand, our effective redshift distributions are somewhat at odds with the conclusions of Wijers et al. (1998) that the faintest bursts observed with BATSE are at redshifts of $3 < z < 6$. According to our results with models D1, D2, and D3, no more than 0.002%, 1%, or 5% (respectively) of the bursts observed with our off-line sample are from redshifts larger than $z = 3.0$; and fewer than 8×10^{-7}%, 0.07%, or 0.25%, respectively, are at redshifts greater than $z = 4.0$. So, while GRBs may be produced at redshifts as high as $z \approx 6$, in the models we considered it is extremely unlikely that any such bursts have been observed.

To summarize, our off-line search of archival BATSE data has explored the distribution of GRB intensities at peak fluxes below the onboard detection threshold. We find a paucity of faint bursts detected on the 4.096 and 8.192 s time scales that were not already detected on the 1.024 s time scale. The differential intensity distribution is consistent with models in which the GRB rate traces the global star formation history of the Universe; and it is marginally consistent with the model in which the GRB rate is independent of redshift. We argue that the models in which the GRB rate traces the star formation rate are nevertheless preferred, based on the paucity of faint bursts detected exclusively on the 4.096 s and 8.192 s time scales, and on the comparison of the inferred effective luminosity and redshift distributions with the bursts for which redshifts have been measured. As an application of the off-line GRB intensity distribution, we set a limit of 10% (99% confidence) on the fractional rate of all GRBs that could belong to a homogeneous (in Euclidean space) subpopulation of burst sources (such as Type Ib/c supernovae).

Table 6-1. Values of $\langle (C_{min}/C_{max})^{3/2} \rangle$ obtained by various GRB detectors.

Detector/Mission	$\langle (C_{min}/C_{max})^{3/2} \rangle$	Reference
PVO	0.46 ± 0.02	Hartmann et al. 1992
Konus/*Venera 11 & 12*	0.45 ± 0.03	Higdon & Schmidt 1990b
A4/*HEAO 1*	0.40 ± 0.08	Schmidt, Higdon, & Hueter 1988
GRS/*SMM*	0.40 ± 0.025	Matz et al. 1992
GBD/*Ginga*	0.35 ± 0.035	Ogasaka et al. 1991
BATSE/*CGRO* (3B)	0.33 ± 0.01	Meegan et al. 1996
BATSE/*CGRO* (off-line, 1.024 s search only)	0.247 ± 0.006	(this paper)
BATSE/*CGRO* (all off-line)	0.177 ± 0.006	(this paper)

Table 6-2. Data for fitting differential peak flux distribution

P_1	P_2	ΔN_{obs}	ΔR (yr^{-1} sr^{-1})
0.180	0.202	87	2.45 ± 0.26
0.202	0.227	83	2.34 ± 0.26
0.227	0.254	99	2.80 ± 0.28
0.254	0.285	111	3.13 ± 0.30
0.285	0.320	92	2.60 ± 0.27
0.320	0.359	96	2.71 ± 0.28
0.359	0.403	95	2.68 ± 0.27
0.403	0.452	114	3.22 ± 0.30
0.452	0.507	93	2.62 ± 0.27
0.507	0.569	79	2.23 ± 0.25
0.569	0.639	82	2.31 ± 0.26
0.639	0.717	91	2.57 ± 0.27
0.717	0.804	73	2.06 ± 0.24
0.804	0.902	83	2.34 ± 0.26
0.902	1.000	52	1.47 ± 0.20
1.000	1.259	117	3.30 ± 0.31
1.259	1.584	111	3.13 ± 0.30
1.584	1.995	104	2.93 ± 0.29
1.995	2.511	72	2.03 ± 0.24
2.511	3.162	59	1.66 ± 0.22
3.162	3.981	48	1.35 ± 0.20
3.981	5.011	40	1.13 ± 0.18
5.011	6.309	27	0.76 ± 0.15
6.309	7.943	26	0.73 ± 0.14
7.943	20.00	64	1.80 ± 0.23

Table 6-3. Best fit parameters for monoluminous cosmological models

$\rho(z)$	R_0 (h_{70}^3 Gpc^{-3} yr^{-1} sr^{-1})	L_0 (10^{51} h_{70}^{-2} erg s^{-1})	χ^2 (23 d.o.f)
D1 (constant)	$9.5^{+0.4}_{-0.8}$	$0.40^{+0.06}_{-0.02}$	32.3
D2 (SFR)	2.0 ± 0.1	1.5 ± 0.1	64.1
D3 (AGN)	1.9 ± 0.1	$3.1^{+0.4}_{-0.2}$	27.8

Table 6-4. Best fit parameters for cosmological models with a power-law luminosity function

$\rho(z)$	R_0 (h_{70}^3 Gpc^{-3} yr^{-1} sr^{-1})	L_{min} (10^{51} h_{70}^{-2} erg s^{-1})	β	χ^2 (22 d.o.f)
D1 (constant)	8.8 ± 1.3	$0.29^{+0.08}_{-0.06}$	$4.6_{-1.4}$[a]	32.9
D2 (SFR)	2.2 ± 0.3	$0.48^{+0.20}_{-0.10}$	$2.1^{+0.3}_{-0.2}$	17.9
D3 (AGN)	2.1 ± 0.2	$1.44^{+0.53}_{-0.40}$	$2.6^{+1.0}_{-0.4}$	17.4

[a]This parameter is not constrained above the best fit value when the other parameters are free to vary.

Table 6-5. Co-moving $z = 0$ burst rate for monoluminous cosmological models

$\rho(z)$	ρ_0 (h_{70}^3 Gpc^{-3} yr^{-1})	GEM[a] (Myr^{-1})
D1 (constant)	$11.9^{+0.5}_{-1.0}$	~ 2
D2 (SFR)	0.78 ± 0.04	~ 0.2
D3 (AGN)	0.46 ± 0.02	~ 0.1

[a]Galactic Events per Million years.

Table 6-6. Co-moving $z = 0$ burst rate for cosmological models with a power-law luminosity function

$\rho(z)$	ρ_0 (h_{70}^3 Gpc^{-3} yr^{-1})	GEM[a] (Myr^{-1})
D1 (constant)	11.1 ± 1.6	~ 2
D2 (SFR)	0.87 ± 0.12	~ 0.2
D3 (AGN)	0.51 ± 0.05	~ 0.1

[a]Galactic Events per Million years.

Table 6-7. Upper limits on fractional GRB rate due to a possible homogeneous (in Euclidean space) sub-population of GRBs

$\rho(z)$	90%	99%
D1 (constant)	5.1%	6.2%
D2 (SFR)	6.9%	10.0%
D3 (AGN)	7.7%	11.2%

Chapter 7

Conclusions

This chapter summarizes the main results of the search for non-triggered events.

- A search of 1.33×10^8 s of archival data from BATSE yields 873 events that appear to be gamma-ray bursts (GRBs) and that did *not* activate the onboard burst detection (or "trigger") system. During the time spanned by the off-line search, the onboard trigger detected 1815 GRBs, of which 1392 were also detected with the off-line search. **Thus the off-line search increases the number of GRBs detected with BATSE by 48%.** (Section 5.2.)

- On the 1.024 s time scale, the detection threshold of the off-line search is a factor of ~ 2 lower in the 50–300 keV range than that of the onboard burst trigger. On the longer time scales (4.096 s and 8.192 s) the off-line search is sensitive to even fainter bursts that have durations at least as long as the corresponding time scale. **The events detected with the off-line search extend knowledge of the GRB peak flux distribution to values a factor of ~ 2 lower than could be studied previously.** (Section 4.4.)

- The value of the $\langle V/V_{\rm max} \rangle$ statistic (in Euclidean space) for the GRBs detected with the off-line search is 0.177 ± 0.006. **This is the lowest value so far obtained for a global sample of GRBs, indicating the strongest deviation from a homogeneous (in Euclidean space) source population.**

(Section 6.3.2.)

- **The direction distribution of all GRBs detected with the off-line search is consistent with an isotropic source population.** Among the GRBs that are below the onboard threshold there is some evidence for clustering towards the poles of the equatorial coordinate system; this most likely reflects a tendency to classify faint GRBs that have source directions consistent with the Sun as solar flares. (Section 5.5.)

- **The peak flux distribution of the GRBs detected with the off-line search is consistent with cosmological models of the source population in which the co-moving GRB rate approximately traces the star-formation history of the Universe.** The inferred distributions of peak luminosity and source redshift in these models are in better agreement with the apparent peak luminosities of the three bursts for which redshifts have been measured than in the model for which the co-moving GRB rate is constant. (Section 6.5.)

- **If the cosmological GRB rate traces the star-formation history of the Universe, the faintest bursts observed with the off-line search are at redshifts of $z \approx 3$.** (Section 6.4.1.)

- The peak flux distribution of the GRBs detected with the off-line search sets upper limits on the rate of bursts from a hypothetical sub-population that is homogeneously distributed in Euclidean space. For example, if the Type Ib/c supernova 1998bw that was discovered in the X-ray error box of GRB 980425 is responsible for that GRB, then it represents a separate population of GRB sources that is expected to appear homogeneously distributed in Euclidean space given the sensitivities of current instruments. **Depending on the model for the co-moving rate of the cosmological GRB population, the peak flux distribution sets 90% confidence upper limits of 5% to 10% on**

the fraction of observed GRBs that may come from a homogeneous, "nearby" sub-population of GRB sources. (Section 6.4.2.)

- The onboard burst trigger relies on a background average that is re-computed every 17.408 s. If a GRB has a time profile that rises on a time scale long compared this, it will artificially raise the background estimate and thus raise the detection threshold. This has been proposed as a significant source of incompleteness in the BATSE catalogs. The off-line search is more sensitive to such "slow-rising" events, so it can be used to evaluate the effect of the "slow-rising" bias on the BATSE catalogs. **Only $\sim$ 3% of the non-triggered GRBs detected with the off-line search were missed by the onboard burst trigger because they were "slow-risers".** (Section C.6.1.)

- The off-line search yields 25 bursts that appear to be from soft gamma-ray repeaters (SGRs). At least 24 of these are consistent with activity from the known source SGR 1806−20 based on source direction and time of arrival. Only one is clearly inconsistent with both the position and periods of activity of SGR 1806−20. It may represent a previously unknown SGR or it may be a spectrally soft GRB of short (< 1 s) duration.

- The off-line search detects 50 events of unknown origin. These have nearly all of their counts in the 25–100 keV range. Their direction distribution is isotropic, and their instrumental hardness ratios are consistent with the hypothesis that they represent the low-energy tail of the GRB spectral distribution. Their times of arrival are not uniform, however. This could indicate the presence of multiple classes of sources (one or more of which does not burst uniformly in time) or variations in the sensitivity of the off-line search and classification procedures.

Appendix A

Catalog of Nontriggered Gamma Ray Bursts

Table A-1 lists the BATSE trigger numbers for the onboard-triggered bursts that were detected with the off-line search. The trigger number can be used to look up the physical parameters of these bursts in the BATSE catalogs (Fishman et al. 1994; Meegan et al. 1996; Paciesas et al. 1999; Meegan et al. 1998a).

Table A-2 lists the physical parameters of 873 the nontriggered GRB candidates identified in a search of 6 years of archival DISCLA data. Each entry in the table occupies a group of 3 lines. The first column gives the name of the nontriggered burst and the time of the peak flux of the event in terms of the Truncated Julian Day (TJD) number and the time of day expressed as seconds UT. The second column gives the best-fit source direction for the event in terms of equatorial right ascension and declination (J2000.0) expressed in decimal degrees along with the statistical uncertainty in the source direction. The full uncertainty in the best-fit source direction is the result of combining the statistical uncertainty in quadrature with a 4° random systematic uncertainty. The third column gives the ratio of the maximum count rate found in DISCLA channels 2 and 3 during the burst to the minimum count rate required for detection on each of the three time scales of the search (1.024 s, 4.096 s, and 8.192 s). The fourth column gives the minimum counts required for detection on the three

time scales. Missing entries are denoted with an ellipsis (...) and indicate that the event was not detected on the corresponding time scale. The fifth column lists the T_{50} and T_{90} duration estimates in seconds. For some bursts, there is no T_{50} estimate; this indicates that the T_{90} duration was estimated by eye. The sixth column gives the peak flux and fluence estimates in DISCLA channels 2 and 3 (roughly 50–300 keV). For further information on these quantities, see section 5.3.

Table A-1. Onboard triggers detected in off-line search

Trigger Number														
1159	1466	1662	2037	2191	2368	2521	2715	2900	3040	3159	3335	3505	3770	3926
1167	1467	1663	2039	2193	2371	2522	2719	2901	3042	3160	3336	3509	3771	3929
1190	1468	1664	2040	2197	2372	2523	2725	2910	3044	3163	3337	3510	3772	3930
1192	1469	1665	2041	2201	2373	2530	2727	2913	3046	3164	3338	3511	3773	3935
1196	1472	1667	2043	2202	2375	2533	2728	2916	3055	3166	3339	3512	3774	3936
1197	1473	1676	2044	2203	2377	2537	2732	2917	3056	3167	3340	3514	3776	3938
1200	1480	1678	2047	2204	2381	2538	2736	2918	3057	3168	3345	3516	3779	3939
1204	1481	1679	2049	2205	2382	2542	2748	2919	3058	3171	3347	3523	3781	3940
1211	1482	1682	2053	2206	2383	2551	2749	2922	3062	3173	3349	3527	3782	3941
1212	1484	1683	2056	2211	2385	2560	2750	2924	3066	3174	3350	3528	3788	3954
1213	1485	1687	2061	2213	2387	2569	2751	2925	3067	3177	3351	3530	3789	4039
1218	1489	1690	2067	2217	2388	2570	2753	2927	3068	3178	3352	3545	3791	4048
1221	1492	1693	2068	2219	2389	2581	2755	2929	3070	3193	3356	3552	3792	4095
1223	1503	1694	2069	2220	2391	2583	2760	2931	3071	3212	3357	3567	3800	4146
1235	1515	1698	2070	2228	2392	2585	2767	2932	3072	3215	3358	3569	3801	4157
1244	1518	1700	2074	2230	2393	2586	2770	2933	3074	3217	3359	3571	3805	4216
1279	1524	1701	2077	2232	2394	2588	2773	2939	3075	3218	3360	3580	3806	4251
1288	1533	1709	2079	2233	2401	2589	2774	2940	3076	3220	3361	3588	3807	4256
1289	1540	1711	2080	2240	2405	2592	2775	2944	3080	3227	3364	3590	3810	4312
1291	1541	1712	2081	2244	2419	2593	2780	2945	3084	3229	3366	3593	3811	4327
1297	1546	1714	2083	2252	2423	2597	2787	2947	3085	3237	3369	3594	3812	4350
1298	1551	1717	2087	2253	2424	2600	2788	2948	3087	3238	3370	3598	3814	4368
1301	1552	1719	2090	2254	2428	2603	2790	2950	3088	3241	3374	3606	3815	4388
1303	1553	1723	2093	2265	2430	2606	2793	2951	3089	3242	3378	3608	3819	4469
1306	1558	1730	2099	2267	2431	2608	2794	2952	3091	3245	3379	3611	3840	4556
1307	1559	1731	2101	2268	2432	2609	2795	2953	3093	3246	3403	3618	3843	4569
1308	1561	1733	2102	2273	2434	2611	2797	2961	3094	3247	3405	3634	3853	4653
1310	1567	1734	2103	2277	2435	2614	2798	2964	3096	3248	3406	3637	3860	4660
1311	1574	1736	2105	2283	2436	2617	2799	2966	3099	3251	3407	3639	3864	4701
1318	1578	1740	2110	2286	2437	2619	2800	2973	3100	3253	3408	3640	3866	4710
1319	1579	1741	2111	2287	2438	2620	2810	2975	3101	3255	3410	3642	3867	4744
1321	1580	1742	2112	2288	2440	2621	2812	2977	3102	3256	3412	3643	3868	4745
1346	1586	1743	2114	2294	2441	2623	2814	2978	3103	3257	3415	3644	3869	4776
1359	1588	1747	2115	2298	2442	2628	2815	2980	3105	3259	3416	3647	3870	4814
1365	1590	1760	2117	2304	2443	2632	2821	2984	3108	3266	3431	3648	3871	4871
1382	1601	1791	2119	2306	2446	2633	2825	2985	3109	3267	3436	3649	3875	4898
1384	1603	1806	2122	2307	2447	2634	2828	2986	3110	3269	3437	3651	3879	4939
1385	1604	1807	2123	2309	2448	2636	2831	2987	3113	3273	3439	3652	3886	4955
1388	1606	1815	2125	2310	2450	2640	2834	2988	3114	3278	3440	3654	3887	4959
1390	1609	1819	2126	2311	2452	2641	2844	2990	3115	3279	3441	3655	3888	5079
1396	1611	1830	2129	2315	2453	2649	2846	2992	3118	3280	3442	3657	3891	5080
1404	1614	1851	2132	2316	2454	2660	2848	2993	3119	3282	3443	3658	3892	5206
1406	1623	1883	2133	2317	2458	2661	2849	2994	3120	3283	3448	3662	3893	5212
1413	1624	1885	2138	2318	2460	2662	2850	2995	3121	3284	3458	3663	3894	5255
1416	1625	1886	2140	2320	2464	2663	2851	2996	3125	3287	3464	3664	3895	5277
1419	1626	1922	2142	2321	2472	2664	2853	2998	3127	3290	3465	3665	3899	5304
1422	1628	1924	2143	2324	2476	2665	2855	3001	3128	3291	3466	3668	3900	5305
1425	1634	1934	2145	2325	2477	2671	2856	3003	3129	3292	3467	3671	3901	5337
1430	1635	1948	2148	2327	2482	2676	2857	3005	3130	3293	3471	3709	3902	5339
1432	1636	1953	2149	2328	2484	2677	2860	3011	3131	3294	3472	3711	3903	5377
1435	1637	1956	2151	2329	2489	2679	2861	3012	3132	3295	3473	3717	3905	5379
1439	1642	1967	2152	2330	2490	2681	2862	3015	3134	3297	3476	3722	3906	5387
1440	1643	1968	2155	2338	2495	2688	2864	3016	3135	3298	3477	3728	3908	5389
1443	1646	1973	2156	2340	2496	2690	2877	3017	3136	3301	3480	3733	3909	5407
1446	1648	1974	2159	2343	2500	2691	2880	3026	3138	3303	3481	3735	3910	5409
1447	1650	1982	2160	2344	2502	2693	2881	3027	3139	3306	3485	3736	3911	5410
1449	1651	1989	2161	2345	2504	2695	2889	3028	3141	3307	3486	3737	3912	5411
1452	1652	1991	2163	2347	2505	2696	2890	3029	3142	3308	3487	3740	3913	5412
1453	1653	1993	2167	2349	2507	2698	2891	3030	3143	3319	3488	3742	3914	5413
1456	1655	1997	2169	2352	2508	2700	2892	3032	3144	3320	3489	3745	3915	5415
1458	1656	2003	2181	2353	2511	2701	2893	3035	3146	3321	3491	3751	3916	5416
1459	1657	2018	2187	2357	2512	2703	2894	3036	3152	3322	3493	3764	3917	5417
1462	1659	2019	2188	2358	2513	2706	2896	3037	3153	3323	3494	3765	3918	5419
1463	1660	2029	2189	2360	2514	2709	2897	3038	3155	3324	3502	3766	3921	5420
1465	1661	2035	2190	2367	2519	2711	2898	3039	3156	3330	3503	3768	3924	5421

Table A-1—Continued

Trigger Number						
5423	5515	5624	6101	6228	6335	6453
5427	5516	5626	6102	6229	6336	6454
5428	5517	5627	6103	6230	6337	6469
5429	5518	5628	6104	6233	6338	6472
5433	5523	5629	6105	6234	6339	6476
5434	5524	5631	6109	6235	6341	6479
5436	5526	5632	6111	6236	6342	6486
5439	5527	5633	6113	6237	6344	6487
5446	5528	5634	6115	6238	6345	6488
5448	5529	5635	6117	6240	6346	6489
5450	5530	5637	6118	6241	6347	6490
5451	5531	5638	6119	6242	6349	6497
5452	5532	5640	6123	6243	6351	6498
5453	5533	5643	6124	6244	6353	6504
5454	5534	5644	6125	6249	6355	6519
5456	5537	5645	6127	6260	6358	6520
5457	5538	5646	6128	6262	6366	6521
5459	5539	5647	6131	6263	6368	6522
5461	5540	5648	6134	6265	6369	6523
5463	5541	5650	6135	6266	6370	6525
5464	5542	5654	6136	6267	6372	6526
5465	5545	5655	6137	6269	6375	6527
5466	5546	5664	6139	6270	6376	6528
5467	5547	5666	6141	6271	6380	6529
5469	5548	5667	6142	6272	6385	6531
5470	5551	5669	6144	6273	6386	6533
5471	5553	5693	6145	6274	6388	6534
5472	5554	5697	6147	6275	6389	
5473	5555	5704	6148	6276	6390	
5474	5556	5706	6149	6279	6393	
5475	5559	5710	6151	6280	6395	
5476	5560	5711	6152	6281	6396	
5477	5561	5713	6154	6283	6397	
5478	5562	5715	6158	6284	6398	
5479	5563	5716	6159	6285	6399	
5480	5564	5718	6160	6288	6400	
5482	5565	5719	6162	6292	6401	
5483	5566	5721	6165	6293	6404	
5484	5567	5723	6167	6294	6405	
5485	5568	5724	6168	6295	6408	
5486	5569	5725	6176	6296	6409	
5487	5571	5726	6178	6298	6411	
5488	5572	5729	6180	6299	6412	
5489	5573	5730	6182	6300	6413	
5490	5574	5731	6186	6301	6414	
5491	5575	5733	6188	6303	6419	
5492	5581	5736	6189	6304	6422	
5493	5585	5740	6190	6305	6425	
5494	5601	5770	6194	6306	6427	
5495	5603	5773	6198	6307	6432	
5497	5604	5867	6205	6308	6433	
5498	5605	5890	6206	6309	6435	
5499	5606	5955	6207	6314	6436	
5500	5607	5983	6209	6315	6437	
5501	5608	5989	6212	6317	6439	
5502	5609	5992	6214	6319	6440	
5503	5610	5995	6215	6320	6443	
5504	5612	6004	6216	6321	6444	
5505	5614	6082	6220	6322	6445	
5507	5615	6083	6221	6323	6446	
5508	5617	6090	6222	6328	6447	
5509	5618	6091	6223	6329	6448	
5510	5619	6096	6225	6330	6450	
5512	5621	6098	6226	6331	6451	
5513	5622	6100	6227	6334	6452	

Table A-2. Nontriggered GRB catalog

Name (NTB) Date (TJD) Time (s UT)	R.A. (°) Decl. (°) Err. (°)	C_{max}/C_{min} (4.096 s) (8.192 s)	C_{min} (4.096 s) (8.192 s)	T_{50} (s) T_{90} (s)	P (ph cm^{-2} s^{-1}) F (erg cm^{-2}) (50–300 keV)
911214.77	81.8	1.55	113	3.07 ± 1.45	0.50 ± 0.08
8604	-46.1	2.25	218	7.17 ± 1.45	(4.87 ± 0.17)E-7
67344.5	13.0	2.10	322		
911216.20	94.3	2.93	142	35.84 ± 3.24	0.46 ± 0.05
8606	5.3	5.19	283	(1.22 ± 0.10)E+2	(3.38 ± 0.12)E-6
18008.2	2.1	6.92	393		
911217.40	176.7	1.42	147	...	0.20 ± 0.04
8607	57.5	1.32	379	4.10 ± 2.05	(8.76 ± 0.18)E-8
35298.4	21.3	...	...		
911220.57	47.2	5.05	131	5.12 ± 1.45	0.80 ± 0.05
8610	82.6	9.65	247	12.29 ± 2.29	(1.48 ± 0.10)E-6
49938.5	2.7	10.75	341		
911222.86	344.2	1.49	151	14.34 ± 2.29	0.22 ± 0.04
8612	65.7	2.70	315	38.91 ± 12.33	(5.46 ± 0.06)E-7
74410.1	7.7	3.22	436		
911224.69	140.6	1.35	115	17.41 ± 1.45	0.17 ± 0.04
8614	12.0	2.42	266	43.01 ± 10.29	(7.48 ± 0.49)E-7
59873.4	8.1	2.79	327		
911225.65	149.3	1.38	157	12.29 ± 2.29	0.19 ± 0.04
8615	24.5	2.26	295	27.65 ± 18.69	(3.25 ± 0.29)E-7
56521.8	14.2	2.44	452		
911228.81	138.4	5.30	184	...	1.40 ± 0.08
8618	20.7	2.97	303	2.05 ± 1.02	(4.04 ± 0.11)E-7
70058.1	16.4	2.36	453		
920107.89	211.8	1.31	189	41.98 ± 2.29	0.18 ± 0.04
8628	-16.6	2.39	375	(1.15 ± 0.07)E+2	(1.27 ± 0.08)E-6
77342.8	5.0	3.11	505		
920117.42	52.1	1.74	120	17.41 ± 1.45	0.41 ± 0.05
8638	-46.8	3.21	237	47.10 ± 7.24	(1.07 ± 0.15)E-6
36696.2	2.7	3.79	340		
920120.00	182.6	1.65	174	12.29 ± 1.45	0.24 ± 0.04
8641	-9.3	2.71	345	29.70 ± 2.29	(5.10 ± 0.66)E-7
656.5	4.1	3.18	509		
920121.55	144.9	...	...	23.55 ± 1.45	0.10 ± 0.04
8642	-0.1	1.17	233	53.25 ± 1.45	(2.02 ± 0.10)E-7
48109.7	30.6	1.47	354		
920123.22	11.6	1.57	183	10.24 ± 1.45	0.22 ± 0.04
8644	22.9	2.82	361	33.79 ± 7.24	(6.35 ± 0.60)E-7
19017.8	4.7	3.71	515		
920126.26	34.7	3.13	147	...	0.77 ± 0.07
8647	-37.1	2.19	250	4.10 ± 2.05	(2.44 ± 0.06)E-7
22582.4	7.6	1.43	322		
920128.14	155.3	3.40	173	2.05 ± 1.45	0.60 ± 0.05
8649	-25.2	3.99	310	9.22 ± 5.22	(3.02 ± 0.77)E-7
12897.4	5.3	3.21	480		
920128.93	36.0	1.16	155	21.50 ± 2.29	0.17 ± 0.04
8649	-8.9	1.85	238	75.78 ± 9.27	(7.10 ± 0.35)E-7
80843.9	21.2	2.06	329		
920130.58	227.0	1.56	148	...	0.43 ± 0.07
8651	-23.5	1.56	347	5.12 ± 3.07	(2.04 ± 0.05)E-7
50457.7	19.5	1.22	389		
920202.80	248.6	...	...	5.12 ± 1.45	(8.07 ± 3.05)E-2
8654	86.1	1.68	300	21.50 ± 6.23	(1.62 ± 0.33)E-7
69197.9	19.3	1.94	432		
920214.98	123.5	4.51	165	12.29 ± 1.45	0.65 ± 0.05
8666	-18.8	8.35	323	40.96 ± 1.45	(2.31 ± 0.09)E-6
85364.8	1.4	11.52	473		
920215.81	248.0	1.17	163	6.14 ± 1.45	0.17 ± 0.04
8667	-44.6	2.10	372	13.31 ± 3.69	(3.14 ± 0.72)E-7
70585.5	11.1	2.80	562		

Table A-2—Continued

Name (NTB) Date (TJD) Time (s UT)	R.A. (°) Decl. (°) Err. (°)	C_{max}/C_{min} (4.096 s) (8.192 s)	C_{min} (4.096 s) (8.192 s)	T_{50} (s) T_{90} (s)	P (ph cm^{-2} s^{-1}) F (erg cm^{-2}) (50–300 keV)
920215.84	230.9	1.17	173	3.07 ± 2.29	0.17 ± 0.04
8667	23.1	1.77	365	15.36 ± 6.56	(1.38 ± 0.04)E-7
73237.6	17.7	1.47	459		
920216.52	240.5	1.40	133	9.22 ± 2.29	0.19 ± 0.04
8668	17.6	2.31	344	24.58 ± 2.29	(2.40 ± 0.37)E-7
45566.1	11.7	1.99	502		
920216.67	324.9	14.16	126	24.58 ± 2.29	2.41 ± 0.07
8668	18.0	23.39	245	46.08 ± 2.29	(6.05 ± 0.40)E-6
58683.5	0.4	24.71	346		
920219.12	275.1	1.39	167	...	0.23 ± 0.05
8671	27.1	1.18	375	4.10 ± 2.05	(9.39 ± 0.20)E-8
10914.9	13.8	1.03	475		
920225.13	14.0	1.85	143	22.53 ± 5.51	0.25 ± 0.04
8677	-49.0	2.91	273	(1.23 ± 0.27)E+2	(5.64 ± 3.26)E-7
11553.9	5.5	3.39	386		
920227.55	201.3	1.46	178	29.70 ± 1.45	0.19 ± 0.04
8679	-5.8	2.50	313	69.63 ± 4.58	(1.45 ± 0.01)E-6
48278.6	2.9	2.91	485		
920229.81	185.4	6.52	145	4.10 ± 1.45	0.95 ± 0.05
8681	-51.3	6.31	295	30.72 ± 1.45	(4.17 ± 0.83)E-7
70747.2	6.7	5.49	427		
920303.28	318.5	10.47	174	3.07 ± 1.45	1.75 ± 0.06
8684	-12.5	13.22	343	31.74 ± 4.34	(1.06 ± 0.18)E-6
24522.9	6.4	10.50	495		
920306.17	278.4	2.30	160	11.26 ± 1.45	0.35 ± 0.04
8687	1.2	3.81	326	29.70 ± 3.24	(6.36 ± 0.59)E-7
15262.8	10.1	4.65	459		
920307.70	156.0	...	...	45.06 ± 1.45	0.15 ± 0.04
8688	-25.5	1.62	253	56.32 ± 3.24	(3.37 ± 0.50)E-7
60735.6	53.4	1.93	376		
920314.73	342.1	2.24	156	14.34 ± 1.45	0.28 ± 0.04
8695	-58.9	4.16	333	48.13 ± 5.22	(1.21 ± 0.11)E-6
63736.9	3.4	5.59	468		
920319.04	28.7	1.20	126	7.17 ± 1.45	0.19 ± 0.04
8700	-9.7	1.99	271	13.31 ± 2.29	(2.45 ± 0.31)E-7
3637.4	14.0	2.23	366		
920321.19	220.1	1.34	150	9.22 ± 1.45	0.19 ± 0.04
8702	-6.0	2.58	236	27.65 ± 3.24	(3.28 ± 0.57)E-7
16640.1	12.0	2.94	389		
920321.53	230.7	1.56	118	6.14 ± 1.45	0.28 ± 0.04
8702	45.6	2.76	273	28.67 ± 5.22	(3.06 ± 0.56)E-7
45908.1	20.6	2.64	378		
920330.80	79.7	1.35	131	12.29 ± 1.45	0.20 ± 0.04
8711	13.3	2.42	312	23.55 ± 1.45	(3.19 ± 0.57)E-7
69508.2	11.7	2.75	460		
920401.40	111.1	1.81	119	6.14 ± 2.29	0.28 ± 0.04
8713	47.4	2.47	253	48.13 ± 11.31	(2.31 ± 0.55)E-7
35038.3	9.4	2.33	357		
920402.05	306.1	1.25	177	19.46 ± 1.45	0.15 ± 0.05
8714	12.1	1.78	332	33.79 ± 8.26	(3.67 ± 0.05)E-7
4948.1	7.8	1.99	462		
920411.79	286.0	1.81	139	...	0.27 ± 0.04
8723	-63.3	1.57	298	6.14 ± 3.07	(9.15 ± 0.32)E-8
68643.9	28.0	1.08	318		
920417.79	239.0	1.38	151	14.34 ± 1.45	0.14 ± 0.04
8729	-31.2	1.71	302	36.86 ± 8.69	(3.39 ± 0.59)E-7
69074.0	23.9	2.01	458		
920423.85	305.1	...	...	...	0.12 ± 0.04
8735	53.4	1.50	326	9.22 ± 3.07	(1.23 ± 0.02)E-7
73647.2	16.0	1.40	438		

Table A-2—Continued

Name (NTB) Date (TJD) Time (s UT)	R.A. (°) Decl. (°) Err. (°)	C_{max}/C_{min} (4.096 s) (8.192 s)	C_{min} (4.096 s) (8.192 s)	T_{50} (s) T_{90} (s)	P (ph cm^{-2} s^{-1}) F (erg cm^{-2}) (50–300 keV)
920424.67	269.6	2.40	189	...	0.64 ± 0.07
8736	7.6	2.05	354	3.07 ± 2.05	(2.34 ± 0.07)E-7
58425.4	20.3	1.66	507		
920425.55	341.4	1.04	167	6.14 ± 1.45	0.14 ± 0.04
8737	-7.2	1.69	294	18.43 ± 1.45	(1.29 ± 0.24)E-7
48147.6	14.7	1.79	483		
920428.63	187.0	1.91	111	30.72 ± 2.29	0.30 ± 0.04
8740	53.9	3.08	234	(1.06 ± 0.18)E+2	(1.49 ± 0.10)E-6
55017.6	5.0	4.45	331		
920430.40	358.4	6.60	181	5.12 ± 1.45	1.05 ± 0.05
8742	-8.1	11.01	357	23.55 ± 4.22	(1.63 ± 0.08)E-6
34896.0	1.1	11.55	519		
920503.16	16.9	1.33	144	27.65 ± 2.29	0.20 ± 0.04
8745	59.7	2.15	295	61.44 ± 9.44	(7.35 ± 0.47)E-7
13855.8	8.3	2.78	387		
920509.08	94.2	1.26	176	12.29 ± 4.22	0.18 ± 0.05
8751	-32.2	2.02	231	23.55 ± 1.45	(2.50 ± 0.39)E-7
7668.8	12.1	2.19	415		
920509.33	178.5	1.27	164	64.51 ± 1.45	0.17 ± 0.04
8751	66.4	2.38	334	(1.40 ± 0.43)E+2	(6.35 ± 0.61)E-7
29074.5	11.0	2.93	486		
920510.17	185.1	1.42	133	13.31 ± 1.45	0.29 ± 0.05
8752	-17.6	2.00	289	29.70 ± 6.56	(7.27 ± 0.06)E-7
15222.9	5.0	2.52	425		
920511.79	63.1	1.19	192	10.24 ± 2.29	0.20 ± 0.05
8753	-47.6	1.54	392	32.77 ± 5.22	(2.88 ± 0.39)E-7
68554.9	9.1	1.66	509		
920513.46	125.2	1.76	120	17.41 ± 1.45	0.29 ± 0.04
8755	-17.1	3.28	245	40.96 ± 2.29	(8.03 ± 0.60)E-7
40058.0	3.5	4.12	364		
920514.82	147.6	...	...	...	0.25 ± 0.07
8756	84.5	1.63	342	31.74 ± 10.24	(6.04 ± 0.11)E-7
70936.7	42.3	1.91	450		
920514.83	36.7	1.13	162	12.29 ± 3.24	0.17 ± 0.04
8756	22.1	1.97	295	33.79 ± 2.29	(3.52 ± 0.49)E-7
72214.6	13.8	2.49	397		
920518.25	172.7	1.46	122	5.12 ± 1.45	0.18 ± 0.04
8760	42.9	2.01	234	21.50 ± 5.51	(2.08 ± 0.40)E-7
21831.8	13.3	2.31	330		
920518.30	30.2	1.24	163	18.43 ± 1.45	0.21 ± 0.04
8760	19.7	1.88	230	52.22 ± 9.44	(8.12 ± 0.89)E-7
26429.5	3.8	2.85	326		
920518.68	295.7	4.35	180	6.14 ± 1.45	0.66 ± 0.05
8760	15.7	6.73	370	20.48 ± 5.51	(7.51 ± 0.80)E-7
59203.7	5.2	7.21	529		
920521.22	238.2	1.23	160	8.19 ± 3.24	0.22 ± 0.05
8763	23.4	1.63	365	18.43 ± 3.24	(1.85 ± 1.60)E-7
19248.2	4.9	1.83	452		
920602.25	356.6	1.18	165	...	0.18 ± 0.04
8775	-44.3	1.44	291	5.12 ± 3.07	(1.09 ± 0.03)E-7
21656.7	22.2	1.18	370		
920604.65	240.4	1.20	177	9.22 ± 1.45	0.15 ± 0.06
8777	-2.1	1.97	325	29.70 ± 2.29	(3.86 ± 1.22)E-7
56876.1	4.7	2.35	500		
920605.79	85.9	...	...	...	(8.12 ± 3.72)E-2
8778	61.9	1.45	335	5.12 ± 3.07	(8.51 ± 0.57)E-8
68417.6	27.4	1.28	493		
920606.67	119.0	1.41	116	...	0.19 ± 0.04
8779	-34.0	1.01	320	4.10 ± 2.05	(5.14 ± 0.15)E-8
58057.8	56.8	...	...		

Table A-2—Continued

Name (NTB) Date (TJD) Time (s UT)	R.A. (°) Decl. (°) Err. (°)	C_{max}/C_{min} (4.096 s) (8.192 s)	C_{min} (4.096 s) (8.192 s)	T_{50} (s) T_{90} (s)	P (ph cm^{-2} s^{-1}) F (erg cm^{-2}) (50–300 keV)
920615.36	309.4	...	...	14.34 ± 3.24	(7.38 ± 3.99)E-2
8788	62.8	1.20	287	41.98 ± 8.75	(2.82 ± 0.11)E-7
31594.6	12.0	1.43	329		
920617.21	76.0	...	...	...	0.15 ± 0.05
8790	42.9	1.40	299	11.26 ± 3.07	(1.82 ± 0.13)E-7
18737.3	7.3	1.58	485		
920617.87	276.5	1.13	118	15.36 ± 1.45	0.15 ± 0.04
8790	78.2	1.53	338	31.74 ± 2.29	(2.70 ± 0.57)E-7
75184.2	25.2	1.83	457		
920619.25	107.2	1.41	166	15.36 ± 1.45	0.13 ± 0.04
8792	33.8	1.76	288	40.96 ± 10.09	(2.76 ± 0.29)E-7
22326.4	10.3	2.20	460		
920619.36	179.5	2.74	184	2.05 ± 1.45	0.48 ± 0.05
8792	-4.8	3.59	345	7.17 ± 4.58	(2.90 ± 0.53)E-7
31668.3	5.8	3.16	529		
920619.57	108.9	1.04	136	8.19 ± 1.45	0.16 ± 0.04
8792	-54.1	1.53	301	20.48 ± 2.29	(2.27 ± 0.06)E-7
49539.2	13.6	1.89	435		
920619.75	253.8	4.04	156	21.50 ± 2.29	0.79 ± 0.06
8792	24.9	7.19	326	59.39 ± 6.23	(2.28 ± 0.15)E-6
64805.0	1.8	8.96	462		
920621.83	45.3	1.21	125	18.43 ± 6.23	0.23 ± 0.05
8794	-2.9	1.88	252	68.61 ± 2.29	(7.13 ± 0.89)E-7
72143.0	33.6	2.66	356		
920622.27	147.6	6.42	134	...	0.90 ± 0.05
8795	-39.7	12.44	278	90.11 ± 10.24	(5.44 ± 0.15)E-6
23825.5	0.9	15.84	387		
920622.30	138.2	1.39	146	28.67 ± 2.29	0.21 ± 0.04
8795	53.3	2.45	290	78.85 ± 23.64	(1.19 ± 0.08)E-6
26059.9	4.4	3.13	405		
920625.09	174.7	1.66	138	24.58 ± 7.24	0.24 ± 0.04
8798	34.0	2.17	235	86.02 ± 7.38	(6.88 ± 0.47)E-7
8491.1	7.0	2.67	302		
920626.74	12.9	15.06	143	(1.52 ± 0.02)E+2	1.97 ± 0.05
8799	55.5	22.47	276	(1.94 ± 0.02)E+2	(3.96 ± 0.14)E-6
64279.7	1.3	20.02	388		
920626.96	110.7	1.14	163	4.10 ± 1.45	0.19 ± 0.05
8799	11.6	1.27	295	12.29 ± 3.69	0.00 ± 0.00
83508.3	31.3	1.25	351		
920711.49	227.8	5.45	160	7.17 ± 1.45	1.01 ± 0.06
8814	-47.5	8.39	318	21.50 ± 2.90	(1.66 ± 0.06)E-6
42663.0	3.9	10.78	457		
920717.66	141.9	1.84	160	4.10 ± 1.45	0.29 ± 0.04
8820	-72.4	2.19	320	10.24 ± 1.45	(2.17 ± 0.33)E-7
57642.1	15.2	1.88	522		
920719.70	292.8	1.35	171	...	0.18 ± 0.04
8822	-49.3	1.86	339	6.14 ± 2.05	(9.57 ± 1.94)E-8
60697.7	14.5	1.51	370		
920721.28	331.7	1.55	187	...	0.25 ± 0.04
8824	51.2	1.23	353	1.02 ± 1.44	(4.97 ± 0.18)E-8
24637.6	66.0	...	...		
920722.75	309.3	1.02	126	...	0.14 ± 0.05
8825	58.3	1.51	321	7.17 ± 3.07	0.00 ± 0.00
65343.6	59.3	1.61	404		
920727.03	180.1	1.14	165	...	0.21 ± 0.05
8830	-7.7	...	...	1.02 ± 1.02	(4.73 ± 0.13)E-8
3177.6	55.3	...	...		
920727.67	106.2	1.07	159	...	0.18 ± 0.06
8830	11.9	1.56	364	32.77 ± 7.17	(4.44 ± 0.19)E-7
58109.1	6.0	1.86	469		

Table A-2—Continued

Name (NTB) Date (TJD) Time (s UT)	R.A. (°) Decl. (°) Err. (°)	C_{max}/C_{min} (4.096 s) (8.192 s)	C_{min} (4.096 s) (8.192 s)	T_{50} (s) T_{90} (s)	P (ph cm^{-2} s^{-1}) F (erg cm^{-2}) (50–300 keV)
920802.72	179.2	1.07	116	...	0.14 ± 0.05
8836	-52.4	...	...	4.10 ± 2.05	(2.40 ± 0.06)E-8
62385.3	78.4	...	...		
920803.92	10.1	2.83	187	...	0.51 ± 0.05
8837	68.7	2.00	376	2.05 ± 1.02	(1.54 ± 0.04)E-7
80054.4	8.1	1.42	440		
920805.21	187.5	1.30	169	15.36 ± 1.45	0.13 ± 0.04
8839	35.8	2.29	353	38.91 ± 7.80	(5.94 ± 0.32)E-7
18962.6	2.4	2.71	477		
920808.72	130.8	5.40	167	5.12 ± 1.45	0.95 ± 0.06
8842	-37.7	8.63	321	24.58 ± 5.22	(1.08 ± 0.12)E-6
62459.0	2.1	8.47	468		
920818.36	323.0	1.83	126	4.10 ± 1.45	0.33 ± 0.05
8852	-1.8	2.56	291	11.26 ± 4.22	(1.66 ± 1.05)E-7
31204.5	9.7	2.35	416		
920821.39	356.8	5.39	208	41.98 ± 5.22	0.97 ± 0.06
8855	28.4	4.79	394	96.26 ± 48.00	(1.60 ± 0.12)E-6
33994.9	108.1	4.60	591		
920823.97	24.9	2.40	155	36.86 ± 1.45	0.37 ± 0.04
8857	-62.9	2.51	308	65.54 ± 2.29	(8.40 ± 0.66)E-7
84291.7	7.6	2.71	456		
920826.68	162.9	2.53	118	13.31 ± 2.29	0.42 ± 0.05
8860	23.2	4.91	231	35.84 ± 3.24	(9.96 ± 0.96)E-7
59186.3	2.9	5.51	327		
920901.63	237.5	1.18	118	10.24 ± 1.45	0.26 ± 0.05
8866	2.0	2.02	243	17.41 ± 3.69	(3.69 ± 0.50)E-7
55139.5	6.6	2.62	344		
920904.14	209.3	4.30	151	18.43 ± 1.45	0.70 ± 0.05
8869	34.1	5.46	313	31.74 ± 3.24	(6.43 ± 0.71)E-7
12742.8	11.8	4.37	411		
920907.29	79.4	2.37	192	...	0.35 ± 0.04
8872	18.9	1.35	348	1.02 ± 1.44	(8.00 ± 1.97)E-8
25894.0	15.3	1.31	465		
920907.71	86.7	1.84	141	28.67 ± 3.24	0.28 ± 0.04
8872	47.9	3.48	302	77.82 ± 4.22	(1.08 ± 0.04)E-6
61891.7	3.1	4.33	407		
920909.69	239.8	1.67	139	...	0.18 ± 0.04
8874	-51.7	1.74	307	3.07 ± 2.05	(1.01 ± 0.39)E-7
59965.6	11.0	1.40	460		
920912.55	61.2	1.29	192	...	0.22 ± 0.05
8877	38.3	1.18	378	5.12 ± 2.05	(8.57 ± 0.72)E-8
48233.6	8.4	1.01	533		
920914.34	259.1	1.28	176	8.19 ± 1.45	0.34 ± 0.08
8879	-35.6	2.02	368	21.50 ± 1.45	(1.09 ± 0.02)E-6
29997.2	3.8	2.74	522		
920916.17	205.0	1.30	134	6.14 ± 2.29	0.34 ± 0.07
8881	25.3	2.03	315	11.26 ± 2.29	(4.32 ± 0.09)E-7
14981.2	9.2	2.53	386		
920920.05	146.6	1.89	143	7.17 ± 1.45	0.30 ± 0.05
8885	17.0	2.91	306	14.34 ± 4.22	(3.95 ± 0.92)E-7
4516.0	6.7	2.92	442		
920920.90	121.8	1.41	188	...	0.24 ± 0.05
8885	30.8	1.96	316	8.19 ± 4.10	(1.88 ± 0.72)E-7
78227.6	8.7	2.12	493		
920924.38	350.6	1.24	177	...	0.44 ± 0.10
8889	-7.2	1.35	324	5.12 ± 3.07	(2.70 ± 0.07)E-7
32993.4	34.9	1.12	476		
920930.21	297.1	1.00	134	2.05 ± 1.45	0.15 ± 0.04
8895	-50.9	1.73	283	4.10 ± 1.45	(1.22 ± 0.51)E-7
18862.2	41.0	1.63	389		

Table A-2—Continued

Name (NTB) Date (TJD) Time (s UT)	R.A. (°) Decl. (°) Err. (°)	C_{max}/C_{min} (4.096 s) (8.192 s)	C_{min} (4.096 s) (8.192 s)	T_{50} (s) T_{90} (s)	P (ph cm^{-2} s^{-1}) F (erg cm^{-2}) (50–300 keV)
921002.18	24.0	1.88	144	...	0.30 ± 0.04
8897	-72.1	1.26	303	2.05 ± 1.44	(6.36 ± 4.18)E-8
16136.3	15.5	1.08	542		
921004.51	52.1	...	...	4.10 ± 2.29	0.23 ± 0.09
8899	-3.2	1.40	378	14.34 ± 4.34	(3.81 ± 0.08)E-7
44206.2	14.4	1.49	499		
921007.05	321.5	1.55	143	5.12 ± 1.45	0.26 ± 0.04
8902	26.5	2.97	293	16.38 ± 3.24	(3.27 ± 0.71)E-7
4969.6	9.1	3.21	370		
921008.15	59.4	1.18	172	4.10 ± 1.45	0.18 ± 0.04
8903	29.5	1.26	348	5.12 ± 1.45	(6.43 ± 0.45)E-8
13162.6	45.3	1.25	504		
921008.78	354.1	1.22	157	5.12 ± 1.45	0.18 ± 0.04
8903	68.1	1.68	258	13.31 ± 6.56	(2.17 ± 0.31)E-7
67813.5	12.1	2.13	382		
921013.34	315.3	1.29	172	...	0.21 ± 0.05
8908	18.8	1.95	390	7.17 ± 3.07	(1.42 ± 0.35)E-7
30076.0	11.3	1.66	534		
921018.85	248.6	...	...	12.29 ± 3.24	(7.10 ± 3.23)E-2
8913	-79.1	1.18	239	28.67 ± 2.29	(2.15 ± 0.02)E-7
73887.9	17.1	1.53	451		
921023.09	257.3	1.47	184	...	0.22 ± 0.05
8918	22.6	2.27	333	5.12 ± 2.05	(1.78 ± 0.03)E-7
8191.1	7.3	1.82	456		
921025.56	85.2	1.23	142	21.50 ± 4.22	0.17 ± 0.04
8920	-33.8	2.10	314	55.30 ± 3.24	(4.81 ± 0.31)E-7
48389.2	5.3	2.60	415		
921025.66	248.5	1.78	125	13.31 ± 3.24	0.53 ± 0.08
8920	-15.9	1.90	278	17.41 ± 6.48	(2.13 ± 0.04)E-7
57504.9	34.7	1.58	314		
921025.99	189.3	1.69	144	5.12 ± 2.29	0.27 ± 0.04
8920	24.4	2.40	269	12.29 ± 1.45	(2.18 ± 0.40)E-7
85621.9	8.2	1.97	381		
921025.99	193.4	1.71	143	6.14 ± 1.45	0.28 ± 0.04
8920	19.0	2.41	269	20.48 ± 9.27	(2.67 ± 0.21)E-7
85757.1	13.3	1.98	381		
921026.32	62.7	1.27	170	...	0.18 ± 0.04
8921	-44.8	1.68	339	11.26 ± 3.07	(2.06 ± 0.06)E-7
28489.9	14.7	1.75	501		
921027.95	232.6	1.43	141	22.53 ± 2.29	0.15 ± 0.04
8922	24.1	2.03	332	41.98 ± 3.24	(3.96 ± 0.04)E-7
82277.5	36.0	2.03	505		
921028.73	84.0	...	...	10.24 ± 2.29	0.14 ± 0.04
8923	35.1	1.03	248	31.74 ± 6.23	(4.20 ± 0.52)E-7
63137.9	11.9	1.53	351		
921029.51	57.2	1.24	162	10.24 ± 3.24	0.15 ± 0.03
8924	70.0	2.01	329	28.67 ± 2.29	(4.46 ± 0.27)E-7
44383.4	15.8	2.84	490		
921104.01	86.3	1.25	173	...	0.16 ± 0.04
8930	73.4	1.65	352	8.19 ± 2.05	(1.06 ± 0.24)E-7
1463.4	20.2	1.46	509		
921104.50	96.6	1.21	184	5.12 ± 2.29	0.16 ± 0.04
8930	4.3	1.49	356	17.41 ± 7.80	(1.28 ± 0.59)E-7
43482.2	18.9	1.58	524		
921105.28	160.2	11.02	112	20.48 ± 1.45	1.69 ± 0.06
8931	-5.5	16.46	229	50.18 ± 2.29	(4.18 ± 0.24)E-6
24210.6	0.7	19.76	333		
921109.25	230.0	1.14	164	7.17 ± 2.29	0.17 ± 0.04
8935	48.4	2.02	348	20.48 ± 5.12	(1.45 ± 0.32)E-7
22356.1	16.1	2.31	509		

Table A-2—Continued

Name (NTB) Date (TJD) Time (s UT)	R.A. (°) Decl. (°) Err. (°)	C_{max}/C_{min} (4.096 s) (8.192 s)	C_{min} (4.096 s) (8.192 s)	T_{50} (s) T_{90} (s)	P (ph cm^{-2} s^{-1}) F (erg cm^{-2}) (50–300 keV)
921110.56	148.3	2.29	134	6.14 ± 1.45	0.37 ± 0.04
8936	-77.4	4.00	268	13.31 ± 2.90	(5.96 ± 0.75)E-7
49245.3	5.7	5.03	358		
921111.15	211.0	1.33	135	4.10 ± 1.45	0.22 ± 0.05
8937	47.3	2.34	293	7.17 ± 1.45	(2.22 ± 0.44)E-7
13727.9	6.3	2.70	447		
921111.54	291.4	1.00	178	12.29 ± 2.29	0.15 ± 0.05
8937	0.3	1.52	360	18.43 ± 5.51	(2.08 ± 0.20)E-7
47430.8	5.7	1.50	488		
921112.61	126.6	8.09	163	...	1.23 ± 0.05
8938	18.5	4.01	339	1.02 ± 1.02	(2.63 ± 0.24)E-7
52980.9	5.8	2.72	525		
921115.87	222.3	4.21	153	(1.31 ± 0.02)E+2	0.79 ± 0.06
8941	-6.6	5.65	284	(2.48 ± 0.16)E+2	(2.75 ± 0.10)E-6
75931.8	3.0	6.78	409		
921116.47	4.2	1.37	165	...	0.22 ± 0.04
8942	-26.7	1.28	374	6.14 ± 2.05	(7.72 ± 1.64)E-8
40860.8	30.8	1.17	541		
921120.35	94.1	1.85	123	28.67 ± 3.24	0.31 ± 0.05
8946	-34.3	2.41	266	70.66 ± 13.74	(1.01 ± 0.06)E-6
30778.5	8.3	2.67	371		
921122.28	304.6	9.10	195	1.02 ± 1.45	4.32 ± 0.16
8948	-17.2	8.35	387	2.05 ± 1.45	(1.84 ± 0.11)E-6
25031.8	4.6	6.03	541		
921123.60	211.3	2.47	136	...	0.61 ± 0.07
8949	15.2	2.01	246	4.10 ± 2.05	(2.56 ± 0.06)E-7
51943.6	12.1	1.58	414		
921124.06	137.4	2.78	157	...	0.38 ± 0.04
8950	-5.0	1.99	299	3.07 ± 2.05	(1.39 ± 0.34)E-7
6016.1	10.3	1.60	456		
921125.38	173.4	...	...	11.26 ± 2.29	0.12 ± 0.04
8951	64.5	1.65	333	25.60 ± 2.29	(3.47 ± 0.05)E-7
33577.1	21.6	1.91	456		
921127.54	29.0	1.02	170	8.19 ± 1.45	0.15 ± 0.04
8953	-35.0	1.62	312	18.43 ± 8.44	(1.93 ± 0.41)E-7
46946.4	17.4	1.89	463		
921128.11	242.5	1.60	182	30.72 ± 2.29	0.25 ± 0.04
8954	40.5	2.74	326	95.23 ± 5.12	(1.72 ± 0.09)E-6
10030.2	2.3	3.44	430		
921128.80	351.5	9.23	123	...	2.54 ± 0.10
8954	-38.8	5.04	266	2.05 ± 1.02	(5.69 ± 0.20)E-7
69344.4	3.1	3.62	370		
921202.54	11.6	1.30	137	1.02 ± 1.45	0.20 ± 0.04
8958	29.6	1.02	224	1.02 ± 1.45	(5.93 ± 2.70)E-8
47262.9	30.1	...	...		
921206.49	122.5	...	...	20.48 ± 2.29	0.12 ± 0.04
8962	5.6	1.54	234	51.20 ± 3.24	(3.49 ± 0.35)E-7
42366.1	15.2	1.82	397		
921208.60	154.1	1.05	134	9.22 ± 5.22	0.15 ± 0.04
8964	-38.0	1.65	280	22.53 ± 5.22	(2.32 ± 0.07)E-7
52460.7	12.1	1.89	411		
921209.33	91.4	1.69	172	17.41 ± 1.45	0.25 ± 0.04
8965	-60.7	2.61	394	22.53 ± 1.45	(4.16 ± 0.35)E-7
28569.7	10.4	2.33	505		
921211.33	29.4	1.13	175	14.34 ± 3.24	0.16 ± 0.04
8967	-39.0	1.73	291	47.10 ± 9.44	(4.06 ± 0.31)E-7
28889.2	8.3	2.20	475		
921212.16	302.4	1.05	138	...	0.18 ± 0.05
8968	25.7	...	...	3.07 ± 1.02	(4.60 ± 0.56)E-8
13980.8	65.7	...	...		

Table A-2—Continued

Name (NTB) Date (TJD) Time (s UT)	R.A. (°) Decl. (°) Err. (°)	C_{max}/C_{min} (4.096 s) (8.192 s)	C_{min} (4.096 s) (8.192 s)	T_{50} (s) T_{90} (s)	P (ph cm^{-2} s^{-1}) F (erg cm^{-2}) (50–300 keV)
921213.63	19.0	1.17	118	12.29 ± 2.29	0.17 ± 0.05
8969	-14.9	1.93	307	32.77 ± 5.51	(4.34 ± 0.34)E-7
54714.5	4.3	2.46	439		
921218.20	231.8	...	...	18.43 ± 2.29	0.10 ± 0.04
8974	24.6	1.23	380	52.22 ± 11.45	(4.20 ± 0.06)E-7
17749.1	5.5	1.51	440		
921228.60	100.5	1.26	177	3.07 ± 1.45	0.19 ± 0.04
8984	11.1	2.27	355	7.17 ± 1.45	(1.86 ± 0.51)E-7
52163.7	18.4	2.42	515		
930102.30	340.2	1.91	132	3.07 ± 96.26	0.23 ± 0.04
8989	-52.5	2.40	264	9.22 ± 4.22	(2.20 ± 0.06)E-7
26028.2	15.0	2.32	369		
930103.38	301.1	1.79	154	38.91 ± 3.24	0.32 ± 0.05
8990	63.0	3.05	350	87.04 ± 6.48	(1.00 ± 0.11)E-6
33445.0	7.2	3.48	506		
930106.60	178.0	2.07	157	38.91 ± 1.45	0.35 ± 0.05
8993	3.0	3.82	343	79.87 ± 7.24	(1.43 ± 0.55)E-6
52138.1	1.2	4.39	479		
930108.31	173.0	1.61	151	...	0.27 ± 0.05
8995	8.1	1.05	336	2.05 ± 1.44	(6.86 ± 0.22)E-8
27101.3	15.3	...	...		
930110.82	294.7	1.31	169	8.19 ± 1.45	0.20 ± 0.05
8997	47.1	2.32	357	21.50 ± 1.45	(3.69 ± 0.35)E-7
71569.5	4.9	2.69	483		
930118.74	218.3	27.18	176	2.05 ± 1.45	4.66 ± 0.08
9005	-31.9	31.02	350	3.07 ± 1.45	(2.20 ± 0.51)E-6
64425.6	0.8	23.05	498		
930205.90	248.4	1.09	145	...	0.15 ± 0.04
9023	27.6	...	308	2.05 ± 1.05	(2.58 ± 0.52)E-8
77957.2	58.7	...	432		
930209.18	239.3	14.04	144	9.22 ± 1.45	1.95 ± 0.05
9027	-58.2	26.75	286	27.65 ± 1.45	(4.96 ± 0.26)E-6
15730.3	0.7	33.05	405		
930211.88	287.6	1.56	140	22.53 ± 2.29	0.20 ± 0.04
9029	23.1	2.95	326	78.85 ± 8.44	(7.44 ± 0.43)E-7
76428.9	4.8	3.62	433		
930216.63	40.0	1.33	150	24.58 ± 1.45	0.23 ± 0.05
9034	-10.6	2.50	326	53.25 ± 12.95	(7.21 ± 0.80)E-7
54956.7	7.5	2.68	461		
930227.83	216.2	...	111	37.89 ± 1.45	0.13 ± 0.04
9045	80.4	1.86	311	57.34 ± 1.45	(3.13 ± 0.10)E-7
71910.5	14.1	2.09	371		
930228.85	28.6	...	117	27.65 ± 1.45	0.12 ± 0.04
9046	16.8	1.71	272	94.21 ± 8.75	(6.58 ± 1.21)E-7
73728.6	6.7	2.16	456		
930302.20	207.9	...	359	15.36 ± 1.45	0.12 ± 0.04
9048	42.6	1.50	341	51.20 ± 4.22	(6.01 ± 0.04)E-7
17613.4	8.5	2.16	504		
930303.65	347.6	1.36	182	33.79 ± 1.45	0.13 ± 0.04
9049	-52.5	2.17	338	73.73 ± 10.29	(7.92 ± 0.43)E-7
56726.7	5.7	2.99	501		
930305.70	279.1	1.60	121	5.12 ± 1.45	0.45 ± 0.07
9051	60.1	2.89	256	11.26 ± 1.45	(7.49 ± 0.14)E-7
60923.0	4.0	3.22	350		
930307.54	101.8	1.17	144	5.12 ± 1.45	0.16 ± 0.04
9053	-24.2	1.56	307	17.41 ± 8.26	0.00 ± 0.00
46677.1	13.7	1.71	419		
930308.30	86.4	1.63	144	23.55 ± 1.45	0.45 ± 0.08
9054	-35.2	3.05	304	56.32 ± 7.45	(2.09 ± 0.02)E-6
26710.7	4.1	3.80	398		

Table A-2—Continued

Name (NTB) Date (TJD) Time (s UT)	R.A. (°) Decl. (°) Err. (°)	C_{max}/C_{min} (4.096 s) (8.192 s)	C_{min} (4.096 s) (8.192 s)	T_{50} (s) T_{90} (s)	P (ph cm^{-2} s^{-1}) F (erg cm^{-2}) (50–300 keV)
930310.08	314.9	1.14	113	8.19 ± 2.29	0.25 ± 0.04
9056	-67.9	2.46	227	15.36 ± 1.45	(2.59 ± 0.31)E-7
7334.5	4.9	2.48	321		
930315.46	238.3	1.00	167	15.36 ± 1.45	0.13 ± 0.05
9061	-34.4	1.81	378	35.84 ± 7.38	(8.54 ± 0.47)E-7
40070.8	3.9	2.32	471		
930316.74	292.3	1.58	133	...	0.21 ± 0.04
9062	-78.9	1.16	234	3.07 ± 1.02	(6.42 ± 0.65)E-8
64295.0	20.9	...	373		
930318.18	6.7	1.14	146	14.34 ± 3.24	0.16 ± 0.04
9064	45.0	2.20	317	35.84 ± 4.34	(3.43 ± 0.42)E-7
15764.1	10.9	2.52	419		
930320.94	222.1	4.47	165	25.60 ± 1.45	0.81 ± 0.06
9066	71.9	5.95	320	59.39 ± 3.24	(3.02 ± 0.04)E-6
81767.0	8.2	7.10	437		
930325.65	51.9	...	116	8.19 ± 1.45	0.21 ± 0.04
9071	42.8	2.16	233	17.41 ± 3.24	(3.85 ± 0.31)E-7
56254.1	8.8	2.85	348		
930327.46	172.2	1.39	180	13.31 ± 1.45	0.35 ± 0.06
9073	-8.2	2.75	401	34.82 ± 8.26	(9.29 ± 0.94)E-7
40594.6	3.2	3.51	531		
930330.91	103.9	...	110	10.24 ± 1.45	0.17 ± 0.05
9076	-59.6	1.47	337	18.43 ± 4.22	(3.26 ± 0.26)E-7
79132.8	4.6	1.72	487		
930403.84	249.3	1.14	110	12.29 ± 1.45	0.24 ± 0.04
9080	-63.3	2.55	261	41.98 ± 6.23	(4.89 ± 0.46)E-7
73239.2	6.3	3.03	358		
930408.07	271.7	8.68	169	1.02 ± 1.45	4.39 ± 0.18
9085	-59.2	7.34	335	2.05 ± 1.45	(1.98 ± 0.11)E-6
6846.1	2.5	5.59	470		
930409.13	309.5	2.27	112	11.26 ± 2.29	0.34 ± 0.05
9086	61.6	2.73	224	27.65 ± 4.22	(5.31 ± 0.40)E-7
11442.8	7.2	2.74	317		
930409.20	302.6	8.83	116	24.58 ± 1.45	1.40 ± 0.06
9086	44.6	15.70	231	(1.17 ± 0.18)E+2	(5.53 ± 0.32)E-6
17335.4	0.5	19.17	327		
930409.91	277.1	8.62	181	13.31 ± 1.45	1.32 ± 0.05
9086	-17.6	12.55	368	54.27 ± 1.45	(3.15 ± 0.29)E-6
78639.7	0.9	12.78	503		
930410.76	195.2	1.62	140	24.58 ± 1.45	0.23 ± 0.04
9087	-67.7	2.17	315	74.75 ± 4.22	(8.40 ± 0.89)E-7
65711.8	23.2	2.95	367		
930416.56	104.7	...	105	5.12 ± 1.45	0.20 ± 0.04
9093	-27.6	2.90	310	14.34 ± 4.22	(2.92 ± 0.47)E-7
48602.2	16.9	3.48	400		
930417.78	196.2	1.10	165	5.12 ± 1.45	0.16 ± 0.04
9094	-1.0	1.51	247	13.31 ± 1.45	(1.29 ± 0.24)E-7
68020.4	11.9	1.81	382		
930421.11	15.0	...	119	48.13 ± 8.44	0.12 ± 0.04
9098	-22.4	1.43	305	(1.11 ± 0.06)E+2	(8.46 ± 0.08)E-7
10164.9	30.3	1.90	506		
930422.58	48.8	1.81	112	13.31 ± 1.45	0.30 ± 0.04
9099	-9.1	3.71	223	30.72 ± 3.24	(8.23 ± 0.84)E-7
50820.2	2.7	4.61	316		
930424.45	230.0	7.58	179	43.01 ± 2.29	1.24 ± 0.06
9101	-55.4	14.96	369	(1.13 ± 0.06)E+2	(1.34 ± 0.03)E-5
38903.4	0.5	20.78	525		
930424.97	258.5	2.02	164	13.31 ± 1.45	0.28 ± 0.04
9101	65.6	2.83	252	32.77 ± 5.22	(7.80 ± 0.89)E-7
84156.0	6.1	3.66	354		

Table A-2—Continued

Name (NTB) Date (TJD) Time (s UT)	R.A. (°) Decl. (°) Err. (°)	C_{max}/C_{min} (4.096 s) (8.192 s)	C_{min} (4.096 s) (8.192 s)	T_{50} (s) T_{90} (s)	P (ph cm^{-2} s^{-1}) F (erg cm^{-2}) (50–300 keV)
930426.48	20.4	4.30	135	1.02 ± 1.45	0.68 ± 0.05
9103	-81.4	2.92	236	11.26 ± 4.22	(1.49 ± 0.37)E-7
41832.1	9.3	2.17	381		
930427.59	72.5	...	115	14.34 ± 5.22	0.14 ± 0.04
9104	38.1	1.90	295	29.70 ± 15.39	(2.45 ± 0.27)E-7
51155.6	16.7	2.19	469		
930429.75	34.7	2.39	126	43.01 ± 1.45	0.36 ± 0.04
9106	-24.8	4.29	259	(1.11 ± 0.14)E+2	(2.00 ± 0.14)E-6
65094.3	6.2	5.75	357		
930501.34	178.9	1.09	114	...	0.18 ± 0.04
9108	-32.2	...	320	2.05 ± 1.02	(4.66 ± 0.60)E-8
29834.4	27.0	...	361		
930506.63	260.4	1.02	152	18.43 ± 1.45	0.17 ± 0.04
9113	35.0	1.69	358	39.94 ± 5.22	(5.20 ± 0.46)E-7
55244.4	11.0	2.14	559		
930508.95	80.8	1.89	180	4.10 ± 1.45	0.24 ± 0.04
9115	41.7	2.93	326	11.26 ± 3.24	(2.89 ± 0.60)E-7
82814.6	12.0	3.27	485		
930519.39	288.9	1.41	132	...	0.25 ± 0.05
9126	-9.2	...	292	1.02 ± 1.44	(4.95 ± 0.18)E-8
34288.8	51.5	...	366		
930608.95	240.5	1.37	141	13.31 ± 1.45	0.23 ± 0.05
9146	-22.9	2.25	335	47.10 ± 6.23	(3.76 ± 0.72)E-7
82418.3	3.5	2.95	480		
930612.63	255.8	9.41	140	8.19 ± 2.29	1.25 ± 0.05
9150	35.2	12.11	279	58.37 ± 4.22	(9.21 ± 0.90)E-7
55165.1	3.1	10.13	393		
930616.27	184.8	11.66	165	1.02 ± 1.45	2.63 ± 0.08
9154	-2.0	5.74	344	1.02 ± 1.45	(5.95 ± 0.20)E-7
23806.6	11.0	4.10	473		
930617.23	246.2	1.00	105	54.27 ± 1.45	0.20 ± 0.04
9155	-11.2	2.38	233	75.78 ± 10.69	(9.63 ± 0.68)E-7
20027.0	6.8	2.56	299		
930617.59	224.9	1.17	123	22.53 ± 1.45	0.29 ± 0.04
9155	-15.9	3.65	260	40.96 ± 1.45	(1.01 ± 0.01)E-6
51037.8	3.0	4.29	358		
930626.94	341.3	1.74	187	11.26 ± 1.45	0.26 ± 0.04
9164	-35.5	3.15	367	22.53 ± 2.29	(5.82 ± 0.57)E-7
81935.0	3.9	3.54	493		
930630.71	59.4	1.65	163	10.24 ± 2.29	0.23 ± 0.04
9168	37.9	2.58	295	41.98 ± 5.97	(3.90 ± 0.44)E-7
61420.2	24.4	3.00	440		
930701.62	223.0	2.03	119	21.50 ± 1.45	0.44 ± 0.05
9169	46.8	3.47	238	39.94 ± 4.22	(1.01 ± 0.09)E-6
54302.9	3.9	4.38	338		
930705.52	284.1	7.70	125	19.46 ± 1.45	1.33 ± 0.06
9173	-41.8	14.21	253	87.04 ± 3.24	(6.41 ± 0.26)E-6
45503.1	1.3	18.61	359		
930705.64	188.4	...	118	10.24 ± 1.45	0.20 ± 0.04
9173	-64.7	1.56	236	26.62 ± 2.29	(3.36 ± 0.47)E-7
55983.3	9.2	1.96	334		
930717.20	188.9	1.19	148	3.07 ± 1.45	0.19 ± 0.04
9185	56.4	1.65	333	12.29 ± 7.24	(1.11 ± 0.55)E-7
18101.4	12.1	1.47	412		
930717.98	210.2	1.84	123	6.14 ± 1.45	0.31 ± 0.05
9185	-70.3	2.95	249	12.29 ± 2.29	(3.55 ± 0.48)E-7
85357.7	5.6	3.07	352		
930722.84	312.5	...	109	...	0.15 ± 0.05
9190	-53.2	1.44	278	41.98 ± 10.24	(5.95 ± 0.47)E-7
73297.6	4.6	2.00	406		

Table A-2—Continued

Name (NTB) Date (TJD) Time (s UT)	R.A. (°) Decl. (°) Err. (°)	C_{max}/C_{min} (4.096 s) (8.192 s)	C_{min} (4.096 s) (8.192 s)	T_{50} (s) T_{90} (s)	P (ph cm^{-2} s^{-1}) F (erg cm^{-2}) (50–300 keV)
930728.54	88.5	1.17	125	28.67 ± 1.45	0.16 ± 0.04
9196	10.5	2.49	371	95.23 ± 1.45	(1.06 ± 0.07)E-6
47072.9	6.2	3.30	501		
930804.71	33.0	1.39	107	19.46 ± 2.29	0.30 ± 0.05
9203	69.7	2.91	215	41.98 ± 8.26	(8.09 ± 0.91)E-7
61858.5	4.6	3.68	324		
930811.62	71.1	1.60	117	17.41 ± 3.24	0.24 ± 0.05
9210	84.3	2.38	231	38.91 ± 9.27	(5.60 ± 0.72)E-7
53728.4	11.9	2.86	323		
930812.27	199.9	2.04	134	29.70 ± 1.45	0.35 ± 0.05
9211	-38.1	3.68	260	77.82 ± 2.29	(1.65 ± 0.12)E-6
23904.9	3.7	4.83	398		
930813.76	92.0	2.12	120	99.33 ± 2.29	0.33 ± 0.04
9212	76.0	3.65	230	(1.33 ± 0.05)E+2	(1.31 ± 0.06)E-6
65850.5	7.0	3.91	325		
930816.67	150.8	1.49	143	14.34 ± 3.24	0.17 ± 0.03
9215	55.9	2.93	297	30.72 ± 3.24	(4.32 ± 0.37)E-7
58569.4	6.4	3.66	424		
930820.76	61.7	1.57	168	...	0.23 ± 0.04
9219	39.0	2.29	245	12.29 ± 3.07	(2.75 ± 0.49)E-7
65885.3	9.3	2.79	387		
930821.64	145.7	1.17	123	...	0.19 ± 0.04
9220	-46.0	1.11	387	2.05 ± 1.44	(6.64 ± 0.18)E-8
56096.9	10.9	...	521		
930825.48	96.5	...	126	4.10 ± 1.45	(7.40 ± 3.64)E-2
9224	53.7	1.46	292	9.22 ± 1.45	(8.16 ± 0.57)E-8
41775.3	32.9	1.40	384		
930826.49	3.3	1.26	103	11.26 ± 1.45	0.19 ± 0.04
9225	24.7	2.20	210	22.53 ± 5.22	(4.38 ± 0.69)E-7
43172.0	7.1	2.44	293		
930827.60	350.1	...	115	14.34 ± 3.24	0.13 ± 0.03
9226	75.2	2.02	361	43.01 ± 10.29	(3.83 ± 0.39)E-7
51963.0	15.2	2.49	508		
930902.45	197.7	...	112	24.58 ± 2.29	0.15 ± 0.04
9232	17.5	1.54	254	59.39 ± 9.44	(5.98 ± 0.46)E-7
39001.8	10.7	2.10	369		
930917.10	129.5	...	121	4.10 ± 1.45	0.12 ± 0.05
9247	-54.2	1.08	267	8.19 ± 2.29	(7.15 ± ****)E-8
9233.6	14.6	1.03	356		
930918.46	320.2	1.10	108	14.34 ± 1.45	0.17 ± 0.04
9248	-76.4	1.96	217	37.89 ± 16.19	(4.24 ± 0.56)E-7
39913.1	5.4	2.70	320		
930921.84	81.0	2.04	116	12.29 ± 1.45	0.33 ± 0.05
9251	-0.1	1.54	226	16.38 ± 1.45	(2.08 ± 0.35)E-7
73133.2	19.1	1.18	415		
930922.66	110.7	1.53	131	...	0.46 ± 0.08
9252	-55.5	...	289	2.05 ± 1.02	(8.82 ± 0.25)E-8
57274.5	49.4	...	355		
930924.37	96.3	1.43	126	8.19 ± 1.45	0.18 ± 0.04
9254	-6.4	2.57	286	19.46 ± 2.29	(4.62 ± 0.44)E-7
32251.0	12.2	3.21	402		
930927.24	253.4	...	165	17.41 ± 1.45	0.13 ± 0.04
9257	-65.4	1.58	396	44.03 ± 12.33	(3.95 ± 0.05)E-7
21537.4	12.5	1.91	472		
930928.93	264.8	1.43	200	3.07 ± 1.45	0.20 ± 0.04
9258	-62.4	2.24	353	7.17 ± 2.29	(1.81 ± 0.30)E-7
81199.3	33.6	2.49	522		
930928.94	91.6	...	110	14.34 ± 2.29	0.14 ± 0.05
9258	39.4	1.38	274	30.72 ± 13.93	(3.33 ± 0.32)E-7
81393.3	10.1	1.75	363		

Table A-2—Continued

Name (NTB) Date (TJD) Time (s UT)	R.A. (°) Decl. (°) Err. (°)	C_{max}/C_{min} (4.096 s) (8.192 s)	C_{min} (4.096 s) (8.192 s)	T_{50} (s) T_{90} (s)	P (ph cm^{-2} s^{-1}) F (erg cm^{-2}) (50–300 keV)
931001.06	207.8	3.18	193	4.10 ± 1.45	0.64 ± 0.06
9261	13.4	5.37	402	13.31 ± 1.45	(7.18 ± 0.96)E-7
5859.5	2.2	5.72	586		
931001.72	10.9	1.25	123	13.31 ± 1.45	0.26 ± 0.04
9261	13.8	2.63	344	56.32 ± 8.00	(6.75 ± 0.84)E-7
62917.3	3.5	3.38	490		
931007.20	307.1	1.15	119	...	0.18 ± 0.04
9267	-4.9	1.97	240	16.38 ± 7.17	(2.48 ± 0.44)E-7
17771.7	9.9	2.27	347		
931007.26	288.9	1.51	155	3.07 ± 1.45	0.23 ± 0.04
9267	-7.7	2.66	288	10.24 ± 1.45	(1.58 ± 6.02)E-7
22952.6	9.4	2.64	416		
931007.33	354.9	1.23	135	...	0.25 ± 0.07
9267	37.2	1.41	261	8.19 ± 3.07	(2.74 ± 0.07)E-7
29319.3	19.1	1.73	360		
931008.05	344.0	1.15	184	...	0.33 ± 0.08
9268	-68.1	1.22	319	2.05 ± 1.02	(1.37 ± 0.04)E-7
5024.9	27.5	...	442		
931008.63	43.0	1.80	160	50.18 ± 5.22	0.23 ± 0.04
9268	49.3	3.42	348	(1.24 ± 0.10)E+2	(2.31 ± 0.14)E-6
54916.8	3.2	4.59	492		
931011.96	260.3	...	117	...	0.15 ± 0.04
9271	55.5	1.04	374	2.05 ± 1.44	(4.64 ± 1.61)E-8
83718.3	33.6	...	566		
931014.08	10.6	1.51	147	...	0.23 ± 0.04
9274	15.6	...	254	4.10 ± 3.07	(4.67 ± 0.33)E-8
7552.2	65.5	...	315		
931017.22	227.2	...	124	5.12 ± 1.45	0.11 ± 0.03
9277	-68.8	1.54	381	15.36 ± 5.51	(1.38 ± 0.21)E-7
19221.7	24.2	1.73	448		
931020.10	289.0	...	392	21.50 ± 1.45	0.12 ± 0.04
9280	9.0	1.30	315	74.75 ± 3.69	(4.73 ± 0.05)E-7
8697.5	20.3	1.66	445		
931025.93	168.6	1.40	173	5.12 ± 1.45	0.19 ± 0.04
9285	20.2	2.36	329	14.34 ± 2.29	(2.30 ± 0.29)E-7
80462.5	11.0	2.63	431		
931031.23	192.0	3.01	163	...	0.45 ± 0.04
9291	66.2	1.60	274	1.02 ± 1.02	(1.01 ± 0.21)E-7
20519.6	16.7	1.04	382		
931102.59	338.5	1.22	166	3.07 ± 1.45	0.19 ± 0.04
9293	19.3	2.02	352	12.29 ± 3.24	(1.27 ± 0.57)E-7
51568.8	19.8	1.88	430		
931106.48	35.9	1.49	116	34.82 ± 5.22	0.23 ± 0.04
9297	75.7	2.86	277	91.14 ± 4.58	(1.34 ± 0.07)E-6
42228.4	15.0	3.72	411		
931106.90	178.5	2.28	154	5.12 ± 1.45	0.33 ± 0.04
9297	-38.4	2.61	275	17.41 ± 5.22	(2.09 ± 0.33)E-7
78310.6	16.8	2.37	411		
931107.31	99.4	1.57	183	43.01 ± 1.45	0.30 ± 0.05
9298	-40.7	3.08	437	(1.16 ± 0.03)E+2	(1.95 ± 0.07)E-6
26896.0	4.8	3.82	599		
931111.71	239.2	4.36	118	62.46 ± 2.29	0.71 ± 0.05
9302	37.9	7.87	237	(1.97 ± 0.02)E+2	(6.58 ± 0.24)E-6
61941.4	0.7	9.09	336		
931113.04	56.7	1.25	131	10.24 ± 1.45	0.18 ± 0.04
9304	-38.4	1.85	298	21.50 ± 4.58	(3.06 ± 0.30)E-7
3669.7	10.4	1.96	392		
931115.77	273.5	2.18	196	17.41 ± 1.45	0.36 ± 0.05
9306	2.8	3.21	360	36.86 ± 2.29	(5.41 ± 0.42)E-7
66557.6	8.0	3.06	538		

Table A-2—Continued

Name (NTB) Date (TJD) Time (s UT)	R.A. (°) Decl. (°) Err. (°)	C_{max}/C_{min} (4.096 s) (8.192 s)	C_{min} (4.096 s) (8.192 s)	T_{50} (s) T_{90} (s)	P (ph cm^{-2} s^{-1}) F (erg cm^{-2}) (50–300 keV)
931125.86	159.7	5.72	182	6.14 ± 1.45	0.68 ± 0.04
9316	-79.4	10.36	374	15.36 ± 1.45	(1.13 ± 0.10)E-6
74847.4	3.5	12.15	530		
931206.45	175.2	1.53	134	12.29 ± 3.24	0.21 ± 0.04
9327	-0.2	2.66	271	27.65 ± 6.23	(4.15 ± 0.44)E-7
39631.5	13.0	3.02	386		
931209.89	28.4	...	110	36.86 ± 2.29	0.17 ± 0.04
9330	-31.7	2.46	297	(1.02 ± 0.14)E+2	(1.20 ± 0.05)E-6
77266.1	2.5	3.26	445		
931214.38	186.1	1.54	125	3.07 ± 1.45	0.28 ± 0.04
9335	72.1	2.39	260	6.14 ± 3.24	(1.97 ± 0.04)E-7
33424.5	7.1	2.29	353		
931215.12	318.1	1.59	118	4.10 ± 1.45	0.34 ± 0.05
9336	-1.5	2.34	293	13.31 ± 1.45	(2.60 ± 0.54)E-7
10491.5	8.8	2.20	370		
931220.16	119.1	1.80	146	4.10 ± 1.45	0.28 ± 0.05
9341	48.0	2.83	276	8.19 ± 1.45	(3.05 ± 0.05)E-7
13826.7	6.0	3.11	437		
931220.73	45.2	3.88	162	7.17 ± 1.45	0.61 ± 0.05
9341	19.2	6.48	318	20.48 ± 4.22	(8.91 ± 0.58)E-7
63345.3	6.0	7.20	438		
931222.11	277.9	...	188	20.48 ± 2.29	0.13 ± 0.04
9343	30.6	1.49	431	58.37 ± 5.12	(4.50 ± 0.05)E-7
10361.5	5.1	1.88	577		
931222.82	210.2	6.09	178	1.02 ± 1.45	1.73 ± 0.09
9343	-34.6	2.83	326	1.02 ± 1.45	(4.13 ± 0.17)E-7
70972.1	13.8	2.00	486		
931223.07	190.1	1.51	196	...	0.22 ± 0.04
9344	33.4	1.36	309	3.07 ± 2.05	(8.96 ± 0.27)E-8
6589.6	52.9	1.19	519		
931225.46	264.8	...	...	...	0.15 ± 0.04
9346	40.7	1.43	348	11.26 ± 4.10	(1.31 ± 0.04)E-7
40442.0	8.5	1.40	404		
931226.85	226.2	2.09	166	12.29 ± 2.29	0.32 ± 0.04
9347	-18.2	3.53	371	33.79 ± 5.22	(5.58 ± 0.33)E-7
73656.5	12.2	4.19	506		
931226.88	93.8	1.02	159	...	0.17 ± 0.05
9347	-28.7	...	...	2.05 ± 1.02	(1.99 ± 1.82)E-8
76813.5	66.1	...	...		
931229.36	97.3	1.61	132	12.29 ± 2.29	0.30 ± 0.05
9350	75.2	2.50	264	32.77 ± 7.38	(7.10 ± 0.55)E-7
31105.2	8.0	3.44	485		
940102.49	310.2	1.35	118	9.22 ± 1.45	0.23 ± 0.05
9354	14.4	2.35	247	23.55 ± 14.37	(3.53 ± 0.37)E-7
43090.1	14.7	2.47	348		
940102.55	24.3	1.51	132	15.36 ± 2.29	0.20 ± 0.04
9354	-53.4	2.63	336	37.89 ± 3.24	(7.68 ± 0.75)E-7
47745.2	6.0	3.41	454		
940103.26	8.8	1.15	186	3.07 ± 1.45	0.19 ± 0.04
9355	-28.2	1.52	335	8.19 ± 2.29	(1.08 ± 0.50)E-7
22470.8	8.7	1.42	465		
940104.79	46.7	1.13	156	9.22 ± 3.24	0.19 ± 0.04
9356	54.9	1.91	340	23.55 ± 6.48	(3.42 ± 0.03)E-7
68722.8	38.2	2.14	468		
940106.99	112.1	2.20	145	26.62 ± 1.45	0.35 ± 0.05
9358	-69.4	3.47	273	53.25 ± 1.45	(1.10 ± 0.11)E-6
85608.6	6.2	4.16	423		
940107.94	229.7	1.68	143	71.68 ± 5.12	0.23 ± 0.04
9359	-11.5	1.82	252	(1.31 ± 0.09)E+2	(5.84 ± 1.01)E-7
81415.3	15.0	1.56	340		

Table A-2—Continued

Name (NTB) Date (TJD) Time (s UT)	R.A. (°) Decl. (°) Err. (°)	C_{max}/C_{min} (4.096 s) (8.192 s)	C_{min} (4.096 s) (8.192 s)	T_{50} (s) T_{90} (s)	P (ph cm^{-2} s^{-1}) F (erg cm^{-2}) (50–300 keV)
940111.10	268.9	...	...	13.31 ± 5.22	(6.93 ± 4.39)E-2
9363	-11.1	...	...	23.55 ± 6.23	(1.62 ± 0.06)E-7
9501.8	45.9	1.19	504		
940111.84	109.6	1.21	148	28.67 ± 2.29	0.17 ± 0.04
9363	-61.6	1.92	285	(1.19 ± 0.07)E+2	(6.68 ± 0.08)E-7
73408.7	11.3	1.93	416		
940113.63	238.3	...	...	22.53 ± 9.27	0.13 ± 0.04
9365	50.8	1.59	275	73.73 ± 10.24	(3.66 ± 0.04)E-7
54979.7	23.5	1.49	319		
940116.52	353.4	1.13	189	...	0.15 ± 0.04
9368	24.4	...	...	2.05 ± 1.02	(4.34 ± 0.15)E-8
45538.5	38.1	...	...		
940116.83	59.5	1.94	128	2.05 ± 1.45	0.39 ± 0.05
9368	16.7	3.02	256	7.17 ± 2.29	(1.90 ± 0.95)E-7
72261.8	5.9	2.52	362		
940119.39	48.4	3.40	119	13.31 ± 1.45	0.63 ± 0.05
9371	18.4	2.47	238	26.62 ± 9.71	(4.19 ± 1.33)E-7
33932.4	6.7	2.65	333		
940121.05	9.0	1.82	139	...	0.54 ± 0.08
9373	-47.4	1.43	337	3.07 ± 1.44	(2.01 ± 0.06)E-7
5084.3	62.5	1.20	380		
940125.55	193.8	1.72	119	77.82 ± 2.90	0.28 ± 0.04
9377	2.3	2.62	297	(1.30 ± 0.03)E+2	(7.41 ± 0.35)E-7
47740.1	36.2	2.24	332		
940131.68	353.5	1.62	118	12.29 ± 1.45	0.26 ± 0.04
9383	-12.5	2.67	237	31.74 ± 8.26	(7.92 ± 0.86)E-7
58971.3	8.2	3.65	336		
940131.78	188.6	1.49	162	45.06 ± 1.45	0.28 ± 0.05
9383	-51.3	2.22	391	77.82 ± 15.39	(7.50 ± 0.73)E-7
67605.7	6.8	2.35	565		
940203.71	240.2	10.57	160	...	1.82 ± 0.06
9386	-23.8	5.99	333	3.07 ± 1.02	(3.92 ± 1.11)E-7
62085.3	2.3	4.31	478		
940218.81	114.1	1.33	148	10.24 ± 4.22	0.11 ± 0.05
9401	-17.5	1.91	359	23.55 ± 39.99	(3.59 ± 0.31)E-7
70793.4	6.1	2.50	521		
940222.09	197.2	12.76	156	9.22 ± 1.45	1.77 ± 0.05
9405	19.6	16.18	313	22.53 ± 4.34	(1.91 ± 0.16)E-6
7906.5	3.3	12.45	445		
940304.58	3.0	1.47	182	8.19 ± 1.45	0.23 ± 0.04
9415	-72.0	2.50	388	18.43 ± 4.22	(3.07 ± 0.36)E-7
50618.5	8.1	2.85	503		
940312.55	356.0	2.27	180	10.24 ± 1.45	0.36 ± 0.05
9423	15.8	3.54	395	26.62 ± 2.29	(6.24 ± 0.84)E-7
48183.4	106.6	4.21	553		
940316.81	57.6	1.29	139	...	0.21 ± 0.04
9427	54.6	1.52	315	4.10 ± 1.02	(7.49 ± 9.14)E-8
70462.6	55.1	1.33	380		
940318.33	121.6	2.96	178	...	0.45 ± 0.05
9429	87.2	1.61	369	1.02 ± 1.02	(1.10 ± 0.27)E-7
29183.1	8.2	1.26	471		
940319.39	256.7	1.42	131	11.26 ± 1.45	0.18 ± 0.05
9430	34.5	2.44	310	37.89 ± 9.66	(6.75 ± 1.17)E-7
34457.8	4.0	3.30	432		
940321.58	149.1	1.46	164	7.17 ± 1.45	0.22 ± 0.04
9432	-14.3	1.17	264	8.19 ± 1.45	(1.27 ± 0.02)E-7
50806.9	17.6	1.34	413		
940324.13	200.1	1.05	182	6.14 ± 2.29	0.13 ± 0.03
9435	14.0	1.91	351	18.43 ± 9.27	(1.86 ± 0.25)E-7
11726.0	14.1	2.23	462		

Table A-2—Continued

Name (NTB) Date (TJD) Time (s UT)	R.A. (°) Decl. (°) Err. (°)	C_{max}/C_{min} (4.096 s) (8.192 s)	C_{min} (4.096 s) (8.192 s)	T_{50} (s) T_{90} (s)	P (ph cm^{-2} s^{-1}) F (erg cm^{-2}) (50–300 keV)
940325.19	105.0	1.37	183	...	0.37 ± 0.07
9436	26.8	1.66	373	3.07 ± 1.02	(2.29 ± 0.05)E-7
16649.4	23.1	1.23	477		
940327.40	50.2	1.83	115	13.31 ± 1.45	0.41 ± 0.05
9438	-3.9	3.11	237	36.86 ± 15.50	(5.91 ± 0.95)E-7
34910.4	4.8	2.76	342		
940330.04	173.7	2.12	187	...	0.32 ± 0.06
9441	-56.7	1.16	295	2.05 ± 1.02	(8.83 ± 0.26)E-8
3828.9	15.8	...	...		
940330.33	47.5	1.88	130	26.62 ± 1.45	0.33 ± 0.05
9441	14.6	1.96	251	48.13 ± 4.22	(1.34 ± 0.06)E-6
28883.1	2.9	2.50	355		
940330.57	351.3	...	...	1.02 ± 1.45	0.16 ± 0.05
9441	4.5	1.12	379	5.12 ± 1.45	(8.52 ± 0.87)E-8
50095.3	25.6	...	...		
940330.95	189.3	1.21	205	...	0.17 ± 0.04
9441	-58.9	2.03	311	10.24 ± 5.12	(1.55 ± 0.07)E-7
82334.9	17.3	1.62	461		
940331.57	217.6	8.37	137	20.48 ± 1.45	1.67 ± 0.08
9442	-74.2	12.97	247	30.72 ± 1.45	(4.46 ± 0.18)E-6
50028.7	1.1	17.93	335		
940402.39	240.1	...	...	54.27 ± 3.24	0.11 ± 0.04
9444	-29.2	1.19	346	99.33 ± 9.27	(6.80 ± 0.15)E-7
34152.6	11.4	1.51	412		
940402.43	162.5	1.87	144	72.70 ± 2.29	0.31 ± 0.05
9444	22.0	3.16	257	(1.29 ± 0.03)E+2	(1.63 ± 0.07)E-6
37832.9	10.7	2.95	341		
940407.24	47.0	...	...	60.42 ± 1.45	0.13 ± 0.04
9449	19.3	1.41	336	(1.02 ± 0.06)E+2	(5.87 ± 0.49)E-7
21284.0	11.1	1.67	457		
940407.82	73.2	1.39	167	...	0.27 ± 0.06
9449	8.4	...	...	2.05 ± 1.02	(4.05 ± 0.75)E-8
71371.9	14.1	...	...		
940407.86	27.9	...	...	14.34 ± 1.45	0.14 ± 0.04
9449	-63.4	1.68	251	35.84 ± 7.38	(3.80 ± 0.07)E-7
74951.8	18.3	2.07	350		
940409.09	191.2	5.68	155	3.07 ± 1.45	0.93 ± 0.06
9451	-23.2	8.79	320	25.60 ± 1.45	(8.68 ± 0.93)E-7
7933.1	4.0	6.78	439		
940411.33	80.7	1.18	114	28.67 ± 1.45	0.21 ± 0.04
9453	41.2	2.28	229	61.44 ± 6.23	(1.26 ± 0.08)E-6
28646.6	3.2	3.40	370		
940412.25	306.1	1.60	128	15.36 ± 2.29	0.25 ± 0.05
9454	-29.8	2.78	354	36.86 ± 2.29	(7.62 ± 0.52)E-7
21602.5	9.3	3.57	531		
940413.24	28.7	1.62	152	7.17 ± 1.45	0.39 ± 0.07
9455	1.3	2.33	321	23.55 ± 3.24	(5.90 ± 0.13)E-7
21206.2	15.4	2.43	391		
940414.51	225.6	1.05	132	6.14 ± 2.29	0.17 ± 0.04
9456	2.9	1.79	358	14.34 ± 3.24	(2.02 ± 0.08)E-7
44093.6	15.4	1.87	541		
940414.91	206.3	2.37	137	4.10 ± 1.45	0.43 ± 0.05
9456	-15.3	3.47	259	12.29 ± 1.45	(3.40 ± 0.37)E-7
79167.6	5.8	3.30	400		
940417.42	136.6	2.04	123	9.22 ± 1.45	0.30 ± 0.04
9459	0.4	3.93	277	27.65 ± 3.24	(4.84 ± 3.13)E-7
36379.8	6.4	5.00	417		
940418.27	141.9	...	...	13.31 ± 1.45	0.11 ± 0.04
9460	-29.0	1.15	352	36.86 ± 5.51	(3.37 ± 0.03)E-7
23814.3	19.7	1.50	453		

Table A-2—Continued

Name (NTB) Date (TJD) Time (s UT)	R.A. (°) Decl. (°) Err. (°)	C_{max}/C_{min} (4.096 s) (8.192 s)	C_{min} (4.096 s) (8.192 s)	T_{50} (s) T_{90} (s)	P (ph cm^{-2} s^{-1}) F (erg cm^{-2}) (50–300 keV)
940418.56	232.6	1.62	176	2.05 ± 1.45	0.42 ± 0.08
9460	-8.9	2.21	351	7.17 ± 2.29	(3.04 ± 0.08)E-7
48832.7	14.1	1.84	448		
940419.24	183.2	1.48	134	7.17 ± 1.45	0.22 ± 0.05
9461	-4.4	2.50	237	25.60 ± 4.34	(3.88 ± 0.34)E-7
21200.0	6.4	2.91	354		
940424.96	213.6	1.13	205	11.26 ± 1.45	0.15 ± 0.05
9466	-68.2	2.12	348	26.62 ± 10.29	(3.03 ± 0.38)E-7
83646.6	18.5	2.63	453		
940503.09	150.8	1.30	154	3.07 ± 1.45	0.17 ± 0.04
9475	-60.9	1.98	281	7.17 ± 3.24	(1.25 ± 0.30)E-7
8466.6	12.7	1.72	358		
940506.93	26.9	1.13	158	39.94 ± 3.24	0.15 ± 0.05
9478	-29.3	2.00	275	(1.10 ± 0.17)E+2	(1.09 ± 0.04)E-6
81103.0	7.3	2.57	420		
940507.03	278.8	1.17	173	3.07 ± 1.45	0.20 ± 0.05
9479	51.5	1.39	319	6.14 ± 2.29	(1.15 ± 0.03)E-7
3296.4	20.3	1.29	491		
940508.43	95.6	...	...	11.26 ± 6.23	0.10 ± 0.04
9480	32.3	1.54	365	32.77 ± 9.71	(2.44 ± 0.04)E-7
37804.2	19.7	1.76	542		
940511.10	142.7	1.43	117	9.22 ± 1.45	0.25 ± 0.04
9483	82.9	2.75	245	22.53 ± 3.24	(6.90 ± 0.34)E-7
9102.5	4.6	3.43	347		
940512.59	119.2	1.13	183	15.36 ± 1.45	0.18 ± 0.04
9484	-17.3	1.93	360	37.89 ± 8.26	(4.58 ± 0.46)E-7
51213.5	8.5	2.34	510		
940514.66	93.1	...	...	10.24 ± 4.22	(6.62 ± 3.97)E-2
9486	-23.8	...	...	23.55 ± 9.27	(2.44 ± 0.03)E-7
57454.7	20.4	1.33	528		
940517.21	214.3	1.69	123	10.24 ± 1.45	0.27 ± 0.04
9489	13.1	3.17	273	28.67 ± 8.26	(5.07 ± 0.48)E-7
18525.3	8.8	3.85	411		
940517.30	276.5	2.66	143	4.10 ± 1.45	0.51 ± 0.05
9489	8.8	4.85	291	14.34 ± 4.22	(5.22 ± 1.03)E-7
26381.5	3.9	4.62	435		
940517.77	55.6	1.65	165	31.74 ± 2.29	0.27 ± 0.04
9489	-53.0	2.76	317	63.49 ± 8.26	(1.08 ± 0.07)E-6
66680.0	2.4	3.34	472		
940521.60	69.2	...	...	4.10 ± 1.45	0.17 ± 0.09
9493	40.7	...	...	11.26 ± 4.22	(3.18 ± 0.07)E-7
51887.3	25.3	1.17	381		
940521.98	66.0	...	...	12.29 ± 1.45	(9.89 ± 4.58)E-2
9493	-40.0	1.48	337	35.84 ± 4.58	(3.92 ± 0.08)E-7
84796.6	7.8	1.87	406		
940523.97	243.8	1.61	185	25.60 ± 1.45	0.27 ± 0.05
9495	23.3	3.12	373	52.22 ± 2.29	(1.04 ± 0.07)E-6
84186.3	5.6	3.97	485		
940524.31	143.5	6.36	162	1.02 ± 1.45	1.06 ± 0.05
9496	-9.1	6.21	329	3.07 ± 1.45	(4.08 ± 1.92)E-7
27048.1	5.7	4.73	445		
940526.33	77.6	1.42	129	10.24 ± 1.45	0.21 ± 0.04
9498	-12.1	1.91	235	26.62 ± 10.29	(3.01 ± 0.41)E-7
29079.7	12.7	2.39	332		
940530.24	283.2	1.58	131	...	0.25 ± 0.05
9502	-79.6	1.20	259	3.07 ± 1.02	(7.73 ± 0.19)E-8
21461.1	40.3	...	...		
940604.27	342.7	1.18	150	21.50 ± 6.23	0.33 ± 0.08
9507	71.1	1.90	304	61.44 ± 3.69	(1.37 ± 0.02)E-6
23481.5	11.7	2.40	395		

Table A-2—Continued

Name (NTB) Date (TJD) Time (s UT)	R.A. (°) Decl. (°) Err. (°)	C_{max}/C_{min} (4.096 s) (8.192 s)	C_{min} (4.096 s) (8.192 s)	T_{50} (s) T_{90} (s)	P (ph cm^{-2} s^{-1}) F (erg cm^{-2}) (50–300 keV)
940610.96	114.2	1.61	187	15.36 ± 2.29	0.20 ± 0.04
9513	-73.7	1.62	373	32.77 ± 2.29	(6.02 ± 0.05)E-7
83489.9	10.1	2.11	548		
940611.66	333.0	2.67	167	2.05 ± 1.45	0.50 ± 0.05
9514	42.6	2.94	349	11.26 ± 5.22	(2.52 ± 0.84)E-7
57137.3	5.3	2.49	496		
940611.86	157.7	2.14	127	10.24 ± 1.45	0.33 ± 0.05
9514	-31.6	3.27	242	28.67 ± 2.90	(5.63 ± 1.05)E-7
74590.4	6.9	3.72	342		
940612.19	167.1	...	...	14.34 ± 1.45	0.14 ± 0.04
9515	-31.8	1.54	336	29.70 ± 6.48	(1.94 ± 0.04)E-7
16749.7	32.0	1.54	501		
940613.37	295.7	7.46	133	7.17 ± 1.45	1.33 ± 0.06
9516	-55.9	10.64	265	21.50 ± 4.22	(1.84 ± 0.22)E-6
32102.6	1.3	12.13	375		
940616.14	52.3	1.67	135	11.26 ± 1.45	0.24 ± 0.04
9519	74.7	3.03	263	27.65 ± 3.24	(7.18 ± 0.92)E-7
12512.4	3.9	4.14	365		
940616.43	51.0	1.06	127	9.22 ± 1.45	0.14 ± 0.04
9519	76.4	1.12	228	21.50 ± 8.26	(1.55 ± 0.28)E-7
37471.4	19.7	1.31	387		
940617.00	19.8	...	...	23.55 ± 2.29	0.14 ± 0.04
9520	-64.3	1.54	304	69.63 ± 8.44	(6.30 ± 0.36)E-7
262.3	6.3	1.92	382		
940620.97	304.4	1.53	118	6.14 ± 1.45	0.24 ± 0.04
9523	-51.2	2.31	243	13.31 ± 7.24	(2.10 ± 0.46)E-7
83830.9	14.5	2.08	335		
940621.89	20.3	1.31	161	16.38 ± 1.45	0.19 ± 0.04
9524	-39.0	2.13	317	44.03 ± 5.22	(6.11 ± 0.32)E-7
77385.9	7.7	2.70	446		
940622.64	71.2	1.21	210	20.48 ± 2.29	0.32 ± 0.07
9525	3.2	1.87	400	62.46 ± 4.22	(1.15 ± 0.02)E-6
55862.4	8.5	2.45	576		
940623.15	183.0	2.09	191	6.14 ± 1.45	0.37 ± 0.05
9526	4.6	2.58	398	17.41 ± 2.29	(3.99 ± 0.89)E-7
13033.6	6.7	3.35	559		
940623.99	209.4	1.58	159	40.96 ± 3.24	0.25 ± 0.04
9526	-44.7	2.85	312	(1.14 ± 0.16)E+2	(1.38 ± 0.08)E-6
85606.6	4.6	3.75	415		
940628.23	266.8	4.70	190	83.97 ± 4.22	0.70 ± 0.05
9531	74.7	8.40	384	(1.62 ± 0.02)E+2	(2.14 ± 0.08)E-6
20448.4	2.3	9.83	554		
940702.36	88.8	1.58	147	21.50 ± 1.45	0.24 ± 0.05
9535	64.0	2.78	322	47.10 ± 2.29	(1.51 ± 0.07)E-6
31516.8	7.6	3.10	515		
940704.26	175.9	...	...	10.24 ± 1.45	0.13 ± 0.04
9537	-29.6	1.12	355	18.43 ± 2.29	(2.02 ± 0.07)E-7
23060.7	20.9	1.23	453		
940704.84	329.4	1.38	188	19.46 ± 2.29	0.18 ± 0.04
9537	29.4	2.17	277	53.25 ± 8.26	(8.49 ± 0.43)E-7
73371.8	6.2	2.83	344		
940705.29	296.0	1.05	126	...	0.16 ± 0.04
9538	56.0	1.51	330	11.26 ± 5.12	(1.66 ± 0.35)E-7
25345.2	14.6	1.62	449		
940706.14	333.7	2.69	201	16.38 ± 1.45	0.38 ± 0.04
9539	46.8	4.80	368	35.84 ± 5.22	(9.24 ± 0.65)E-7
12239.0	4.1	5.63	517		
940708.01	112.3	3.80	206	2.05 ± 1.45	0.68 ± 0.05
9541	-25.2	4.81	441	16.38 ± 15.39	(4.26 ± 0.90)E-7
1712.3	3.1	3.71	622		

Table A-2—Continued

Name (NTB) Date (TJD) Time (s UT)	R.A. (°) Decl. (°) Err. (°)	C_{max}/C_{min} (4.096 s) (8.192 s)	C_{min} (4.096 s) (8.192 s)	T_{50} (s) T_{90} (s)	P (ph cm^{-2} s^{-1}) F (erg cm^{-2}) (50–300 keV)
940708.41	176.9	...	...	22.53 ± 6.48	0.20 ± 0.08
9541	-33.6	1.09	256	57.34 ± 6.87	(1.13 ± 0.01)E-6
35911.9	10.9	1.28	367		
940710.41	99.4	1.18	176	16.38 ± 1.45	0.11 ± 0.04
9543	-33.3	1.90	384	47.10 ± 2.29	(6.17 ± 0.10)E-7
35465.4	3.4	2.42	499		
940712.00	58.0	19.07	136	5.12 ± 1.45	4.07 ± 0.08
9545	-71.1	21.82	273	11.26 ± 2.29	(2.90 ± 0.46)E-6
69.8	0.7	18.47	386		
940713.48	316.5	1.40	168	9.22 ± 4.22	0.20 ± 0.04
9546	53.3	2.21	354	27.65 ± 2.29	(2.41 ± 0.03)E-7
41819.3	15.0	2.08	512		
940716.56	353.5	1.33	184	...	0.36 ± 0.07
9549	49.9	...	...	3.07 ± 2.05	(8.23 ± 0.25)E-8
48860.3	29.5	...	...		
940719.20	334.6	...	...	9.22 ± 2.29	0.23 ± 0.08
9552	-25.8	1.16	336	32.77 ± 10.44	(5.95 ± 0.09)E-7
18078.9	35.7	1.45	440		
940720.08	252.3	1.34	159	...	0.20 ± 0.04
9553	31.1	1.05	366	5.12 ± 3.07	(4.60 ± 0.64)E-8
7026.9	31.5	...	...		
940720.40	330.9	1.30	176	23.55 ± 1.45	0.16 ± 0.04
9553	-51.2	2.10	373	38.91 ± 4.22	(6.23 ± 0.61)E-7
35074.2	16.8	2.57	503		
940722.33	347.5	1.79	145	32.77 ± 2.90	0.26 ± 0.04
9555	36.1	2.98	311	(1.04 ± 0.03)E+2	(1.17 ± 0.03)E-6
28528.8	6.2	3.09	463		
940726.63	349.6	2.69	185	76.80 ± 19.48	1.30 ± 0.14
9559	27.5	4.73	403	(1.25 ± 0.08)E+2	(5.31 ± 0.08)E-6
55163.1	3.2	5.49	542		
940727.47	308.3	11.98	163	50.18 ± 1.45	2.13 ± 0.06
9560	-8.7	21.59	328	80.90 ± 1.45	(9.60 ± 0.87)E-6
40864.9	6.0	23.92	465		
940727.82	234.9	...	...	9.22 ± 1.45	0.13 ± 0.04
9560	-76.2	1.29	364	19.46 ± 3.24	(2.35 ± 0.20)E-7
71046.3	8.0	1.76	373		
940729.06	352.9	3.90	184	19.46 ± 1.45	0.62 ± 0.05
9562	-0.1	5.84	364	45.06 ± 5.22	(1.45 ± 0.09)E-6
5403.8	2.4	7.11	513		
940729.45	102.0	1.00	134	...	0.15 ± 0.04
9562	-49.0	1.71	352	5.12 ± 1.44	(1.14 ± 0.36)E-7
39711.9	15.9	1.48	481		
940730.45	82.5	19.09	179	11.26 ± 1.45	3.78 ± 0.08
9563	-65.3	33.90	361	20.48 ± 1.45	(9.41 ± 0.37)E-6
39690.4	0.7	27.85	504		
940803.44	90.2	1.55	139	12.29 ± 2.29	0.25 ± 0.05
9567	-32.2	2.02	362	30.72 ± 2.90	(4.38 ± 0.41)E-7
38263.0	8.7	2.29	518		
940811.31	94.8	1.46	144	29.70 ± 4.22	0.21 ± 0.04
9575	29.0	1.77	259	80.90 ± 20.33	(4.13 ± 0.15)E-7
27547.8	25.8	1.49	386		
940812.28	237.8	1.35	180	23.55 ± 1.45	0.16 ± 0.04
9576	-26.7	2.38	360	56.32 ± 13.35	(5.78 ± 0.39)E-7
24874.2	13.7	2.60	521		
940813.13	272.1	1.23	166	2.05 ± 1.45	0.19 ± 0.04
9577	17.3	1.35	357	6.14 ± 3.24	(8.54 ± 0.16)E-8
11688.1	51.9	1.10	494		
940814.53	99.0	1.70	166	32.77 ± 1.45	0.25 ± 0.04
9578	-24.1	2.83	363	(1.04 ± 0.17)E+2	(1.94 ± 0.11)E-6
45849.8	2.1	3.75	532		

Table A-2—Continued

Name (NTB) Date (TJD) Time (s UT)	R.A. (°) Decl. (°) Err. (°)	C_{max}/C_{min} (4.096 s) (8.192 s)	C_{min} (4.096 s) (8.192 s)	T_{50} (s) T_{90} (s)	P (ph cm^{-2} s^{-1}) F (erg cm^{-2}) (50–300 keV)
940815.78	73.1	1.29	154	13.31 ± 1.45	0.15 ± 0.04
9579	18.2	1.45	284	28.67 ± 17.44	(2.39 ± 0.18)E-7
68196.5	43.0	1.34	465		
940815.86	148.8	...	...	8.19 ± 3.24	0.11 ± 0.04
9579	-18.7	1.26	241	21.50 ± 1.45	(2.53 ± 0.03)E-7
74662.1	11.2	1.77	397		
940902.23	138.0	...	...	5.12 ± 2.29	0.13 ± 0.04
9597	50.4	1.49	254	17.41 ± 9.44	(1.95 ± 0.42)E-7
20164.8	30.9	1.82	405		
940906.73	104.7	...	...	4.10 ± 1.45	0.11 ± 0.04
9601	29.3	1.06	343	9.22 ± 4.34	(9.86 ± 1.00)E-8
63695.0	11.1	1.17	400		
940908.87	308.8	1.22	184	11.26 ± 1.45	0.19 ± 0.05
9603	31.3	1.80	386	30.72 ± 7.45	(3.82 ± 0.42)E-7
75245.7	4.5	2.27	599		
940909.00	105.5	1.26	193	14.34 ± 2.29	0.22 ± 0.05
9604	63.4	1.90	355	29.70 ± 7.80	(3.65 ± 0.54)E-7
699.6	43.0	2.15	445		
940909.47	194.1	9.90	204	33.79 ± 6.23	1.92 ± 0.07
9604	19.5	8.30	419	86.02 ± 1.45	(2.17 ± 0.10)E-6
40875.2	2.4	6.53	573		
940913.95	156.8	1.14	146	41.98 ± 5.22	0.15 ± 0.04
9608	29.3	2.11	354	65.54 ± 4.22	(5.62 ± 0.44)E-7
82402.5	23.4	2.61	485		
940916.33	74.8	4.92	206	4.10 ± 1.45	1.27 ± 0.08
9611	-39.5	5.93	429	48.13 ± 2.90	(1.07 ± 0.04)E-6
29184.2	17.2	5.63	579		
940917.29	301.8	1.47	136	10.24 ± 3.24	0.21 ± 0.04
9612	1.7	2.68	317	32.77 ± 5.79	(6.71 ± NaN)E-7
25416.9	11.9	2.88	476		
940923.31	259.3	2.54	164	12.29 ± 1.45	0.31 ± 0.04
9618	66.7	4.69	297	38.91 ± 5.12	(8.83 ± 0.85)E-7
27198.6	3.1	5.60	411		
940923.81	254.1	1.40	154	27.65 ± 2.29	0.20 ± 0.04
9618	-49.9	2.48	375	75.78 ± 13.66	(5.08 ± 0.45)E-7
70474.9	10.9	3.09	518		
940923.94	91.9	1.32	143	21.50 ± 3.24	0.42 ± 0.09
9618	11.8	2.04	309	51.20 ± 13.47	(2.00 ± 0.03)E-6
81698.0	4.2	2.63	420		
940924.30	227.1	1.46	179	12.29 ± 3.24	0.25 ± 0.05
9619	11.8	2.36	355	47.10 ± 4.58	(5.76 ± 0.47)E-7
26306.7	5.6	2.87	597		
940924.97	154.5	1.87	168	4.10 ± 1.45	0.34 ± 0.05
9619	-9.9	2.36	332	7.17 ± 2.29	(1.96 ± 6.16)E-7
84644.0	4.3	2.70	440		
940926.05	31.6	1.55	177	25.60 ± 8.26	0.40 ± 0.07
9621	-40.7	1.90	317	48.13 ± 5.12	(6.83 ± 0.08)E-7
4565.2	11.4	1.64	500		
940926.48	187.6	1.14	144	3.07 ± 1.45	0.19 ± 0.05
9621	-12.0	2.08	263	7.17 ± 3.24	(1.52 ± 0.47)E-7
41896.1	24.1	2.12	391		
940930.06	87.1	1.37	188	...	0.30 ± 0.06
9625	59.7	1.48	334	3.07 ± 1.44	(1.55 ± 0.03)E-7
5214.4	22.2	1.20	407		
940930.26	80.4	7.08	204	16.38 ± 1.45	0.97 ± 0.05
9625	33.0	11.97	385	74.75 ± 8.26	(2.21 ± 0.14)E-6
23013.6	10.7	12.65	544		
940930.57	187.5	...	...	8.19 ± 1.45	(9.71 ± 4.48)E-2
9625	75.0	1.31	391	17.41 ± 1.45	(2.36 ± 0.04)E-7
49696.9	10.5	1.45	507		

Table A-2—Continued

Name (NTB) Date (TJD) Time (s UT)	R.A. (°) Decl. (°) Err. (°)	C_{max}/C_{min} (4.096 s) (8.192 s)	C_{min} (4.096 s) (8.192 s)	T_{50} (s) T_{90} (s)	P (ph cm^{-2} s^{-1}) F (erg cm^{-2}) (50–300 keV)
940930.88	123.0	1.61	113	4.10 ± 1.45	0.19 ± 0.04
9625	55.3	2.33	297	14.34 ± 10.44	(1.64 ± 0.51)E-7
76697.8	56.2	2.40	406		
941001.89	301.8	1.27	155	7.17 ± 2.29	0.18 ± 0.04
9626	30.6	1.48	357	24.58 ± 12.37	(1.65 ± 0.90)E-7
77083.8	53.1	1.60	518		
941004.97	158.2	2.80	141	45.06 ± 2.90	0.40 ± 0.05
9629	-2.5	5.15	280	(2.32 ± 0.16)E+2	(4.96 ± 0.17)E-6
83810.5	2.0	6.99	406		
941005.32	100.9	1.37	162	(1.04 ± 0.02)E+2	0.13 ± 0.04
9630	-31.8	2.37	285	(1.90 ± 0.16)E+2	(1.11 ± 0.06)E-6
28380.3	5.9	3.01	422		
941008.07	358.7	1.49	158	76.80 ± 5.51	0.29 ± 0.05
9633	76.5	2.44	297	(1.05 ± 0.03)E+2	(9.32 ± 1.04)E-7
6885.6	6.1	2.32	510		
941008.73	270.7	1.25	194	49.15 ± 5.22	0.19 ± 0.05
9633	-4.3	1.83	360	82.94 ± 4.22	(7.61 ± 0.07)E-7
63897.8	5.3	2.00	530		
941010.18	132.8	2.33	162	46.08 ± 9.27	0.34 ± 0.04
9635	-76.0	3.81	332	(1.03 ± 0.34)E+2	(1.08 ± 0.03)E-6
15902.9	6.7	4.62	472		
941011.15	290.0	...	...	14.34 ± 1.45	0.26 ± 0.12
9636	-58.4	1.39	314	44.03 ± 8.44	(1.42 ± 0.02)E-6
13094.1	56.8	1.65	340		
941011.36	351.5	...	...	7.17 ± 1.45	0.20 ± 0.06
9636	-36.0	1.44	325	15.36 ± 4.58	(3.21 ± 0.05)E-7
31270.1	41.3	1.62	504		
941015.97	22.0	1.84	121	12.29 ± 1.45	0.23 ± 0.04
9640	20.9	2.41	289	32.77 ± 4.34	(4.05 ± 0.68)E-7
84432.0	13.4	3.06	376		
941018.55	55.0	...	...	8.19 ± 2.29	0.14 ± 0.04
9643	-0.2	1.66	365	17.41 ± 5.22	(2.06 ± 0.03)E-7
48228.5	15.5	1.77	495		
941018.90	308.9	1.64	163	16.38 ± 1.45	0.26 ± 0.04
9643	35.7	2.36	335	60.42 ± 8.26	(6.65 ± 0.68)E-7
78180.5	27.0	2.76	470		
941020.22	5.0	...	...	28.67 ± 12.46	0.12 ± 0.05
9645	67.6	1.37	315	46.08 ± 2.29	(3.59 ± 1.48)E-7
19081.4	5.4	1.60	479		
941022.42	45.3	2.44	125	75.78 ± 3.24	0.57 ± 0.05
9647	28.3	5.15	251	(1.50 ± 0.01)E+2	(2.65 ± 0.10)E-6
37101.7	4.3	5.42	378		
941023.03	112.0	1.23	156	8.19 ± 1.45	0.22 ± 0.05
9648	19.4	2.25	316	21.50 ± 3.24	(4.41 ± 0.58)E-7
3402.9	10.9	2.58	414		
941023.19	338.9	1.46	163	...	0.37 ± 0.07
9648	65.4	1.25	300	10.24 ± 3.07	(2.88 ± 0.07)E-7
16590.0	28.8	1.49	473		
941026.25	243.3	1.90	167	4.10 ± 1.45	0.28 ± 0.05
9651	-51.5	2.96	306	14.34 ± 1.45	(2.73 ± 0.36)E-7
22067.4	56.2	2.90	451		
941031.39	36.4	2.06	175	6.14 ± 1.45	0.26 ± 0.04
9656	45.6	3.54	353	15.36 ± 1.45	(4.72 ± 0.32)E-7
33813.7	21.2	4.06	532		
941031.58	257.2	1.57	140	4.10 ± 1.45	0.18 ± 0.03
9656	50.9	2.32	310	11.26 ± 1.45	(2.64 ± 0.37)E-7
50199.7	14.5	3.08	485		
941101.41	243.5	...	...	10.24 ± 1.45	0.16 ± 0.05
9657	4.9	1.89	289	25.60 ± 2.90	(3.58 ± 1.20)E-7
36036.8	5.5	2.24	401		

Table A-2—Continued

Name (NTB) Date (TJD) Time (s UT)	R.A. (°) Decl. (°) Err. (°)	C_{max}/C_{min} (4.096 s) (8.192 s)	C_{min} (4.096 s) (8.192 s)	T_{50} (s) T_{90} (s)	P (ph cm^{-2} s^{-1}) F (erg cm^{-2}) (50–300 keV)
941102.67	141.6	...	...	29.70 ± 2.29	0.22 ± 0.07
9658	-36.5	1.79	330	79.87 ± 3.69	(1.09 ± 0.01)E-6
58524.8	18.9	2.17	431		
941104.40	338.3	3.65	166	4.10 ± 1.45	0.56 ± 0.05
9660	22.2	6.18	302	14.34 ± 4.58	(6.88 ± 0.85)E-7
35171.5	4.0	7.35	439		
941108.55	48.1	1.48	178	13.31 ± 1.45	0.24 ± 0.05
9664	67.3	2.64	362	25.60 ± 3.24	(5.72 ± 0.37)E-7
48100.5	5.4	2.95	464		
941109.25	329.8	...	...	13.31 ± 2.29	0.12 ± 0.05
9665	-14.8	1.27	338	30.72 ± 10.44	(2.13 ± 0.39)E-7
22294.7	57.7	1.61	462		
941116.36	284.6	1.31	197	3.07 ± 2.29	0.38 ± 0.08
9672	30.5	1.36	376	7.17 ± 2.29	(3.07 ± 0.09)E-7
31954.1	19.3	1.57	561		
941119.05	4.7	1.77	175	8.19 ± 1.45	0.26 ± 0.05
9675	24.4	3.13	321	20.48 ± 1.45	(6.28 ± 0.61)E-7
4896.9	6.1	3.94	433		
941123.70	26.8	1.08	157	7.17 ± 1.45	0.14 ± 0.04
9679	55.8	1.53	375	15.36 ± 1.45	(2.41 ± 0.49)E-7
61235.4	12.6	2.01	519		
941125.46	246.5	1.87	162	12.29 ± 3.24	0.22 ± 0.03
9681	19.4	2.90	304	36.86 ± 19.48	(3.84 ± 0.48)E-7
40288.4	8.1	3.23	406		
941201.27	79.8	1.20	129	44.03 ± 1.45	0.14 ± 0.04
9687	-31.7	2.01	279	77.82 ± 3.24	(1.59 ± 0.12)E-6
23396.5	7.0	2.70	358		
941205.12	276.0	1.07	128	13.31 ± 2.29	0.25 ± 0.05
9691	-37.9	2.36	313	29.70 ± 1.45	(4.68 ± 1.00)E-7
11223.2	6.0	2.69	424		
941210.34	187.5	1.95	156	8.19 ± 2.29	0.31 ± 0.05
9696	-27.8	3.43	337	19.46 ± 4.22	(6.31 ± 0.80)E-7
30053.6	60.9	4.14	438		
941211.17	139.4	1.35	140	20.48 ± 2.29	0.19 ± 0.04
9697	-20.6	2.27	320	59.39 ± 6.23	(5.74 ± 0.34)E-7
14758.1	20.2	3.05	445		
941216.45	257.7	1.79	206	8.19 ± 1.45	0.28 ± 0.04
9702	31.0	3.00	417	30.72 ± 5.22	(5.56 ± 0.53)E-7
38991.0	9.6	3.87	588		
941222.16	74.7	1.04	126	8.19 ± 1.45	0.14 ± 0.04
9708	-5.6	1.39	234	18.43 ± 1.45	(3.10 ± 0.41)E-7
14524.6	9.9	2.32	331		
941222.26	95.1	...	...	22.53 ± 3.24	0.10 ± 0.04
9708	60.2	1.53	245	65.54 ± 23.57	(4.93 ± 0.04)E-7
22658.2	8.3	1.92	399		
941230.82	149.7	3.52	125	8.19 ± 1.45	0.59 ± 0.05
9716	11.8	5.84	245	21.50 ± 3.24	(9.72 ± 1.16)E-7
70921.4	2.3	6.60	348		
950103.79	11.1	1.15	181	20.48 ± 6.48	0.15 ± 0.04
9720	73.0	1.83	281	58.37 ± 13.47	(6.12 ± 0.77)E-7
68336.8	8.0	2.38	354		
950104.25	9.8	1.01	155	...	0.21 ± 0.06
9721	7.4	1.29	393	11.26 ± 5.12	(1.68 ± 0.12)E-7
22341.8	16.1	1.33	475		
950104.32	273.2	4.38	174	...	1.89 ± 0.13
9721	-24.4	2.77	394	1.02 ± 1.02	(4.50 ± 0.27)E-7
28350.6	7.2	2.25	515		
950104.37	220.8	4.07	176	9.22 ± 1.45	0.69 ± 0.05
9721	49.7	7.08	304	36.86 ± 1.45	(1.39 ± 0.18)E-6
32438.4	2.4	8.02	425		

Table A-2—Continued

Name (NTB) Date (TJD) Time (s UT)	R.A. (°) Decl. (°) Err. (°)	C_{max}/C_{min} (4.096 s) (8.192 s)	C_{min} (4.096 s) (8.192 s)	T_{50} (s) T_{90} (s)	P (ph cm^{-2} s^{-1}) F (erg cm^{-2}) (50–300 keV)
950104.86	12.0	3.75	114	10.24 ± 1.45	0.56 ± 0.05
9721	-55.8	6.09	229	49.15 ± 5.12	(1.01 ± 0.15)E-6
74453.2	3.2	5.67	324		
950111.53	23.1	15.30	136	24.58 ± 1.45	2.43 ± 0.07
9728	-6.1	26.65	280	44.03 ± 1.45	(1.02 ± 0.06)E-5
46523.6	0.5	32.77	398		
950123.65	216.0	2.27	175	10.24 ± 1.45	0.34 ± 0.04
9740	-82.8	3.98	373	30.72 ± 8.26	(4.84 ± 1.34)E-7
56456.4	20.0	4.60	548		
950129.78	249.4	1.13	137	46.08 ± 9.27	0.18 ± 0.05
9746	-47.4	2.06	320	86.02 ± 5.22	(8.75 ± 0.09)E-7
67577.0	3.2	2.67	436		
950129.81	180.6	...	...	...	0.20 ± 0.07
9746	39.1	1.36	354	21.50 ± 5.12	(4.29 ± 0.06)E-7
70184.1	21.8	1.54	513		
950131.90	318.4	2.68	143	6.14 ± 1.45	0.39 ± 0.04
9748	-47.7	4.49	317	14.34 ± 2.29	(4.25 ± 3.62)E-7
78591.2	5.7	5.40	454		
950203.09	274.0	71.24	139	6.14 ± 1.45	13.94 ± 0.14
9751	39.0	86.99	277	31.74 ± 1.45	(1.72 ± 0.24)E-5
8452.3	0.2	104.85	390		
950207.83	177.8	3.89	167	25.60 ± 1.45	1.13 ± 0.09
9755	-18.7	7.09	392	78.85 ± 9.71	(1.02 ± 0.01)E-5
72388.8	0.8	9.77	544		
950210.81	238.0	1.25	192	11.26 ± 1.45	0.18 ± 0.04
9758	-3.8	1.83	348	23.55 ± 3.69	(3.21 ± 0.50)E-7
70100.1	8.6	2.25	527		
950211.18	324.4	22.91	177	7.17 ± 1.45	4.62 ± 0.09
9759	0.4	37.55	357	29.70 ± 2.29	(9.93 ± 0.33)E-6
15919.3	0.4	49.08	504		
950213.83	87.8	1.44	172	...	0.19 ± 0.05
9761	-6.7	1.91	265	6.14 ± 2.05	(1.27 ± 0.42)E-7
72200.4	29.7	1.64	362		
950220.37	9.3	1.46	188	7.17 ± 1.45	0.20 ± 0.04
9768	-75.2	2.80	395	27.65 ± 9.27	(4.77 ± 0.79)E-7
32425.1	9.8	3.67	534		
950224.39	321.0	1.07	120	13.31 ± 1.45	0.26 ± 0.04
9772	60.0	2.23	250	35.84 ± 2.29	(1.04 ± 0.05)E-6
33797.3	2.8	3.14	354		
950228.54	102.8	1.76	142	51.20 ± 3.24	0.44 ± 0.07
9776	-44.2	2.97	259	94.21 ± 13.35	(2.30 ± 0.02)E-6
46711.0	3.8	4.17	352		
950304.09	67.7	1.44	128	...	0.32 ± 0.05
9780	-34.4	1.32	246	5.12 ± 2.05	(8.67 ± 5.43)E-8
8305.8	19.8	...	...		
950305.63	208.0	1.01	117	39.94 ± 4.22	0.15 ± 0.04
9781	-20.5	1.92	302	(1.21 ± 0.33)E+2	(1.12 ± 0.09)E-6
54585.5	6.5	2.37	393		
950305.65	337.9	2.59	183	...	0.38 ± 0.04
9781	36.2	2.12	356	6.14 ± 2.05	(1.37 ± 0.63)E-7
56910.0	11.0	1.76	514		
950310.90	1.5	8.84	191	82.94 ± 3.24	1.95 ± 0.07
9786	20.6	16.13	382	(1.93 ± 0.02)E+2	(9.17 ± 0.54)E-6
78552.2	5.8	20.91	548		
950313.84	30.8	...	...	21.50 ± 1.45	(7.53 ± 4.19)E-2
9789	-38.1	1.37	275	55.30 ± 7.24	(4.89 ± 0.10)E-7
73042.1	20.4	1.77	431		
950320.26	209.3	1.73	134	...	0.35 ± 0.05
9796	-28.3	1.49	377	2.05 ± 1.02	(8.88 ± 0.18)E-8
22893.7	33.3	1.31	448		

Table A-2—Continued

Name (NTB) Date (TJD) Time (s UT)	R.A. (°) Decl. (°) Err. (°)	C_{max}/C_{min} (4.096 s) (8.192 s)	C_{min} (4.096 s) (8.192 s)	T_{50} (s) T_{90} (s)	P (ph cm^{-2} s^{-1}) F (erg cm^{-2}) (50–300 keV)
950320.53	192.4	1.41	136	16.38 ± 5.22	0.21 ± 0.04
9796	-1.1	2.45	321	49.15 ± 9.44	(4.88 ± 0.50)E-7
46245.0	19.3	3.09	441		
950320.77	147.2	...	...	19.46 ± 1.45	0.23 ± 0.08
9796	19.9	1.27	281	50.18 ± 4.22	(1.40 ± 0.01)E-6
67134.6	11.8	1.74	555		
950325.27	360.0	2.68	165	...	0.41 ± 0.04
9801	-74.9	1.37	305	1.02 ± 1.02	(8.93 ± 1.89)E-8
23699.6	15.6	...	...		
950330.80	12.0	...	...	10.24 ± 2.29	0.12 ± 0.04
9806	22.8	1.53	335	22.53 ± 5.51	(2.73 ± 0.60)E-7
69975.2	18.4	2.15	509		
950403.16	25.3	1.62	157	35.84 ± 2.29	0.22 ± 0.04
9810	23.2	3.12	360	78.85 ± 5.79	(7.27 ± 0.68)E-7
14163.1	13.8	3.88	510		
950406.84	45.6	2.94	133	13.31 ± 2.29	0.44 ± 0.04
9813	52.1	4.29	270	41.98 ± 6.56	(8.22 ± 1.45)E-7
72863.9	4.8	4.86	390		
950407.25	316.6	1.13	119	20.48 ± 7.24	0.17 ± 0.04
9814	38.7	1.83	240	38.91 ± 7.24	(4.12 ± 0.45)E-7
22265.0	8.5	1.92	339		
950410.91	360.0	1.64	184	...	0.25 ± 0.04
9817	-28.3	2.29	347	5.12 ± 2.05	(1.76 ± 0.03)E-7
79345.8	48.6	1.82	523		
950411.47	121.6	1.88	169	...	0.32 ± 0.05
9818	-73.1	1.68	363	5.12 ± 2.05	(1.01 ± 0.15)E-7
41374.9	50.7	1.34	490		
950411.62	75.9	1.97	190	6.14 ± 1.45	0.34 ± 0.05
9818	-83.6	3.54	386	17.41 ± 3.24	(4.48 ± 0.75)E-7
54060.2	10.4	4.12	548		
950413.09	41.5	2.02	160	...	0.58 ± 0.08
9820	75.7	2.12	341	4.10 ± 2.05	(2.86 ± 0.10)E-7
8213.7	14.3	1.72	451		
950414.81	305.6	1.19	135	9.22 ± 2.29	0.17 ± 0.04
9821	80.0	1.83	364	19.46 ± 7.80	(2.51 ± 0.16)E-7
70199.5	65.8	2.16	500		
950416.10	333.1	1.42	172	...	0.51 ± 0.10
9823	15.1	2.14	326	5.12 ± 2.05	(3.90 ± 0.13)E-7
9396.4	18.0	1.69	412		
950417.30	155.5	1.93	175	9.22 ± 1.45	0.28 ± 0.04
9824	-41.2	3.34	347	26.62 ± 5.22	(6.00 ± 0.48)E-7
26256.6	10.2	4.03	481		
950421.23	291.0	1.07	137	12.29 ± 1.45	0.13 ± 0.03
9828	-51.0	1.64	342	48.13 ± 7.45	(2.66 ± 0.02)E-7
20407.5	41.0	1.84	488		
950422.15	222.9	1.10	128	11.26 ± 3.24	0.15 ± 0.04
9829	72.2	1.75	266	29.70 ± 3.24	(2.91 ± 0.14)E-7
13578.4	9.9	2.10	388		
950424.24	90.7	1.12	136	5.12 ± 1.45	0.15 ± 0.04
9831	-6.4	1.80	273	13.31 ± 4.22	(1.66 ± 0.17)E-7
21135.5	22.9	1.84	390		
950428.71	217.1	...	...	5.12 ± 2.29	(8.51 ± 4.08)E-2
9835	13.3	1.37	362	17.41 ± 3.24	(1.71 ± 0.05)E-7
61421.7	17.8	1.72	500		
950430.11	47.6	1.24	157	...	0.30 ± 0.07
9837	-82.7	...	...	1.02 ± 1.02	(6.97 ± 0.22)E-8
9506.0	28.6	...	...		
950430.30	340.5	1.52	167	28.67 ± 1.45	0.35 ± 0.07
9837	-79.8	2.30	331	43.01 ± 6.48	(1.03 ± 0.01)E-6
25977.0	12.7	2.37	442		

Table A-2—Continued

Name (NTB) Date (TJD) Time (s UT)	R.A. (°) Decl. (°) Err. (°)	C_{max}/C_{min} (4.096 s) (8.192 s)	C_{min} (4.096 s) (8.192 s)	T_{50} (s) T_{90} (s)	P (ph cm^{-2} s^{-1}) F (erg cm^{-2}) (50–300 keV)
950501.08	316.3	1.92	187	...	0.28 ± 0.04
9838	-36.0	1.30	290	1.02 ± 1.02	(6.38 ± 1.83)E-8
6939.8	40.8	...	...		
950503.91	359.0	2.40	179	75.78 ± 3.24	0.32 ± 0.04
9840	38.5	4.38	372	(2.39 ± 0.07)E+2	(5.37 ± 0.23)E-6
79217.8	6.6	5.90	531		
950506.58	310.8	1.53	144	4.10 ± 1.45	0.19 ± 0.04
9843	-72.4	1.97	241	12.29 ± 7.24	(1.07 ± 0.55)E-7
50286.8	42.6	1.40	352		
950509.99	331.1	2.44	131	...	0.76 ± 0.09
9846	29.2	1.07	250	1.02 ± 1.02	(1.72 ± 0.08)E-7
85837.0	13.2	...	...		
950510.35	56.8	1.36	141	7.17 ± 1.45	0.21 ± 0.04
9847	72.1	1.80	366	24.58 ± 1.45	(2.66 ± 0.35)E-7
30370.0	48.4	1.84	483		
950510.76	244.4	1.55	176	14.34 ± 2.29	0.28 ± 0.05
9847	14.6	2.94	389	41.98 ± 5.79	(1.06 ± 0.10)E-6
66156.7	3.0	4.03	563		
950510.91	331.3	2.58	195	27.65 ± 1.45	0.46 ± 0.05
9847	-23.5	3.38	376	67.58 ± 7.24	(1.57 ± 0.04)E-6
79370.4	6.2	3.38	553		
950510.95	229.0	5.78	182	19.46 ± 1.45	1.42 ± 0.08
9847	-30.0	8.46	381	44.03 ± 1.45	(3.68 ± 0.06)E-6
82114.7	3.5	9.68	520		
950511.93	220.8	2.01	175	20.48 ± 2.29	0.33 ± 0.05
9848	-71.7	3.41	295	33.79 ± 2.29	(6.95 ± 1.30)E-7
81050.8	3.7	4.06	435		
950514.73	261.9	1.11	182	31.74 ± 5.22	0.18 ± 0.05
9851	-17.2	1.78	359	64.51 ± 19.48	(6.82 ± 0.35)E-7
63338.7	10.4	1.88	479		
950514.90	78.1	1.09	182	17.41 ± 2.29	0.19 ± 0.05
9851	13.4	1.77	362	46.08 ± 6.23	(4.16 ± 0.87)E-7
78033.1	5.9	2.18	566		
950515.64	307.4	2.85	149	...	0.51 ± 0.05
9852	13.3	2.19	254	4.10 ± 2.05	(1.45 ± 0.61)E-7
55536.8	7.3	1.39	317		
950518.12	159.0	1.20	137	2.05 ± 1.45	0.17 ± 0.04
9855	-45.4	1.35	227	6.14 ± 2.90	(8.77 ± 0.35)E-8
10920.1	15.5	1.17	399		
950518.81	32.6	3.75	148	5.12 ± 1.45	0.55 ± 0.05
9855	-62.4	6.28	291	18.43 ± 11.31	(6.93 ± 0.56)E-7
70228.1	4.7	6.41	405		
950519.44	156.6	2.19	150	...	0.67 ± 0.08
9856	-22.8	1.40	256	3.07 ± 1.44	(1.95 ± 0.07)E-7
38407.3	19.2	1.36	441		
950519.92	326.3	2.05	164	13.31 ± 2.29	0.39 ± 0.05
9856	-50.3	3.75	325	60.42 ± 15.63	(8.36 ± 0.89)E-7
79609.0	6.0	4.25	469		
950521.42	61.8	5.64	204	92.16 ± 1.45	0.84 ± 0.05
9858	23.3	5.78	399	(1.15 ± 0.16)E+2	(7.36 ± 0.45)E-7
36936.9	9.6	5.01	559		
950522.78	26.6	1.64	175	7.17 ± 1.45	0.20 ± 0.04
9859	80.7	2.65	326	15.36 ± 1.45	(3.32 ± 0.87)E-7
68155.6	30.7	3.07	483		
950523.70	27.4	1.18	127	10.24 ± 2.29	0.18 ± 0.04
9860	10.9	1.75	247	22.53 ± 1.45	(2.54 ± 0.30)E-7
60744.9	24.6	2.28	356		
950524.89	298.4	3.79	144	9.22 ± 1.45	0.82 ± 0.06
9861	4.0	6.55	269	28.67 ± 2.29	(1.07 ± 0.11)E-6
77389.0	2.7	7.41	397		

Table A-2—Continued

Name (NTB) Date (TJD) Time (s UT)	R.A. (°) Decl. (°) Err. (°)	C_{max}/C_{min} (4.096 s) (8.192 s)	C_{min} (4.096 s) (8.192 s)	T_{50} (s) T_{90} (s)	P (ph cm^{-2} s^{-1}) F (erg cm^{-2}) (50–300 keV)
950530.17	55.1	...	...	19.46 ± 2.29	0.14 ± 0.04
9867	-4.9	1.56	376	37.89 ± 8.44	(2.83 ± 0.28)E-7
15198.4	42.6	1.96	535		
950531.22	49.4	2.02	135	8.19 ± 1.45	0.33 ± 0.05
9868	9.9	2.74	247	22.53 ± 2.29	(4.31 ± 0.21)E-7
19158.2	8.1	3.23	395		
950601.50	50.4	1.23	171	14.34 ± 3.24	0.17 ± 0.04
9869	-17.4	2.10	368	38.91 ± 8.26	(4.87 ± 0.43)E-7
43862.2	9.0	2.90	496		
950602.54	41.0	1.67	136	14.34 ± 1.45	0.26 ± 0.04
9870	-35.1	2.85	284	43.01 ± 6.23	(6.81 ± 0.59)E-7
47076.5	8.4	3.41	376		
950603.24	56.2	14.43	136	10.24 ± 1.45	2.57 ± 0.07
9871	-33.9	16.19	275	40.96 ± 8.26	(2.26 ± 0.17)E-6
21252.3	1.4	14.93	386		
950604.07	309.7	...	...	22.53 ± 3.24	0.14 ± 0.04
9872	81.0	1.54	341	38.91 ± 8.00	(5.92 ± 0.14)E-7
6905.0	5.3	1.74	456		
950605.13	114.2	1.32	168	...	0.21 ± 0.04
9873	40.8	1.03	366	3.07 ± 1.44	(4.52 ± 1.97)E-8
11380.9	31.0	...	...		
950611.94	211.0	1.16	179	13.31 ± 2.29	0.12 ± 0.04
9879	32.7	1.72	387	35.84 ± 4.22	(3.63 ± 0.55)E-7
81750.2	9.5	2.26	546		
950614.00	164.6	2.18	126	4.10 ± 1.45	0.31 ± 0.04
9882	-72.0	4.25	253	20.48 ± 3.24	(3.82 ± 0.06)E-7
769.2	3.3	3.91	358		
950615.14	301.7	4.13	132	47.10 ± 1.45	0.67 ± 0.05
9883	-49.4	7.49	250	79.87 ± 1.45	(3.62 ± 0.28)E-6
12103.9	4.9	9.06	345		
950616.43	297.7	...	...	10.24 ± 2.29	(9.83 ± 4.11)E-2
9884	-50.7	1.14	354	28.67 ± 8.26	(2.00 ± 0.10)E-7
37666.0	30.3	1.33	435		
950619.55	154.5	1.88	147	8.19 ± 2.29	0.29 ± 0.04
9887	50.2	3.03	267	26.62 ± 7.24	(6.17 ± 0.45)E-7
47876.3	9.6	3.80	373		
950620.64	234.4	2.00	183	...	0.38 ± 0.06
9888	39.4	1.69	430	4.10 ± 1.44	(1.13 ± 0.62)E-7
55434.4	5.0	1.13	524		
950621.78	324.6	2.67	180	...	0.42 ± 0.05
9889	-67.2	1.01	260	1.02 ± 1.02	(8.58 ± 0.28)E-8
68084.9	13.8	...	...		
950621.91	253.8	1.06	153	9.22 ± 2.29	0.19 ± 0.05
9889	-40.1	1.69	315	38.91 ± 19.88	(2.80 ± 0.44)E-7
79427.8	7.4	1.94	544		
950622.82	209.3	8.29	162	2.05 ± 1.45	1.23 ± 0.05
9890	8.3	9.56	324	17.41 ± 8.26	(7.20 ± 1.47)E-7
71468.2	4.8	8.22	484		
950624.75	140.3	1.07	155	10.24 ± 2.29	0.19 ± 0.05
9892	-55.6	1.93	378	25.60 ± 4.22	(3.64 ± 0.38)E-7
65471.7	6.7	2.37	540		
950625.11	140.3	9.01	204	16.38 ± 1.45	1.52 ± 0.06
9893	41.2	16.07	406	23.55 ± 1.45	(3.05 ± 0.59)E-6
9681.1	1.7	15.99	585		
950625.14	132.7	...	...	14.34 ± 1.45	0.13 ± 0.04
9893	7.1	1.11	324	28.67 ± 6.23	0.00 ± 0.00
12959.9	10.3	1.15	374		
950626.76	153.5	2.48	166	...	0.40 ± 0.05
9894	-41.6	1.53	362	2.05 ± 1.02	(1.08 ± 0.02)E-7
65979.6	10.5	1.22	475		

Table A-2—Continued

Name (NTB) Date (TJD) Time (s UT)	R.A. (°) Decl. (°) Err. (°)	C_{max}/C_{min} (4.096 s) (8.192 s)	C_{min} (4.096 s) (8.192 s)	T_{50} (s) T_{90} (s)	P (ph cm^{-2} s^{-1}) F (erg cm^{-2}) (50–300 keV)
950628.89	268.4	1.36	174	4.10 ± 2.29	0.22 ± 0.04
9896	47.9	2.24	316	16.38 ± 3.69	(2.46 ± 0.56)E-7
77202.6	18.9	2.60	431		
950629.07	288.4	1.76	176	8.19 ± 1.45	0.25 ± 0.05
9897	-4.7	3.13	366	26.62 ± 6.56	(5.33 ± 1.03)E-7
6806.7	6.3	3.77	515		
950701.23	175.0	1.81	151	...	0.49 ± 0.07
9899	-39.7	1.22	326	2.05 ± 1.44	(1.56 ± 0.05)E-7
20363.4	28.6	...	...		
950704.44	192.4	...	...	18.43 ± 3.69	0.13 ± 0.05
9902	24.6	1.08	264	37.89 ± 3.69	(4.25 ± 0.13)E-7
38040.8	7.8	1.44	410		
950705.15	216.5	1.27	184	12.29 ± 3.24	0.18 ± 0.04
9903	62.8	2.41	361	27.65 ± 5.22	(5.34 ± 0.45)E-7
13494.4	28.0	3.24	526		
950709.84	11.1	1.65	160	12.29 ± 1.45	0.27 ± 0.05
9907	-14.0	3.09	336	32.77 ± 5.22	(7.35 ± 1.26)E-7
73330.9	2.7	3.85	440		
950713.66	295.5	1.64	184	20.48 ± 1.45	0.24 ± 0.04
9911	-72.9	2.81	356	36.86 ± 4.22	(5.74 ± 0.52)E-7
57143.5	11.6	3.23	478		
950713.78	342.8	2.52	164	4.10 ± 1.45	0.48 ± 0.05
9911	-27.1	4.15	297	13.31 ± 5.22	(4.45 ± 0.58)E-7
67907.8	8.0	4.89	437		
950715.19	66.4	2.42	160	9.22 ± 2.29	0.37 ± 0.05
9913	-59.8	4.03	318	24.58 ± 8.26	(4.95 ± 0.79)E-7
17039.5	6.0	4.08	440		
950717.11	225.5	2.82	141	10.24 ± 1.45	0.42 ± 0.04
9915	1.1	3.69	306	39.94 ± 8.26	(6.89 ± 1.37)E-7
9861.3	5.3	5.09	446		
950717.81	140.2	2.96	151	5.12 ± 1.45	0.45 ± 0.04
9915	4.1	3.91	307	31.74 ± 6.23	(4.81 ± 0.35)E-7
70596.8	24.7	3.96	395		
950719.37	204.9	1.87	139	29.70 ± 1.45	0.23 ± 0.04
9917	31.8	1.63	331	48.13 ± 9.71	(2.63 ± 0.03)E-7
32426.2	14.7	1.60	491		
950721.58	63.2	3.17	158	47.10 ± 2.29	0.51 ± 0.05
9919	25.2	4.17	302	(1.55 ± 0.08)E+2	(2.49 ± 0.09)E-6
50454.7	6.7	4.64	419		
950722.74	73.6	10.95	191	26.62 ± 1.45	1.56 ± 0.05
9920	28.8	14.17	385	55.30 ± 4.22	(3.50 ± 0.16)E-6
64126.1	1.7	14.71	559		
950727.39	297.8	1.22	203	34.82 ± 3.69	0.26 ± 0.06
9925	-3.3	1.94	398	77.82 ± 4.58	(1.21 ± 0.02)E-6
33818.8	3.2	2.56	555		
950728.50	337.8	1.89	164	...	0.50 ± 0.07
9926	-74.2	1.23	328	2.05 ± 1.02	(1.55 ± 0.04)E-7
43502.8	11.1	1.06	497		
950728.52	280.0	4.78	205	6.14 ± 1.45	0.79 ± 0.05
9926	22.1	7.88	386	12.29 ± 1.45	(1.10 ± 0.06)E-6
45741.2	2.9	8.32	541		
950729.27	324.5	1.49	161	21.50 ± 1.45	0.21 ± 0.04
9927	-50.5	2.56	321	56.32 ± 2.90	(8.61 ± 0.87)E-7
23974.1	5.5	3.51	475		
950730.88	217.5	19.43	200	4.10 ± 1.45	3.51 ± 0.08
9928	-15.6	24.68	392	23.55 ± 3.24	(2.74 ± 0.52)E-6
76123.3	0.7	21.91	555		
950804.55	35.9	3.39	161	39.94 ± 2.29	0.55 ± 0.05
9933	40.8	5.35	356	(1.16 ± 0.08)E+2	(1.96 ± 0.06)E-6
48259.2	2.5	7.12	503		

Table A-2—Continued

Name (NTB) Date (TJD) Time (s UT)	R.A. (°) Decl. (°) Err. (°)	C_{max}/C_{min} (4.096 s) (8.192 s)	C_{min} (4.096 s) (8.192 s)	T_{50} (s) T_{90} (s)	P (ph cm^{-2} s^{-1}) F (erg cm^{-2}) (50–300 keV)
950805.90	12.0	1.82	196	12.29 ± 1.45	0.31 ± 0.05
9934	25.0	3.12	346	29.70 ± 2.29	(8.12 ± 0.83)E-7
78107.8	5.0	4.00	493		
950815.23	275.0	1.23	154	27.65 ± 3.24	0.11 ± 0.04
9944	-39.7	1.99	347	64.51 ± 19.48	(5.55 ± 0.32)E-7
20217.0	5.6	2.45	408		
950816.74	188.4	1.77	147	20.48 ± 2.29	0.25 ± 0.04
9945	33.1	2.10	371	37.89 ± 23.57	(2.18 ± 0.03)E-7
64397.5	6.9	1.89	485		
950826.14	240.9	...	...	23.55 ± 3.24	(8.01 ± 3.88)E-2
9955	86.1	1.18	329	72.70 ± 8.69	(3.77 ± 0.08)E-7
12116.1	13.0	1.39	424		
950827.05	126.9	1.92	120	3.07 ± 1.45	0.34 ± 0.05
9956	4.4	2.59	279	17.41 ± 5.22	(2.87 ± 0.50)E-7
4918.4	17.7	2.23	360		
950904.28	189.0	1.04	162	...	0.13 ± 0.04
9964	-27.2	1.45	343	5.12 ± 2.05	0.00 ± 0.00
24880.3	21.6	1.15	419		
950904.61	194.8	14.87	179	10.24 ± 1.45	2.64 ± 0.07
9964	36.6	27.67	360	24.58 ± 1.45	(4.30 ± 0.68)E-6
52772.0	1.5	33.44	502		
950905.62	93.4	2.82	200	3.07 ± 1.45	0.45 ± 0.05
9965	47.4	4.08	405	13.31 ± 1.45	(4.54 ± 0.49)E-7
54380.7	12.3	4.62	585		
950912.39	334.2	1.55	191	17.41 ± 7.24	0.24 ± 0.04
9972	-30.3	2.56	329	43.01 ± 14.91	(4.47 ± 0.36)E-7
34112.7	8.0	3.00	469		
950920.22	174.9	1.75	164	15.36 ± 2.29	0.26 ± 0.04
9980	37.1	3.28	356	40.96 ± 3.24	(6.04 ± 0.49)E-7
19754.2	50.4	4.04	508		
950930.77	191.3	1.16	146	9.22 ± 1.45	0.16 ± 0.04
9990	-41.1	2.07	299	20.48 ± 2.29	(4.37 ± 0.35)E-7
67283.1	10.8	2.75	406		
951001.41	147.5	1.96	180	14.34 ± 1.45	0.62 ± 0.09
9991	26.2	2.29	369	46.08 ± 2.29	(1.14 ± 0.07)E-6
36051.1	4.2	3.21	492		
951001.48	131.1	14.16	197	29.70 ± 1.45	1.90 ± 0.05
9991	7.3	18.23	396	45.06 ± 1.45	(3.62 ± 0.16)E-6
41867.4	3.3	21.81	561		
951005.17	234.0	11.69	170	3.07 ± 1.45	1.79 ± 0.06
9995	-79.7	14.62	340	28.67 ± 4.22	(1.35 ± 0.25)E-6
14840.0	1.4	12.49	472		
951009.21	254.6	3.90	128	3.07 ± 1.45	0.62 ± 0.05
9999	-37.4	4.17	272	10.24 ± 2.29	(2.91 ± 0.57)E-7
18421.9	9.2	3.16	396		
951010.09	166.7	4.07	147	...	0.69 ± 0.05
10000	-16.1	2.09	285	1.02 ± 1.44	(1.44 ± 0.06)E-7
7822.5	9.3	1.46	391		
951010.10	1.9	1.04	193	16.38 ± 5.97	0.27 ± 0.07
10000	-14.4	1.08	259	28.67 ± 4.22	(3.85 ± 0.05)E-7
9465.0	51.9	1.52	494		
951010.85	171.5	1.43	184	...	0.47 ± 0.09
10000	-8.4	...	...	1.02 ± 1.02	(1.07 ± 0.05)E-7
73753.8	34.2	...	...		
951013.66	294.9	7.72	178	...	1.19 ± 0.05
10003	-10.0	3.98	355	1.02 ± 1.44	(2.47 ± 0.09)E-7
57090.2	3.5	2.97	487		
951014.23	184.2	...	...	...	0.12 ± 0.05
10004	8.1	1.06	321	17.41 ± 5.12	(1.51 ± 0.09)E-7
20565.2	15.2	1.20	502		

Table A-2—Continued

Name (NTB) Date (TJD) Time (s UT)	R.A. (°) Decl. (°) Err. (°)	C_{max}/C_{min} (4.096 s) (8.192 s)	C_{min} (4.096 s) (8.192 s)	T_{50} (s) T_{90} (s)	P (ph cm^{-2} s^{-1}) F (erg cm^{-2}) (50–300 keV)
951017.78	199.8	1.27	131	...	0.17 ± 0.04
10007	-40.2	1.01	267	2.05 ± 1.44	(5.02 ± 0.80)E-8
68224.2	27.5	...	...		
951018.52	210.8	...	...	16.38 ± 2.29	0.12 ± 0.04
10008	-32.5	1.13	223	51.20 ± 5.97	(5.06 ± 0.32)E-7
45401.3	8.5	1.90	315		
951018.88	41.8	...	...	15.36 ± 3.24	0.12 ± 0.04
10008	37.6	1.00	221	36.86 ± 3.24	(3.85 ± 0.05)E-7
76129.5	9.4	1.65	340		
951020.96	115.5	2.21	171	33.79 ± 1.45	0.34 ± 0.04
10010	61.9	2.31	317	74.75 ± 16.42	(1.11 ± 0.01)E-6
83576.0	4.2	2.67	468		
951022.99	344.1	1.14	158	13.31 ± 1.45	0.21 ± 0.05
10012	-28.7	1.35	276	31.74 ± 6.23	(2.82 ± 0.15)E-7
85644.5	11.3	1.53	466		
951025.69	200.1	1.14	180	24.58 ± 3.24	0.16 ± 0.04
10015	-71.6	2.10	369	46.08 ± 5.12	(4.84 ± 0.59)E-7
60332.2	11.6	2.64	496		
951111.95	308.7	1.67	159	7.17 ± 1.45	0.23 ± 0.04
10032	33.7	2.64	357	14.34 ± 1.45	(2.21 ± 0.39)E-7
82877.6	11.1	2.64	505		
951112.78	227.0	7.61	186	16.38 ± 1.45	1.25 ± 0.06
10033	18.4	13.74	365	40.96 ± 5.22	(3.15 ± 0.39)E-6
67850.4	1.1	16.37	522		
951114.95	300.0	1.02	189	3.07 ± 1.45	0.20 ± 0.06
10035	-42.2	1.61	392	7.17 ± 1.45	(1.44 ± 0.43)E-7
82524.3	9.0	1.46	569		
951117.40	93.9	1.39	175	7.17 ± 1.45	0.18 ± 0.04
10038	41.2	2.33	383	16.38 ± 3.24	(4.42 ± 0.55)E-7
34716.9	8.3	3.16	479		
951118.56	126.3	...	...	14.34 ± 4.22	0.15 ± 0.07
10039	20.9	1.42	356	39.94 ± 5.22	(8.19 ± 0.08)E-7
48451.8	9.4	1.84	449		
951120.40	199.5	4.79	182	6.14 ± 1.45	0.75 ± 0.05
10041	14.0	8.71	368	32.77 ± 9.27	(1.49 ± 0.14)E-6
34928.8	2.0	10.66	518		
951124.29	158.4	4.89	190	(2.38 ± 0.01)E+2	0.78 ± 0.05
10045	46.4	9.06	370	(2.81 ± 0.02)E+2	(7.18 ± 0.32)E-6
25127.1	0.9	11.76	519		
951126.45	65.5	...	...	17.41 ± 2.90	0.13 ± 0.04
10047	58.9	1.49	243	49.15 ± 6.48	(4.56 ± 0.44)E-7
39624.9	15.2	2.11	378		
951127.64	235.0	...	...	6.14 ± 2.29	0.13 ± 0.04
10048	-14.7	1.52	273	13.31 ± 2.90	(1.86 ± 0.08)E-7
55899.3	21.7	1.88	408		
951129.34	187.7	1.44	153	17.41 ± 3.24	0.23 ± 0.04
10050	31.9	2.25	297	61.44 ± 10.54	(5.66 ± 0.74)E-7
29619.4	7.4	2.85	425		
951203.05	275.6	1.05	127	35.84 ± 2.29	0.15 ± 0.05
10054	-13.8	1.80	296	95.23 ± 12.46	(1.04 ± 0.06)E-6
4447.4	6.7	2.48	409		
951207.34	76.3	1.06	137	31.74 ± 1.45	0.15 ± 0.05
10058	-6.4	1.77	341	82.94 ± 15.22	(7.24 ± 0.40)E-7
29846.7	5.0	2.15	493		
951209.36	40.6	1.14	201	5.12 ± 1.45	0.19 ± 0.05
10060	-35.7	1.96	414	15.36 ± 3.24	(2.97 ± 0.53)E-7
31313.1	4.0	2.36	586		
951211.00	226.5	1.73	119	39.94 ± 1.45	0.28 ± 0.04
10062	-20.9	2.45	252	97.28 ± 17.44	(1.46 ± 0.13)E-6
421.0	3.5	2.94	434		

Table A-2—Continued

Name (NTB) Date (TJD) Time (s UT)	R.A. (°) Decl. (°) Err. (°)	C_{max}/C_{min} (4.096 s) (8.192 s)	C_{min} (4.096 s) (8.192 s)	T_{50} (s) T_{90} (s)	P (ph cm^{-2} s^{-1}) F (erg cm^{-2}) (50–300 keV)
951211.98	36.6	1.18	148	5.12 ± 2.29	0.36 ± 0.08
10062	-41.6	1.29	373	20.48 ± 8.26	(3.62 ± 0.07)E-7
85269.7	12.8	1.23	528		
951212.80	238.3	2.24	166	5.12 ± 1.45	0.37 ± 0.05
10063	-45.3	3.87	387	17.41 ± 2.29	(4.59 ± 0.59)E-7
69640.4	4.0	3.98	535		
951213.02	225.3	1.14	146	...	0.17 ± 0.04
10064	-19.9	...	...	1.02 ± 1.02	(4.91 ± 0.17)E-8
2066.6	24.0	...	...		
951213.37	325.4	7.33	174	2.05 ± 1.45	1.27 ± 0.05
10064	38.3	6.23	350	10.24 ± 3.24	(4.11 ± 1.28)E-7
32670.9	6.5	4.99	478		
951213.37	96.2	2.18	142	14.34 ± 1.45	0.51 ± 0.06
10064	13.1	2.66	303	50.18 ± 2.29	(1.16 ± 0.01)E-6
32736.4	14.5	3.61	443		
951214.51	355.9	2.38	144	8.19 ± 1.45	0.81 ± 0.09
10065	64.1	3.03	288	11.26 ± 2.29	(9.11 ± 0.24)E-7
44116.1	5.3	2.61	377		
951215.84	104.5	5.20	112	41.98 ± 2.29	0.83 ± 0.05
10066	86.7	7.91	225	(1.27 ± 0.03)E+2	(3.48 ± 0.10)E-6
73420.0	1.3	8.41	319		
951216.02	67.5	2.71	144	33.79 ± 2.29	0.45 ± 0.05
10067	24.1	4.79	326	95.23 ± 13.35	(1.81 ± 0.11)E-6
2552.0	2.3	6.11	436		
951217.16	292.1	1.63	140	22.53 ± 1.45	0.30 ± 0.05
10068	-63.7	2.98	277	40.96 ± 6.23	(5.66 ± 1.20)E-7
13972.7	5.6	3.44	367		
951217.80	330.5	1.36	182	9.22 ± 2.29	0.20 ± 0.04
10068	5.2	2.46	400	18.43 ± 3.24	(4.24 ± 0.30)E-7
69568.7	7.2	3.03	566		
951218.33	20.0	6.71	180	59.39 ± 1.45	1.17 ± 0.06
10069	-22.3	11.77	374	(1.18 ± 0.02)E+2	(8.74 ± 0.28)E-6
28741.8	0.5	14.31	528		
951218.77	189.6	4.24	192	2.05 ± 1.45	0.82 ± 0.06
10069	17.6	5.76	396	5.12 ± 1.45	(5.15 ± 1.79)E-7
66592.9	1.6	5.44	572		
951219.71	12.7	10.53	166	2.05 ± 1.45	1.65 ± 0.06
10070	7.2	12.53	341	7.17 ± 2.29	(1.10 ± 0.08)E-6
61414.6	6.5	11.35	476		
951224.31	236.5	1.34	181	21.50 ± 2.29	0.16 ± 0.04
10075	21.7	2.21	358	47.10 ± 3.24	(5.64 ± 0.08)E-7
27637.9	10.9	2.56	451		
951224.57	170.9	2.37	204	29.70 ± 1.45	0.32 ± 0.04
10075	-13.2	4.10	398	54.27 ± 3.24	(8.95 ± 0.65)E-7
49352.9	12.6	4.61	553		
951226.23	25.8	2.05	134	...	0.58 ± 0.08
10077	-40.6	1.26	320	1.02 ± 1.02	(1.18 ± 0.05)E-7
19945.7	50.0	...	...		
951227.83	326.5	1.19	153	11.26 ± 1.45	0.16 ± 0.05
10078	13.5	1.83	300	21.50 ± 2.90	(4.04 ± 0.45)E-7
72256.7	8.8	2.27	426		
951231.35	85.9	4.70	161	...	2.33 ± 0.15
10082	-44.4	2.55	358	1.02 ± 1.02	(4.72 ± 0.36)E-7
30686.4	19.3	1.91	449		
951231.89	169.8	1.62	137	12.29 ± 1.45	0.24 ± 0.04
10082	66.7	2.39	303	26.62 ± 7.38	(5.02 ± 0.46)E-7
77069.5	10.7	2.95	461		
960101.46	131.5	2.52	184	48.13 ± 3.69	0.74 ± 0.08
10083	26.6	2.96	374	86.02 ± 13.35	(2.35 ± 0.02)E-6
39783.6	5.5	3.25	570		

Table A-2—Continued

Name (NTB) Date (TJD) Time (s UT)	R.A. (°) Decl. (°) Err. (°)	C_{max}/C_{min} (4.096 s) (8.192 s)	C_{min} (4.096 s) (8.192 s)	T_{50} (s) T_{90} (s)	P (ph cm^{-2} s^{-1}) F (erg cm^{-2}) (50–300 keV)
960102.83	119.3	1.70	154	...	0.27 ± 0.04
10084	58.5	2.50	349	6.14 ± 2.05	(1.67 ± 0.39)E-7
72536.3	9.6	1.92	517		
960104.02	303.0	4.66	123	...	1.40 ± 0.09
10086	-36.8	2.64	258	1.02 ± 1.44	(3.40 ± 0.18)E-7
2418.9	4.8	1.54	339		
960105.78	312.2	3.77	178	4.10 ± 1.45	0.56 ± 0.05
10087	-22.0	5.20	322	14.34 ± 1.45	(4.67 ± 0.55)E-7
67820.7	18.4	4.45	446		
960107.51	211.2	9.18	196	44.03 ± 1.45	1.44 ± 0.06
10089	-35.2	7.30	376	80.90 ± 3.24	(1.88 ± 0.18)E-6
44246.2	1.9	6.69	528		
960107.79	208.9	9.04	155	18.43 ± 1.45	2.98 ± 0.11
10089	61.7	15.70	307	31.74 ± 1.45	(7.87 ± 0.16)E-6
68601.0	1.2	20.08	439		
960108.45	97.1	1.95	152	13.31 ± 1.45	0.32 ± 0.05
10090	-37.0	2.03	294	49.15 ± 4.58	(5.48 ± 0.34)E-7
39057.6	6.5	1.84	403		
960109.56	140.4	4.28	159	29.70 ± 2.29	0.67 ± 0.05
10091	18.4	5.98	339	(1.76 ± 0.07)E+2	(2.78 ± 0.11)E-6
48817.4	3.1	7.34	460		
960110.67	255.8	2.63	171	...	0.75 ± 0.08
10092	-30.3	2.69	370	4.10 ± 2.05	(3.33 ± 0.10)E-7
58110.2	20.4	2.04	546		
960113.24	175.1	...	...	31.74 ± 4.22	0.14 ± 0.04
10095	22.5	1.46	304	(1.10 ± 0.33)E+2	(8.88 ± 0.09)E-7
21200.1	25.2	1.81	421		
960113.63	104.9	2.52	186	10.24 ± 6.48	0.43 ± 0.05
10095	16.1	2.96	372	24.58 ± 2.90	(3.94 ± 0.53)E-7
54947.0	23.2	2.39	516		
960113.65	142.9	1.10	156	23.55 ± 2.29	0.16 ± 0.04
10095	7.3	1.90	358	53.25 ± 7.24	(4.81 ± 0.12)E-7
56915.1	9.7	2.26	459		
960114.46	56.9	1.19	146	...	0.20 ± 0.04
10096	51.0	1.89	316	4.10 ± 2.05	(1.32 ± 0.36)E-7
40130.8	9.6	1.52	423		
960115.36	130.9	11.54	153	10.24 ± 1.45	1.49 ± 0.05
10097	-43.3	16.50	299	43.01 ± 3.24	(1.82 ± 0.50)E-6
31956.2	2.1	19.18	424		
960116.85	295.7	4.14	189	5.12 ± 1.45	0.67 ± 0.05
10098	-28.9	5.10	380	34.82 ± 11.31	(5.66 ± 1.05)E-7
73580.7	3.7	4.57	554		
960117.25	342.2	2.28	141	...	0.38 ± 0.05
10099	85.7	1.74	303	3.07 ± 1.44	(1.09 ± 0.38)E-7
21966.0	28.7	1.25	440		
960119.38	278.8	3.63	188	4.10 ± 1.45	0.50 ± 0.04
10101	3.7	6.56	391	14.34 ± 3.24	(6.74 ± 0.53)E-7
32988.4	4.8	7.32	568		
960119.41	276.1	2.52	193	14.34 ± 1.45	0.39 ± 0.05
10101	-59.8	4.87	405	40.96 ± 4.22	(1.35 ± 0.14)E-6
35980.5	4.0	6.21	556		
960120.46	1.9	2.88	142	(1.00 ± 0.02)E+2	0.43 ± 0.04
10102	52.1	5.49	278	(1.50 ± 0.04)E+2	(1.38 ± 0.22)E-6
40196.3	2.8	6.67	394		
960120.90	118.1	1.89	152	8.19 ± 1.45	0.34 ± 0.05
10102	17.4	2.17	282	28.67 ± 11.31	(2.47 ± 0.98)E-7
78481.6	5.8	1.93	424		
960123.50	296.1	8.34	178	5.12 ± 1.45	3.51 ± 0.16
10105	-34.7	13.62	340	10.24 ± 1.45	(7.69 ± 0.37)E-6
43638.0	1.1	18.07	477		

Table A-2—Continued

Name (NTB) Date (TJD) Time (s UT)	R.A. (°) Decl. (°) Err. (°)	C_{max}/C_{min} (4.096 s) (8.192 s)	C_{min} (4.096 s) (8.192 s)	T_{50} (s) T_{90} (s)	P (ph cm^{-2} s^{-1}) F (erg cm^{-2}) (50–300 keV)
960124.28	253.9	1.09	109	25.60 ± 1.45	0.19 ± 0.04
10106	2.5	2.01	269	56.32 ± 4.22	(8.57 ± 5.11)E-7
24873.2	2.3	2.70	372		
960125.39	289.3	...	...	...	0.11 ± 0.05
10107	-29.5	1.31	371	6.14 ± 4.10	(1.21 ± 0.09)E-7
34172.1	9.4	1.26	568		
960129.64	159.4	4.78	153	33.79 ± 1.45	0.81 ± 0.05
10111	-57.4	8.01	310	53.25 ± 1.45	(1.01 ± 0.22)E-6
55428.3	49.9	7.66	444		
960201.95	153.9	4.28	145	2.05 ± 1.45	1.70 ± 0.12
10114	-15.7	6.38	307	5.12 ± 2.29	(1.21 ± 0.05)E-6
82190.5	6.9	4.84	439		
960201.96	182.8	1.09	179	...	0.17 ± 0.04
10114	-52.9	1.76	328	7.17 ± 2.05	(1.40 ± 0.34)E-7
82944.2	23.1	1.69	418		
960202.06	109.3	9.31	174	30.72 ± 1.45	1.73 ± 0.07
10115	52.2	16.70	340	(1.23 ± 0.03)E+2	(9.05 ± 0.26)E-6
5971.1	0.6	21.14	477		
960202.52	104.4	2.38	163	6.14 ± 2.29	0.37 ± 0.05
10115	64.7	3.95	299	22.53 ± 11.31	(6.28 ± 0.54)E-7
45489.4	3.2	4.28	421		
960202.90	166.2	1.18	193	(1.41 ± 1.01)E+2	0.18 ± 0.04
10115	26.3	1.74	343	(2.14 ± 0.44)E+2	(1.95 ± 0.11)E-6
78107.9	7.3	2.28	549		
960203.00	251.3	5.08	132	2.05 ± 1.45	0.82 ± 0.05
10116	-15.4	3.76	246	13.31 ± 12.95	(2.95 ± 0.50)E-7
835.8	2.7	2.68	348		
960204.40	172.2	1.45	186	8.19 ± 1.45	0.23 ± 0.04
10117	12.0	2.14	388	17.41 ± 6.23	(3.30 ± 0.53)E-7
34596.0	12.2	2.53	520		
960205.96	235.9	1.59	174	7.17 ± 1.45	0.27 ± 0.05
10118	-13.3	2.82	347	19.46 ± 20.51	(3.56 ± 0.36)E-7
83718.3	6.7	3.07	461		
960207.75	12.4	21.38	156	27.65 ± 1.45	3.37 ± 0.07
10120	34.9	25.10	311	44.03 ± 2.29	(7.17 ± 0.23)E-6
65026.2	0.8	26.31	450		
960207.94	128.1	...	...	23.55 ± 2.29	0.14 ± 0.04
10120	-27.1	1.56	385	49.15 ± 5.12	(6.30 ± 0.48)E-7
81797.3	13.2	2.05	530		
960210.41	145.3	1.54	155	25.60 ± 2.29	0.27 ± 0.05
10123	1.1	2.77	321	63.49 ± 8.81	(1.02 ± 0.06)E-6
35867.8	4.9	3.68	419		
960211.79	254.8	1.52	170	4.10 ± 1.45	0.16 ± 0.05
10124	58.5	2.51	266	7.17 ± 3.24	(1.58 ± 0.06)E-7
68501.7	19.6	2.29	383		
960215.20	169.1	1.91	180	70.66 ± 1.45	0.28 ± 0.05
10128	16.3	3.15	345	(1.27 ± 0.05)E+2	(1.01 ± 0.05)E-6
17438.9	4.2	3.40	471		
960215.68	292.0	1.78	167	21.50 ± 2.29	0.29 ± 0.05
10128	-20.4	3.13	366	58.37 ± 7.24	(9.69 ± 1.32)E-7
58872.0	11.1	3.98	548		
960217.39	47.6	1.19	126	28.67 ± 3.24	0.23 ± 0.05
10130	-17.4	2.54	261	90.11 ± 8.44	(8.89 ± 0.99)E-7
33786.1	3.4	3.32	364		
960225.78	206.7	1.16	172	4.10 ± 1.45	0.16 ± 0.04
10138	-57.1	1.94	381	9.22 ± 4.22	(1.32 ± 0.06)E-7
67588.3	19.8	1.99	501		
960301.07	121.7	5.31	191	2.05 ± 1.45	0.79 ± 0.05
10143	-25.6	4.50	389	7.17 ± 2.90	(3.13 ± 0.33)E-7
6087.9	12.3	3.82	559		

Table A-2—Continued

Name (NTB) Date (TJD) Time (s UT)	R.A. (°) Decl. (°) Err. (°)	C_{max}/C_{min} (4.096 s) (8.192 s)	C_{min} (4.096 s) (8.192 s)	T_{50} (s) T_{90} (s)	P (ph cm^{-2} s^{-1}) F (erg cm^{-2}) (50–300 keV)
960302.86	194.7	2.03	191	27.65 ± 5.12	0.25 ± 0.04
10144	-59.3	2.97	379	93.18 ± 16.42	(1.42 ± 0.09)E-6
74733.8	5.0	3.65	528		
960303.31	194.4	...	...	9.22 ± 1.45	0.27 ± 0.08
10145	16.3	1.24	333	14.34 ± 3.24	(4.25 ± 0.08)E-7
27634.9	31.1	1.35	516		
960304.56	72.3	4.12	165	17.41 ± 1.45	0.75 ± 0.06
10146	25.5	7.16	357	31.74 ± 2.29	(1.64 ± 0.14)E-6
48771.3	1.5	8.83	485		
960305.41	346.6	...	...	8.19 ± 4.22	0.11 ± 0.04
10147	57.8	1.01	285	20.48 ± 8.44	(2.09 ± 0.08)E-7
35732.7	9.3	1.42	480		
960305.85	74.5	1.25	153	16.38 ± 1.45	0.16 ± 0.04
10147	-47.9	2.10	287	38.91 ± 11.31	(6.01 ± 0.50)E-7
74083.5	4.3	2.52	451		
960307.37	183.8	1.47	155	27.65 ± 2.29	0.12 ± 0.04
10149	-7.5	2.32	371	99.33 ± 2.29	(7.93 ± 1.26)E-7
32754.9	4.7	2.59	522		
960309.06	264.5	1.09	191	13.31 ± 3.24	0.20 ± 0.05
10151	-13.0	1.61	336	38.91 ± 16.03	(4.63 ± 0.43)E-7
5745.9	7.4	2.06	489		
960315.14	166.6	1.21	124	25.60 ± 5.22	0.21 ± 0.05
10157	-2.8	2.08	309	56.32 ± 10.44	(6.13 ± 0.34)E-7
12852.4	7.3	2.65	441		
960315.59	215.2	...	...	11.26 ± 1.45	0.12 ± 0.04
10157	-54.6	1.44	360	38.91 ± 4.22	(2.02 ± 0.02)E-7
51315.9	21.0	1.44	534		
960315.87	1.7	...	...	...	0.10 ± 0.05
10157	40.0	1.42	315	20.48 ± 10.24	(2.53 ± 0.13)E-7
75433.2	9.2	1.56	494		
960318.95	114.0	2.99	131	10.24 ± 1.45	0.46 ± 0.05
10160	-1.2	5.53	282	46.08 ± 9.66	(1.29 ± 0.14)E-6
82772.2	4.0	7.40	389		
960320.74	226.6	1.52	197	5.12 ± 2.29	0.23 ± 0.04
10162	17.7	1.66	344	15.36 ± 2.29	(2.16 ± 0.32)E-7
64069.8	18.5	1.84	457		
960321.22	14.5	8.17	189	22.53 ± 1.45	1.58 ± 0.06
10163	49.2	7.51	368	27.65 ± 1.45	(2.02 ± 0.07)E-6
19657.9	1.5	6.97	517		
960322.67	195.6	1.20	155	13.31 ± 1.45	0.19 ± 0.04
10164	-24.7	1.96	382	35.84 ± 3.69	(5.29 ± 0.49)E-7
58540.2	29.5	2.51	585		
960326.88	219.4	1.12	147	4.10 ± 1.45	0.18 ± 0.05
10168	-66.3	1.96	272	9.22 ± 1.45	(2.43 ± 0.50)E-7
76550.3	9.5	2.22	415		
960328.00	90.9	1.32	176	16.38 ± 4.22	0.21 ± 0.04
10170	11.2	1.85	324	49.15 ± 4.22	(5.74 ± 0.05)E-7
809.2	19.9	2.18	520		
960329.23	106.3	2.49	120	1.02 ± 1.45	0.45 ± 0.05
10171	-1.3	2.37	240	2.05 ± 1.45	(1.80 ± 0.28)E-7
20643.0	9.3	1.66	325		
960331.24	117.4	1.01	126	8.19 ± 1.45	0.17 ± 0.04
10173	-26.5	1.70	307	33.79 ± 1.45	(3.15 ± 0.43)E-7
21581.0	9.5	2.14	450		
960402.44	146.6	2.01	206	17.41 ± 2.29	0.38 ± 0.05
10175	6.3	3.32	336	46.08 ± 4.58	(1.50 ± 0.12)E-6
38708.4	4.0	4.51	485		
960403.08	267.4	1.14	165	...	0.26 ± 0.06
10176	14.4	...	...	2.05 ± 1.02	(1.06 ± 0.03)E-7
6958.3	51.3	...	...		

Table A-2—Continued

Name (NTB) Date (TJD) Time (s UT)	R.A. (°) Decl. (°) Err. (°)	C_{max}/C_{min} (4.096 s) (8.192 s)	C_{min} (4.096 s) (8.192 s)	T_{50} (s) T_{90} (s)	P (ph cm^{-2} s^{-1}) F (erg cm^{-2}) (50–300 keV)
960404.30	235.9	1.19	145	10.24 ± 1.45	0.21 ± 0.05
10177	77.2	1.58	345	44.03 ± 2.29	(3.53 ± 0.05)E-7
26344.7	9.4	1.95	506		
960408.12	269.5	...	...	14.34 ± 2.29	0.18 ± 0.05
10181	57.2	1.60	337	61.44 ± 31.76	(5.92 ± 0.05)E-7
11197.6	10.3	1.84	417		
960410.51	45.2	1.22	189	19.46 ± 1.45	0.17 ± 0.04
10183	-52.0	2.10	299	55.30 ± 8.26	(6.96 ± 0.96)E-7
44768.5	9.5	2.69	359		
960415.46	75.2	1.81	140	10.24 ± 1.45	0.26 ± 0.05
10188	12.3	2.89	292	24.58 ± 7.24	(6.05 ± 0.42)E-7
40532.2	4.4	3.16	440		
960415.84	100.9	1.74	166	6.14 ± 1.45	0.26 ± 0.04
10188	32.8	3.04	317	20.48 ± 3.24	(3.62 ± 1.94)E-7
72648.9	6.2	3.59	460		
960418.09	303.0	9.28	183	17.41 ± 1.45	1.51 ± 0.06
10191	37.8	14.55	362	29.70 ± 2.29	(2.05 ± 0.28)E-6
8264.9	1.7	15.67	519		
960421.20	284.7	1.19	125	25.60 ± 3.69	0.13 ± 0.04
10194	51.0	2.10	290	67.58 ± 8.26	(7.75 ± 0.48)E-7
17705.2	6.8	2.61	380		
960422.57	287.3	...	...	...	0.19 ± 0.05
10195	-63.7	...	...	12.29 ± 4.10	(1.23 ± 0.41)E-7
50019.5	9.5	1.14	585		
960422.69	137.5	2.15	144	7.17 ± 1.45	0.28 ± 0.04
10195	23.9	3.58	303	19.46 ± 3.24	(4.08 ± 0.56)E-7
60089.5	7.8	3.78	400		
960426.50	316.5	2.14	121	4.10 ± 2.29	0.35 ± 0.05
10199	17.1	2.77	251	10.24 ± 4.22	(2.29 ± 0.39)E-7
43829.4	10.0	2.29	336		
960427.77	199.0	1.26	191	...	0.23 ± 0.05
10200	-18.0	1.08	316	8.19 ± 4.10	(1.16 ± 0.05)E-7
67287.2	25.9	1.14	539		
960429.88	60.5	4.11	181	8.19 ± 2.90	0.61 ± 0.06
10202	34.5	6.35	332	14.34 ± 2.29	(9.10 ± 1.30)E-7
76804.3	2.8	7.80	486		
960504.21	306.6	6.48	221	68.61 ± 1.45	1.17 ± 0.06
10207	-48.1	10.09	370	99.33 ± 3.69	(3.51 ± 0.34)E-6
18775.2	1.9	10.08	528		
960510.59	234.3	1.20	192	7.17 ± 1.45	0.19 ± 0.04
10213	-14.1	1.77	347	26.62 ± 2.29	(2.07 ± 0.57)E-7
51379.4	11.6	1.82	479		
960516.73	80.6	1.13	137	4.10 ± 1.45	0.17 ± 0.04
10219	5.1	1.97	306	9.22 ± 2.29	(1.78 ± 0.29)E-7
63190.2	9.1	2.05	443		
960518.50	332.9	1.57	131	...	0.52 ± 0.09
10221	5.4	1.01	285	3.07 ± 1.02	(1.42 ± 0.05)E-7
43659.5	27.7	1.05	436		
960526.73	90.4	1.60	159	11.26 ± 5.12	0.23 ± 0.04
10229	13.1	1.59	273	33.79 ± 13.93	(2.30 ± 0.09)E-7
63671.5	20.4	1.35	424		
960528.38	143.9	1.10	193	...	0.47 ± 0.13
10231	15.0	...	...	2.05 ± 1.02	(1.83 ± 0.08)E-7
33458.4	35.0	...	...		
960531.08	16.6	...	...	15.36 ± 1.45	(9.28 ± 3.48)E-2
10234	-27.9	1.19	337	34.82 ± 4.22	(2.95 ± 0.12)E-7
7276.7	22.9	1.55	502		
960531.08	155.7	1.07	113	4.10 ± 1.45	0.18 ± 0.04
10234	16.4	1.80	374	8.19 ± 1.45	(2.05 ± 0.47)E-7
7538.9	12.2	1.95	494		

Table A-2—Continued

Name (NTB) Date (TJD) Time (s UT)	R.A. (°) Decl. (°) Err. (°)	C_{max}/C_{min} (4.096 s) (8.192 s)	C_{min} (4.096 s) (8.192 s)	T_{50} (s) T_{90} (s)	P (ph cm^{-2} s^{-1}) F (erg cm^{-2}) (50–300 keV)
960602.02	343.9	1.33	127	11.26 ± 2.29	0.20 ± 0.04
10236	-49.1	2.01	258	25.60 ± 3.69	(3.43 ± 0.30)E-7
2121.9	9.5	2.15	361		
960602.10	208.4	1.94	158	...	0.40 ± 0.05
10236	11.9	1.20	328	2.05 ± 1.02	(1.23 ± 0.03)E-7
9389.3	18.5	...	...		
960602.49	64.9	8.44	172	...	1.28 ± 0.05
10236	-16.2	4.38	348	1.02 ± 1.44	(2.82 ± 0.10)E-7
42664.1	4.2	2.93	454		
960603.70	124.1	2.46	121	15.36 ± 1.45	0.40 ± 0.05
10237	-30.4	4.22	238	38.91 ± 1.45	(1.13 ± 0.12)E-6
60925.1	2.1	4.90	330		
960604.04	161.4	1.08	136	9.22 ± 1.45	0.20 ± 0.05
10238	26.5	1.51	248	28.67 ± 6.56	(5.17 ± 0.48)E-7
3988.7	31.6	2.00	351		
960604.66	318.6	4.40	177	16.38 ± 1.45	0.65 ± 0.04
10238	-20.4	5.75	371	53.25 ± 19.48	(8.69 ± 0.58)E-7
57659.6	7.0	6.10	525		
960609.76	110.6	1.14	163	...	0.58 ± 0.14
10243	36.9	1.23	309	2.05 ± 1.02	(2.82 ± 0.21)E-7
65897.7	19.9	...	...		
960609.87	328.7	1.15	144	4.10 ± 1.45	0.30 ± 0.05
10243	-46.7	2.43	288	8.19 ± 2.29	(3.09 ± 0.41)E-7
75746.5	4.9	2.13	386		
960611.11	174.0	1.13	183	34.82 ± 2.29	0.15 ± 0.04
10245	74.9	1.79	291	92.16 ± 9.27	(8.86 ± 0.11)E-7
10237.1	8.2	2.41	446		
960611.65	242.7	1.93	128	35.84 ± 1.45	0.29 ± 0.04
10245	55.1	2.76	242	41.98 ± 1.45	(5.39 ± 0.78)E-7
56503.5	12.5	3.11	354		
960614.96	103.1	1.47	146	33.79 ± 1.45	0.25 ± 0.05
10248	-32.0	2.63	390	83.97 ± 3.24	(1.26 ± 0.11)E-6
83620.0	2.8	3.46	560		
960618.92	123.5	1.21	197	22.53 ± 1.45	0.18 ± 0.04
10252	52.9	2.26	372	59.39 ± 14.37	(6.16 ± 0.65)E-7
79862.0	9.2	2.91	512		
960619.52	197.0	...	...	15.36 ± 25.78	0.12 ± 0.05
10253	82.3	1.23	318	38.91 ± 10.69	0.00 ± 0.00
45569.2	9.5	1.40	440		
960623.34	201.4	1.21	172	17.41 ± 2.29	0.17 ± 0.04
10257	4.3	2.16	390	35.84 ± 9.71	(5.54 ± 0.05)E-7
29828.3	34.4	2.37	551		
960625.20	197.3	1.89	158	...	0.25 ± 0.04
10259	-65.9	1.21	358	5.12 ± 3.07	(8.53 ± 0.13)E-8
17448.1	31.3	1.10	527		
960715.67	16.8	8.33	185	19.46 ± 2.29	1.29 ± 0.06
10279	-7.0	8.40	377	67.58 ± 4.22	(3.70 ± 0.15)E-6
58322.1	2.7	11.08	522		
960715.75	88.3	2.26	168	32.77 ± 1.45	0.22 ± 0.04
10279	42.7	3.37	352	(1.05 ± 0.03)E+2	(1.23 ± 0.05)E-6
64806.1	2.1	4.12	476		
960717.38	72.6	1.25	116	14.34 ± 4.22	0.24 ± 0.05
10281	-0.1	1.85	240	40.96 ± 5.22	(4.61 ± 0.39)E-7
33594.6	8.9	1.74	330		
960719.85	29.2	2.69	129	11.26 ± 1.45	0.42 ± 0.04
10283	52.2	4.68	283	30.72 ± 4.22	(7.77 ± 0.82)E-7
73458.9	5.3	5.74	423		
960724.42	357.7	1.08	180	7.17 ± 1.45	0.18 ± 0.05
10288	-64.7	1.43	401	16.38 ± 1.45	(1.38 ± 0.10)E-7
36935.9	24.0	1.13	480		

Table A-2—Continued

Name (NTB) Date (TJD) Time (s UT)	R.A. (°) Decl. (°) Err. (°)	C_{max}/C_{min} (4.096 s) (8.192 s)	C_{min} (4.096 s) (8.192 s)	T_{50} (s) T_{90} (s)	P (ph cm^{-2} s^{-1}) F (erg cm^{-2}) (50–300 keV)
960725.73	90.3	1.80	182	32.77 ± 2.90	0.27 ± 0.04
10289	45.1	2.63	376	71.68 ± 8.26	(8.67 ± 0.73)E-7
63534.3	7.5	3.52	534		
960728.08	164.3	1.25	198	2.05 ± 1.45	0.20 ± 0.07
10292	-11.6	1.50	296	5.12 ± 1.45	(1.85 ± 0.06)E-7
7604.4	29.1	1.36	359		
960730.21	306.6	2.25	189	17.41 ± 1.45	0.35 ± 0.05
10294	-54.0	3.43	450	35.84 ± 1.45	(6.82 ± 0.79)E-7
18333.9	3.3	4.38	630		
960802.25	183.9	...	...	10.24 ± 2.29	0.20 ± 0.06
10297	-24.1	1.62	386	46.08 ± 9.44	(3.52 ± 0.10)E-7
22205.6	14.1	1.63	455		
960804.32	68.1	1.42	200	10.24 ± 6.23	0.22 ± 0.05
10299	-56.5	1.94	291	25.60 ± 16.42	(1.97 ± 0.09)E-7
27671.8	49.9	1.91	426		
960804.73	358.9	1.46	163	36.86 ± 1.45	0.25 ± 0.05
10299	24.0	2.55	365	61.44 ± 14.66	(8.12 ± 0.50)E-7
63878.3	4.7	2.93	562		
960807.65	42.7	1.55	165	68.61 ± 3.69	0.24 ± 0.04
10302	-36.1	2.39	288	(1.55 ± 0.12)E+2	(2.05 ± 0.05)E-6
56523.0	14.1	2.92	494		
960810.53	135.6	2.43	155	...	0.46 ± 0.05
10305	-19.1	1.86	348	3.07 ± 1.44	(1.07 ± 0.37)E-7
46171.3	30.3	1.40	486		
960811.04	159.8	1.64	211	...	0.26 ± 0.04
10306	-39.9	1.58	365	5.12 ± 1.02	(1.04 ± 0.49)E-7
3555.5	8.0	1.30	560		
960811.91	253.9	...	...	12.29 ± 2.29	0.11 ± 0.04
10306	-25.2	1.53	362	27.65 ± 4.34	(3.38 ± 0.15)E-7
79098.1	6.9	1.93	540		
960817.28	203.7	3.27	147	11.26 ± 2.29	0.61 ± 0.05
10312	42.4	5.61	307	51.20 ± 11.45	(8.41 ± 2.11)E-7
24602.8	10.3	6.14	464		
960822.25	325.9	1.21	195	6.14 ± 2.29	0.21 ± 0.05
10317	15.4	1.96	383	24.58 ± 3.24	(2.70 ± 0.04)E-7
22398.2	11.0	1.96	502		
960825.40	158.4	...	...	13.31 ± 5.22	0.14 ± 0.05
10320	-29.1	1.69	332	57.34 ± 3.24	(2.92 ± 0.57)E-7
35092.7	7.2	2.23	509		
960826.66	187.8	1.89	175	26.62 ± 1.45	0.23 ± 0.04
10321	20.4	2.50	361	53.25 ± 13.47	(9.37 ± 0.78)E-7
57167.1	10.8	3.17	521		
960826.67	179.8	1.65	199	23.55 ± 1.45	0.38 ± 0.07
10321	21.3	2.84	378	39.94 ± 7.24	(1.63 ± 0.02)E-6
58072.3	5.3	3.46	542		
960911.12	311.8	1.38	129	54.27 ± 1.45	0.25 ± 0.04
10337	30.6	1.90	296	72.70 ± 4.22	(3.51 ± 0.32)E-7
10775.8	21.1	1.79	438		
960912.99	207.3	2.44	154	32.77 ± 1.45	0.45 ± 0.05
10338	-46.8	3.37	349	53.25 ± 1.45	(1.18 ± 0.10)E-6
86192.3	4.0	3.49	389		
960913.23	78.9	2.52	186	10.24 ± 1.45	0.36 ± 0.04
10339	44.1	3.36	364	33.79 ± 9.27	(4.91 ± 0.34)E-7
20718.8	12.2	3.39	516		
960913.25	89.3	5.24	151	2.05 ± 1.45	0.94 ± 0.06
10339	-39.4	4.08	295	3.07 ± 1.45	(2.96 ± 1.20)E-7
22068.4	4.7	3.31	457		
960921.84	222.0	1.15	163	28.67 ± 3.24	0.20 ± 0.05
10347	-73.5	1.55	343	79.87 ± 4.58	(7.34 ± 0.42)E-7
72975.6	6.0	1.69	461		

Table A-2—Continued

Name (NTB) Date (TJD) Time (s UT)	R.A. (°) Decl. (°) Err. (°)	C_{max}/C_{min} (4.096 s) (8.192 s)	C_{min} (4.096 s) (8.192 s)	T_{50} (s) T_{90} (s)	P (ph cm^{-2} s^{-1}) F (erg cm^{-2}) (50–300 keV)
960923.36	215.2	1.39	175	...	0.23 ± 0.05
10349	-3.5	1.03	363	4.10 ± 2.05	(8.06 ± 0.17)E-8
31200.5	51.6	...	...		
960927.58	261.0	1.20	129	61.44 ± 11.31	0.14 ± 0.04
10353	20.7	2.06	318	(1.40 ± 0.10)E+2	(7.38 ± 0.44)E-7
50463.9	7.8	2.75	481		
960929.57	33.4	1.66	142	...	0.24 ± 0.04
10355	27.1	...	...	1.02 ± 1.02	(4.62 ± 0.30)E-8
49852.6	22.8	...	...		
960930.51	39.1	1.79	131	11.26 ± 3.24	0.30 ± 0.05
10356	23.6	2.71	290	25.60 ± 3.69	(3.70 ± 0.37)E-7
44124.4	5.1	2.81	368		
961003.24	285.5	1.26	129	29.70 ± 4.22	0.24 ± 0.05
10359	-11.8	2.51	297	65.54 ± 7.24	(1.30 ± 0.01)E-6
21415.1	5.4	3.50	411		
961003.43	254.9	1.44	194	10.24 ± 1.45	0.22 ± 0.04
10359	27.2	2.21	358	25.60 ± 9.27	(3.51 ± 0.44)E-7
37620.9	11.4	2.74	462		
961006.75	254.1	...	...	5.12 ± 2.90	0.12 ± 0.05
10362	24.3	1.19	370	11.26 ± 3.69	(2.65 ± 0.05)E-7
65526.0	16.8	1.57	482		
961009.58	80.0	1.29	199	18.43 ± 1.45	0.17 ± 0.04
10365	-80.6	2.06	316	52.22 ± 7.24	(9.68 ± 0.85)E-7
50287.8	3.9	2.77	417		
961009.72	267.6	1.43	129	19.46 ± 1.45	0.24 ± 0.05
10365	55.3	2.34	330	44.03 ± 2.90	(7.91 ± 0.68)E-7
62704.8	11.3	2.69	460		
961010.25	151.2	1.30	146	...	0.25 ± 0.05
10366	-64.1	1.34	354	5.12 ± 1.44	(9.59 ± 0.86)E-8
21875.9	11.9	1.02	559		
961010.77	114.0	1.39	164	8.19 ± 2.29	0.19 ± 0.05
10366	-68.7	2.20	321	30.72 ± 6.23	(2.93 ± 0.65)E-7
67016.9	9.9	2.55	483		
961013.15	283.3	1.25	197	...	0.18 ± 0.04
10369	-13.8	2.01	368	17.41 ± 5.12	(2.91 ± 0.08)E-7
13313.2	21.8	2.40	547		
961013.86	186.1	...	...	30.72 ± 2.29	0.12 ± 0.04
10369	49.4	1.23	299	74.75 ± 6.23	(3.83 ± 0.20)E-7
74530.0	17.9	1.52	367		
961017.27	163.9	5.10	180	6.14 ± 1.45	0.93 ± 0.06
10373	42.6	8.57	377	34.82 ± 7.24	(1.34 ± 0.16)E-6
23645.4	1.6	8.13	522		
961019.51	262.8	1.15	199	14.34 ± 1.45	0.14 ± 0.04
10375	-65.9	1.73	327	51.20 ± 1.45	(3.60 ± 0.06)E-7
44432.6	16.2	2.06	516		
961024.25	32.7	1.65	167	...	0.25 ± 0.05
10380	25.4	1.64	394	5.12 ± 3.07	(1.05 ± 0.09)E-7
21713.1	13.7	1.31	559		
961025.41	36.1	...	...	11.26 ± 2.29	0.14 ± 0.05
10381	-15.7	1.36	248	31.74 ± 10.29	(3.01 ± 0.19)E-7
35734.7	16.0	1.72	455		
961030.92	141.8	1.39	191	14.34 ± 1.45	0.22 ± 0.04
10386	47.7	2.37	379	44.03 ± 9.16	(4.63 ± 1.01)E-7
80068.8	7.1	3.13	543		
961102.88	301.4	...	...	15.36 ± 1.45	0.12 ± 0.05
10389	23.1	1.50	303	38.91 ± 2.90	(5.73 ± 0.47)E-7
76647.6	7.9	2.09	399		
961104.19	219.5	1.78	121	2.05 ± 1.45	0.28 ± 0.04
10391	25.9	3.27	281	5.12 ± 1.45	(2.46 ± 0.39)E-7
16831.7	10.5	3.01	343		

Table A-2—Continued

Name (NTB) Date (TJD) Time (s UT)	R.A. (°) Decl. (°) Err. (°)	C_{max}/C_{min} (4.096 s) (8.192 s)	C_{min} (4.096 s) (8.192 s)	T_{50} (s) T_{90} (s)	P (ph cm^{-2} s^{-1}) F (erg cm^{-2}) (50–300 keV)
961106.49	296.9	1.40	156	...	0.26 ± 0.05
10393	68.7	1.75	340	13.31 ± 5.12	(2.01 ± 0.03)E-7
43027.7	15.7	1.50	470		
961108.96	358.6	1.93	176	14.34 ± 1.45	0.29 ± 0.05
10395	33.8	3.23	315	43.01 ± 7.24	(1.24 ± 0.07)E-6
83234.0	2.5	4.37	461		
961110.31	61.1	2.96	142	94.21 ± 1.45	0.47 ± 0.05
10397	59.0	5.29	297	(1.24 ± 0.01)E+2	(1.60 ± 0.15)E-6
26946.8	7.9	5.27	409		
961111.14	344.9	2.89	125	13.31 ± 1.45	0.51 ± 0.05
10398	-13.5	5.15	234	28.67 ± 1.45	(2.30 ± 0.12)E-6
12431.6	1.3	6.82	320		
961111.61	338.0	1.73	126	8.19 ± 1.45	0.32 ± 0.05
10398	-7.0	2.94	252	21.50 ± 1.45	(4.45 ± 0.55)E-7
52849.9	7.9	3.06	368		
961112.72	300.4	2.12	168	23.55 ± 2.90	0.25 ± 0.04
10399	28.4	3.78	354	63.49 ± 8.75	(1.58 ± 0.13)E-6
62332.1	2.0	5.16	476		
961119.44	67.0	1.42	177	15.36 ± 2.29	0.24 ± 0.05
10406	29.5	2.69	333	52.22 ± 9.16	(8.28 ± 0.79)E-7
38625.5	5.3	3.64	533		
961120.35	286.8	2.78	177	...	0.42 ± 0.04
10407	43.6	2.92	382	3.07 ± 1.44	(1.92 ± 0.39)E-7
30430.4	15.0	2.26	519		
961123.68	64.6	9.63	202	...	2.98 ± 0.11
10410	65.9	4.96	411	1.02 ± 1.02	(6.84 ± 0.31)E-7
59310.3	16.7	3.58	576		
961128.06	58.4	1.42	132	7.17 ± 1.45	0.25 ± 0.05
10415	80.2	2.62	320	17.41 ± 1.45	(4.83 ± 0.49)E-7
5618.9	7.1	3.49	497		
961130.43	44.0	1.81	191	31.74 ± 2.29	0.33 ± 0.07
10417	-28.2	3.21	410	80.90 ± 9.27	(1.94 ± 0.14)E-6
37848.3	1.4	4.26	587		
961206.39	16.7	...	...	12.29 ± 2.29	0.11 ± 0.04
10423	-53.1	1.43	303	38.91 ± 17.41	0.00 ± 0.00
34487.5	18.0	1.92	530		
961207.62	113.0	1.07	165	9.22 ± 2.29	0.15 ± 0.04
10424	-59.1	1.66	367	16.38 ± 6.23	(2.27 ± 0.03)E-7
54182.1	26.4	2.04	428		
961208.21	345.6	1.10	163	9.22 ± 1.45	0.17 ± 0.04
10425	-30.7	1.83	298	25.60 ± 6.23	(3.95 ± 0.05)E-7
18574.5	17.6	2.35	408		
961208.58	73.5	1.13	196	12.29 ± 1.45	0.15 ± 0.04
10425	-69.7	1.74	316	28.67 ± 2.29	(4.51 ± 0.43)E-7
50939.1	32.1	2.21	461		
961208.78	61.4	2.27	184	20.48 ± 3.24	0.37 ± 0.05
10425	-44.9	2.80	391	24.58 ± 5.22	(3.31 ± 0.08)E-7
68228.3	50.0	2.31	552		
961209.32	141.6	1.29	183	15.36 ± 3.24	0.22 ± 0.05
10426	-37.5	1.86	390	45.06 ± 1.45	(6.47 ± 0.39)E-7
27746.5	7.4	2.29	576		
961209.86	180.3	4.91	146	38.91 ± 4.22	0.77 ± 0.05
10426	28.4	6.50	287	(1.68 ± 0.02)E+2	(3.42 ± 0.15)E-6
74676.4	2.3	7.86	414		
961212.30	190.7	1.44	165	43.01 ± 1.45	0.19 ± 0.04
10429	73.7	2.63	389	88.06 ± 3.24	(1.20 ± 0.03)E-6
26297.5	5.7	3.44	545		
961213.57	191.9	7.87	123	(1.00 ± 0.02)E+2	1.62 ± 0.06
10430	51.5	10.88	246	(1.32 ± 0.01)E+2	(5.88 ± 0.44)E-6
49965.3	0.7	13.76	347		

Table A-2—Continued

Name (NTB) Date (TJD) Time (s UT)	R.A. (°) Decl. (°) Err. (°)	C_{max}/C_{min} (4.096 s) (8.192 s)	C_{min} (4.096 s) (8.192 s)	T_{50} (s) T_{90} (s)	P (ph cm^{-2} s^{-1}) F (erg cm^{-2}) (50–300 keV)
961216.87	248.3	1.70	180	6.14 ± 2.29	0.22 ± 0.04
10433	38.7	2.73	347	22.53 ± 6.23	(4.90 ± 0.05)E-7
75488.5	5.8	3.63	516		
961216.94	347.2	1.08	172	7.17 ± 1.45	0.16 ± 0.04
10433	26.1	1.61	379	11.26 ± 1.45	(1.50 ± 0.32)E-7
81346.8	25.1	1.56	462		
961217.82	19.9	1.46	207	...	0.16 ± 0.06
10434	-0.8	1.53	373	5.12 ± 2.05	(9.65 ± 0.26)E-8
70860.0	72.5	...	...		
961219.55	211.7	1.84	195	38.91 ± 1.45	0.30 ± 0.05
10436	-24.9	2.62	330	64.51 ± 2.29	(5.75 ± 0.69)E-7
47636.7	28.5	2.85	445		
961219.58	307.5	1.69	158	...	0.28 ± 0.05
10436	41.4	1.35	421	2.05 ± 1.02	(8.12 ± 2.85)E-8
50356.4	16.2	1.02	483		
961220.02	5.3	1.17	167	24.58 ± 1.45	0.18 ± 0.05
10437	-0.7	1.91	371	39.94 ± 2.29	(5.91 ± 0.46)E-7
2460.9	5.5	2.31	568		
961222.50	302.9	2.32	172	37.89 ± 3.24	0.57 ± 0.07
10439	-12.1	3.68	323	69.63 ± 7.45	(2.03 ± 0.02)E-6
43201.7	6.1	3.99	436		
961224.42	319.5	5.20	131	11.26 ± 1.45	0.97 ± 0.06
10441	14.5	8.02	262	36.86 ± 2.29	(2.38 ± 0.07)E-6
36644.0	1.3	9.98	371		
961227.62	186.9	2.02	168	9.22 ± 1.45	0.31 ± 0.05
10444	-15.9	3.92	345	46.08 ± 2.29	(7.95 ± 0.75)E-7
53713.1	3.0	4.86	497		
961231.29	102.5	1.18	155	20.48 ± 2.29	0.21 ± 0.05
10448	2.0	1.73	395	(1.50 ± 0.03)E+2	(5.79 ± 0.44)E-7
25571.5	6.0	1.56	579		
970108.63	25.1	1.50	156	14.34 ± 1.45	0.19 ± 0.04
10456	-35.1	2.75	376	57.34 ± 6.23	(8.04 ± 0.58)E-7
54782.2	18.5	3.75	530		
970110.45	46.8	2.56	133	...	0.40 ± 0.05
10458	58.2	1.61	232	1.02 ± 1.44	(9.52 ± 0.31)E-8
39248.1	18.7	1.25	337		
970111.65	150.9	1.11	130	7.17 ± 1.45	0.24 ± 0.05
10459	27.1	2.19	313	13.31 ± 2.90	(3.98 ± 0.61)E-7
56765.6	11.2	2.65	414		
970111.92	324.9	2.37	154	...	0.81 ± 0.09
10459	22.0	1.69	279	1.02 ± 1.44	(2.09 ± 0.10)E-7
80082.1	21.4	1.15	352		
970115.11	304.6	2.40	189	...	0.45 ± 0.06
10463	-26.7	2.73	393	4.10 ± 1.02	(2.73 ± 0.08)E-7
10128.6	7.2	2.11	562		
970116.37	52.0	2.40	146	...	0.42 ± 0.05
10464	53.0	2.01	269	4.10 ± 2.05	(1.67 ± 0.03)E-7
32519.4	20.1	1.38	367		
970116.67	190.1	6.42	154	18.43 ± 1.45	1.07 ± 0.05
10464	-44.8	12.12	321	57.34 ± 2.29	(4.55 ± 0.51)E-6
58239.2	3.3	15.88	445		
970117.09	301.8	1.90	198	3.07 ± 1.45	0.25 ± 0.04
10465	-58.5	2.94	380	11.26 ± 3.24	(2.50 ± 0.40)E-7
7994.6	11.2	2.83	542		
970119.49	206.8	4.60	180	(1.05 ± 0.77)E+2	0.63 ± 0.04
10467	79.9	7.97	362	(1.37 ± 0.04)E+2	(2.01 ± 0.08)E-6
42595.5	2.0	9.39	528		
970120.62	109.7	1.00	145	...	0.10 ± 0.04
10468	9.5	1.32	251	10.24 ± 5.12	(1.64 ± 0.05)E-7
54215.9	15.5	1.66	436		

Table A-2—Continued

Name (NTB) Date (TJD) Time (s UT)	R.A. (°) Decl. (°) Err. (°)	C_{max}/C_{min} (4.096 s) (8.192 s)	C_{min} (4.096 s) (8.192 s)	T_{50} (s) T_{90} (s)	P (ph cm^{-2} s^{-1}) F (erg cm^{-2}) (50–300 keV)
970121.28	149.7	1.61	122	...	0.40 ± 0.06
10469	-7.8	1.21	237	3.07 ± 2.05	(1.44 ± 0.04)E-7
25048.3	39.7	1.07	410		
970126.27	207.1	1.85	164	15.36 ± 1.45	0.35 ± 0.05
10474	-35.8	3.17	325	38.91 ± 9.71	(9.13 ± 0.96)E-7
23367.9	5.6	3.94	457		
970126.39	51.2	1.92	144	8.19 ± 1.45	0.35 ± 0.05
10474	70.9	3.26	260	25.60 ± 10.09	(7.73 ± 0.78)E-7
33796.3	3.2	4.47	414		
970126.40	281.8	2.02	174	...	0.29 ± 0.04
10474	23.9	2.21	321	14.34 ± 5.12	(2.38 ± 0.31)E-7
35408.1	26.8	2.36	460		
970128.44	61.9	1.92	178	4.10 ± 1.45	0.33 ± 0.05
10476	-73.5	3.42	338	12.29 ± 1.45	(4.25 ± 0.42)E-7
38795.5	2.9	3.58	502		
970129.55	113.9	1.08	181	5.12 ± 3.24	0.16 ± 0.04
10477	55.4	1.90	355	11.26 ± 3.24	(2.21 ± 0.29)E-7
48170.2	18.9	2.25	568		
970131.21	287.7	1.07	162	8.19 ± 1.45	0.12 ± 0.04
10479	34.4	1.79	353	16.38 ± 1.45	(2.77 ± 0.04)E-7
18181.3	9.3	1.99	503		
970203.38	44.4	1.80	174	...	0.25 ± 0.05
10482	34.1	2.31	295	10.24 ± 5.12	(3.01 ± 0.44)E-7
32985.3	5.5	2.59	470		
970205.06	155.2	1.79	156	3.07 ± 1.45	0.30 ± 0.05
10484	-71.7	2.77	385	6.14 ± 1.45	(2.86 ± 0.52)E-7
5931.2	4.6	2.68	543		
970205.09	67.7	1.54	180	13.31 ± 1.45	0.21 ± 0.04
10484	-77.1	2.70	347	45.06 ± 2.90	(4.62 ± 0.31)E-7
8222.9	17.9	3.14	514		
970206.05	164.1	1.09	186	28.67 ± 1.45	0.29 ± 0.08
10485	20.5	1.85	381	53.25 ± 1.45	(1.10 ± 0.01)E-6
5106.9	9.5	1.93	534		
970221.15	33.6	1.04	161	11.26 ± 1.45	0.16 ± 0.04
10500	68.8	1.82	420	26.62 ± 3.24	(4.66 ± 0.36)E-7
13744.3	38.2	2.35	559		
970221.34	297.1	1.19	191	...	0.19 ± 0.04
10500	44.9	1.57	379	10.24 ± 5.12	(1.91 ± 0.05)E-7
30056.7	21.1	1.80	494		
970223.31	330.2	1.34	181	...	0.45 ± 0.09
10502	-26.1	1.32	364	3.07 ± 2.05	(2.31 ± 0.12)E-7
27511.0	22.9	1.35	533		
970226.14	139.7	1.12	127	16.38 ± 1.45	0.18 ± 0.04
10505	55.3	1.51	248	47.10 ± 3.24	(5.70 ± 0.51)E-7
12236.0	7.2	2.11	351		
970306.87	134.4	1.38	194	66.56 ± 4.22	0.26 ± 0.05
10513	-81.9	2.01	384	(1.41 ± 0.16)E+2	(1.99 ± 0.10)E-6
75756.7	2.9	2.53	534		
970310.04	62.4	1.20	120	14.34 ± 1.45	0.17 ± 0.05
10517	-33.4	1.63	240	46.08 ± 10.29	(5.31 ± 0.33)E-7
3945.7	6.8	2.20	359		
970310.27	62.3	1.44	163	17.41 ± 1.45	0.23 ± 0.04
10517	68.4	2.02	347	52.22 ± 14.37	(5.59 ± 0.64)E-7
23932.1	25.5	2.55	546		
970311.35	20.7	2.27	181	10.24 ± 1.45	0.41 ± 0.05
10518	-1.9	3.84	286	30.72 ± 5.22	(9.26 ± 1.51)E-7
30253.3	3.6	4.99	411		
970323.81	201.8	1.40	176	3.07 ± 1.45	0.31 ± 0.06
10530	-30.9	2.43	367	8.19 ± 1.45	(2.24 ± 2.11)E-7
70209.7	5.0	2.27	492		

Table A-2—Continued

Name (NTB) Date (TJD) Time (s UT)	R.A. (°) Decl. (°) Err. (°)	C_{max}/C_{min} (4.096 s) (8.192 s)	C_{min} (4.096 s) (8.192 s)	T_{50} (s) T_{90} (s)	P (ph cm^{-2} s^{-1}) F (erg cm^{-2}) (50–300 keV)
970331.84	344.1	2.02	134	4.10 ± 1.45	0.37 ± 0.05
10538	13.7	3.30	293	15.36 ± 12.33	(3.40 ± 0.82)E-7
72915.1	8.5	3.40	418		
970404.29	60.5	1.58	175	9.22 ± 1.45	0.48 ± 0.09
10542	25.7	1.58	389	23.55 ± 10.44	(7.21 ± 0.11)E-7
25616.6	22.6	1.81	531		
970406.29	287.6	3.26	220	14.34 ± 1.45	0.63 ± 0.06
10544	-30.3	5.95	416	46.08 ± 4.58	(2.30 ± 0.15)E-6
25471.2	2.3	7.90	594		
970407.82	186.4	1.33	197	...	0.29 ± 0.06
10545	43.8	...	...	1.02 ± 1.02	(8.69 ± 0.25)E-8
71030.0	21.4	...	...		
970409.32	151.6	1.39	119	5.12 ± 1.45	0.21 ± 0.04
10547	29.3	2.05	236	13.31 ± 2.29	(3.49 ± 3.95)E-7
27649.2	3.9	2.92	381		
970414.36	111.1	1.68	197	33.79 ± 1.45	0.22 ± 0.04
10552	5.0	2.97	335	86.02 ± 2.29	(1.94 ± 0.13)E-6
31461.6	21.6	3.95	468		
970415.82	225.8	1.01	194	10.24 ± 2.29	0.16 ± 0.05
10553	-2.7	1.61	384	51.20 ± 10.29	(3.68 ± 0.37)E-7
71050.4	5.8	1.94	524		
970421.24	24.2	1.49	141	16.38 ± 1.45	0.23 ± 0.04
10559	-44.0	1.81	251	45.06 ± 3.69	(3.28 ± 0.19)E-7
21304.5	13.1	2.08	384		
970425.70	208.8	1.14	176	4.10 ± 1.45	0.19 ± 0.05
10563	-24.7	1.45	328	23.55 ± 8.26	(1.91 ± 0.03)E-7
61336.8	25.1	1.45	533		
970426.13	48.7	1.04	145	5.12 ± 1.45	0.19 ± 0.04
10564	-61.9	1.73	246	14.34 ± 1.45	(2.54 ± 0.13)E-7
11346.1	8.3	1.67	317		
970427.28	300.3	1.42	132	14.34 ± 1.45	0.25 ± 0.05
10565	-13.6	2.57	278	43.01 ± 1.45	(4.99 ± 0.46)E-7
24726.7	8.5	3.10	410		
970427.86	179.4	...	...	14.34 ± 3.24	0.16 ± 0.04
10565	36.2	1.11	350	45.06 ± 12.37	(2.75 ± 0.14)E-7
74779.9	24.5	1.39	568		
970501.12	294.6	...	...	11.26 ± 2.29	0.18 ± 0.05
10569	64.5	1.40	269	34.82 ± 11.99	(3.03 ± 0.07)E-7
10378.4	37.8	1.63	402		
970502.77	205.2	1.10	168	...	0.17 ± 0.04
10570	17.4	1.85	387	14.34 ± 4.10	(2.47 ± 0.51)E-7
67029.2	15.6	2.23	537		
970506.08	88.5	1.49	144	11.26 ± 1.45	0.25 ± 0.04
10574	40.3	2.59	311	24.58 ± 2.29	(6.84 ± 0.68)E-7
7233.7	9.5	3.31	455		
970511.68	328.1	1.32	145	3.07 ± 1.45	0.20 ± 0.04
10579	31.8	2.15	254	9.22 ± 6.23	(2.28 ± 0.33)E-7
59122.9	5.9	1.99	360		
970518.40	85.3	...	...	17.41 ± 1.45	0.13 ± 0.05
10586	48.7	1.17	254	47.10 ± 7.24	(5.36 ± 0.06)E-7
35414.2	8.9	1.78	404		
970522.05	194.7	1.18	187	12.29 ± 4.22	0.46 ± 0.11
10590	-25.5	2.18	389	30.72 ± 9.27	(1.02 ± 0.02)E-6
4989.1	9.2	2.44	536		
970525.36	149.5	1.20	166	10.24 ± 1.45	0.17 ± 0.04
10593	50.8	2.19	330	28.67 ± 2.90	(5.56 ± 0.46)E-7
31778.0	6.1	2.93	457		
970526.56	195.3	1.45	160	...	0.21 ± 0.05
10594	-61.2	1.32	301	3.07 ± 2.05	(1.07 ± 0.03)E-7
48627.9	22.6	1.17	439		

Table A-2—Continued

Name (NTB) Date (TJD) Time (s UT)	R.A. (°) Decl. (°) Err. (°)	C_{max}/C_{min} (4.096 s) (8.192 s)	C_{min} (4.096 s) (8.192 s)	T_{50} (s) T_{90} (s)	P (ph cm^{-2} s^{-1}) F (erg cm^{-2}) (50–300 keV)
970527.57	153.3	1.44	154	7.17 ± 1.45	0.20 ± 0.04
10595	-68.2	2.33	308	25.60 ± 3.24	(3.26 ± 0.46)E-7
49577.2	11.3	2.90	473		
970531.65	5.4	1.86	183	4.10 ± 1.45	0.27 ± 0.04
10599	-87.3	2.10	275	12.29 ± 1.45	(1.54 ± 0.31)E-7
56532.2	14.2	1.74	468		
970604.77	1.0	1.61	172	...	0.27 ± 0.05
10603	74.7	1.87	300	4.10 ± 1.44	(1.49 ± 0.03)E-7
67013.8	45.4	1.47	533		
970605.51	212.0	2.10	208	...	0.39 ± 0.05
10604	-70.6	1.57	415	2.05 ± 1.44	(9.64 ± 2.59)E-8
44845.3	17.6	1.19	570		
970607.41	32.4	2.45	147	20.48 ± 1.45	0.44 ± 0.05
10606	17.9	4.12	246	74.75 ± 11.68	(2.05 ± 0.19)E-6
35799.2	3.1	5.66	394		
970607.47	355.7	1.20	200	21.50 ± 2.29	0.20 ± 0.04
10606	-50.6	2.01	257	52.22 ± 15.39	(7.95 ± 0.52)E-7
41150.7	3.3	2.57	363		
970610.41	32.7	3.81	163	88.06 ± 3.24	0.75 ± 0.06
10609	41.8	3.72	335	(1.01 ± 0.01)E+2	(6.82 ± 0.78)E-7
36150.5	12.1	3.65	495		
970610.76	33.8	1.43	168	24.58 ± 2.29	0.28 ± 0.05
10609	8.8	2.18	321	57.34 ± 6.23	(5.40 ± 0.69)E-7
65897.7	16.2	2.54	435		
970611.79	255.9	1.34	183	...	0.47 ± 0.10
10610	34.6	1.15	291	3.07 ± 1.44	(1.86 ± 0.08)E-7
68776.1	31.1	...	...		
970614.99	205.9	2.92	138	25.60 ± 2.29	0.53 ± 0.05
10613	-25.3	2.49	257	39.94 ± 4.22	(5.41 ± 1.22)E-7
85845.2	9.5	2.56	364		
970616.92	327.6	1.39	200	...	0.22 ± 0.05
10615	-2.6	1.13	281	6.14 ± 3.07	(8.97 ± 1.78)E-8
79715.5	35.2	1.07	443		
970617.71	161.7	1.17	192	20.48 ± 1.45	0.17 ± 0.04
10616	10.6	1.65	434	49.15 ± 5.51	(7.42 ± 0.44)E-7
61460.7	7.2	2.22	625		
970626.90	186.1	1.28	152	3.07 ± 1.45	0.23 ± 0.04
10625	-70.1	1.83	310	6.14 ± 3.24	(1.26 ± 0.35)E-7
78484.7	24.6	1.59	414		
970629.88	322.6	1.40	154	2.05 ± 1.45	0.21 ± 0.05
10628	-12.5	1.48	265	3.07 ± 60.49	(8.51 ± 1.41)E-8
76306.6	20.9	1.25	356		
970709.57	23.9	...	...	7.17 ± 1.45	0.15 ± 0.05
10638	52.8	1.49	312	15.36 ± 4.22	(1.87 ± 0.39)E-7
49732.8	10.1	1.94	458		
970709.61	240.3	3.10	200	7.17 ± 1.45	0.53 ± 0.05
10638	22.5	4.02	374	16.38 ± 2.90	(5.36 ± 0.85)E-7
53038.3	4.9	3.95	543		
970712.33	47.1	1.28	136	26.62 ± 2.29	0.14 ± 0.04
10641	7.0	2.02	410	61.44 ± 4.34	(8.30 ± 0.12)E-7
29120.7	16.1	2.21	574		
970714.57	10.7	3.96	192	3.07 ± 1.45	0.68 ± 0.05
10643	-22.9	6.54	381	10.24 ± 1.45	(6.61 ± 2.85)E-7
49754.3	3.4	6.83	532		
970724.36	202.4	1.05	199	11.26 ± 1.45	0.23 ± 0.06
10653	41.8	1.82	293	28.67 ± 5.22	(3.98 ± 0.06)E-7
31275.2	7.7	1.68	416		
970726.94	62.0	1.45	190	21.50 ± 5.22	0.28 ± 0.05
10655	-8.9	2.37	396	52.22 ± 7.24	(7.89 ± 0.11)E-7
81588.5	3.7	2.92	611		

Table A-2—Continued

Name (NTB) Date (TJD) Time (s UT)	R.A. (°) Decl. (°) Err. (°)	C_{max}/C_{min} (4.096 s) (8.192 s)	C_{min} (4.096 s) (8.192 s)	T_{50} (s) T_{90} (s)	P (ph cm^{-2} s^{-1}) F (erg cm^{-2}) (50–300 keV)
970728.43	296.2	1.30	149	25.60 ± 1.45	0.17 ± 0.05
10657	42.1	2.12	338	53.25 ± 10.29	(8.86 ± 0.79)E-7
37654.8	6.5	2.59	527		
970801.33	308.0	10.58	178	10.24 ± 1.45	1.57 ± 0.05
10661	-54.3	18.33	339	20.48 ± 1.45	(3.48 ± 0.47)E-6
29047.0	1.5	22.00	477		
970801.69	206.8	1.96	150	...	0.51 ± 0.05
10661	-18.8	1.72	331	7.17 ± 4.10	(1.76 ± 0.88)E-7
59873.5	15.1	1.64	564		
970804.50	68.0	1.45	229	...	0.18 ± 0.06
10664	81.6	...	...	1.02 ± 0.00	(3.43 ± 0.14)E-8
43965.7	38.7	...	...		
970812.09	305.9	1.58	211	16.38 ± 1.45	0.27 ± 0.05
10672	-14.4	2.34	423	34.82 ± 2.29	(6.76 ± 0.59)E-7
8000.7	10.5	2.68	631		
970816.57	292.9	1.31	194	6.14 ± 1.45	0.21 ± 0.05
10676	69.9	1.87	308	9.22 ± 1.45	(3.36 ± 0.52)E-7
49715.4	15.7	2.49	509		
970817.80	50.3	...	...	27.65 ± 2.29	0.11 ± 0.04
10677	50.5	1.83	329	55.30 ± 5.22	(6.01 ± 0.28)E-7
69683.4	12.7	2.40	436		
970823.35	300.0	1.91	161	...	0.38 ± 0.05
10683	27.3	2.98	335	4.10 ± 2.05	(2.31 ± 0.25)E-7
30810.3	6.2	2.76	528		
970825.47	29.2	1.11	127	29.70 ± 1.45	0.21 ± 0.05
10685	-47.8	2.19	370	61.44 ± 1.45	(1.02 ± 0.05)E-6
40624.4	11.8	2.77	536		
970827.29	287.6	4.50	214	19.46 ± 1.45	0.88 ± 0.06
10687	-23.8	7.49	405	50.18 ± 3.24	(2.11 ± 0.09)E-6
25868.5	1.7	8.52	561		
970906.24	168.3	1.28	134	28.67 ± 3.24	0.21 ± 0.05
10697	19.8	2.33	410	75.78 ± 5.22	(9.50 ± 0.70)E-7
21537.0	2.5	2.90	587		
970906.70	235.0	1.36	130	...	0.21 ± 0.05
10697	44.7	2.12	283	18.43 ± 6.14	(3.05 ± 0.49)E-7
60883.2	20.3	2.12	395		
970909.79	176.8	...	...	8.19 ± 2.90	0.20 ± 0.11
10700	40.2	1.03	348	18.43 ± 5.12	(5.97 ± 0.13)E-7
68320.5	14.7	1.26	567		
970910.32	21.6	1.34	211	18.43 ± 1.45	0.19 ± 0.05
10701	-28.3	2.43	420	47.10 ± 4.58	(9.17 ± 0.66)E-7
27779.3	3.0	3.25	562		
970912.68	52.4	1.25	208	...	0.23 ± 0.05
10703	34.7	1.81	396	6.14 ± 2.05	(1.47 ± 0.42)E-7
58917.1	10.9	1.62	538		
970914.58	283.1	1.09	164	23.55 ± 3.69	0.13 ± 0.05
10705	37.1	1.61	291	59.39 ± 15.50	(6.39 ± 0.55)E-7
50456.8	18.2	1.68	367		
970914.91	356.8	1.61	145	...	0.30 ± 0.05
10705	63.5	1.91	308	4.10 ± 2.05	(1.54 ± 0.42)E-7
79085.8	29.2	1.50	453		
970916.84	210.4	1.48	139	12.29 ± 1.45	0.35 ± 0.05
10707	-15.7	2.75	279	30.72 ± 6.23	(9.07 ± 0.95)E-7
72978.7	3.1	3.22	395		
970917.02	298.9	2.39	163	24.58 ± 2.29	0.35 ± 0.04
10708	24.1	4.39	352	79.87 ± 7.24	(1.75 ± 0.15)E-6
1807.6	33.8	5.86	502		
970917.88	88.1	1.37	187	3.07 ± 1.45	0.32 ± 0.06
10708	22.0	1.66	388	11.26 ± 5.12	(1.94 ± 0.65)E-7
76578.0	6.9	1.57	586		

Table A-2—Continued

Name (NTB) Date (TJD) Time (s UT)	R.A. (°) Decl. (°) Err. (°)	C_{max}/C_{min} (4.096 s) (8.192 s)	C_{min} (4.096 s) (8.192 s)	T_{50} (s) T_{90} (s)	P (ph cm^{-2} s^{-1}) F (erg cm^{-2}) (50–300 keV)
970926.92	160.4	4.58	191	22.53 ± 1.45	0.82 ± 0.05
10717	-37.9	7.38	360	72.70 ± 2.29	(2.43 ± 0.11)E-6
79649.0	2.6	8.63	525		
970927.01	315.4	1.94	153	33.79 ± 3.24	0.34 ± 0.05
10718	-6.6	3.36	343	72.70 ± 10.89	(2.17 ± 0.06)E-6
1514.7	3.5	4.45	472		
971013.87	87.5	4.26	180	1.02 ± 1.45	0.72 ± 0.05
10734	20.9	4.96	379	5.12 ± 1.45	(3.00 ± 1.31)E-7
75583.7	7.5	3.78	556		
971015.23	290.5	6.76	213	5.12 ± 1.45	1.31 ± 0.06
10736	-81.2	6.99	427	7.17 ± 1.45	(7.08 ± 2.12)E-7
20356.3	2.7	6.80	582		
971017.02	44.1	1.24	178	11.26 ± 2.29	0.23 ± 0.05
10738	79.1	1.80	381	40.96 ± 14.26	(5.15 ± 0.63)E-7
1895.6	4.9	2.27	609		
971018.51	244.2	1.91	148	5.12 ± 1.45	0.62 ± 0.05
10739	51.0	3.33	299	15.36 ± 4.58	(9.60 ± 0.60)E-7
44359.9	2.5	3.65	423		
971026.16	161.4	1.62	187	23.55 ± 1.45	0.25 ± 0.04
10747	13.0	2.54	419	57.34 ± 3.69	(8.61 ± 0.40)E-7
13857.0	31.7	2.93	567		
971027.11	205.7	33.21	189	4.10 ± 1.45	4.75 ± 0.07
10748	59.2	53.91	375	13.31 ± 1.45	(6.89 ± 0.41)E-6
9805.0	1.9	64.17	533		
971027.82	276.9	...	...	9.22 ± 1.45	0.13 ± 0.04
10748	27.3	1.59	373	27.65 ± 1.45	(2.60 ± 0.07)E-7
71019.7	10.3	1.75	511		
971030.81	347.8	1.78	238	6.14 ± 1.45	0.39 ± 0.06
10751	-9.0	2.97	484	13.31 ± 3.24	(6.49 ± 1.55)E-7
70113.5	3.7	3.73	679		
971101.27	356.6	78.03	186	3.07 ± 1.45	13.70 ± 0.12
10753	10.4	106.59	362	8.19 ± 1.45	(1.04 ± 0.05)E-5
23480.5	0.5	85.31	510		
971102.22	282.8	1.83	167	...	0.35 ± 0.05
10754	-59.2	2.52	290	8.19 ± 3.07	(2.49 ± 0.08)E-7
19455.2	13.9	2.32	456		
971102.22	293.8	1.48	143	(1.66 ± 0.04)E+2	0.31 ± 0.05
10754	-59.0	2.30	320	(2.16 ± 0.01)E+2	(2.70 ± 0.15)E-6
19676.4	4.8	2.70	405		
971103.83	30.1	1.13	138	23.55 ± 3.69	0.18 ± 0.04
10755	-42.1	1.99	324	79.87 ± 11.99	(9.22 ± 0.47)E-7
72026.3	7.6	2.54	493		
971106.11	197.5	1.73	183	11.26 ± 1.45	0.31 ± 0.05
10758	-22.5	3.25	357	31.74 ± 4.58	(6.73 ± 0.69)E-7
9587.9	3.8	3.85	493		
971108.37	95.9	1.01	136	3.07 ± 2.29	0.17 ± 0.05
10760	42.8	1.65	257	6.14 ± 4.58	(1.36 ± 0.51)E-7
32785.6	20.0	1.37	363		
971108.97	42.9	...	...	...	0.16 ± 0.05
10760	13.3	1.55	353	14.34 ± 5.12	(2.76 ± 0.05)E-7
84331.7	6.4	1.79	539		
971110.21	58.2	1.03	221	15.36 ± 1.45	0.23 ± 0.05
10762	38.9	1.82	308	33.79 ± 1.45	(4.85 ± 0.58)E-7
18414.8	9.9	2.17	408		
971110.56	303.8	1.80	172	6.14 ± 1.45	0.34 ± 0.05
10762	-38.9	2.84	339	14.34 ± 1.45	(4.34 ± 0.73)E-7
49030.4	8.3	2.75	454		
971110.78	206.6	1.99	150	59.39 ± 3.24	0.38 ± 0.05
10762	32.1	3.68	273	(1.13 ± 0.11)E+2	(2.27 ± 0.14)E-6
67679.5	2.7	4.76	386		

Table A-2—Continued

Name (NTB) Date (TJD) Time (s UT)	R.A. (°) Decl. (°) Err. (°)	C_{max}/C_{min} (4.096 s) (8.192 s)	C_{min} (4.096 s) (8.192 s)	T_{50} (s) T_{90} (s)	P (ph cm^{-2} s^{-1}) F (erg cm^{-2}) (50–300 keV)
971117.65	44.3	1.73	134	33.79 ± 1.45	0.27 ± 0.05
10769	39.8	1.54	275	61.44 ± 5.51	(1.03 ± 0.06)E-6
56746.2	66.2	1.95	375		
971119.27	26.1	1.55	135	59.39 ± 1.45	0.25 ± 0.05
10771	75.6	2.91	321	89.09 ± 2.29	(1.58 ± 0.07)E-6
23922.9	17.3	3.89	440		
971121.50	279.0	6.86	136	3.07 ± 1.45	1.35 ± 0.06
10773	-68.3	10.20	273	8.19 ± 1.45	(1.08 ± 0.07)E-6
43993.3	1.3	9.14	386		
971123.47	21.5	1.61	136	...	0.28 ± 0.05
10775	18.4	1.47	261	6.14 ± 2.05	(1.40 ± 0.45)E-7
40929.5	15.6	1.74	370		
971125.04	148.6	...	...	...	0.17 ± 0.05
10777	17.6	1.45	365	6.14 ± 3.07	(1.31 ± 0.02)E-7
4239.6	10.6	1.24	471		
971127.43	41.8	1.21	168	...	0.17 ± 0.04
10779	63.1	...	...	2.05 ± 1.02	(4.49 ± 0.33)E-8
37360.9	17.7	...	...		
971201.24	253.6	3.12	152	...	0.55 ± 0.06
10783	52.1	2.28	280	3.07 ± 2.05	(1.89 ± 0.06)E-7
21035.2	8.3	1.68	395		
971201.25	47.0	1.20	169	10.24 ± 4.22	0.20 ± 0.05
10783	16.1	2.20	304	30.72 ± 13.35	(4.18 ± 0.52)E-7
22223.1	12.7	2.69	462		
971203.28	297.1	1.78	129	...	0.36 ± 0.05
10785	-46.7	2.79	259	7.17 ± 3.07	(2.54 ± 0.43)E-7
24285.4	8.3	2.42	407		
971207.78	96.1	2.25	129	23.55 ± 1.45	0.44 ± 0.05
10789	53.0	3.58	254	69.63 ± 4.22	(2.26 ± 0.15)E-6
67895.5	1.9	4.58	383		
971207.87	138.2	9.00	191	13.31 ± 1.45	1.45 ± 0.05
10789	71.0	8.18	384	16.38 ± 1.45	(9.22 ± 1.87)E-7
75489.5	7.5	6.20	509		
971210.88	288.9	...	...	2.05 ± 1.45	0.14 ± 0.05
10792	33.7	1.33	409	2.05 ± 1.45	(7.35 ± 0.25)E-8
76819.7	18.1	1.31	565		
971214.08	208.5	1.37	152	12.29 ± 1.45	0.19 ± 0.05
10796	54.5	1.92	261	38.91 ± 4.22	(7.37 ± 0.80)E-7
7476.4	7.1	2.80	413		

Appendix B

Catalog of Unknown 25–50 keV Transients

Table B-1 lists the physical parameters of the 25 non-triggered events detected in the off-line search that appear to be emission from soft gamma-ray repeaters (SGRs). Each entry in the table occupies a group of 3 lines. The first column gives the name of the non-triggered burst and the time of the peak flux of the event in terms of the Truncated Julian Day (TJD) number and the time of day expressed as seconds UT. The second column gives the best-fit source direction for the event in terms of equatorial right ascension and declination (J2000.0) expressed in decimal degrees along with the statistical uncertainty in the source direction. The full uncertainty in the best-fit source direction is the result of combining the statistical uncertainty in quadrature with a 6° random systematic uncertainty. The third column lists the T_{50} and T_{90} duration estimates in seconds. For some bursts, there is no T_{50} estimate; this indicates that the T_{90} duration was estimated by eye. The fourth column gives the peak flux and fluence estimates in DISCLA channels 1 and 2 (roughly 25–100 keV). For further information on these quantities, see section 5.3.

Table B-2 lists the physical parameters of the 50 non-triggered "low-energy" events that did not appear to be obviously GRBs, activity from SGRs, solar flares, or terrestrial phenomena. The description of the table is the same as for Table B-1.

Table B-1. Non-triggered SGR events

Name (NTB) Date (TJD) Time (s UT)	R.A. (°) Decl. (°) Err. (°)	T_{50} (s) T_{90} (s)	P (ph cm^{-2} s^{-1}) F (erg cm^{-2}) (25–100 keV)
930930.16	270.1	...	0.98 ± 0.14
9260	-14.3	1.02 ± 1.44	(2.75 ± 0.83)E-8
14295.2	6.6		
930930.37	280.7	...	0.86 ± 0.16
9260	-32.5	1.02 ± 1.44	(1.77 ± 0.59)E-8
32273.6	48.7		
930930.87	259.9	...	0.38 ± 0.10
9260	-17.8	7.17 ± 3.00	(6.63 ± 2.08)E-8
75878.6	51.3		
931005.95	271.4	...	1.35 ± 0.12
9265	-5.8	1.02 ± 1.44	(3.37 ± 0.80)E-8
82287.3	17.4		
931007.00	264.8	...	0.44 ± 0.11
9267	0.0	2.05 ± 1.44	(2.79 ± 1.50)E-8
499.9	40.5		
931009.93	268.9	...	1.61 ± 0.16
9269	-46.9	1.02 ± 1.44	(3.62 ± 1.17)E-8
80698.5	69.2		
941022.58	28.3	...	1.31 ± 0.12
9647	56.1	1.02 ± 1.44	(8.10 ± 6.12)E-8
50780.3	6.6		
961014.14	318.7	...	1.60 ± 0.23
10370	-17.8	1.02 ± 1.44	(3.34 ± 1.17)E-8
12269.8	9.7		
961101.45	269.6	...	0.83 ± 0.13
10388	-27.9	1.02 ± 1.44	(1.55 ± 0.42)E-8
39301.3	16.4		
961118.19	275.0	...	1.32 ± 0.14
10405	-19.5	1.02 ± 1.44	(3.43 ± 1.01)E-8
16909.5	10.2		
961118.20	269.9	...	5.33 ± 0.18
10405	-21.5	1.02 ± 1.44	(1.29 ± 0.45)E-7
17548.5	2.2		
961118.44	271.6	...	0.82 ± 0.16
10405	-22.7	1.02 ± 1.44	(1.81 ± 0.59)E-8
38617.3	10.3		
961118.46	268.5	...	0.67 ± 0.12
10405	-9.9	1.02 ± 1.44	(1.51 ± 0.39)E-8
40046.8	23.5		
961118.51	269.4	...	1.06 ± 0.16
10405	-26.1	1.02 ± 1.44	(2.63 ± 0.91)E-8
44478.7	26.2		
961119.24	270.7	...	9.65 ± 0.17
10406	-17.4	2.05 ± 1.44	(5.14 ± 2.29)E-7
21321.9	1.8		
961119.24	270.0	...	2.66 ± 0.13
10406	-18.8	1.02 ± 1.44	(9.00 ± 6.37)E-8
21534.9	4.0		
961119.27	273.8	...	1.11 ± 0.12
10406	-16.8	1.02 ± 1.44	(4.78 ± 1.99)E-8
23765.2	52.9		
961119.28	268.7	...	0.66 ± 0.16
10406	-29.0	1.02 ± 1.44	(1.30 ± 0.44)E-8
24249.5	34.2		
961119.30	267.2	...	2.39 ± 0.11
10406	-11.8	1.02 ± 1.44	(1.80 ± 0.38)E-7
26171.6	2.4		
961119.31	273.9	...	1.37 ± 0.10
10406	-8.7	2.05 ± 1.44	(1.45 ± 0.23)E-7
26958.0	6.0		

Table B-1—Continued

Name (NTB) Date (TJD) Time (s UT)	R.A. (°) Decl. (°) Err. (°)	T_{50} (s) T_{90} (s)	P (ph cm^{-2} s^{-1}) F (erg cm^{-2}) (25–100 keV)
970314.89	272.5	...	1.65 ± 0.21
10521	-17.1	1.02 ± 1.44	(3.51 ± 1.52)E-8
77124.8	4.3		
970407.65	280.2	...	1.39 ± 0.16
10545	3.4	1.02 ± 1.44	(5.20 ± 2.39)E-8
56337.6	13.6		
970419.33	275.7	...	2.18 ± 0.12
10557	-25.1	1.02 ± 1.44	(8.36 ± 2.82)E-8
28894.4	16.6		
970907.18	267.2	...	1.95 ± 0.13
10698	-20.1	1.02 ± 0.00	(7.54 ± 3.14)E-8
15779.0	4.7		
971113.15	261.2	...	1.00 ± 0.15
10765	-13.9	1.02 ± 1.44	(3.33 ± 1.10)E-8
13304.0	49.2		

Table B-2. Non-triggered "unknown" events

Name (NTB) Date (TJD) Time (s UT)	R.A. (°) Decl. (°) Err. (°)	T_{50} (s) T_{90} (s)	P (ph cm^{-2} s^{-1}) F (erg cm^{-2}) (25–100 keV)
911211.33	135.4	...	0.73 ± 0.15
8601	-41.5	3.07 ± 1.44	(6.09 ± 2.87)E-8
29060.2	61.0		
920314.62	139.2	(1.01 ± 0.01)E+2	0.59 ± 0.08
8695	-34.3	(1.61 ± 0.25)E+2	(5.73 ± 0.58)E-7
53902.4	26.3		
920419.02	189.9	...	0.75 ± 0.12
8731	-46.9	4.10 ± 1.44	(4.74 ± 0.89)E-8
2258.0	18.1		
920601.30	313.5	5.12 ± 1.45	0.82 ± 0.13
8774	-59.8	14.34 ± 2.90	(1.94 ± 0.46)E-7
26654.8	18.1		
920612.16	102.4	24.58 ± 5.22	0.28 ± 0.13
8785	-44.6	57.34 ± 4.22	(3.46 ± 0.15)E-7
13954.2	3.9		
920723.91	48.2	7.17 ± 4.22	0.52 ± 0.10
8826	46.4	13.31 ± 2.29	(5.53 ± 0.65)E-8
78910.6	36.8		
921003.83	186.0	...	0.49 ± 0.12
8898	-0.8	1.02 ± 1.44	(1.76 ± 0.48)E-8
72114.3	27.7		
921011.29	49.7	...	0.61 ± 0.21
8906	35.2	11.26 ± 3.00	(8.39 ± 1.34)E-8
25597.1	13.4		
921016.95	157.7	...	0.57 ± 0.12
8911	-22.2	1.02 ± 1.44	(1.78 ± 0.52)E-8
82642.0	33.3		
921025.57	133.2	...	0.68 ± 0.13
8920	14.8	1.02 ± 1.44	(1.93 ± 0.57)E-8
49368.2	22.0		
921106.87	272.6	2.05 ± 28.75	0.40 ± 0.11
8932	48.0	6.14 ± 17.50	(7.05 ± ****)E-9
75948.2	42.5		
921114.46	88.9	...	0.52 ± 0.16
8940	-12.9	2.05 ± 1.44	(1.44 ± 0.36)E-8
40270.0	134.5		
921225.33	29.5	...	0.32 ± 0.10
8981	20.1	5.12 ± 2.00	(3.51 ± 0.64)E-8
28694.7	54.3		
930109.31	57.3	...	0.58 ± 0.15
8996	-29.6	1.02 ± 1.44	(7.41 ± 1.77)E-9
26927.2	67.8		
930309.60	168.0	...	0.40 ± 0.09
9055	3.5	3.07 ± 1.44	(5.11 ± 3.01)E-8
52598.9	31.6		
930328.55	162.9	28.67 ± 1.45	0.52 ± 0.11
9074	32.7	65.54 ± 12.33	(4.37 ± 0.36)E-7
48368.3	15.8		
930606.65	141.5	4.10 ± 1.45	0.55 ± 0.08
9144	12.4	9.22 ± 1.45	(1.96 ± 0.50)E-7
56465.5	10.3		
930612.78	261.4	68.61 ± 5.22	0.95 ± 0.15
9150	-40.5	(1.88 ± 0.18)E+2	(1.91 ± 0.13)E-6
67963.5	5.9		
930623.08	24.1	...	0.80 ± 0.13
9161	-50.3	2.05 ± 1.44	(3.75 ± 1.56)E-8
6953.1	59.5		
930812.49	237.4	6.14 ± 1.45	0.61 ± 0.12
9211	43.0	19.46 ± 5.22	(3.29 ± 0.70)E-7
42827.9	2.3		

Table B-2—Continued

Name (NTB) Date (TJD) Time (s UT)	R.A. (°) Decl. (°) Err. (°)	T_{50} (s) T_{90} (s)	P (ph cm^{-2} s^{-1}) F (erg cm^{-2}) (25–100 keV)
930825.48	330.9	...	0.31 ± 0.08
9224	63.5	6.14 ± 2.00	(1.38 ± 0.56)E-7
41775.3	52.3		
930905.00	15.1	11.26 ± 1.45	0.47 ± 0.10
9235	-58.5	30.72 ± 4.22	(3.04 ± 0.30)E-7
800.9	14.7		
931011.97	303.9	26.62 ± 1.45	0.69 ± 0.09
9271	-19.5	70.66 ± 4.58	(1.11 ± 0.13)E-6
84430.0	9.0		
931108.42	182.9	...	1.23 ± 0.11
9299	49.3	24.58 ± 6.00	(2.22 ± 0.30)E-7
36823.7	5.4		
931110.79	95.5	...	0.72 ± 0.14
9301	7.9	3.07 ± 1.44	(3.67 ± 0.81)E-8
68393.1	14.5		
931115.09	36.8	...	0.64 ± 0.11
9306	-21.9	7.17 ± 3.00	(1.61 ± 0.39)E-7
8035.5	11.1		
931116.78	123.2	...	0.77 ± 0.13
9307	34.0	4.10 ± 1.44	(7.64 ± 3.03)E-8
68241.6	9.2		
931202.75	304.7	...	0.72 ± 0.13
9323	-67.9	4.10 ± 2.05	(4.18 ± 1.91)E-8
65493.1	18.6		
931222.27	294.1	...	0.57 ± 0.16
9343	37.0	1.02 ± 1.44	(1.98 ± 0.78)E-8
23403.7	19.3		
940716.46	236.0	...	1.20 ± 0.17
9549	36.2	1.02 ± 1.44	(3.30 ± 2.15)E-8
40061.1	63.3		
940808.67	181.6	...	0.44 ± 0.09
9572	-42.8	4.10 ± 2.05	(9.51 ± 2.99)E-8
57922.7	14.3		
940927.72	246.1	73.73 ± 18.46	0.50 ± 0.10
9622	-27.5	(1.63 ± 0.05)E+2	(8.42 ± 0.72)E-7
62647.5	7.7		
941012.61	181.5	...	0.41 ± 0.14
9637	-33.5	4.10 ± 2.05	(2.45 ± 0.50)E-8
53364.9	41.0		
941208.93	292.8	...	0.69 ± 0.13
9694	31.1	8.19 ± 4.10	(9.34 ± 3.73)E-8
80558.3	6.8		
941211.98	239.9	17.41 ± 1.45	0.71 ± 0.10
9697	33.5	26.62 ± 1.45	(2.16 ± 0.37)E-7
85227.7	28.5		
941213.55	307.6	2.05 ± 1.45	0.78 ± 0.11
9699	-27.4	4.10 ± 1.45	(2.39 ± 0.51)E-7
47641.8	48.4		
950523.47	276.7	...	0.69 ± 0.13
9860	43.5	11.26 ± 4.10	(1.53 ± 0.49)E-7
40660.1	13.5		
951024.89	290.7	...	0.68 ± 0.13
10014	69.0	4.10 ± 2.05	(5.39 ± 3.51)E-8
76933.3	11.6		
951025.30	156.2	10.24 ± 1.45	0.58 ± 0.14
10015	2.0	43.01 ± 17.04	(3.82 ± 0.70)E-7
26544.3	5.4		
951122.87	245.2	...	0.59 ± 0.17
10043	22.8	1.02 ± 1.44	(1.94 ± 0.77)E-8
75532.5	61.6		

Table B-2—Continued

Name (NTB) Date (TJD) Time (s UT)	R.A. (°) Decl. (°) Err. (°)	T_{50} (s) T_{90} (s)	P (ph cm^{-2} s^{-1}) F (erg cm^{-2}) (25–100 keV)
960407.23	147.9	...	1.98 ± 0.18
10180	5.6	9.22 ± 3.07	(3.49 ± 0.95)E-7
20052.2	4.8		
960706.25	342.2	13.31 ± 1.45	2.03 ± 0.17
10270	-55.5	38.91 ± 6.48	(3.69 ± 0.59)E-7
21745.9	3.7		
961204.66	121.2	...	0.62 ± 0.17
10421	35.0	4.10 ± 2.05	(6.14 ± 3.73)E-8
57316.6	82.4		
970124.49	94.3	...	0.82 ± 0.12
10472	-17.0	10.24 ± 3.00	(1.81 ± 0.36)E-7
42852.6	23.0		
970414.23	168.2	...	0.71 ± 0.12
10552	39.5	4.10 ± 2.00	(9.67 ± 3.10)E-8
20025.5	39.9		
970529.59	233.8	...	0.68 ± 0.10
10597	2.5	6.14 ± 2.00	(1.95 ± 0.45)E-7
51705.0	15.8		
970619.67	344.5	...	0.88 ± 0.10
10618	63.4	18.43 ± 6.00	(3.89 ± 0.68)E-7
58235.1	4.3		
970829.33	14.3	11.26 ± 1.45	1.88 ± 0.18
10689	-12.6	26.62 ± 2.29	(3.92 ± 0.91)E-7
29063.4	6.2		
971019.66	230.4	6.14 ± 1.45	1.29 ± 0.13
10740	67.7	18.43 ± 10.29	(3.49 ± 0.84)E-7
57426.1	6.5		
971217.19	118.8	...	1.51 ± 0.21
10799	-28.6	4.10 ± 1.44	(6.92 ± 1.58)E-8
16615.7	10.2		

Appendix C

"A Search for Nontriggered Gamma-ray Bursts in the BATSE Data Base"

This appendix is a self-contained paper entitled, "A Search for Nontriggered Gamma-ray Bursts in the BATSE Data Base." It has appeared in the *Astrophysical Journal* (Kommers et al. 1997).

C.1 Abstract

We describe a search of archival data from the Burst and Transient Source Experiment (BATSE). The purpose of the search is to find astronomically interesting transients that did *not* activate the burst detection (or "trigger") system onboard the spacecraft. Our search is sensitive to events with peak fluxes (on the 1.024 s time scale) that are lower by a factor of ~ 2 than can be detected with the onboard burst trigger. In a search of 345 days of archival data, we detected 91 events in the 50–300 keV range that resemble classical gamma ray bursts but that did not activate the onboard burst trigger. We also detected 110 low-energy (25–50 keV) events of unknown origin which may include activity from SGR 1806−20 and bursts and flares from X-ray binaries. This paper gives the occurrence times, estimated source directions, durations, peak fluxes, and fluences for the 91 gamma ray burst candidates. The direction and inten-

sity distributions of these bursts imply that the biases inherent in the onboard trigger mechanism have not significantly affected the completeness of the published BATSE gamma ray burst catalogs.

C.2 Introduction

Since 1991 April 19 the Burst and Transient Source Experiment (BATSE) on the *Compton Gamma Ray Observatory* (*CGRO*) has been detecting gamma ray bursts (GRBs) and other high-energy transients with unprecedented sensitivity (Fishman et al. 1989; Fishman et al. 1994; Meegan et al. 1996). The 1122 GRBs in the 3B catalog show an isotropic angular distribution and a spatially inhomogeneous intensity distribution (Meegan et al. 1992; Meegan et al. 1996). Despite extensive analysis, however, the origin of GRBs remains unknown; see recent reviews by Fishman & Meegan (1995), Briggs (1995), and Hartmann (1995).

The detection of GRBs and other high-energy transients with BATSE is controlled by a real-time burst detection algorithm running onboard the spacecraft (Fishman et al. 1989). The onboard computer continuously monitors the count rates in each of the eight Large Area Detectors (LADs). When the count rates exceed a certain threshold, the computer signals a "burst trigger" and data are collected at high temporal and spectral resolution for a limited time interval. Even in the absence of a burst trigger, however, data are recorded at lower resolution in the continuous data types. For most of the mission, the criteria for a burst trigger have been that the 50–300 keV count rates in two detectors simultaneously increase by more than 5.5 times the expected root-mean-square background fluctuations on any of three time scales: 64 ms, 256 ms, or 1024 ms. The average background rate for each detector is recomputed every 17.408 s (Fishman et al. 1989).

By definition all of the GRBs listed in the 1B, 2B, and 3B catalogs satisfy the requirements for a burst trigger (Fishman et al. 1994; Meegan et al. 1996). Other transient phenomena that are unrelated to GRBs can also lead to a burst trigger.

Examples include solar flares, terrestrial magnetospheric disturbances, bursts and flares from X-ray binaries, and activity from soft gamma ray repeaters (SGRs). Such events are classified appropriately by the BATSE team.

A GRB or other transient phenomenon may have characteristics such that it does *not* lead to a burst trigger onboard the spacecraft but it nevertheless leaves a statistically significant signal in the continuous data. For example, a GRB or other transient may be too faint to achieve the necessary statistical significance for a trigger; it may have a time profile that biases the onboard background average; or it may have too few counts in the 50–300 keV range.

A burst can also occur while the onboard trigger is disabled for technical reasons. Following a burst trigger, the high resolution data collected during the burst accumulation interval are gradually telemetered to the ground during the following 90 minutes. During this read out period the onboard burst trigger is disabled on the 256 ms and 1024 ms time scales, and the 64 ms threshold is set to the maximum rate of the burst being read out. The onboard burst trigger is also disabled when the spacecraft passes through regions with a high probability of triggering on atmospheric particle precipitation events (Fishman et al. 1994).

In this paper, we describe a retrospective search of the archival continuous data from BATSE for statistically significant GRBs and other transients that did *not* cause a burst trigger onboard the spacecraft. A search for these "nontriggered" (or "untriggered") events in the 50–300 keV range is expected to find GRBs that are generally fainter than those cataloged previously. A concurrent search for nontriggered events in the lowest discriminator channel (25–50 keV) is expected to find activity from other astronomical sources, including bursts and flares from X-ray binaries and activity from SGRs. This ongoing project is an extension of previous work by Rubin et al. (1993), Van Paradijs et al. (1993), and Kommers et al. (1996). Other retrospective searches for GRBs in the BATSE data (using techniques different from those described here) have been discussed by Skelton & Mahoney (1994) and by Young et al. (1996).

C.3 Search Algorithm

A retrospective search of archival data can take advantage of burst detection algorithms that would have been impractical to implement onboard the spacecraft. The choice of a detection scheme to look for nontriggered events therefore involves tradeoffs between the detection efficiency of the method for a given class of events and the resources (both computational and human) needed to implement it. In this section we describe a search algorithm which is loosely based on the one used onboard the spacecraft but which has proved more sensitive. The next section will discuss its efficiency for detecting transients with certain characteristics.

We will refer to all events detected by our off-line search of archival data as "laboratory triggers." The events previously detected by the onboard burst trigger mechanism will be called "onboard triggers." Some onboard triggers will be flagged by our off-line search and so they will also be laboratory triggers. Events that were detected *only* by our off-line search will be called "nontriggered events."

For most of the mission the onboard trigger criterion has required that the count rate in two detectors simultaneously increase by at least $5.5\sigma_B$ above the nominal background level, where σ_B is the standard deviation of the expected background counts due to counting statistics. As a result, the BATSE detectors provide anisotropic sky exposure over short time periods (Fishman et al. 1989; Fishman et al. 1994). The cosine-like change in the detectors' effective area with source viewing direction causes the onboard trigger to be less sensitive to faint bursts with directions directly in front of one of the detectors than to ones with directions mid-way between two detector normals (Brock et al. 1991). For example, a $10\sigma_B$ event occurring directly in front of a detector may produce only a $3.5\sigma_B$ signal in the second most brightly illuminated detector and it would thus fail to trigger onboard. On the other hand, the same event incident along a direction mid-way between two detector normals would register approximately $7.1\sigma_B$ in both detectors and would comfortably cause an onboard trigger.

The onboard trigger mechanism relies on a background rate that is computed during a 17.408 s time interval occurring before the time bin being tested. A rising or falling background can therefore bias the background estimate to be too low or too high, respectively. A slowly rising transient may itself bias the background estimate upwards to such an extent that it fails to cause an onboard burst trigger, even though it is otherwise intense enough to be above the minimum detection threshold.

Our retrospective search procedure partially combats the directional detection anisotropy and the rising/falling background bias. We form a time series to be searched by combining the relevant energy channels from the DISCLA data. This data type provides the count rates in each detector integrated over 1024 ms time bins. Four discriminator energy channels (numbered 1 through 4) are available: 25–50 keV, 50–100 keV, 100–300 keV, and > 300 keV. When searching for GRBs, the sum of channels 2 and 3 (50–300 keV) gives optimal sensitivity. When searching for low-energy transients such as bursts and flares from X-ray binaries or SGRs the lowest energy channel (channel 1, 25–50 keV) is most sensitive. A sum of channels 1,2, and 3 provides a further "catch-all" search. After summing the appropriate energy channels, the time series are rebinned in time (if necessary) to search on time scales longer than the 1024 ms DISCLA sampling period. The resulting time series are then searched sequentially to see if any data meet our laboratory trigger criteria.

To signal a laboratory trigger, we first determine from the time series being searched a nominal background level for each detector. To estimate $B_d(k)$, the number of background counts expected in detector d for the time bin k, we use a linear fit to the data in time bins $k-N_b, \ldots, k-1$ and $k+1+N_b, \ldots, k+2N_b$. Here the number of background bins, N_b, is specified for each time scale. Unlike the onboard trigger, the off-line search uses data before and after the time bin being tested.[1] This method

[1]The bin, k, being tested is not centered in the gap of N_b bins which separates the fitted intervals. This somewhat arbitrary choice evolved out of various triggering schemes which were tried, including one where the background was always estimated based on the N_b bins immediately prior to the one being tested. The scheme chosen performed well on 14 days of data that were used to test various

reduces the bias (discussed above) caused by slowly rising or falling background levels.

Temporally contiguous data are not always available because of telemetry gaps and spacecraft passages through regions of high particle flux, such as the South Atlantic Anomaly (SAA). In such cases the background estimate discussed here cannot be formed. We only test bins for which we can estimate the background with the above procedure, so our search is not sensitive to bursts that occur during the N_b bins after, or the $2N_b$ bins before, a data gap.

Let $C_d(k)$ be the measured number of counts in time bin k for detector d. We define the "significance" of that detector to be $S_d(k) = [C_d(k) - B_d(k)]/\sqrt{B_d(k)}$. Our laboratory trigger criteria are that the two greatest values of the 8 significances $S_d(k)$, call them s_1 and s_2, must be such that $s_1 \geq s_2 \geq M$ and $s_1 + s_2 \geq \Sigma$. These criteria ensure that at least two detectors simultaneously experience a statistically significant upward fluctuation, but they are also more sensitive to events incident along detector normals than the onboard criteria.

The values chosen for M, Σ, and N_b for the searches reported here are shown in Table C-1. They were chosen to keep the actual number of detections per day of data searched (due to the activity of real sources) at a manageable level of about 20 per day.

A more sensitive search could be conducted using other laboratory trigger criteria. For example, the effective detector area achieved by adding the rates in each set of 3 contiguous detectors would produce time series with higher signal-to-noise ratios for activity from real sources. The caveat to a more sensitive search is the corresponding increase in the rate of "false triggers" due to solar activity, variability from X-ray binaries, particle precipitation events, Earth occultation steps, and phosphorescence spikes (which occur when high-energy particles interact in the detectors). During outbursts of bright X-ray binaries, our laboratory trigger has detected hundreds of events per day due to variability from Vela X-1, A0535+26, and GRO J0422+32.

---

laboratory trigger criteria.

For our laboratory trigger criteria, the number of detections expected from statistical fluctuations alone can be estimated by considering the "phase space" defined by s_1 and s_2. The number of counts in each time bin of the DISCLA data type is large enough that the Poisson statistics can be treated in the Gaussian approximation, so that the $S_d(k)$ are independent and normally distributed with zero mean and unit variance. The laboratory trigger criteria define a region A in the (s_1, s_2) plane in which measured values s_1^* and s_2^* will be flagged by our search. This area is sketched in Figure C-1.

The probability P_{stat} that a randomly selected set of 8 significances S_d will meet or exceed the laboratory trigger criteria is estimated by first integrating the bivariate normal distribution (centered on the origin) over the allowed area A in the (s_1, s_2) plane. Next, we multiply by 8 ways to select the most significant detector (s_1) and the remaining 7 ways to select the second most significant (s_2). The final expression is

$$P_{stat} = \left[\iint_A \frac{1}{2\pi} \exp\left(-\frac{s_1^2 + s_2^2}{2} \right) ds_1 \, ds_2 \right] \times 7 \times 8 \div 2. \qquad \text{(C.1)}$$

If there are N time bins searched per day, the number of detections expected from purely statistical fluctuations is $P_{stat} \times N$ per day. This quantity is shown in the last column of Table C-1 for a representative value of $N = 5.0 \times 10^4$. Although the searches are not statistically independent, we would expect no more than 8 detections due solely to statistical fluctuations in a search of 100 days of data. Furthermore only a fraction of these will have properties consistent with astronomical source activity.

In practice we find many more laboratory triggers than can be expected from purely statistical fluctuations. This is because the time series we are searching are not Poissonian. They are dominated by the activity of real sources. Astronomical objects, the sun, terrestrial photon sources, and the interaction of particles in the detectors contribute to the count rates. Figure C-2 shows an integral distribution of $S_d(k)$ for a single detector ($d = 0$) taken from a search of one day of data on the 1.024 s time scale. For comparison, the expectation from a normal distribution with

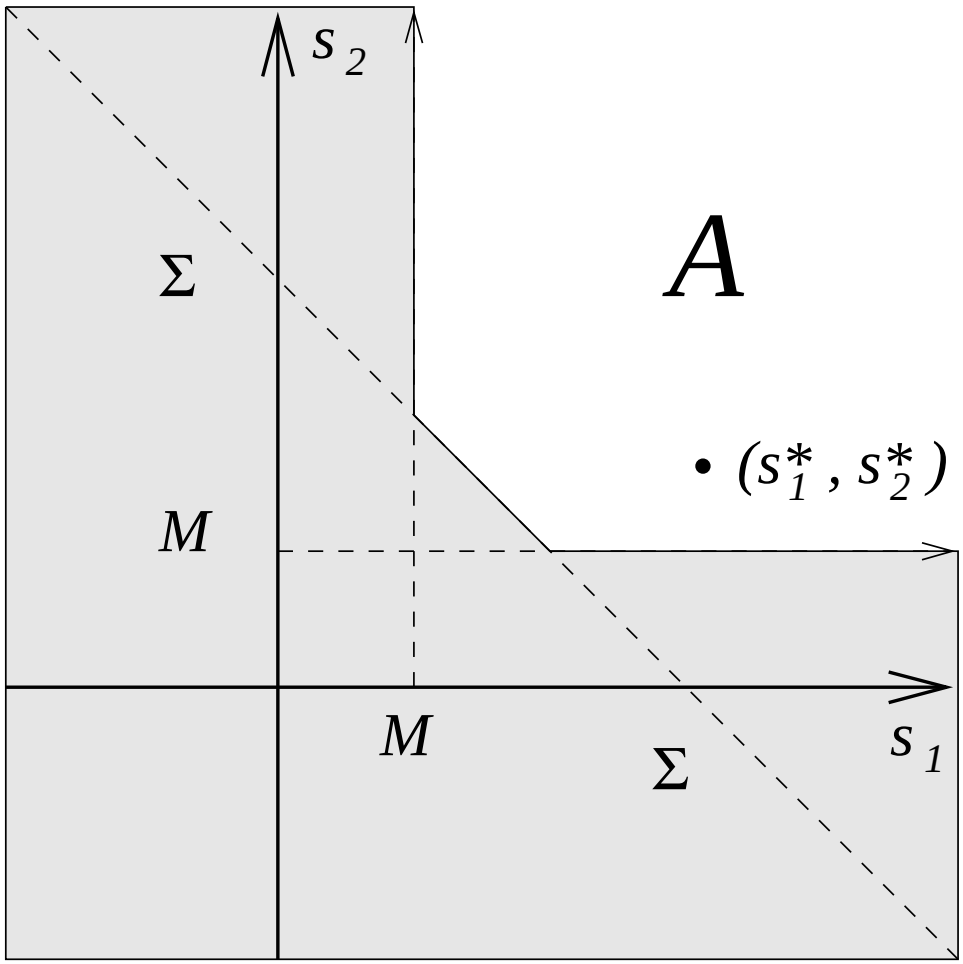

Figure C-1 Schematic diagram of the laboratory (off-line search) trigger criteria. If the significances of the fluctuations measured in the two most brightly illuminated detectors lie in the non-shaded area A, our search will flag that time bin as a laboratory trigger.

zero mean and unit variance is also shown. The excess over what is expected from a normal distribution reflects both deficiencies in the background estimation and the activity of real sources, although no laboratory triggers were detected by our off-line search in this detector on the day shown.

C.4 Sensitivity

The search strategy described above is expected to detect bursts that were fainter than those detected by the onboard trigger mechanism. In this section, we estimate the efficiency of the search algorithm for detecting events with certain physical characteristics. In general the ability of our search strategy to detect an event depends on its peak flux (as measured on the search time scale), its time profile, the background levels in the detectors, and the spacecraft orientation with respect to the source direction. Here we will estimate the trigger efficiency and sky exposure of our off-line search strategy assuming an event profile for which a single time bin completely determines our ability to detect the event. The effects of a more complicated time profile are then considered separately for a simplified case of "slow-rising" events that would have biased the onboard background estimate.

C.4.1 Trigger Efficiency

We define the trigger efficiency $E(P, \nu, \alpha, \delta, t)$ to be the probability that an event with given physical characteristics will satisfy the laboratory trigger criteria. The event is modeled in terms of its peak flux on the time scale of the search (P), power-law photon spectral index (ν), source direction in equatorial coordinates (α, δ), and time of occurrence during the mission (t). The background rates in the detectors, the spacecraft orientation, and the geographic position of the spacecraft must also be known to estimate E, but these quantities are known from the data once t is specified. The time profile of the event is considered to be a square pulse that occupies a single time bin.

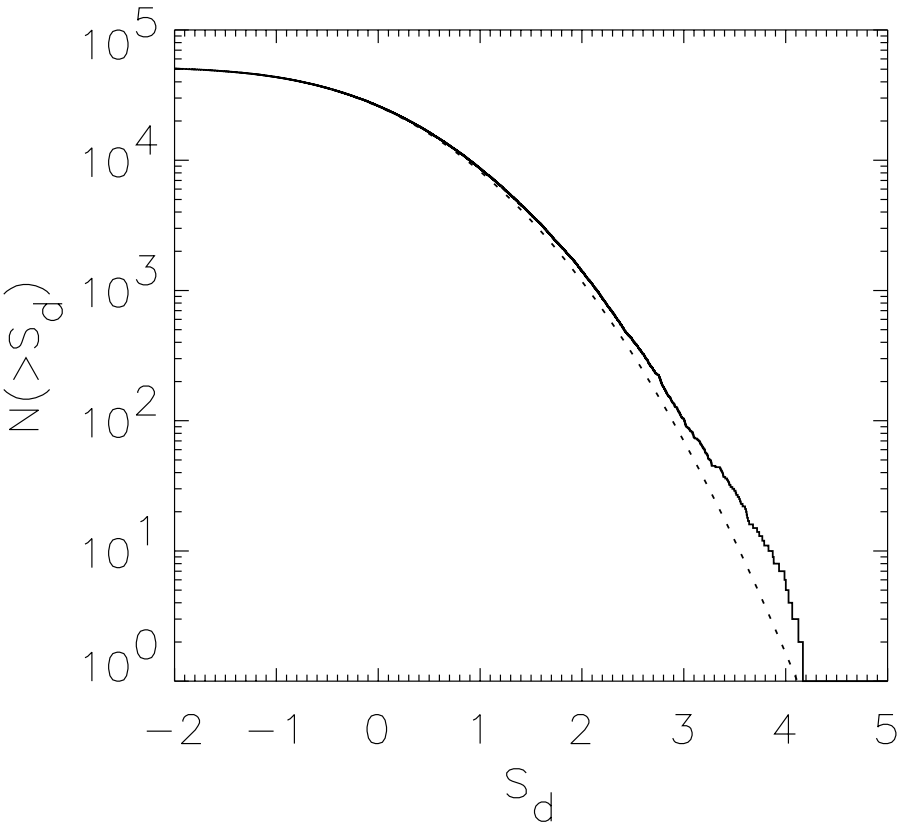

Figure C-2 Integral distribution of $S_d(k)$ for the data of May 27, 1993 (TJD 9135) in detector 0. The dotted line shows the expectation for a Gaussian distribution with zero mean and unit variance. The excess counts are attributed both to deficiencies in the background estimate and to the activity of real sources.

For a particular spacecraft orientation and position, the mean count rates expected from an event with given values of P, ν, α, and δ can be computed by adding the "direct" count rates found from the BATSE instrument response matrix to the "scattered" count rates expected from the scattering of incident photons by the Earth's atmosphere. The instrument response matrices and atmospheric scattering model are described further in Pendleton et al. (1995) and Meegan et al. (1996).[2] The resulting total count rates are multiplied by the time binning interval to obtain the expected counts (above background) in a single bin of the time series for each detector; we denote these quantities by C_d^*. The expected background counts, B_d, are estimated from the measured rates at time t and the expected significances in the detectors are calculated as $S_d^* = C_d^*/\sqrt{B_d}$. Let s_1^* and s_2^* be the greatest and second greatest of the S_d^*, respectively.

The trigger efficiency, E, is the probability that a measurement of a pair (s_1, s_2) will meet the laboratory trigger criteria. The counting statistics imply that our measurement, (s_1, s_2), is drawn from a bivariate normal distribution with unit variances centered on the expected significances, (s_1^*, s_2^*). The probability that we detect the given event is therefore estimated by integrating this distribution over the area, A (shown in Figure C-1), in which the trigger criteria are satisfied:

$$E = \iint_A \frac{1}{2\pi} \exp\left[-\frac{(s_1 - s_1^*)^2}{2}\right] \exp\left[-\frac{(s_2 - s_2^*)^2}{2}\right] ds_1\, ds_2. \qquad \text{(C.2)}$$

We evaluate E on a three-dimensional grid composed of 9 peak fluxes, 252 source directions, and 4992 times per orbital precession period of *CGRO* (i.e., every 15 minutes). The photon spectral index is fixed at $\nu = 2.0$. The 9 peak fluxes were chosen to span an intensity range where the efficiency varies significantly. The 252 source

[2]The detector response and atmospheric scattering matrices used in this work were provided by the BATSE team. We also made use of some elements of the BACODINE burst location code (Scott Barthelmy, private communication) which is based on an early version of the BATSE LOCBURST code.

directions are nearly isotropically distributed on the unit sphere (Tegmark 1996). The 4992 times per orbital precession period were chosen to thoroughly sample the range of background variations. For points where the source direction is behind the Earth or no searchable data are available, E is set to zero. This calculation must be repeated for each time scale and energy channel combination in our search.

Figure C-3 shows E as a function of P for events searched on the 1024 ms and 4096 ms time scales in the 50–300 keV range. The source directions and times of occurrence have been averaged. For comparison, the trigger efficiency on the 1024 ms time scale from the BATSE 1B catalog is also shown (Fishman et al. 1994).

For the 1024 ms time scale, Figure C-3 shows that our search is nearly complete near the BATSE threshold ($\sim$ 0.2 ph cm^{-2} s^{-1}). Our off-line search should detect about 50% of events with peak fluxes lower by a factor of $\sim$ 2 than the onboard 50% completeness limit. For events that maintain their peak flux for at least 4 s or 8 s, the searches on the 4096 ms and 8192 ms time scales can reach even lower peak fluxes. The values of $E(P)$ shown in Figure C-3 vary by only a few percent between spacecraft orbital precession periods (52 days for *CGRO*).

The sky coverage of our search is determined by the angular distribution of $E(P, \nu, \alpha, \delta)$, where P and ν are fixed and t has been averaged. If T is the total time period covered by the data searched, then $T \times E(P, \nu, \alpha, \delta)$ gives the total amount of time that our search was sensitive to an event with the given intensity, spectral index, and source direction. In practice our search covers many orbits, so the dependence on the equatorial right ascension (α) averages out. Figure C-4 shows the sky exposure as a function of declination (δ) for events with $P \geq 0.5$ ph s^{-1} cm^{-2} on the 1024 ms time scale and $\nu = 2.0$. The decreased exposure near the celestial equator is due to Earth blockage. The Southern Hemisphere gets less exposure than the Northern Hemisphere due to passages through the SAA.

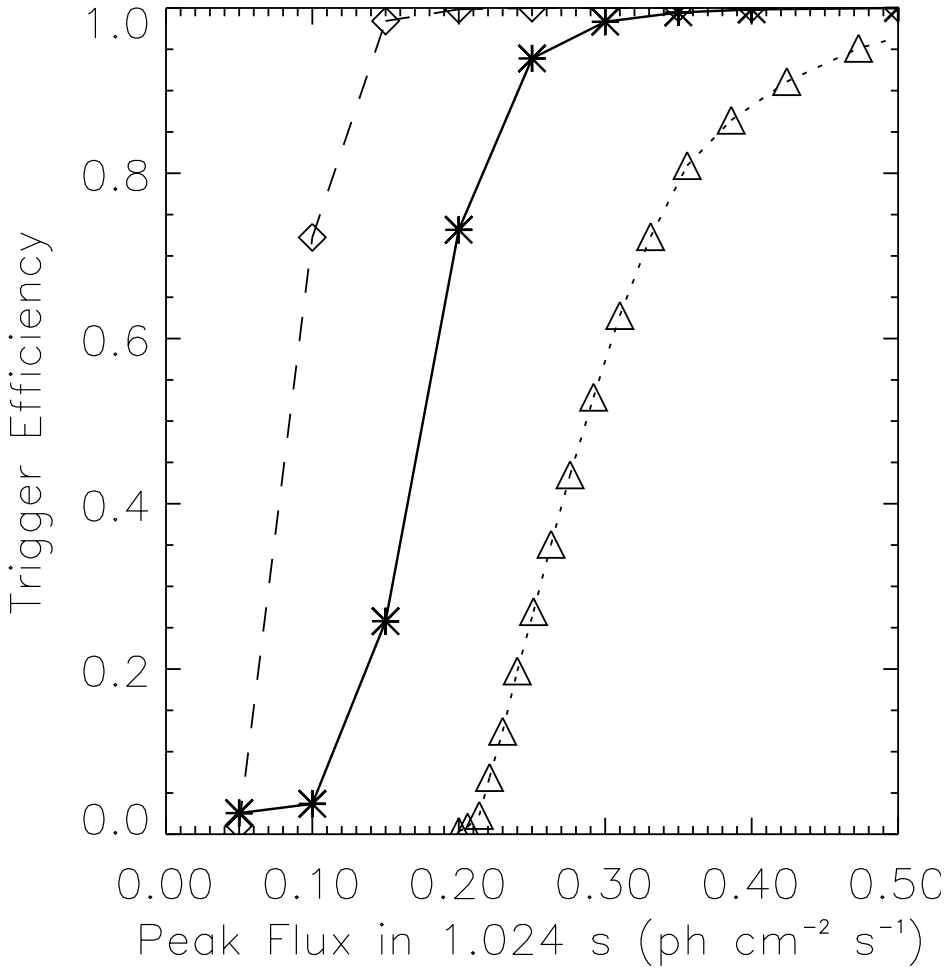

Figure C-3 Off-line trigger efficiency. The solid line shows the efficiency of our off-line search algorithm for detecting an event with a given peak flux in the 50–300 keV range on the 1024 ms time scale. The long-dashed line shows the trigger efficiency for our off-line search on the 4096 ms time scale. The short-dashed line shows the trigger efficiency from the 1B catalog.

Table C-1. Parameters of the time series formed from the DISCLA data.

Search	Time Bin Duration (s)	Energy Channels	M	Σ	N_b	Statistical Detections per day
a	1.024	1	2.5	4.0	20	0.021
b	1.024	2+3	2.5	4.0	20	0.021
c	1.024	1+2+3	2.5	4.0	20	0.021
d	4.096	1	2.5	4.0	15	0.005
e	4.096	2+3	2.5	4.0	15	0.005
f	8.192	1	2.5	4.0	5	0.002
g	8.192	2+3	2.5	4.0	5	0.002

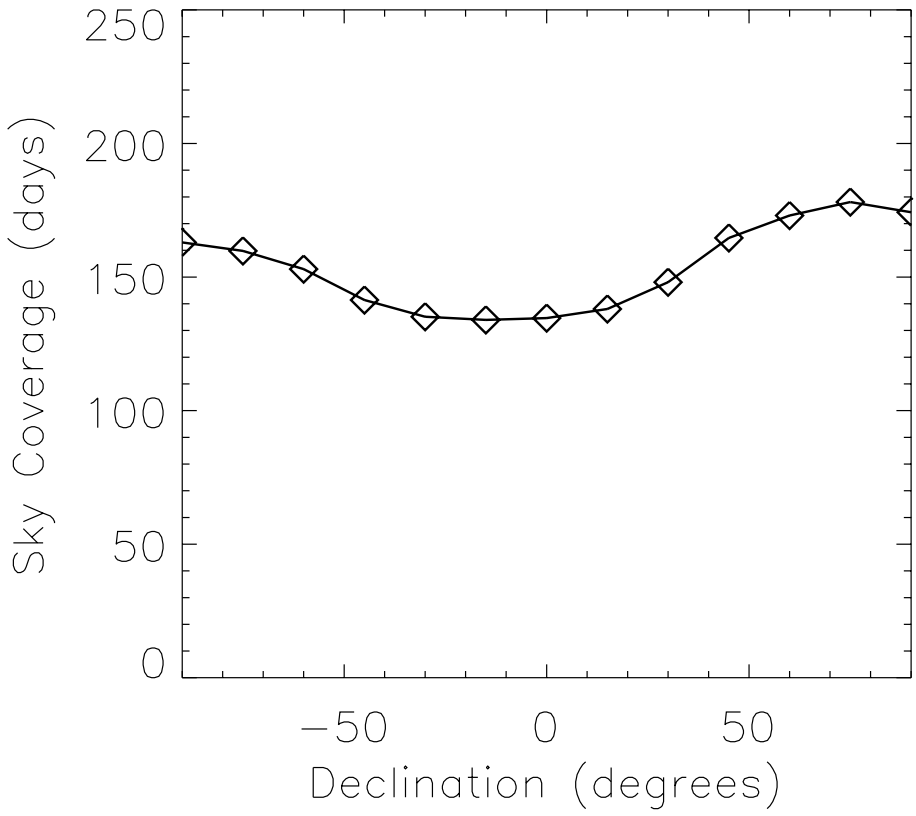

Figure C-4 Sky exposure for our 50-300 keV off-line trigger search as a function of declination, assuming a search spanning 345 days.

C.4.2 Sensitivity to "Slow-risers"

The chances that our search detects a given event also depend on its time profile in our time series. For example, an event with a peak flux near the detection threshold that is shaped like a square pulse occupying N time bins will have N statistical chances to meet or exceed the trigger criteria. In such a case the trigger efficiency calculated above will be an underestimate.

On the other hand, the event profile may be such that it biases the nominal background rate used by the search algorithm and artificially raises the detection threshold. Then the trigger efficiency calculated above is an overestimate. This case is more serious as it implies that the search could miss a population of such events even though their peak flux is well above the nominal minimum detection threshold. Both the onboard trigger mechanism and our off-line search are subject to this limitation.

The most problematic time profile is one which both rises and decays slowly on a time scale long compared to the background averaging with no significant rapid variability. This case is difficult to distinguish from background variations arising from the spacecraft environment. Neither our search nor the onboard trigger has appreciable sensitivity to events of this type. They are even unlikely to be evident in a close visual inspection of the count rates.

An event that rises slowly and then either falls off quickly or subsequently goes into a more complicated profile can usually be identified as a transient, however. We will call such an event a "slow-riser." The onboard trigger mechanism has particular trouble with slow-risers because it can only base its background estimate on count rates measured over some 17.408 s interval that occurred some time during the 34.8 s before the time bin being tested. Lingenfelter & Higdon (1996) have discussed this effect for the onboard burst trigger. Here we estimate the extent to which our off-line search algorithm is sensitive to slow-risers.

The profile of an idealized slow-riser is shown in Figure C-5. The event is characterized by a peak amplitude, s, measured in sigmas above background, and a slope, r, measured in sigmas per second, where one sigma is one standard deviation of the

expected background fluctuations. The total duration of the event is s/r. To estimate our sensitivity to such events, we generated a grid of peak amplitudes and a grid of slopes. For each peak amplitude and slope, we generated 5000 events with a background level of 1000 counts s^{-1} and Poisson noise to mimic the counting statistics. We then used our detection algorithm to find the fraction of events that met our off-line trigger threshold and the fraction of events that met the onboard trigger threshold.

The results are shown in Figure C-6, which shows contours of detection probability for (idealized) events with maximum significance, s, and slope, r, when searching on the 1024 ms time scale. Evidently our laboratory detection algorithm is more sensitive to slow-risers than the onboard trigger mechanism. This is due both to the lower detection threshold and to the use of data before and after the time bin being tested when forming the background estimate. Slow-risers with no subsequent variability that are both longer than about 30 s and fainter than 5σ (about 0.3–0.5 photons cm^{-2} s^{-1} in the 50–300 keV range) are unlikely to be found by our 1024 ms off-line search. The 4096 ms and 8192 ms searches are sensitive to longer events, however.

The idealized profile used for these estimates may not be representative of the faintest or longest transients since the typical profiles of those events are not known a priori. The simple case presented here shows that our search algorithm is more sensitive to *some* slow-rising bursts.

C.5 Classification and Analysis of Events

We visually inspect each laboratory trigger flagged by our off-line search to separate the events into useful categories.

We first examine plots of the count rates in each of the eight detectors at the time of the laboratory trigger. This information is adequate to exclude from further analysis the majority of features in the data that are not interesting in the context of our search. Common examples of such features are occultation steps, phosphorescence

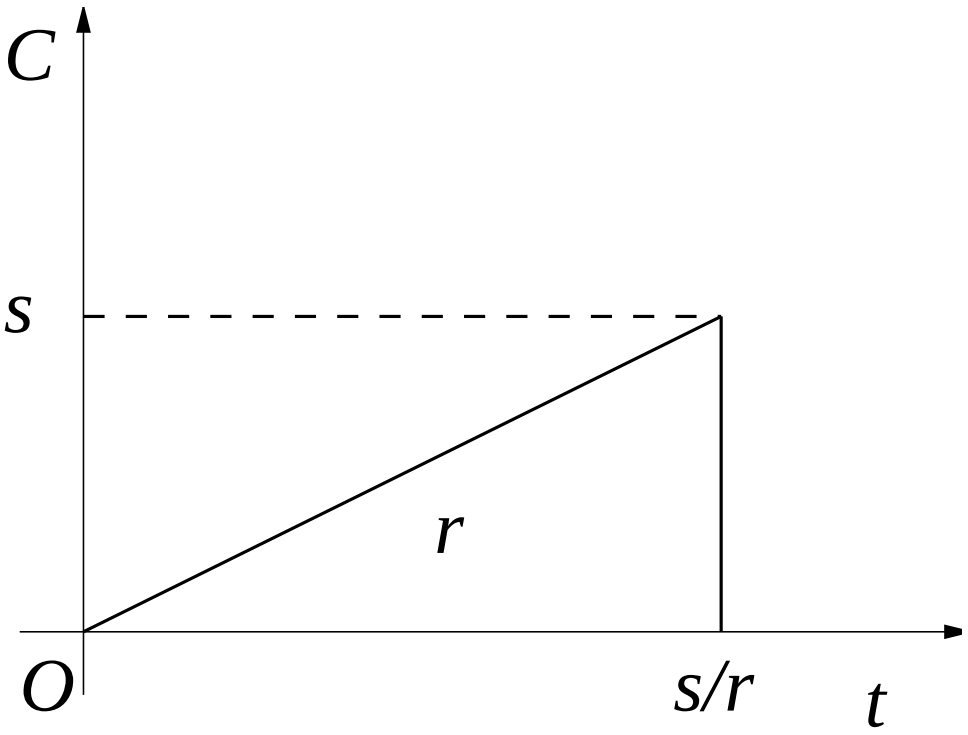

Figure C-5 Simplified profile of a "slow-riser". It reaches maximum significance s by rising with a slope r given in sigmas per second.

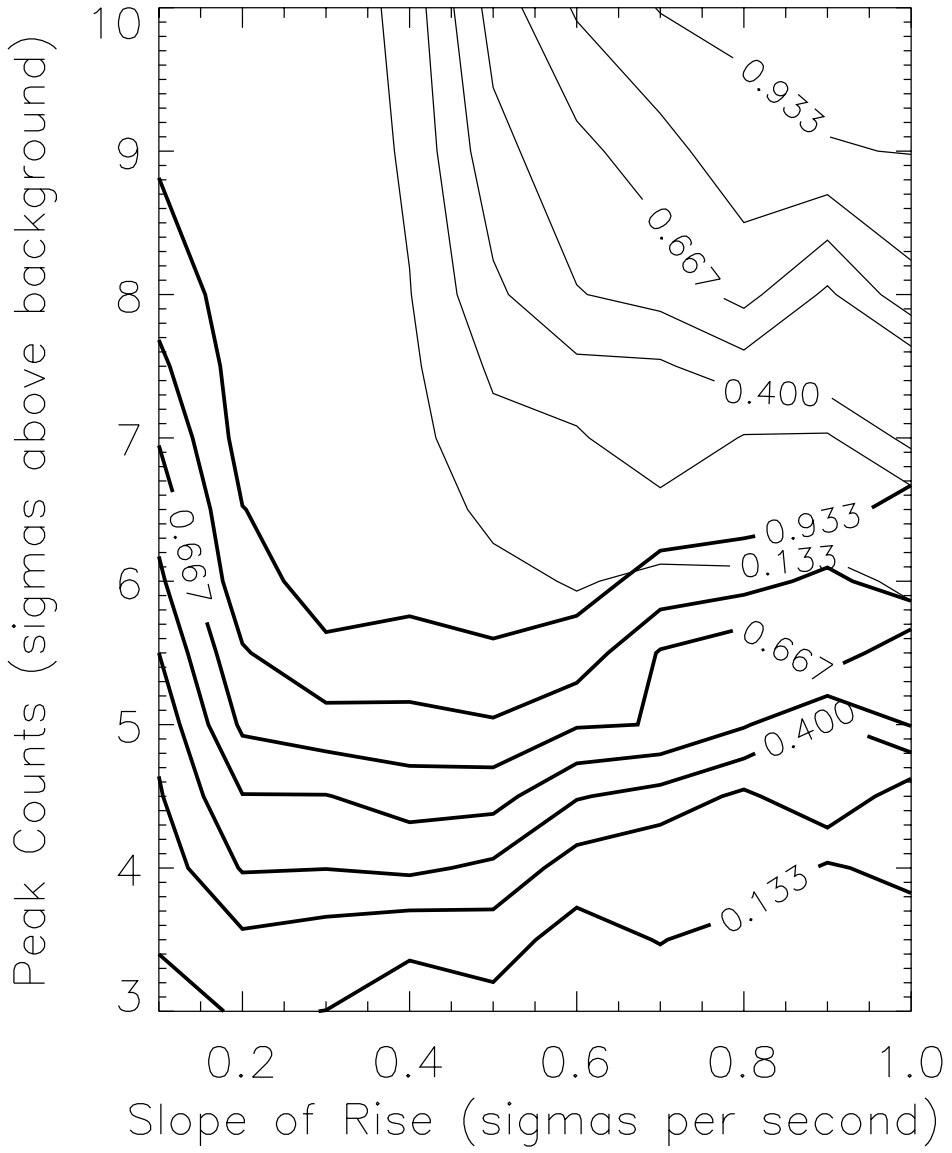

Figure C-6 Contours showing the probability of detecting a "slow-riser" with a given peak significance (relative to the "true" background) and a given slope. Thick contours apply to our off-line search algorithm, and thin contours apply to the onboard burst trigger.

spikes, and magnetospheric particle precipitation events.

Occultation steps due to bright sources (such as Cyg X-1) rising above (or setting below) the Earth's limb typically appear as sustained increases (or decreases) in the count rates in two or more detectors. This signature is not generally consistent with the burst-like transients we seek.

Phosphorescence spikes due to the interaction of high-energy particles in the detectors typically appear in the DISCLA data as short (< 1.024 s), intense (> 1000 counts s^{-1}) spikes in the lowest energy channel (25–50 keV) of a single detector. The intense signal in one detector with no coincident signal in a second detector is inconsistent with a point source of photons.

Magnetospheric particle precipitation events occur when particles (mostly electrons with energies of tens of eV to tens of MeV) that are usually trapped in the radiation belts by the Earth's magnetosphere are released into the upper atmosphere (Burgess & Inan 1993). The LADs detect the bremsstrahlung generated as precipitating particles interact in the atmosphere or in the spacecraft (Horack et al. 1991) and references therein). These events can appear in the data in three different ways as discussed by Horack et al. (1992). Events of the first kind show a smooth rise and decay with comparable intensities in all eight detectors; this signature is inconsistent with a point source of photons. The second kind of event arises when the precipitation occurs at some distance from the spacecraft, so that it appears only in the detectors on one side of the satellite. Because the source of radiation is relatively nearby, however, the orbital motion of *CGRO* gives the event different profiles in different detectors. The third kind of event shows rapid variability with complex temporal structure, and can closely mimic a GRB. Such events can be recognized if they show characteristics from the first two classes, such as appearance in opposite-facing detectors or inconsistent time profiles between detectors. These events also exhibit a bremsstrahlung cutoff in their energy spectrum.

If an event does not appear to be any of the above, we define background intervals by hand and estimate the source direction using our version of the BATSE

LOCBURST software (see below). We also examine the profile of the event in the 4 DISCLA energy channels.

Events with directions estimated to be behind the Earth are classified as "Earth" events. We have not yet done a detailed analysis of this category, but it is likely to include electron precipitation events occurring below the spacecraft, events from other categories for which we obtained poor direction estimates, and possibly terrestrial gamma ray flashes (TGRFs) (Fishman et al. 1994a).

Solar flares are identified based primarily on spectral softness and location. Typical solar flares have most of their counts in DISCLA channel 1, with fewer in channel 2, and fewer still in channel 3. In contrast, typical GRBs have most of their counts in channels 2 and 3, with proportionally less signal in channel 1. Some spectrally hard solar flares are observed, however, so events with directions consistent with the sun (within uncertainties) are classified as solar. For the search described here we did not compare laboratory trigger times with records of solar activity to separate hard solar flares from GRBs.

Events which appear to be neither terrestrial nor solar and which have sufficient spectral hardness to be seen both in channels 2 and 3 are classified as GRB candidates.

Events which do not make it into any of the previous categories are classified as "unknown", a category which includes all the low-energy (channel 1 only) events that are not obviously of terrestrial or solar origin. Events with significant counts in channels 1 and 2 (25–100 keV) but not in channel 3 (100–300 keV) are also included in this category.

The classification of laboratory triggers is subjective in cases where there is not an obvious indication of the nature of the event. To compare our classification methods with those of the BATSE team, we can use the 317 onboard triggers that were also laboratory triggers in our search of 345 days of data (see section C.6; the remaining 256 triggers were not detected because of gaps in the DISCLA data files). Table C-2 shows how these onboard triggers were classified by the BATSE team and by us.

Out of the 221 events that were identified as GRBs by the BATSE team, we

classified 198 as GRBs, 10 as solar flares, 4 as magnetospheric events, and 9 in other categories (such as "unknown" or "Earth"). The 10 events that were classified as GRBs by the BATSE team but as solar flares by us all had estimated directions consistent with the sun. We classified them as solar flares because we could not argue that they were GRBs rather than hard solar flares. The 4 BATSE GRBs that we classified as magnetospheric events occurred while the spacecraft was in the vicinity of the SAA or at a maximum (or minimum) geographic latitude, where particle precipitation events are common. The remaining 9 BATSE GRBs that we put in other categories include very short (duration < 1 s) bursts that were difficult to classify due to low signal-to-noise, events for which we estimated the directions to be behind the Earth, and bursts for which there was an unusually low count rate in channel 3 (100-300 keV).

The results in Table C-2 show that our classifications agree with those of the BATSE team in most cases. When there is uncertainty between a GRB and a non-GRB origin, our classification is "conservative" in that we tend towards the non-GRB classification. There were only 2 events out of 200 that we classified as GRBs but that the BATSE team classified as magnetospheric particle precipitation events. Over the course of a year, our tendency to classify hard events occurring near the sun as solar flares introduces a bias against GRBs that occur in the plane of the ecliptic.

For each of the solar flares, GRB candidates, and unknown events we estimate a source direction, intensity, and power-law spectral index using a modified version

Table C-2. Classification matrix of 317 onboard triggers

	Off-line GRB Candidate	Off-line Solar Flare	Off-line Magnetospheric	Off-line Other
BATSE GRB	198	10	4	9
BATSE Solar Flare	0	50	3	0
BATSE Magnetospheric	2	2	30	4
BATSE Unclassified	0	0	0	5

of the BATSE LOCBURST code. This software uses the BATSE detector response matrices along with a model for the scattering of incident photons by the Earth's atmosphere to find the count rates expected from an event with intensity P (in photons cm^{-2} s^{-1} above 10 keV), power-law spectral index ν, and source direction (θ, ϕ) in *CGRO* coordinates (Fishman et al. 1994; Pendleton et al. 1995). Let $C_d^i(P, \nu, \theta, \phi)$ denote the model count rates expected in energy channel i of detector d, and let $\tilde{C}_d^i$ denote the measured (background subtracted) count rates with associated statistical measurement uncertainties $\tilde{\sigma}_{i,d}$. To estimate $\tilde{P}$, $\tilde{\nu}$, $\tilde{\theta}$, and $\tilde{\phi}$ for a given event, the software minimizes the following measure of goodness-of-fit,

$$\chi^2(\tilde{P}, \tilde{\nu}, \tilde{\theta}, \tilde{\phi}) = \sum_{i,d} \left[\frac{\tilde{C}_d^i - C_d^i(\tilde{P}, \tilde{\nu}, \tilde{\theta}, \tilde{\phi})}{\tilde{\sigma}_{i,d}} \right]^2 . \qquad \text{(C.3)}$$

The measured count rates used for this procedure are mean count rates obtained from the main (most intense) portion of the burst as selected by hand during our visual inspection of the laboratory triggers.

The angular response of the BATSE detectors can allow for multiple, widely separated local minima in the χ^2 parameter space, especially for weak bursts. For example, if a burst has most of its counts in just two detectors it can be equally consistent with two burst directions depending on the choice of the third most brightly illuminated detector. For weak bursts, the statistics may not be good enough to reliably distinguish the third detector. Background variations (due to real source activity) in some detectors can also make it difficult to distinguish the third detector. In such situations, χ^2 can be a strongly non-linear function of the observed rates. The errors on the estimated burst parameters cannot then be reliably estimated from the formal covariance matrix of the fit.

To estimate errors on the model parameters for each burst, we produce 50 sets of "synthetic" burst rates obtained by drawing from a random distribution with the same means and variances as the measured rates. These 50 sets of synthetic count rates are then subjected to the same χ^2 minimization procedure as the real rates.

The variances in the parameters obtained from the synthetic count rates are used to estimate the uncertainty on the parameters ($\tilde{P}$, $\tilde{\nu}$, $\tilde{\theta}$, $\tilde{\phi}$) obtained from the measured count rates.

Using the estimated mean intensity $\tilde{P}$ we obtain a conversion factor from counts s^{-1} in the most brightly illuminated detector to units of ph cm^{-2} s^{-1} in the 50–300 keV range. The peak flux and fluence of each event in physical units are then determined by multiplying the corresponding measured counts by this conversion factor. The durations of events are characterized by the T_{50} and T_{90} duration measures, which are the time intervals during which the burst fluence increases from 25% to 75% and from 5% to 95% (respectively) of the total fluence (Kouveliotou et al. 1993; Koshut et al. 1996). Uncertainties in the peak flux, fluence, and durations are derived from the uncertainties in $\tilde{P}$, $\tilde{\nu}$, and the measured (background subtracted) count rates using the standard techniques for the propagation of small random errors (although the assumptions required by this method are not always satisfied).

We have attempted to ascertain how well the above procedures estimate burst intensities and directions by applying our methods to GRBs from the 3B catalog (Meegan et al. 1996). Because the burst intensities and directions must be estimated simultaneously by folding a model through the detector and atmospheric response matrices, systematic errors in the inferred quantities can arise from the background subtraction, the modeling of the event spectrum, spectral changes during the event, and detector calibration.

To evaluate the accuracy of our intensity measurements, we applied our analysis procedure to 29 GRBs from the 3B catalog (Meegan et al. 1996). We compared our peak fluxes (derived from the DISCLA data) to those obtained by the BATSE team (using the high resolution burst data types) (Pendleton et al. 1996a). In 13 bursts the two measurements agreed to within the 1σ statistical uncertainties, and in 24 bursts they agreed to within 2σ. The largest disagreements (in terms of standard deviations) occur only in the most intense bursts, where the systematic errors are expected to dominate the statistical uncertainties. In those cases, the measurements disagree by

less than 30%.

At least two sources of systematic errors are responsible for the differences between our peak flux measurements (on intense bursts) and those obtained by Pendleton et al. (1996) for the 3B catalog. First, we model the incident photon spectrum as a power law, whereas Pendleton et al. (1996) allow for some curvature in the spectrum. Second, our peak flux measurement on the 1024 ms time scale is based on the DISCLA time bin that contains the most counts above background. The phase of this 1024 ms bin relative to the "true" 1024 ms peak flux depends on the DISCLA sampling times; therefore, the "true" 1024 ms peak flux could be spread over two DISCLA time bins. In contrast, Pendleton et al. (1996) use data with 64 ms time resolution to find which placement of a 1024 ms interval yields the highest peak flux on that time scale.

A similar procedure was used to assess the accuracy of our direction estimates. Comparison of a sample of GRBs from the 3B catalog and hard solar flares which triggered onboard suggests that an additional systematic uncertainty of about 4° should be added in quadrature to our statistical direction uncertainties for events with emission between 50 and 300 keV. This is expected since our version of the LOCBURST code roughly corresponds (with minor improvements) to the version used to produce the BATSE 1B catalog (Fishman et al. 1994). The improvements to LOCBURST that reduced systematic errors to 1.6° for the 3B catalog require more spectral information than is available in the DISCLA data and have not been incorporated into the analysis described in this paper. For the channel 1 only (25–50 keV) events, comparison with solar flares indicates that the additional systematic uncertainty is about 6°.

For faint events the background subtraction can be a substantial source of systematic error because it is not always clear what is background and what is low-level emission before or after the event. The duration estimates (and thus fluence estimates) are particularly sensitive to the choice of background intervals (Koshut et al. 1996).

C.6 Results

We have applied the search and analysis procedures described in sections C.3 and C.5 to the DISCLA data taken between 1993 January 13 and 1993 December 24. The corresponding range of Truncated Julian Day numbers is TJD 9001–9345 (TJD = Julian Day − 2,440,000.5). Figure C-7 shows a sky map which combines events from the GRB candidate ($\diamond$), solar flare ($*$), and unknown ($+$) categories. The concentration of solar events in the ecliptic plane is clearly visible, as is a concentration of low-energy ($+$) events in the vicinity of Cyg X-1 ($\ell = 71.3°$, $b = 3.0°$).

C.6.1 Gamma-ray Burst Candidates

Our search so far yields 91 nontriggered GRB candidates. Tables C-3 and C-4 together are a catalog of these events.

The first column of Table C-3 is a name which specifies the approximate time of the event in the format NTB *yymmdd.ff*, where *yy* is the year, *mm* is the month, and *dd.ff* is the day. The second column gives the time of the laboratory trigger expressed as the TJD and the seconds of day (SOD). The next three columns give the estimated source direction in equatorial (J2000) coordinates and its associated statistical uncertainty. The full 1.0σ uncertainty in the direction estimates is obtained by combining the statistical uncertainty and the 4° systematic uncertainty (see section C.5) in quadrature. The next column gives the largest value (among the three time scales in Table C-1) of C_{max}/C_{min}, which is the ratio of the maximum count rate achieved during the event to the minimum count rate required for detection in the 50–300 keV band. Events with $C_{max}/C_{min} < 1.0$ were detected in the "catch-all" search of the 25–300 keV band (search "c" of Table C-1) and may represent spectrally softer GRBs that had too few counts to trigger in the 50–300 keV band. The next column gives the threshold number of counts in the 50–300 keV band, C_{min}, and (in superscript) the search time scale which yielded the largest value of C_{max}/C_{min}. The next column lists the searches from Table C-1 in which the event was detected.

The last column of Table C-3 gives the reasons in our estimation why the events did not trigger onboard the spacecraft. The notation "R" indicates the event occurred during the readout of a previous onboard trigger. "D" indicates that the event occurred while the onboard trigger was disabled due to passage through a region with a high probability of magnetospheric particle precipitation events. "F" indicates that the event was too faint to meet the onboard burst trigger threshold. "BB" indicates that the event failed to trigger onboard because it biased the onboard background average. In one case, no experiment housekeeping data were available so the state of the onboard trigger at the time of the event could not be determined. A "?" is entered for this event because we cannot determine whether the reason is "D" or "BB". (See below for further discussion of these reasons and examples of events in each category.)

Table C-3. 91 nontriggered GRB candidates.

Name	Time (TJD:s)	RA (°)	Dec (°)	Err. (°)	$\frac{C_{max}}{C_{min}}$	C_{min}	Searches Triggered	Reason Nontriggered
NTB 930118.74	9005:64425.6	219.3	-32.9	0.5	31.0	349^{4}	abcdefg	R
NTB 930211.88	9029:76428.9	285.5	20.0	7.7	3.5	425^{8}	bcdefg	F
NTB 930216.63	9034:54956.7	42.5	-8.7	3.6	2.6	447^{8}	bcdeg	F
NTB 930217.80	9035:69525.6	311.7	-12.0	28.2	0.9	286^{4}	c	F
NTB 930225.86	9043:75141.2	336.6	35.2	38.4	1.1	155^{1}	abc	F
NTB 930227.83	9045:71910.5	241.2	81.0	11.0	2.1	377^{8}	ceg	F
NTB 930228.85	9046:73728.6	18.6	2.5	8.3	2.2	477^{8}	g	F
NTB 930302.20	9048:17613.4	214.1	42.5	6.2	2.4	483^{8}	g	F
NTB 930303.65	9049:56726.7	0.0	-50.8	3.3	3.2	501^{8}	bceg	F
NTB 930305.70	9051:60923.0	275.2	59.8	3.5	3.2	330^{8}	bceg	F
NTB 930307.54	9053:46677.1	94.2	-15.5	12.7	1.7	411^{8}	bc	F
NTB 930308.30	9054:26710.7	88.7	-31.6	3.5	3.8	399^{8}	bceg	F
NTB 930310.08	9056: 7334.5	333.5	-57.2	5.0	2.6	321^{8}	abcdefg	F
NTB 930315.46	9061:40070.8	232.5	-32.1	3.9	2.0	395^{8}	g	F
NTB 930316.74	9062:64295.0	314.1	-87.1	19.8	1.6	132^{1}	bc	F
NTB 930318.18	9064:15764.1	16.2	44.0	8.9	2.4	425^{8}	bceg	F
NTB 930320.94	9066:81767.0	228.3	72.7	15.5	7.2	436^{8}	bcefg	R
NTB 930325.65	9071:56254.1	46.9	46.8	5.8	2.8	383^{8}	bceg	F
NTB 930327.46	9073:40594.6	178.7	-5.5	13.2	3.4	553^{8}	bc	F
NTB 930330.91	9076:79132.8	109.2	-54.4	2.0	1.7	481^{8}	cfg	F
NTB 930403.84	9080:73239.2	245.8	-59.6	6.2	3.0	351^{8}	abcdefg	BB
NTB 930409.13	9086:11442.8	315.6	68.8	4.0	3.3	334^{8}	abcdef	BB
NTB 930409.91	9086:78639.7	275.4	-17.7	0.9	12.8	501^{8}	abcdefg	R
NTB 930410.76	9087:65711.8	182.3	-45.3	7.3	3.0	380^{8}	abcefg	F
NTB 930416.56	9093:48602.2	115.6	-21.0	6.2	3.1	389^{8}	abcdefg	F
NTB 930417.78	9094:68020.4	190.5	8.3	6.7	1.7	351^{8}	abcdf	F
NTB 930421.11	9098:10164.9	23.7	19.3	7.0	2.0	520^{8}	g	F
NTB 930422.58	9099:50820.2	50.4	-7.5	2.1	4.9	315^{8}	bc	?
NTB 930424.45	9101:38903.4	230.3	-55.7	0.4	21.2	523^{8}	abcde	D
NTB 930424.97	9101:84156.0	254.1	68.6	3.2	3.5	332^{8}	abcefg	BB
NTB 930426.48	9103:41832.1	33.2	-81.9	5.4	4.4	133^{1}	abcdefg	R
NTB 930427.59	9104:51155.6	60.1	34.3	11.5	2.2	453^{8}	abd	F
NTB 930429.75	9106:65094.3	35.7	-25.8	5.4	5.7	344^{8}	bcdefg	BB
NTB 930501.34	9108:29834.4	181.4	-32.9	31.7	1.1	114^{1}	ab	F
NTB 930506.63	9113:55244.4	259.8	35.4	8.4	2.4	548^{8}	cg	F
NTB 930508.95	9115:82814.6	82.9	41.4	7.6	3.4	494^{8}	bce	D
NTB 930513.98	9120:85533.8	169.0	12.0	39.5	1.5	384^{8}	bc	F
NTB 930519.39	9126:34288.8	272.4	-24.2	83.8	1.4	134^{1}	bc	F
NTB 930612.63	9150:55165.1	254.5	34.3	2.9	12.1	277^{4}	abcde	R
NTB 930616.27	9154:23806.6	179.5	1.8	4.4	11.7	165^{1}	abcde	R
NTB 930617.23	9155:20027.0	244.9	-12.7	6.1	2.5	299^{8}	bceg	F
NTB 930626.94	9164:81935.0	342.6	-34.9	3.3	3.6	512^{8}	bcdefg	BB
NTB 930630.71	9168:61420.2	70.0	38.1	6.9	3.0	438^{8}	bcdeg	F
NTB 930701.62	9169:54302.9	226.4	39.4	2.5	4.2	338^{8}	abcde	F
NTB 930705.64	9173:55983.3	195.3	-59.5	7.2	2.0	334^{8}	bcefg	F
NTB 930717.20	9185:18101.4	184.3	57.8	10.3	1.5	364^{4}	bcd	F
NTB 930717.98	9185:85357.7	200.5	-66.4	3.5	3.3	374^{8}	abc	F
NTB 930722.84	9190:73297.6	310.5	-48.2	3.5	2.1	412^{8}	eg	F
NTB 930728.54	9196:47072.9	90.8	19.0	21.0	3.3	510^{8}	d	R
NTB 930804.71	9203:61858.5	32.7	66.6	5.0	3.7	317^{8}	bcefg	F
NTB 930811.62	9210:53728.4	347.5	65.0	3.6	2.9	325^{8}	bc	F
NTB 930812.27	9211:23904.9	198.0	-27.8	2.4	4.9	409^{8}	bcdef	BB
NTB 930813.76	9212:65850.5	76.9	77.1	8.1	3.7	336^{8}	abcdefg	F
NTB 930816.67	9215:58569.4	155.1	53.8	5.9	3.5	429^{8}	bceg	F
NTB 930820.76	9219:65885.3	62.7	36.4	7.6	2.8	386^{8}	bceg	F
NTB 930821.64	9220:56096.9	148.0	-40.4	11.7	1.2	123^{1}	bc	F
NTB 930825.48	9224:41775.3	59.7	63.1	21.4	1.5	298^{4}	cg	F
NTB 930827.60	9226:51963.0	349.4	68.5	19.0	2.5	506^{8}	bceg	F
NTB 930902.45	9232:39001.8	224.2	20.8	6.6	2.1	364^{8}	acg	F

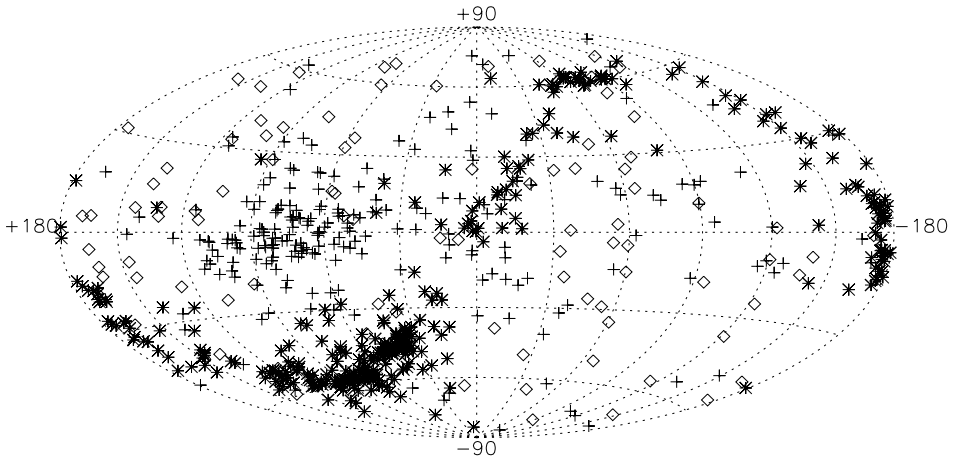

Figure C-7 Sky map of all non-terrestrial nontriggered events in Galactic coordinates. The GRB candidate ($\diamond$), solar flare ($*$), and unknown ($+$) categories are shown. The concentration of solar events in the ecliptic plane is clearly visible, as is a concentration of low-energy ($+$) events in the vicinity of Cyg X-1 ($\ell = 71°.3$, $b = 3°.0$).

Table C-4 gives the durations and intensities (in physical units) of the GRB candidates. The first column gives the name of the GRB candidate. The next two columns give estimates of the T_{50} and T_{90} duration measures. Events with no entry in the T_{50} column had their T_{90} duration estimated by eye. Uncertainties listed as 0.00 indicate that the uncertainty is less than the duration of one DISCLA time bin (1.024 s). The next column gives the peak flux in the 50–300 keV range as measured on the 1024 ms time scale. The next column gives the 50–300 keV fluence estimate.

Table C-3—Continued

Name	Time (TJD:s)	RA (°)	Dec (°)	Err. (°)	$\frac{C_{max}}{C_{min}}$	C_{min}	Searches Triggered	Reason Nontriggered
NTB 930918.46	9248:39913.1	275.3	-81.0	11.8	2.6	310^{8}	bceg	F
NTB 930921.84	9251:73133.2	75.0	-35.7	25.2	1.3	292^{8}	bce	F
NTB 930924.37	9254:32251.0	98.1	-9.6	21.5	3.3	403^{8}	bcde	F
NTB 930928.93	9258:81199.3	260.5	-67.6	10.4	2.2	529^{8}	bcf	F
NTB 930928.94	9258:81393.3	79.8	45.2	7.0	1.7	329^{8}	f	F
NTB 931001.06	9261: 5859.5	207.2	12.6	1.4	5.6	582^{8}	abcde	R
NTB 931001.72	9261:62917.3	8.5	12.5	2.2	3.4	473^{8}	bcefg	BB
NTB 931007.20	9267:17771.7	311.3	-5.2	23.7	2.2	368^{8}	bg	F
NTB 931007.33	9267:29319.3	355.1	36.4	48.7	1.7	363^{8}	bg	F
NTB 931008.05	9268: 5024.9	26.4	-65.6	30.5	1.2	190^{1}	bc	F
NTB 931008.63	9268:54916.8	42.3	42.8	3.7	4.7	492^{8}	ceg	BB
NTB 931011.96	9271:83718.3	248.4	63.9	23.4	1.2	373^{4}	bc	F
NTB 931014.08	9274: 7552.2	65.5	72.0	55.6	1.5	148^{1}	bc	F
NTB 931017.22	9277:19221.7	185.7	-67.5	18.3	1.8	448^{8}	b	F
NTB 931020.10	9280: 8697.5	285.0	16.0	14.0	1.7	447^{8}	c	F
NTB 931025.93	9285:80462.5	173.2	15.9	4.8	2.7	438^{8}	bceg	F
NTB 931031.23	9291:20519.6	173.2	63.4	17.2	3.0	163^{1}	bce	R
NTB 931106.48	9297:42228.4	34.3	69.7	3.7	3.7	406^{8}	bcefg	BB
NTB 931106.90	9297:78310.6	185.7	-38.0	16.1	2.7	279^{4}	bc	R
NTB 931107.31	9298:26896.0	106.0	-27.7	12.6	2.9	578^{8}	abcde	BB
NTB 931111.71	9302:61941.4	244.6	49.5	0.8	9.2	352^{8}	abcdefg	R
NTB 931113.04	9304: 3669.7	50.9	-40.2	10.1	2.1	383^{8}	bce	F
NTB 931115.77	9306:66557.6	279.1	27.9	11.0	3.1	401^{4}	abceg	R
NTB 931125.86	9316:74847.4	177.7	-77.4	2.4	12.0	529^{8}	abcdefg	R
NTB 931206.45	9327:39631.5	174.1	-14.7	15.0	3.1	404^{8}	bceg	F
NTB 931209.89	9330:77266.1	20.0	-37.4	3.0	3.3	443^{8}	bceg	F
NTB 931215.12	9336:10491.5	326.0	-3.5	12.2	2.3	298^{4}	abd	F
NTB 931220.16	9341:13826.7	120.2	45.7	8.5	3.0	414^{8}	bce	F
NTB 931220.73	9341:63345.3	50.0	22.0	3.9	7.3	435^{8}	abcdefg	R
NTB 931222.11	9343:10361.5	278.9	29.5	5.4	1.9	565^{8}	g	F
NTB 931222.82	9343:70972.1	209.6	-35.5	14.8	6.2	178^{1}	abceg	R
NTB 931223.07	9344: 6589.6	212.8	40.0	23.2	1.5	200^{1}	bc	F

Table C-4. Durations and intensities of nontriggered GRB candidates

Name	T_{50} (s)	T_{90} (s)	Peak Flux (ph cm^{-2} s^{-1})	Fluence (ergs cm^{-2})
NTB 930118.74	2.05 ± 0.00	4.10 ± 0.00	4.53 ± 0.14	(3.00 ± 0.19)E-6
NTB 930211.88	19.46 ± 2.90	58.37 ± 6.23	0.26 ± 0.05	(8.46 ± 1.95)E-7
NTB 930216.63	23.55 ± 0.00	40.96 ± 8.44	0.28 ± 0.07	(6.34 ± 1.54)E-7
NTB 930217.80	···	3.07 ± 1.02	0.18 ± 0.10	(5.86 ± 3.50)E-8
NTB 930225.86	···	4.10 ± 1.02	0.18 ± 0.07	(7.72 ± 2.94)E-8
NTB 930227.83	37.89 ± 2.29	57.34 ± 7.24	0.17 ± 0.05	(5.46 ± 1.36)E-7
NTB 930228.85	26.62 ± 3.24	91.14 ± 16.67	0.16 ± 0.04	(9.25 ± 1.98)E-7
NTB 930302.20	21.50 ± 3.24	57.34 ± 15.50	0.26 ± 0.09	(1.44 ± 0.44)E-6
NTB 930303.65	32.77 ± 1.45	70.66 ± 7.17	0.20 ± 0.05	(7.64 ± 1.42)E-7
NTB 930305.70	5.12 ± 1.45	12.29 ± 1.45	0.59 ± 0.19	(8.88 ± 3.73)E-7
NTB 930307.54	5.12 ± 1.02	22.53 ± 16.79	0.18 ± 0.19	(2.26 ± 2.35)E-7
NTB 930308.30	18.43 ± 1.45	38.91 ± 2.29	0.43 ± 0.11	(2.18 ± 0.53)E-6
NTB 930310.08	10.24 ± 0.00	34.82 ± 23.57	0.35 ± 0.05	(4.16 ± 0.68)E-7
NTB 930315.46	15.36 ± 2.29	35.84 ± 4.22	0.23 ± 0.05	(7.61 ± 1.81)E-7
NTB 930316.74	···	3.07 ± 1.02	0.22 ± 0.07	(8.05 ± 2.47)E-8
NTB 930318.18	15.36 ± 2.05	35.84 ± 6.87	0.17 ± 0.04	(3.97 ± 0.94)E-7
NTB 930320.94	25.60 ± 0.00	59.39 ± 3.07	0.96 ± 0.15	(4.09 ± 0.62)E-6
NTB 930325.65	10.24 ± 1.45	20.48 ± 5.12	0.24 ± 0.06	(5.13 ± 1.42)E-7
NTB 930327.46	12.29 ± 3.69	46.08 ± 31.89	0.29 ± 0.07	(7.86 ± 2.88)E-7
NTB 930330.91	12.29 ± 2.29	52.22 ± 14.37	0.24 ± 0.06	(4.99 ± 1.47)E-7
NTB 930403.84	13.31 ± 0.00	92.16 ± 10.69	0.26 ± 0.04	(6.96 ± 0.93)E-7
NTB 930409.13	14.34 ± 1.02	39.94 ± 9.27	0.40 ± 0.05	(7.91 ± 1.20)E-7
NTB 930409.91	12.29 ± 1.02	53.25 ± 0.00	1.19 ± 0.06	(3.06 ± 0.34)E-6
NTB 930410.76	24.58 ± 1.02	74.75 ± 3.07	0.29 ± 0.05	(1.09 ± 0.16)E-6
NTB 930416.56	···	20.48 ± 5.12	0.21 ± 0.04	(3.54 ± 0.58)E-7
NTB 930417.78	5.12 ± 1.45	35.84 ± 26.62	0.21 ± 0.06	(2.05 ± 0.82)E-7
NTB 930421.11	47.10 ± 3.24	(1.29 ± 0.23)E+2	0.15 ± 0.04	(1.28 ± 0.26)E-6
NTB 930422.58	15.36 ± 1.02	44.03 ± 17.41	0.27 ± 0.03	(1.20 ± 0.13)E-6
NTB 930424.45	41.98 ± 1.02	(1.06 ± 0.03)E+2	1.28 ± 0.06	(1.38 ± 0.08)E-5
NTB 930424.97	12.29 ± 1.02	32.77 ± 15.36	0.33 ± 0.04	(8.77 ± 1.30)E-7
NTB 930426.48	···	3.07 ± 1.02	0.70 ± 0.10	(1.66 ± 0.27)E-7
NTB 930427.59	21.50 ± 1.45	46.08 ± 7.17	0.19 ± 0.06	(4.45 ± 1.30)E-7
NTB 930429.75	43.01 ± 1.45	(1.11 ± 0.15)E+2	0.38 ± 0.04	(2.24 ± 0.25)E-6
NTB 930501.34	···	2.05 ± 1.02	0.23 ± 0.14	(5.71 ± 3.59)E-8
NTB 930506.63	34.82 ± 8.26	82.94 ± 5.22	0.18 ± 0.05	(9.14 ± 2.73)E-7
NTB 930508.95	5.12 ± 1.45	22.53 ± 15.39	0.24 ± 0.05	(4.17 ± 1.39)E-7
NTB 930513.98	···	41.98 ± 10.24	0.17 ± 0.05	(3.67 ± 1.07)E-7
NTB 930519.39	···	1.02 ± 0.00	0.35 ± 0.29	(1.15 ± 0.96)E-7
NTB 930612.63	6.14 ± 2.05	50.18 ± 9.22	1.33 ± 0.08	(1.23 ± 0.42)E-6
NTB 930616.27	···	1.02 ± 0.00	3.21 ± 0.77	(7.97 ± 1.94)E-7
NTB 930617.23	51.20 ± 1.02	73.73 ± 5.12	0.29 ± 0.06	(1.35 ± 0.28)E-6
NTB 930626.94	14.34 ± 1.02	61.44 ± 38.01	0.27 ± 0.05	(8.29 ± 1.25)E-7
NTB 930630.71	···	18.43 ± 5.12	0.23 ± 0.05	(3.86 ± 0.71)E-7
NTB 930701.62	20.48 ± 1.02	35.84 ± 3.07	0.45 ± 0.05	(1.07 ± 0.14)E-6
NTB 930705.64	12.29 ± 1.02	48.13 ± 16.38	0.20 ± 0.05	(4.10 ± 0.95)E-7
NTB 930717.20	2.05 ± 1.45	3.07 ± 1.02	0.21 ± 0.09	(1.37 ± 1.11)E-7
NTB 930717.98	6.14 ± 1.45	17.41 ± 3.07	0.32 ± 0.05	(3.93 ± 1.09)E-7
NTB 930722.84	26.62 ± 2.29	72.70 ± 9.44	0.20 ± 0.05	(8.37 ± 1.62)E-7
NTB 930728.54	66.56 ± 15.22	(3.43 ± 0.21)E+2	0.29 ± 0.05	(3.60 ± 0.92)E-6
NTB 930804.71	19.46 ± 1.02	49.15 ± 16.42	0.25 ± 0.04	(9.05 ± 1.10)E-7
NTB 930811.62	18.43 ± 2.29	45.06 ± 4.22	0.29 ± 0.06	(7.27 ± 1.71)E-7
NTB 930812.27	28.67 ± 2.29	77.82 ± 3.24	0.39 ± 0.04	(1.97 ± 0.25)E-6
NTB 930813.76	(1.02 ± 0.02)E+2	(1.36 ± 0.02)E+2	0.29 ± 0.05	(1.16 ± 0.19)E-6
NTB 930816.67	8.19 ± 1.02	24.58 ± 4.10	0.33 ± 0.10	(6.95 ± 2.21)E-7
NTB 930820.76	7.17 ± 1.02	45.06 ± 23.55	0.22 ± 0.05	(4.03 ± 0.98)E-7
NTB 930821.64	···	2.05 ± 1.02	0.30 ± 0.10	(9.30 ± 3.26)E-8
NTB 930825.48	4.10 ± 2.29	20.48 ± 5.12	0.14 ± 0.06	(1.58 ± 1.07)E-7
NTB 930827.60	15.36 ± 3.07	48.13 ± 15.36	0.22 ± 0.07	(5.23 ± 1.80)E-7
NTB 930902.45	28.67 ± 10.69	74.75 ± 16.51	0.16 ± 0.04	(7.53 ± 3.05)E-7

Figure C-8 shows a sky map of the direction estimates for the 91 untriggered GRB candidates. Events are shown as 1.0σ error circles centered on the best-fit location. Using the sky exposure calculated in section C.4.1, the dipole and quadrupole moments of this direction distribution in Galactic coordinates are $\langle \cos\theta \rangle = -0.001 \pm 0.025$ and $\langle \sin^2 b - 1/3 \rangle = -0.022 \pm 0.021$, where θ is the angle between the burst direction and the Galactic center and b is the Galactic longitude. These values are consistent with the values $\langle \cos\theta \rangle = 0.00 \pm 0.06$ and $\langle \sin^2 b - 1/3 \rangle = 0.00 \pm 0.03$ expected from an isotropic distribution with the same number of bursts.

The dipole and quadrupole moments (corrected for sky exposure) with respect to equatorial coordinates are $\langle \sin\delta \rangle = 0.036 \pm 0.027$ and $\langle \sin^2 \delta - 1/3 \rangle = 0.074 \pm 0.024$. The dipole moment is consistent with that expected from an isotropic distribution, $\langle \sin\delta \rangle = 0.00 \pm 0.06$. The quadrupole moment appears to be only marginally consistent with the value $\langle \sin^2 \delta - 1/3 \rangle = 0.00 \pm 0.03$ expected for an isotropic distribution, indicating a weak concentration of events in the direction of the celestial poles. This result may be due to our tendency to classify GRBs with directions consistent with the sun as hard solar flares (see section C.5).

The durations based on the T_{90} interval of these events range from $\lesssim 1.024$ s to ~ 350 s. We have examined the nontriggered GRB candidates to see if any appear to be related to an onboard triggered GRB that occurred within 1 day of a nontriggered event. In a combined sample of 91 nontriggered GRB candidates and 333 bursts from the 3B catalog (covering TJD 8995–9347), we found 7 pairs of bursts occurring within 1 day of each other and having direction measurements compatible within 1σ uncertainties. Only 3 of these 7 pairs involved a nontriggered GRB candidate. We do not consider this to be evidence that any of these pairs share the same burst source. We expect statistically to find 5–8 such pairs in a sample of the same size drawn from bursts randomly distributed uniformly in time and isotropically in space, with median location measurement errors of 8–10°. If one or more convincing pairs had been identified, however, they could have either been interpreted as burst repetition (Wang 1994) or as bursts that extend knowledge of the T_{90} distribution to longer

Table C-4—Continued

Name	T_{50} (s)	T_{90} (s)	Peak Flux (ph cm^{-2} s^{-1})	Fluence (ergs cm^{-2})
NTB 930918.46	16.38 ± 4.10	54.27 ± 14.34	0.20 ± 0.05	(5.54 ± 1.95)E-7
NTB 930921.84	12.29 ± 3.24	56.32 ± 18.43	0.32 ± 0.12	(3.12 ± 1.47)E-7
NTB 930924.37	8.19 ± 1.02	28.67 ± 17.17	0.22 ± 0.05	(5.58 ± 1.23)E-7
NTB 930928.93	2.05 ± 1.02	4.10 ± 2.05	0.19 ± 0.06	(6.92 ± 4.24)E-8
NTB 930928.94	14.34 ± 1.45	28.67 ± 2.29	0.13 ± 0.04	(3.75 ± 1.04)E-7
NTB 931001.06	4.10 ± 0.00	12.29 ± 3.07	0.74 ± 0.08	(8.66 ± 0.93)E-7
NTB 931001.72	16.38 ± 2.29	82.94 ± 8.44	0.28 ± 0.06	(9.18 ± 1.98)E-7
NTB 931007.20	5.12 ± 1.02	35.84 ± 5.12	0.23 ± 0.07	(3.62 ± 1.27)E-7
NTB 931007.33	···	8.19 ± 4.10	0.43 ± 0.74	(4.94 ± 8.59)E-7
NTB 931008.05	···	2.05 ± 1.02	0.28 ± 0.11	(1.19 ± 0.46)E-7
NTB 931008.63	66.56 ± 1.45	(1.98 ± 0.28)E+2	0.26 ± 0.04	(3.34 ± 0.29)E-6
NTB 931011.96	11.26 ± 3.24	50.18 ± 18.55	0.20 ± 0.11	(2.00 ± 1.27)E-7
NTB 931014.08	···	4.10 ± 2.05	0.36 ± 0.14	(1.24 ± 0.52)E-7
NTB 931017.22	9.22 ± 5.22	41.98 ± 23.57	0.16 ± 0.06	(2.72 ± 1.82)E-7
NTB 931020.10	21.50 ± 3.24	73.73 ± 2.29	0.14 ± 0.05	(4.52 ± 1.52)E-7
NTB 931025.93	20.48 ± 9.22	49.15 ± 15.66	0.21 ± 0.05	(5.15 ± 2.55)E-7
NTB 931031.23	···	1.02 ± 0.00	0.40 ± 0.11	(8.95 ± 2.43)E-8
NTB 931106.48	31.74 ± 2.29	90.11 ± 1.45	0.22 ± 0.04	(1.41 ± 0.21)E-6
NTB 931106.90	···	11.26 ± 4.10	0.32 ± 0.06	(2.66 ± 0.50)E-7
NTB 931107.31	30.72 ± 3.24	55.30 ± 9.27	0.41 ± 0.11	(1.57 ± 0.40)E-6
NTB 931111.71	58.37 ± 3.07	(1.86 ± 0.01)E+2	0.77 ± 0.04	(7.24 ± 0.59)E-6
NTB 931113.04	12.29 ± 1.02	52.22 ± 16.67	0.21 ± 0.05	(4.15 ± 0.93)E-7
NTB 931115.77	14.34 ± 1.45	26.62 ± 2.29	0.32 ± 0.06	(3.15 ± 0.76)E-7
NTB 931125.86	5.12 ± 1.02	14.34 ± 1.45	0.83 ± 0.05	(1.27 ± 0.27)E-6
NTB 931206.45	11.26 ± 1.02	29.70 ± 8.44	0.26 ± 0.05	(5.43 ± 1.11)E-7
NTB 931209.89	34.82 ± 1.02	90.11 ± 4.58	0.27 ± 0.06	(1.44 ± 0.21)E-6
NTB 931215.12	3.07 ± 2.05	13.31 ± 11.31	0.28 ± 0.07	(2.25 ± 1.61)E-7
NTB 931220.16	4.10 ± 1.45	11.26 ± 4.10	0.49 ± 0.11	(6.84 ± 2.81)E-7
NTB 931220.73	8.19 ± 0.00	33.79 ± 4.58	0.56 ± 0.05	(9.78 ± 0.89)E-7
NTB 931222.11	18.43 ± 3.24	58.37 ± 12.83	0.18 ± 0.06	(6.86 ± 1.93)E-7
NTB 931222.82	···	2.05 ± 1.02	1.75 ± 0.24	(4.40 ± 0.65)E-7
NTB 931223.07	···	3.07 ± 1.02	0.26 ± 0.19	(9.55 ± 7.28)E-8

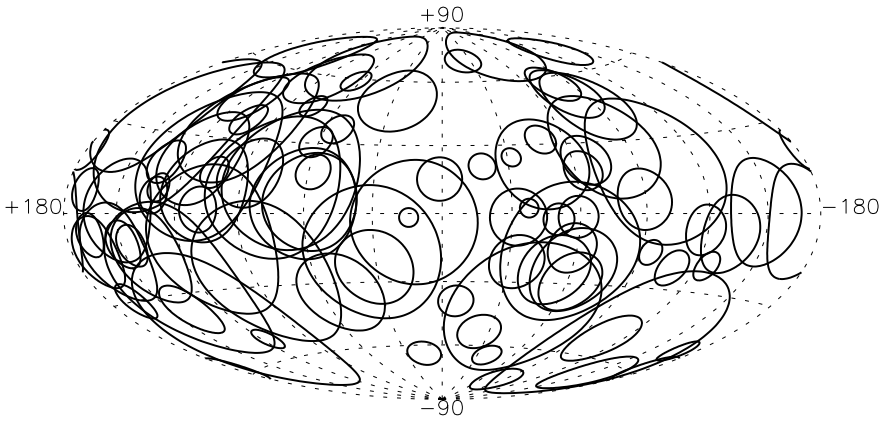

Figure C-8 Sky map of 91 nontriggered GRB candidates, shown as 1σ error circles in Galactic coordinates.

durations.

Figure C-9 shows the integral peak flux distribution on the 1024 ms time scale for the untriggered GRB candidates. These events are concentrated at the faint end of the distribution, as expected for events which were generally too faint to cause an onboard trigger. When the nontriggered bursts are added to the triggered bursts for the same time period, the departure from the $-3/2$ power law slope expected from a homogeneous distribution (in Euclidean space) remains evident.

The top two panels of Figure C-10 show the differential, $n(P)$, and integral, $N(>P)$, distributions of the peak fluxes, P, for the combined sample of 83 nontriggered GRB candidates and 233 onboard triggered GRBs that were detected on the 1024 ms time scale. The bottom panel shows the slope of the logarithmic number versus peak flux distribution, defined by

$$s(P) = \frac{d \log N(>P)}{d \log P} = -P \frac{n(P)}{N(>P)}. \tag{C.4}$$

The dotted histograms in Figure C-10 show the distributions corrected for our laboratory trigger efficiency (see figure C-3). The logarithmic slope $s(P)$ is consistent with a value of -0.5 ± 0.1 at peak fluxes of 0.15–0.35 ph cm^{-2} s^{-1}.

Another measure of the inhomogeneity of the source distribution is reflected in the distribution of the V/V_{max} statistic for these events, given by $(C_{max}/C_{min})^{-3/2}$ (Schmidt et al. 1988). For the 91 nontriggered GRB candidates, the average value $\langle V/V_{max} \rangle = 0.28 \pm 0.03$. This value is biased by the elimination of the strong (triggered) bursts; but it is of interest when considering how biases inherent in the onboard trigger mechanism could affect conclusions about the spatial inhomogeneity of GRB sources. For example, if the onboard trigger's bias against slow-risers had significantly biased the value of $\langle V/V_{max} \rangle = 0.33 \pm 0.01$ obtained for the 3B catalog (Meegan et al. 1996) then the value obtained from the nontriggered GRB candidates alone could be expected to be much higher. For comparison, the value obtained using the cataloged bursts detected during the same time period is $\langle V/V_{max} \rangle = 0.13 \pm 0.02$. For the

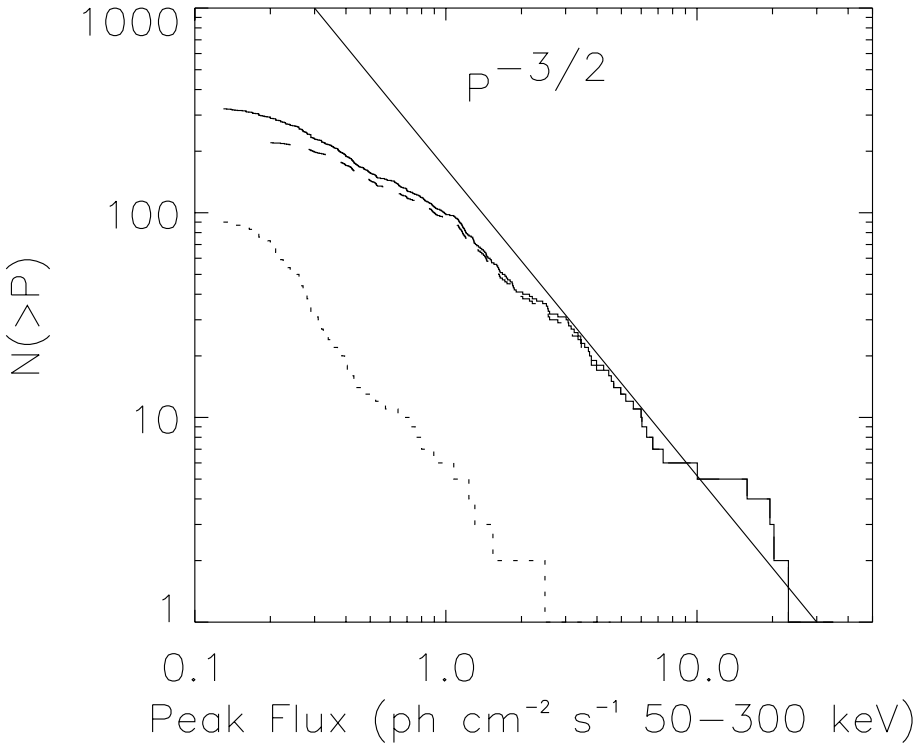

Figure C-9 Integral number versus peak flux distribution of 91 nontriggered GRB candidates (dotted line). No corrections for trigger efficiency have been applied. The distribution for GRBs from the 3B catalog detected during the same time period is also shown (dashed line), as is that for the combined sample (solid line).

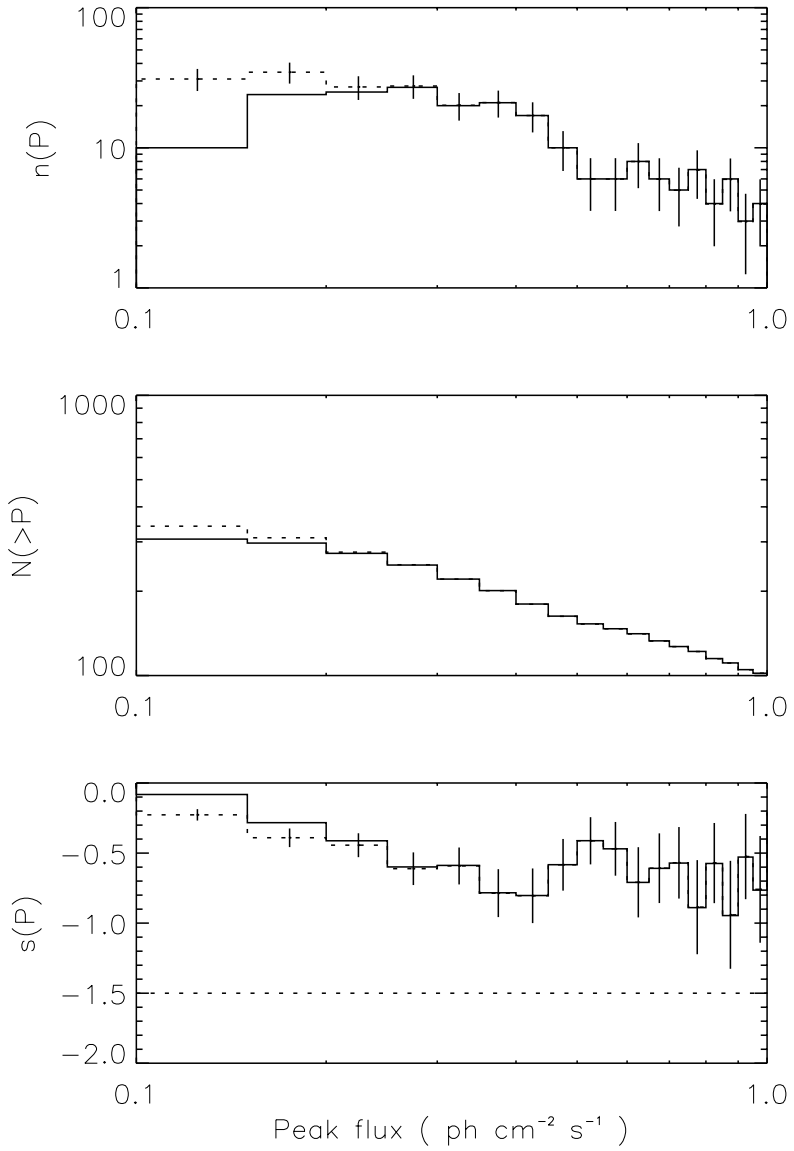

Figure C-10 Peak flux distributions for 83 nontriggered GRB candidates combined with the 233 onboard triggered events (1024 ms time scale) from the same time period. The solid histogram shows the observed numbers and the dotted histogram shows the numbers corrected for laboratory trigger efficiency. $n(P)$ is the differential distribution, $N(P)$ is the integral distribution, and $s(P)$ is the slope of the logarithmic number versus peak flux distribution.

combined nontriggered GRB candidates and cataloged bursts, $\langle V/V_{max} \rangle = 0.18 \pm 0.02$. This value is representative of the entire BATSE sample.

Figures C-11 and C-12 show intensity profiles of some representative GRB candidates. Two adjacent plots are shown for each event. The plots on the left show the burst profile from the detector most brightly illuminated by the burst. The plots on the right show the profile from the second most illuminated (or "second brightest") detector; they illustrate why some of the events did not cause an onboard burst trigger. The dashed lines show our estimate, $B_k^{\rm fit}$ of the background counts in each bin (k) based on polynomial fits to data before and after the event. The dotted lines show the $5.5\sigma_B$ threshold level given by $5.5\sqrt{B_k^{\rm fit}}$. This level represents an "ideal" threshold estimate and it is in general different from the actual onboard background estimate that was in effect at the time the event occurred (see section C.3). The onboard background estimate has a statistical uncertainty resulting from the uncertainty in the mean count rate during the 17.408 s background accumulation interval. The dot–dashed line represents the threshold corresponding to $5.5\sqrt{B_k^{\rm fit}}$ *plus* the uncertainty in the onboard trigger level arising from the onboard background uncertainty. An event with peak counts just slightly above our "ideal" $5.5\sigma_B$ threshold may fall below the onboard burst trigger threshold even though both thresholds are based on background estimates that are statistically consistent with each other. We classify events with peak counts less than $5.5\sqrt{B_k^{\rm fit}}$ plus the onboard threshold uncertainty as too faint to trigger onboard ("F" in table C-3).

The event in row (a) of Figure C-11 failed to trigger onboard because it occurred during the read out period of a previous onboard burst trigger. The event in row (b) occurred while the onboard burst trigger was disabled due to spacecraft passage through a region identified with a high probability of a false trigger due to atmospheric electron precipitation events. The events in row (c) of Figure C-11 and (d) of Figure C-12 failed to trigger onboard because the onboard background estimate was biased upwards by slowly rising burst flux; these are examples of slow-risers. Panels (e) and (f) show events that were too faint to meet the onboard trigger threshold.

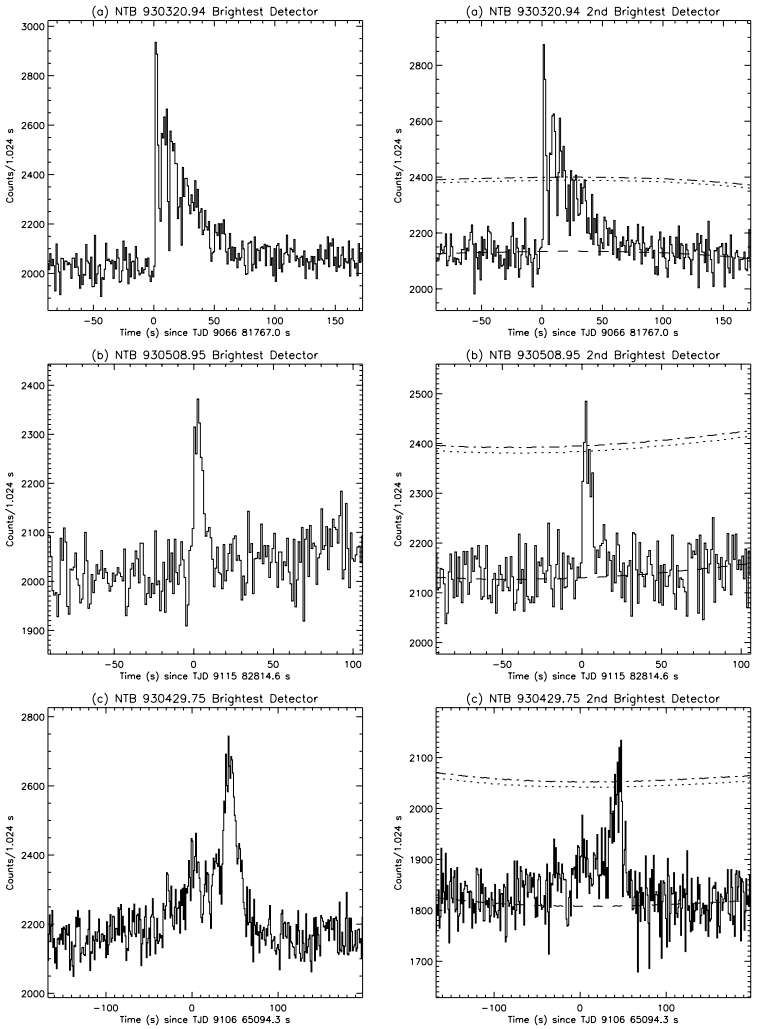

Figure C-11 Intensity profiles of selected GRB candidates in the 50–300 keV bands. Two panels are used for each event. Those on the left represent the count rates observed in the detector most brightly illuminated by the burst. Those on the right represent the count rates in the second most illuminated detector. Dashed lines represent our background estimate derived from polynomial fits to data before and after the event. Dotted lines represent an "ideal" onboard trigger threshold based on our background estimates; the actual onboard trigger threshold is in general different and is based on an average count rate that is recomputed every 17.408 s. The dot-dashed line represents the "ideal" onboard threshold *plus* the uncertainty arising from the statistical uncertainty in onboard background average. The burst in row (a) occurred during the read out period of a more intense event, and that in row (b) occurred while the onboard trigger was disabled. The bursts in row (c) modified the onboard background average.

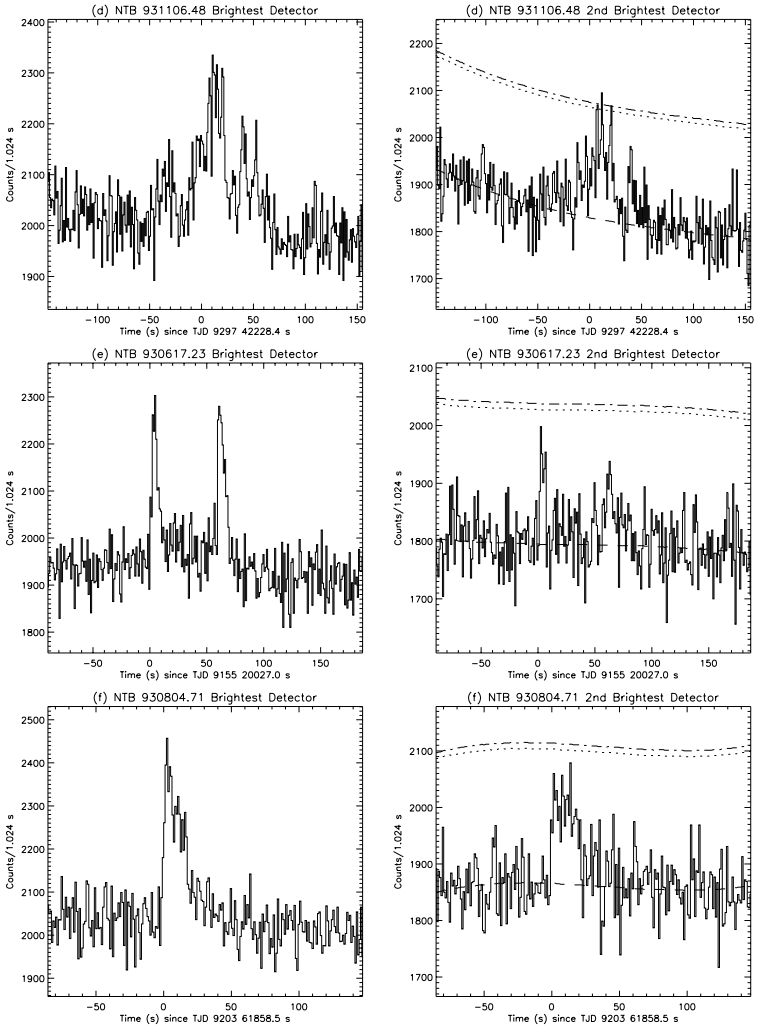

Figure C-12 More light curves of nontriggered GRB candidates. The bursts in rows (c) and (d) modified the onboard background average. Rows (e) and (f) show events that were too faint cause an onboard burst trigger.

We estimate that the 91 GRB candidates failed to trigger onboard the spacecraft for the following reasons: 15 events occurred during the read out of a brighter event, 2 occurred while the onboard trigger was disabled for other reasons, 63 were below the $5.5\sigma_B$ threshold in the second brightest detector, and 10 had a slow rise that modified the onboard background estimate. One occurred during a time for which no spacecraft housekeeping data are available to determine the status of the onboard trigger.

The onboard trigger mechanism's bias against slow-rising GRBs has been discussed by Lingenfelter and Higdon (1996). The 10 (possibly 11) events we find that failed to trigger onboard the spacecraft *solely* because of the slow-rising effect constitute 3.0% (possibly 3.3%) of the total 332 GRBs that have been detected above the onboard threshold while the trigger was active. This is a lower fraction than estimated elsewhere (Lingenfelter & Higdon 1996). We note, however, that our search algorithm is biased against faint events which rise on time scales longer than ~ 30 s on the 1.024 s time scale (see Figure C-6).

C.6.2 Unknown Events

The "unknown" category of laboratory triggers includes all events which were not obviously of terrestrial or solar origin and which do not resemble a GRB. Most of the channel 1 only (low-energy, 25–50 keV) events fall into this category. The major problem with this class of events is that it is dominated by intensity fluctuations from Cyg X-1: of 799 events in the unknown category, 689 are consistent with this source (although they may not *all* be from Cyg X-1); see the clustering of events marked (+) in Figure C-7. If we remove all the events consistent with Cyg X-1 we are left with the sky map shown in Figure C-13, where events are plotted as their 1.0σ error circles. Although Figure C-13 shows some general clustering toward the galactic center, there is no obvious clustering that would indicate the activity of any particular source.

We find two events which can convincingly be attributed to SGR 1806−20 based on intensity, spectral softness, and location. Both occur within one day of the onboard

triggered emission from SGR 1806−20 reported by Kouveliotou et al. (1994). Recent activity from this source suggests that more events from SGR 1806−20 (or other SGRs) may be detectable when this search is extended (Kouveliotou et al. 1996).

C.7 Conclusions

Our search of 345 days of archival BATSE data has uncovered a significant number of astronomically interesting transients.

The 91 nontriggered GRB candidates detected (so far) by this search include some of the faintest GRBs ever observed. When combined with the bursts detected by the onboard trigger during the same 345 days, these events extend knowledge of the peak flux distribution to values a factor of ~ 2 lower than the onboard detection threshold. Near the onboard trigger threshold, the combined sample is expected to be nearly complete (on the 1024 ms time scale). We find the logarithmic slope of the integral number versus peak flux distribution to be -0.5 ± 0.1 at peak fluxes of 0.15–0.35 ph cm $^{-2}$ s^{-1} after correcting for our laboratory trigger efficiency. The value of $\langle V/V_{max} \rangle = 0.32 \pm 0.02$ for the combined sample is consistent with that obtained for the 3B catalog as a whole. We find no evidence for anisotropy in the direction distribution of these events.

These results are consistent with those obtained from analyses of the published BATSE catalogs. The biases inherent in the onboard trigger mechanism do not appear to have significantly undermined its sampling of GRBs, at least for bursts with the characteristics our search can detect.

The nontriggered GRB candidates add to the database of GRBs available for duration studies, searches for burst repetition, and searches for gravitational lensing. See Fishman & Meegan (1995) for an overview and references. The slow-risers and the more intense bursts (which occurred while the onboard trigger was disabled) will probably be the most useful nontriggered GRBs for such purposes.

The low-energy (25–50 keV) events detected by our search arise from a variety

of sources. While intensity fluctuations from Cyg X-1 dominate this class of events, we find a significant number that must be due to other sources. Because of the difficulty in accurately estimating the source directions of these events, identification of the individual sources responsible for them depends on unique repetition patterns or temporal coincidences with other observations (as in the case of events from SGR 1806−20). The possibility remains that we may identify among these events new source activity or completely new burst sources.

The effort to extend this search to cover the more than 5 years of remaining archival data is in progress.

C.8 Acknowledgments

J. M. K. acknowledges support from a National Science Foundation Graduate Research Fellowship during the preliminary phase of this research and subsequent support from NASA Graduate Student Researchers Program Fellowship NGT8-52816. W. H. G. L. acknowledges support from NASA under grant NAG5-3804. C. K. acknowledges support from NASA under grant NAG5-2560. J. v. P. acknowledges support from NASA under grant NAG5-2755. We also thank Scott Barthelmy and James Kuyper for sharing the BACODINE version of the BATSE LOCBURST code, which formed the foundation for our trigger efficiency and burst location algorithms.

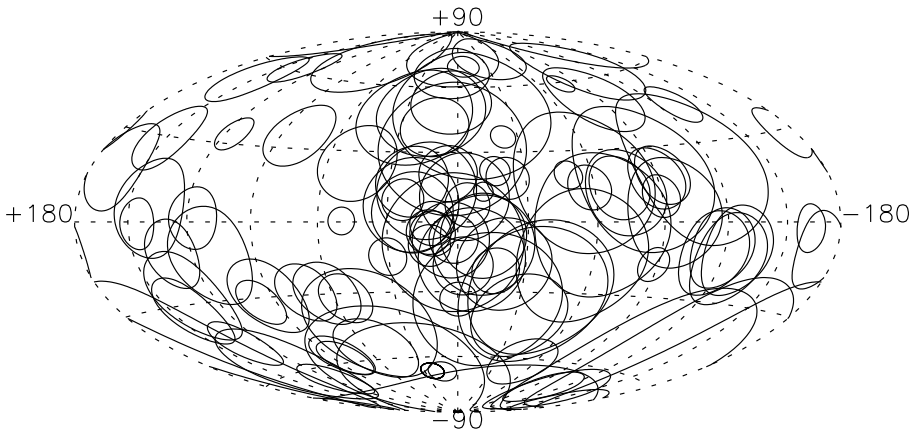

Figure C-13 Low-energy (25–50 keV) events plotted as 1σ error circles in Galactic coordinates (those consistent with Cyg X-1 excluded).

Bibliography

Aftergood, S., Hafemeister, D., Prilutsky, O. F., Primack, J. R., & Rodionov, S. N., 1991, *Scientific American* **264**, 42

Ananthakrishnan, S. & Ramanathan, K. R., 1969, *Nature* **223**, 488

Aschwanden, M. J., Schwartz, R. A., & Dennis, B. R., 1998, *Astrophysical Journal* **502**, 468

Avni, Y., 1976, *Astrophysical Journal* **210**, 642

Band, D., Matteson, J., Ford, L., Schaefer, B., Palmer, D., Teegarden, B., Cline, T., Briggs, M., Paciesas, W., Pendleton, G., Fishman, G., Kouveliotou, C., Meegan, C., Wilson, R., & Lestrade, P., 1993, *Astrophysical Journal* **413**, 281

Barthelmy, S. D. & Butterworth, P., 1998, in (Meegan et al. 1998b), pp 134–138

Belian, R. D., Conner, J. P., & Evans, W. D., 1976, *Astrophysical Journal Letters* **206**, L135

Bloom, J. S., Kulkarni, S. R., Harrison, F., Prince, T., Phinney, E. S., & Frail, D. A., 1998, *Astrophysical Journal Letters* **506**, L105

Bond, H., 1997, *IAU Circ.* 6654

Briggs, M. S., 1995, *Astrophysics and Space Science* **231**, 1

Briggs, M. S., Paciesas, W. S., Pendleton, G. N., Meegan, C. A., Fishman, G. J., Horack, J. M., Brock, M. N., Kouveliotou, C., Hartmann, D. H., & Hakkila, J., 1996, *Astrophysical Journal* **459**, 40

Brock, M. N., Meegan, C. A., Fishman, G. J., Wilson, R. B., Paciesas, W. S., & Pendleton, G. N., 1991, in (Paciesas & Fishman 1991), pp 399–403

Brown, R. T., 1973, *Nature* **246**, 83

Burgess, W. C. & Inan, U. S., 1993, *Journal of Geophysical Research* **98**, 15643

Chakrabarty, D., 1996, PhD dissertation, California Institute of Technology, Pasadena, CA

Cohen, E. & Piran, T., 1995, *Astrophysical Journal Letters* **444**, L25

Costa, E., Frontera, F., Heise, J., Feroci, M., Zand, J. I., Fiore, F., Cinti, M. N., Fiume, D. D., Nicastro, L., Orlandini, M., Palazzi, E., Rapisarda, M., Zavattini, G., Jager, R., Parmar, A., Owens, A., Moleni, S., Cusumano, G., Maccarone, M. C., Giarrusso, S., Coletta, A., Antonelli, L. A., Gimmi, P., Muller, J. M., Piro, L., & Butler, R. C., 1997, *Nature* **387**, 783

Datlowe, D. W., Imhof, W. L., Fishman, G. J., & Finger, M. H., 1995, *Radio Science* **30**, 47

Dean, A. J., Lei, F., & Knight, P. J., 1991, *Space Science Reviews* **57**, 109

Dennis, B. R., Schwartz, R. A., & Tolbert, A. K., 1998, *Access to BATSE Solar Flare Data for the Solar Physics Community*, http://umbra.nascom.nasa.gov/batse/batse_years.html

Djorgovski, S. G., Kulkarni, S. R., Bloom, J. S., Goodrich, R., Frail, D. A., Piro, L., & Palazzi, E., 1998, *Astrophysical Journal Letters* **508**, L17

Doschek, G. A., 1992, in S. P. Maran (ed.), *The Astronomy and Astrophysics Encyclopedia*, pp 632–635, Cambridge University Press, Cambridge

Dunlop, J. S., 1998, in M. N. Bremer et al. (ed.), *Observational Cosmology with the New Radio Surveys*, pp 157–162, Kluwer Academic Publishers, Netherlands

Fall, S. M., Charlot, S., & Pei, Y. C., 1996, *Astrophysical Journal Letters* **464**, L43

Fenimore, E. E. & Bloom, J. S., 1995, *Astrophysical Journal* **453**, 25

Fenimore, E. E., Epstein, R. I., Ho, C., Klebesadel, R. W., Lacey, C., Laros, J. G., Meier, M., Strohmayer, T., Pendleton, G., Fishman, G., Kouveliotou, C., & Meegan, C., 1993, *Nature* **366**, 40

Fishman, G. J., Bhat, P. N., Mallozzi, R., Horack, J. M., Koshut, T., Kouveliotou, C., Pendleton, G. N., Meegan, C. A., Wilson, R. B., Paciesas, W. S., Goodman, S. J., & Christian, H. J., 1994a, *Science* **264**, 1313

Fishman, G. J., Brainerd, J. J., & Hurley, K. (eds.), 1994b, *Gamma Ray Bursts: Proc. 2nd Huntsville Symposium*, No. 307 in AIP Conference Proceedings, Woodbury, NY, AIP

Fishman, G. J. & Inan, U. S., 1988, *Nature* **331**, 418

Fishman, G. J., Kouveliotou, C., van Paradijs, J., Harmon, B. A., Paciesas, W. S., Briggs, M. S., Kommers, J. M., & Lewin, W. H. G., 1995, *IAU Circular* 6272

Fishman, G. J. & Meegan, C. A., 1995, *Annual Reviews of Astronomy and Astrophysics* **33**, 415

Fishman, G. J., Meegan, C. A., Wilson, R. B., Brock, M. N., Horack, J. M., Kouveliotou, C., Howard, S., Paciesas, W. S., Briggs, M. S., Pendleton, G. N., Koshut, T. M., Mallozzi, R. S., Stollberg, M., & Lestrade, J. P., 1994, *Astrophysical Journal Supplement Series* **92**, 229

Fishman, G. J., Meegan, C. A., Wilson, R. B., Paciesas, W. S., Parnell, T. A., Austin, R. W., Rehage, J. R., Matteson, J. L., Teegarden, B. J., Cline, T. L., Schaefer, B. E., Pendleton, G. N., Berry, F. A., Horack, J. M., Storey, S. D., Brock, M. N., & Lestrade, J. P., 1989, in W. N. Johnson (ed.), *Proc. Gamma Ray Observatory Science Workshop*, pp 2–39–2–50, NASA, Greenbelt, MD

Frail, D. A., Kulkarni, S. R., Nicastro, L., Feroci, M., & Taylor, G. B., 1997, *Nature* **389**, 261

Friedlander, M., Gehrels, N., & Macomb, D. J. (eds.), 1993, *Compton Gamma Ray Observatory*, No. 280 in AIP Conference Proceedings, Woodbury, NY, AIP

Galama, T. J., Wijers, R. A. M. J., Bremer, M., Groot, P. J., Strom, R. G., Kouveliotou, C., & van Paradijs, J., 1998, *Astrophysical Journal Letters* **500**, L97

Gotthelf, E. V., Hamilton, T. T., & Helfand, D. J., 1996, *Astrophysical Journal* **466**, 779

Grindlay, J., Gursky, H., Schnopper, H., Parsignault, D. R., Heise, J., Brinkman,

A. C., & Schrijver, J., 1976, *Astrophysical Journal Letters* **205**, L127
Hakkila, J., Meegan, C. A., Horack, J. M., Pendleton, G. N., Briggs, M. S., Mallozzi, R. S., Koshut, T. M., Preece, R. D., & Paciesas, W. S., 1996, *Astrophysical Journal* **462**, 125
Hartmann, D. H., 1995, *Astronomy and Astrophysics Reviews* **6**, 225
Hess, W. N., 1965, *The Radiation Belt and Magnetosphere*, Blaisdell Publishing Co., Waltham, MA
Higdon, J. C. & Lingenfelter, R. E., 1990, *Annual Reviews of Astronomy and Astrophysics* **28**, 401
Horack, J. M., 1991, *Development of the Burst and Transient Source Experiment (BATSE)*, NASA Reference Publication 1268, NASA, Washington, D.C.
Horack, J. M., Fishman, G. J., Meegan, C. A., Wilson, R. B., & Paciesas, W. S., 1991, in (Paciesas & Fishman 1991), pp 373–377
Horack, J. M., Hakkila, J., Emslie, A. G., & Meegan, C. A., 1996, *Astrophysical Journal* **462**, 131
Hughes, D. H., Serjeant, S., Dunlop, J., Rowan-Robinson, M., Blain, A., Mann, R. G., Ivison, R., Peacock, J., Efstathiou, A., Gear, W., Oliver, S., Lawrence, A., Longair, M., Golschmidt, P., & Jenness, T., 1998, *Nature* **394**, 241
Hurley, K., 1995, in (Lewin et al. 1995a), pp 523–535
Hurley, K., 1998, in (Meegan et al. 1998b), pp 87–91
Hurley, K., Dingus, B. L., Mukherjee, R., Sreekumar, P., Kouveliotou, C., Meegan, C., Fishman, G., Band, D., Ford, L., Bertssch, D., Cline, T., Fichtel, C., Hartman, R., Hunter, S., Thompson, D. J., Kanbach, G., Mayer-Hasselwander, H., von Montigny, C., Sommer, M., Lin, Y., Nolan, P., Michelson, P., Kniffen, D., Mattox, J., Schneid, E., Moer, M., & Niel, M., 1994, *Nature* **372**, 652
Hurley, K., Li, P., Smette, A., Kouveliotou, C., Fishman, G., Laros, J., Cline, T., Fenimore, E., Klebesadel, R., Boer, M., Pedersen, H., Niel, M., & Sommer, M., 1996, *Astrophysical Journal* **464**, 342
in't Zand, J. J. M. & Fenimore, E. E., 1994, in (Fishman et al. 1994b), pp 692–696
Iwamoto, K., Mazzali, P. A., Nomoto, K., Umeda, H., Nakamura, T., Patat, F., Danziger, I. J., Young, T. R., Suzuki, T., Shigeyama, T., Augusteijn, T., Doublier, V., Gonzalez, J.-F., Boehnhardt, H., Brewer, J., Hainaut, O. R., Lidman, C., Leibundgut, B., Cappellaro, E., Turatto, M., Galama, T. J., Vreeswijk, P. M., Kouveliotou, C., Van Paradijs, J., Pian, E., Palazzi, E., & Frontera, F., 1998, *Nature* **395**, 672
Johnson, W. N., Kinzer, R. L., Kurfess, J. D., Strickman, M. S., Purcell, W. R., Grabelsky, D. A., Ulmer, M. P., Hillis, D. A., Jung, G. V., & Cameron, R. A., 1993, *Astrophysical Journal Supplement Series* **86**, 693
Kippen, R. M., Briggs, M. S., Kommers, J. M., Kouveliotou, C., Hurley, K., Robinson, C. R., Van Paradijs, J., Hartmann, D. H., Galama, T. J., & Vreeswijk, P. M., 1998, *Astrophysical Journal Letters* **506**, L27
Klebesadel, R. W., 1988, in Y. Tanaka (ed.), *Physics of Neutron Stars and Black Holes*, pp 387–403, Universal Academy Press, Tokyo

Klebesadel, R. W., Strong, I. B., & Olson, R. A., 1973, *Astrophysical Journal Letters* **182**, L85

Kommers, J. M., Lewin, W. H. G., Kouveliotou, C., van Paradijs, J., Pendleton, G. N., Fishman, G. J., & Meegan, C. A., 1998, in (Meegan et al. 1998b), pp 45–49

Kommers, J. M., Lewin, W. H. G., Kouveliotou, C., van Paradijs, J., Pendleton, G. N., Meegan, C. A., & Fishman, G. J., 1997, *Astrophysical Journal* **491**, 704

Kommers, J. M., Lewin, W. H. G., Kouveliotou, C., van Paradijs, J., Pendleton, G. N., Meegan, C. A., & Fishman, G. J., 1999a, *Astrophysical Journal*, in press

Kommers, J. M., Lewin, W. H. G., Kouveliotou, C., van Paradijs, J., Pendleton, G. N., Meegan, C. A., & Fishman, G. J., 1999b, *Astrophysical Journal Supplement Series*, in preparation

Kommers, J. M., Lewin, W. H. G., Kouveliotou, C., van Paradijs, J., Pendleton, G. N., Meegan, C. A., & Fishman, G. J., 1999c, *Astrophysical Journal* 511, in press

Kommers, J. M., Lewin, W. H. G., van Paradijs, J., Kouveliotou, C., Pendleton, G. N., Meegan, C. A., Fishman, G. J., & Briggs, M. S., 1996, in (Kouveliotou et al. 1996), pp 441–445

Koshut, T. M., Paciesas, W. S., Kouveliotou, C., van Paradijs, J., Pendleton, G. N., Fishman, G. J., & Meegan, C. A., 1996, *Astrophysical Journal* **463**, 570

Kouveliotou, C., Briggs, M. S., & Fishman, G. J. (eds.), 1996, *Gamma Ray Bursts: Proc. 3rd Huntsville Symposium*, No. 384 in AIP Conference Proceedings, Woodbury, NY, AIP

Kouveliotou, C., Dieters, S., Strohmayer, T., van Paradijs, J., Fishman, G. J., Meegan, C. A., Hurley, K., Kommers, J., Smith, I., Frail, D., & Murakami, T., 1998a, *Nature* **393**, 235

Kouveliotou, C., Fishman, G., Meegan, C., Paciesas, W., Van Paradijs, J., Norris, J., Preece, R., Briggs, M., Horack, J., Pendleton, G., & Green, D., 1994, *Nature* **368**, 125

Kouveliotou, C., Fishman, G. J., Meegan, C. A., Paciesas, W. S., Wilson, R. B., Van Paradijs, J., Preece, R. D., Briggs, M. S., Pendleton, G. N., & Brock, M. N., 1993, *Nature* **362**, 728

Kouveliotou, C., Fishman, G. J., Meegan, C. A., Van Paradijs, J., Briggs, M. S., Richardson, G., & Hurley, K., 1996, *IAU Circ.* 6501

Kouveliotou, C., Meegan, C. A., Fishman, G. J., Bhat, N. P., Briggs, M. S., Koshut, T. M., Paciesas, W. S., & Pendleton, G. N., 1993, *Astrophysical Journal Letters* **413**, L101

Kouveliotou, C., Strohmayer, T., Hurley, K., van Paradijs, J., Finger, M. H., Dieters, S., Woods, P., Thompson, C., & Duncan, R. C., 1998b, *Astrophysical Journal Letters*, in press

Kouveliotou, C., van Paradijs, J., Fishman, G. J., Briggs, M. S., Kommers, J. M., Harmon, B. A., Meegan, C. A., & Lewin, W. H. G., 1996, *Nature* **379**, 799

Krumholz, M., Thorsett, S. E., & Harrison, F. A., 1998, *Astrophysical Journal Letters* **506**, L81

Kulkarni, S. R., Djorgoski, S. G., Ramaprakash, A. N., Goodrich, R., Bloom, J. S., Adelberger, K. L., Kundic, T., Lubin, L., Frail, D. A., Frontera, F., Feroci, M., Nicastro, L., Barth, A. J., Davis, M., Filippenko, A. V., & Newman, J., 1998, *Nature* **393**, 35

Kulkarni, S. R., Frail, D. A., Wieringa, M. H., Ekers, R. D., Sadler, E. M., Wark, R. M., Higdon, J. L., Phinney, E. S., & Bloom, J. S., 1998, *Nature* **395**, 663

Lewin, W., van Paradijs, J., & Van Den Heuvel, E. (eds.), 1995a, *X-Ray Binaries*, Cambridge University Press

Lewin, W. H. G., Clark, G. W., & Smith, W. B., 1968, *Astrophysical Journal Letters* **152**, L55

Lewin, W. H. G. & Joss, P. C., 1983, in W. Lewin & E. Van Den Heuvel (eds.), *Accretion-driven Stellar X-ray Sources*, pp 41–115, Cambridge University Press, Cambridge

Lewin, W. H. G., van Paradijs, J., & Taam, R. E., 1993, *Space Science Reviews* **62**, 223

Lewin, W. H. G., van Paradijs, J., & Taam, R. E., 1995b, in (Lewin et al. 1995a), pp 175–232

Lilly, S. J., Le Fevre, O., Hammer, F., & Crampton, D., 1996, *Astrophysical Journal Letters* **460**, L1

Lingenfelter, R. E. & Higdon, J. C., 1996, in R. E. Rothschild & R. E. Lingenfelter (eds.), *High Velocity Neutron Stars and Gamma Ray Bursts*, No. 366 in AIP Conference Proceedings, pp 164–169, AIP, Woodbury, NY

Loredo, T. J., 1992, in E. D. Feigelson & G. J. Babu (eds.), *Statistical Challenges in Modern Astronomy*, pp 275–306, Springer-Verlag, New York

Loredo, T. J. & Wasserman, I. M., 1995, *Astrophysical Journal Supplement Series* **96**, 261

Loredo, T. J. & Wasserman, I. M., 1997, *astro-ph/9701111*

Loredo, T. J. & Wasserman, I. M., 1998a, *Astrophysical Journal* **502**, 108

Loredo, T. J. & Wasserman, I. M., 1998b, *Astrophysical Journal* **502**, 75

Loveday, J., Peterson, B. A., Efstathiou, G., & Maddox, S. J., 1992, *Astrophysical Journal* **390**, 338

Madau, P., Della Valle, M., & Panagia, N., 1998a, *Monthly Notices of the Royal Astronomical Society* **297**, L17

Madau, P., Pozzetti, L., & Dickinson, M., 1998b, *Astrophysical Journal* **498**, 106

Mao, S. & Mo, H. J., 1998, *Astronomy & Astrophysics* **339**, L1

Marani, G. F., Nemiroff, R., Norris, J. P., Hurley, K., & Bonnell, J. T., 1998, in (Meegan et al. 1998b), pp 134–138

Mayer, W., 1976, *IAU Circ.* 3006

Meegan, C. A., Fishman, G. J., Wilson, R. B., Horack, J. M., Brock, M. N., Paciesas, W. S., Pendleton, G. N., & Kouveliotou, C., 1992, *Nature* **355**, 143

Meegan, C. A., Pendleton, G. N., Briggs, M. S., Kouveliotou, C., Koshut, T. M., Lestrade, J. P., Paciesas, W. S., McCollough, M. L., Brainerd, J. J., Horack, J. M., Hakkila, J., Henze, W., Preece, R. D., Mallozzi, R. S., & Fishman, G. J.,

1998a, http://www.batse.msfc.nasa.gov

Meegan, C. A., Pendleton, G. N., Briggs, M. S., Kouveliotou, C., Koshut, T. M., Lestrade, J. P., Paciesas, W. S., McCollough, M. L., Brainerd, J. J., Horack, J. M., Hakkila, J., Henze, W., Preece, R. D., Mallozzi, R. S., & Fishman, G. J., 1996, *Astrophysical Journal Supplement Series* **106**, 65

Meegan, C. A., Preece, R. D., & Koshut, T. M. (eds.), 1998b, *Gamma Ray Bursts: Proc. 4th Huntsville Symposium*, No. 428 in AIP Conference Proceedings, Woodbury, NY, AIP

Mészáros, P. & Rees, M. J., 1997, *Astrophysical Journal* **476**, 232

Metzger, M. R., Djorgovski, S. G., Kulkarni, S. R., Steidel, C. C., Adelberger, K. L., Frail, D. A., Costa, E., & Frontera, F., 1997, *Nature* **387**, 878

Norris, J. P., Bonnell, J. T., Nemiroff, R. J., Scargle, J. D., Kouveliotou, C., Paciesas, W. S., Meegan, C. A., & Fishman, G. J., 1995, *Astrophysical Journal* **439**, 542

Norris, J. P., Nemiroff, R. J., Scargle, J. D., Kouveliotou, C., Fishman, G. J., Meegan, C. A., Paciesas, W. S., & Bonnell, J. T., 1994, *Astrophysical Journal* **424**, 540

O'Mongain, E. & Baird, G. A., 1976, *Astrophysics and Space Science* **42**, 63

O'Neill, T. J., Kerrick, A. D., Ait-Ouamer, F., Tumer, O. T., Zych, A. D., & White, R. S., 1989, *Science* **244**, 451

Paciesas, W. S. & Fishman, G. J. (eds.), 1991, *Gamma Ray Bursts: Proc. 1st Huntsville Symposium*, No. 265 in AIP Conference Proceedings, Woodbury, NY, AIP

Paciesas, W. S., Meegan, C. A., Penleton, G. N., Briggs, M. S., Kouveliotou, C., Koshut, T. M., Lestrade, J. P., McCollough, M. L., Brainerd, J. J., Hakkila, J., Henze, W., Preece, R. D., Connaughton, V., Kippen, R. M., Mallozzi, R. S., & Fishman, G. J., 1999, *Astrophysical Journal Supplement Series*, submitted

Pendleton, G. N., Briggs, M. S., & Meegan, C. A., 1996a, in (Kouveliotou et al. 1996), p. 877

Pendleton, G. N., Mallozzi, R. S., Paciesas, W. S., Briggs, M. S., Preece, R. D., Koshut, T. M., Horack, J. M., Meegan, C. A., Fishman, G. J., Hakkila, J., & Kouveliotou, C., 1999, *Astrophysical Journal* **511**, in press

Pendleton, G. N., Mallozzi, R. S., Paciesas, W. S., Briggs, M. S., Preece, R. D., Koshut, T. M., Horack, J. M., Meegan, C. A., Fishman, G. J., Hakkila, J., & Kouveliotou, C., 1996b, *Astrophysical Journal* **464**, 606

Pendleton, G. N., Paciesas, W. S., Mallozzi, R. S., Koshut, T. M., Fishman, G. J., Meegan, C. A., Wilson, R. B., Horack, J. M., & Lestrade, J. P., 1995, *Nuclear Instruments & Methods in Physics Research A* **364**, 567

Piran, T., 1998, astro-ph/9810256

Press, W., Flannery, B., Teukolsky, S., & Vetterling, W., 1995, *Numerical Recipies in C*, Cambridge University Press

Primack, J. R., 1989, *Science* **244**, 407

Ramanamurty, Y. V., Mitra, A. P., & Jain, V. C., 1970, *Journal of Atmospheric and Terrestrial Physics* **32**, 1721

Rieger, E., Vestrand, W. T., Forrest, D. J., Chupp, E. L., Kanbach, G., & Reppin,

C., 1989, *Science* **244**, 441

Rubin, B. C., Finger, M. H., Harmon, B. A., Paciesas, W. S., Fishman, G. J., Wilson, R. B., Wilson, C. A., Brock, M. N., Briggs, M. S., Pendleton, G. N., Cominsky, L. R., & Roberts, M. S., 1996, *Astrophysical Journal* **459**, 259

Rubin, B. C., Horack, J. M., Brock, M. N., Meegan, C. A., Fishman, G. J., Wilson, R. B., Paciesas, W. S., & van Paradijs, J., 1993, in (Friedlander et al. 1993), pp 719–723

Rubin, B. C., Lei, F., Fishman, G. J., Finger, M. H., Harmon, B. A., Kouveliotou, C., Paciesas, W. S., Pendleton, G. N., Wilson, R. B., & Zhang, S. N., 1996, *Astronomy & Astrophysics Supplement Series* **120**, 687

Rutledge, R. E., Hui, L., & Lewin, W. H. G., 1995, *Monthly Notices of the Royal Astronomical Society* **276**, 753

Rutledge, R. E., Lewin, W. H. G., Pendleton, G., Lestrade, J. P., Kouveliotou, C., & Meegan, C., 1996, in (Kouveliotou et al. 1996), pp 527–531

Sahu, K. C., Livio, M., Petro, L., Macchetto, F. D., van Paradijs, J., Kouveliotou, C., Fishman, G. J., Meegan, C. A., Groot, P. J., & Galama, T., 1997, *Nature* **387**, 476

Schaefer, B. E., Cline, T. L., Hurley, K. C., & Laros, J. G., 1997, *Astrophysical Journal* **489**, 693

Schechter, P., 1976, *Astrophysical Journal* **203**, 297

Schmidt, M., Higdon, J. C., & Hueter, G., 1988, *Astrophysical Journal Letters* **329**, L85

Schoenfelder, V., Aarts, H., Bennett, K., De Boer, H., Clear, J., Collmar, W., Connors, A., Deerenberg, A., Diehl, R., Von Dordrecht, A., Den Herder, J. W., Hermsen, W., Kippen, M., Kuiper, L., Lichti, G., Lockwood, J., Macri, J., McConnell, M., Morris, D., Much, R., Ryan, J., Simpson, G., Snelling, M., Stacy, G., Steinle, H., Strong, A., Swanenburg, B. N., Taylor, B., De Vries, C., & Winkler, C., 1993, *Astrophysical Journal Supplement Series* **86**, 657

Schulz, M. & Lanzerotti, L. J., 1974, *Particle Diffusion in the Radiation Belts*, Springer-Verlag, New York

Skelton, R. T. & Mahoney, W. A., 1994, in (Fishman et al. 1994b), pp 706–710

Strohmayer, T. E., Fenimor, E. E., Murakami, T., & Yoshida, A., 1995, *Astrophysical Journal* **445**, 731

Tanaka, Y. & Shibazaki, N., 1996, *Annual Review of Astronomy and Astrophysics* **34**, 607

Tascione, T. F., 1994, *Introduction to the Space Environment*, Krieger Publishing Co., Malabar, FL

Tegmark, M., 1996, *Astrophysical Journal Letters* **470**, L81

Thompson, C. & Duncan, R. C., 1995, *Monthly Notices of the Royal Astronomical Society* **275**, 255

Thompson, D. J., Bertsch, D. L., Fichtel, C. E., Hartman, R. C., Hofstadter, R., Hughes, E. B., Hunter, S. D., Hughlock, B. W., Kanbach, G., Kniffen, D. A., Lin, Y. C., Mattox, J. R., Mayer-Hasselwander, H. A., Von Montigny, C., Nolan, P. L.,

Nel, H. I., Pinkau, K., Rothermel, H., Schneid, E. J., Sommer, M., Sreekumar, P., Tieger, D., & Walker, A. H., 1993, *Astrophysical Journal Supplement Series* **86**, 629

Tinney, C., Stathakis, R., Cannon, R., & Galama, T. J., 1998, *IAU Circular* 6896

Totani, T., 1997, *Astrophysical Journal Letters* **486**, L71

Totani, T., 1998, pp astro–ph/9805263

van der Klis, M., 1995, in (Lewin et al. 1995a), pp 252–307

van Paradijs, J., Groot, P. J., Galama, T., Kouveliotou, C., Strom, R. G., Teltin, J., Rutten, R. G. M., Fishman, G. J., Meegan, C. A., Pettini, M., Tanvir, N., Bloom, J., Pedersen, H., Nordgaard-Nielsen, H. U., andJ. Melnick, M. L.-V., van der Steene, G., Beremer, M., Naber, R., Heise, J., Zand, J. I., Costa, E., Feroci, M., Piro, L., Frontera, F., Zavattini, G., Nicastro, L., Palazzi, E., Bennet, K., Hanlon, L., & Parmar, A., 1997, *Nature* **386**, 686

van Paradijs, J., Rubin, B. C., Kouveliotou, C., Horack, J. M., Fishman, G. J., Meegan, C. A., Wilson, R. B., Paciesas, W. S., Lewin, W. H. G., & van der Klis, M., 1993, in (Friedlander et al. 1993), pp 877–881

Wang, V. C., 1994, PhD dissertation, University of California San Diego, La Jolla, CA

Weekes, T. C., 1976, *Journal of Atmopheric and Terrestrial Physics* **38**, 1021

Wienberg, S., 1972, *Gravitation and Cosmology: Principles and Applications of the General Theory of Relativity*, John Wiley & Sons, New York

Wijers, R. A. M. J., Bloom, J. S., Bagla, J. S., & Natarajan, P., 1998, *Monthly Notices of the Royal Astronomical Society* **294**, L13

Wijers, R. A. M. J., Rees, M. J., & Mészáros, P., 1997, *Monthly Notices of the Royal Astronomical Society* **288**, L51

Young, C. A., Arndt, M. B., Beisecker, D. A., & Ryan, J. M., 1996, in (Kouveliotou et al. 1996), pp 555–559

Zhang, S. N., Fishman, G. J., Harmon, B. A., & Paciesas, W. S., 1993, *Nature* **366**, 245